DOCTORAT BIOLOGIE BRETAGNE SANTE LOIRE

UNIVERSITÉ DE NANTES

THÈSE DE DOCTORAT DE

L'UNIVERSITE DE NANTES

ECOLE DOCTORALE N° 605
Biologie Santé
Spécialité : Neurosciences

Par
Céline SALAUD

Reconstruction in vitro d'un glioblastome par techniques de bioimpression

Thèse présentée et soutenue à Nantes, le 02/12/2020
Unité de recherche : CRCINA Inserm UMR 1232

Rapporteurs avant soutenance :

Marie-Pierre JUNIER, Directeur de recherche INSERM, HDR, Sorbonne Université
Didier WION, Chargé de recherche INSERM HDR, Université Grenoble Alpes

Composition du Jury :

Président :	Kévin BUFFENOIR	Professeur d'Université – Praticien Hospitalier, Université Nantes
Examinateurs :	Marie-Pierre JUNIER	Directeur de Recherche INSERM, HDR, Sorbonne Université
	Didier WION	Chargé de Recherche INSERM, HDR, Université Grenoble Alpes
	Dominique LIGUORO	Professeur d'Université – Praticien Hospitalier, Université Bordeaux
	Lisa OLIVER	Chargée de Recherche INSERM, HDR, Université Nantes
Dir. de thèse :	François VALLETTE	Directeur de Recherche INSERM, HDR, Université Nantes
Co-dir. de thèse :	Kévin BUFFENOIR	Professeur d'Université – Praticien Hospitalier, Université Nantes

REMERCIEMENTS

A Madame Marie-Pierre Junier et à Monsieur Didier Wion

Merci à vous d'avoir accepté d'évaluer mon travail et d'être membres de mon jury. Merci pour votre disponibilité.

A Madame le Professeur Dominique Liguoro

Merci d'avoir accepté de faire partie de mon jury.

A Monsieur François Vallette,

Merci de m'avoir permis de faire partie de ton équipe. Merci de m'avoir fait confiance et de m'aider depuis le début dans la réalisation de ce travail de thèse mais également au-delà. Merci à toi, de me permettre de participer aux différents projets de recherche dans le glioblastome. Ce n'est que le début de notre collaboration entre la recherche et la clinique.

A Monsieur le Professeur Kevin Buffenoir

Merci pour votre soutien depuis ces nombreuses années que ce soit dans les projets chirurgicaux comme scientifiques. J'espère que ce travail, comme on le souhaite, permettra à la neurochirurgie nantaise de rayonner également en neurooncologie.

A Madame Lisa Oliver,

Travailler à tes côtés m'a beaucoup apporté tout au long de ces années. Tu m'as permis d'appréhender les connaissances fondamentales en tumorigenèse beaucoup plus facilement. Merci pour ta bienveillance envers moi, pour ta patience et pour ta bonne humeur. Je n'en serai pas là sans toi. Je te dois énormément.

A Fanny Geraldo,

Merci de m'avoir accueilli à tes côtés sur la paillasse. Ta patience et ta disponibilité m'ont manqué quand tu es partie.

A tous mes collègues du service de neurochirurgie du CHU de Nantes : Dr Stéphane Martin, Dr Vincent Roualdes, Dr Tanguy Riem, Dr Sylvie Raoul, Dr Alexis Moles, Dr Philippe Cam, Dr Constentin Moraru.

Merci de m'avoir aidée tout au long de ce cursus parallèlement à l'activité clinique. Merci à vous pour votre soutien, pour m'avoir remplacée au pied levé lors de la dernière ligne droite.

Au Docteur Caroline Victorri-Vigneau,

Merci pour tes précieux conseils lors de la dernière ligne droite. Je comprends l'affection que te portent les étudiants en médecine. Tu sais trouver les mots pour croire en soi et pour se motiver. Sans toi j'y serai peut-être encore…

À toi Nicolas,

Ma moitié. Sans toi rien n'est possible.

A mes parents,

Merci d'être toujours là pour moi, même après 36 ans.

A mes enfants, Léon et Camille,

Vous comprendrez plus tard pourquoi maman était si souvent au boulot.

TABLE DES MATIERES

LISTE DES ABRÉVIATIONS

A

ADN : Acide Désoxyribonucléique
ARG: Arginase

ASCL : Achaete-Scute

B

BCPC : Brain Cancer-Propagating Cell

BCNU : Bis-Chloroethylnitrosourea

BHE : Barrière Hémato-Encéphalique

C

CAF : Cancer Associated Fibroblasts

CD : Cluster of differentiation

CDK : Cyclin-Dependant Kinase

CHI3L1 : Chitinase 3 Like 1

CMH : Complexe Majeur d'Histocompatibilité

CPA : Cellule Présentatrice d'Antigène

CSC : Cellules Souches Cancéreuse

CSM : Cellules Souches Mésenchymateuse

CXCR :Chemokine Receptor

D

DCX : Doublecortin X

DLL : Delta Like Canonical Notch Ligand

E

ECM: Extracellular Matrix

EGFR : Epidermal Growth Factor

EMT : Epithelial-Mesenchymal Transition

G

GAG : glycoaminoglycanes

GASCS : Glioblastoma Assiated Stromal Cell

GABRA: Gamma-Aminobutyric Acid type A

GBM : Glioblastome

GCSC: Glioblastoma Cancer Stem Cell

GSC : Glioblastoma Stem Cell

H

HIF : Hypoxia-Inductible Factor

I

IDH : Isocitrate Dehydrogenase

IL: Interleukine

IRM : Imagerie par Résonnance Magnétique

M

mARN : Acide Ribonucléique Messager

miARN : Micro Acide Ribonucléique

MDSC : Myeloide-Derived Suppressor Cells

MEC : Matrice Extra-Cellulaire

MERTK : Myeloid-Epithelial-Reproductive Tyrosine Kinase

MET : Microenvironnement Tumoral

MGMT : Methylguanine Methyl Transférase

MMP: Metalloproteinase

c-Myc : Cellular Myelocytomatosis Oncogene

N

NEFL : Neurofilament Light

NES : Nestine

NF1 : Neurofibrine 1

NF KB : Nuclear Factor Kappa B

NG2 : Neural Glial antigen 2

NK : Natural Killer

NOX4 : Nicotinamide Adenine Dinucleotide Oxidase 4

O

Oct4 : Octamer-binding transcription factor 4

OLIG : Oligodendrocyte

OMS : Organisation Mondiale de la Santé

P

PCSC: Peritumoral Cancer Stem Cell

PDGF : Platelet Growth Factor

PI3K : Phosphoinositol 3-Kinase

PTEN : Phosphatase Tensin Homolog

R

ROS : Reactive Oxygen Species

S

SDF : Stromal Derived Factor

SHH : Sonic Hedgehog

SLC : Solute Carrier

alphaSMA : alpha Smooth Muscle Actin

SNC : Système Nerveux Central

SMA : smooth muscle actin

SOX : Sex Determining Region Y-related Hight Mobility Group-box

SYT : Synaptotagmin

T

TA-MSC : Tumor Associated Mesenchymal Stem Cell

TCGA : The Cancer Genome Atlas Consortium

TCF : Transcription Factor

TIC : Tumor Initiating Cell

TGF-ß: Transforming Growth Factor ß

TMZ : Témozolomide

TNF : Tumor Necrosis Factor

TNT : Tunneling Nanotubes

TP53 : Tumor Protein 53

V

VEGF: Vascular Endothelial Growth Factor

Z

ZNF217 : Zinc Finger Protein 217

LISTE DES FIGURES ET TABLEAUX

INTRODUCTION

I. INTRODUCTION

1 LES GLIOMES

1.1 DEFINITION ET CLASSIFICATION DES GLIOMES

Les tumeurs du système nerveux central (SNC) représentent seulement 2% des cancers diagnostiqués chez l'adulte (1). Les tumeurs neuroépithéliales, comportant les gliomes, sont les plus fréquentes des tumeurs primitives du SNC. Les gliomes représentent les tumeurs primitives les plus fréquentes (entre 30 et 40%). Leur incidence est estimée à 5 cas pour 100000 habitants (2).

La classification des gliomes a évolué dans le temps, la plus récente est de 2016 par l'Organisation Mondiale de la Santé (OMS) (3). En 2007, l'OMS classait les tumeurs du SNC à partir de leurs caractéristiques histogénétiques (aspect microscopique des cellules tumorales et leur degré de différentiation) (4). Cependant cette classification était peu reproductible, ne prenait pas en compte l'hétérogénéité tumorale et ne distinguait pas les cellules tumorales du parenchyme résiduel infiltré. Une deuxième classification a été décrite par l'Hôpital Saint Anne, basée sur ces caractéristiques mais en y incluant les données cliniques et iconographiques. Cette classification a permis de distinguer les tumeurs circonscrites des tumeurs infiltrantes ainsi que la présence ou non d'une néoangiogenèse modifiant par sa présence le pronostic des patients (5). En 2016, la nouvelle classification de l'OMS s'est basée sur les critères précédemment cités mais également sur des critères moléculaires. Cette classification est encore mieux corrélée à l'évolution clinique et au pronostique (Tableau 1) (3).

Actuellement, les gliomes sont répartis en 4 grades (de I à IV), les gliomes de bas grade (I astrocytome pilocytique et II astrocytome diffus) et les gliomes de haut grade (III anaplasique et IV glioblastome). Plus le grade est élevé, plus le pronostic est sombre. Les glioblastomes (GBM) sont définis histologiquement par la présence de cellules néoplasiques ayant les caractéristiques astrocytaires et par la présence de prolifération endothéliale et/ou de nécrose (3).

Grades	Tumeurs diffuses astrocytaires et oligodendrogliales
II	Astrocytome diffus, *IDH*-muté Astrocytome gémistocytique, *IDH*-muté
II	*Astrocytome diffus, IDH-non muté*
II	Astrocytome diffus, NOS
III	Astrocytome anaplasique, *IDH*-muté
III	*Astrocytome anaplasique, IDH-non muté*
III	Astrocytome anaplasique, NOS
IV	Glioblastome, *IDH*-non muté Glioblastome à cellules géantes Gliosarcome *Glioblastome épithélioïde*
IV	Glioblastome, *IDH*-muté
IV	Glioblastome, NOS
IV	Gliome diffus de la ligne médiane, H3 K27M-muté
II	Oligodendrogliome, *IDH*-muté et codélétion 1p-19q
II	Oligodendrogliome, NOS
III	Oligodendrogliome anaplasique, *IDH*-muté et codélétion 1p-19q
III	*Oligodendrogliome anaplasique, NOS*
II	*Oligoastrocytome, NOS*
III	*Oligoastrocytome anaplasique, NOS*
	Autres tumeurs astrocytaires
I	Astrocytome pilocytique Astrocytome pilomyxoïde
I	Astrocytome subépendymaire à cellules géantes
II	Xanthoastrocytome pléomorphe
III	Xanthoastrocytome pléomorphe anaplasique
	Tumeurs épendymaires
I	Subépendymome
I	Ependymome myxopapillaire
I	Ependymome Ependymome papillaire Ependymome à cellules claires Ependymome tanacytique
II ou III	Ependymome, *RELA* fusion-positif
III	Ependymome anaplasique
	Autres gliomes
II	Gliome chordoïde du 3e ventricule
I	Gliome angiocentrique
–	Astroblastome

Tableau 1: Classification des gliomes selon l'OMS 2016. Traduit en français dans la revue médicale suisse 2017. Les glioblastomes sont les tumeurs diffuses astrocytaires de grade IV (6) (3).

1.2 LES GLIOBLASTOMES

1.2.1 Épidémiologie

Les glioblastomes multiformes représentent la forme la plus agressive et la plus fréquente des astrocytomes, environ 50% des tumeurs malignes du SNC. Ils peuvent être « de novo » (GBM primaires) ou évoluer à partir d'un gliome de bas grade (GBM secondaires)(7).

L'incidence des GBM a augmenté au cours des dernières décennies. Elle est d'environ 5/100000 habitants en France (1). Elle augmente de manière linéaire chez l'adulte jusqu'à 75 ans (Figure 1). Cette augmentation s'explique en partie avec le développement et l'accessibilité des imageries cérébrales (scanner et IRM) ainsi que par le vieillissement de la population. Ils sont plus fréquents chez l'homme dans un rapport de 1,5 à 1,8/1. Les principaux facteurs modifiant le risque de survenue d'un GBM sont l'âge, le sexe masculin, les syndromes de prédisposition, le polymorphisme génétique et la radiothérapie encéphalique(7).

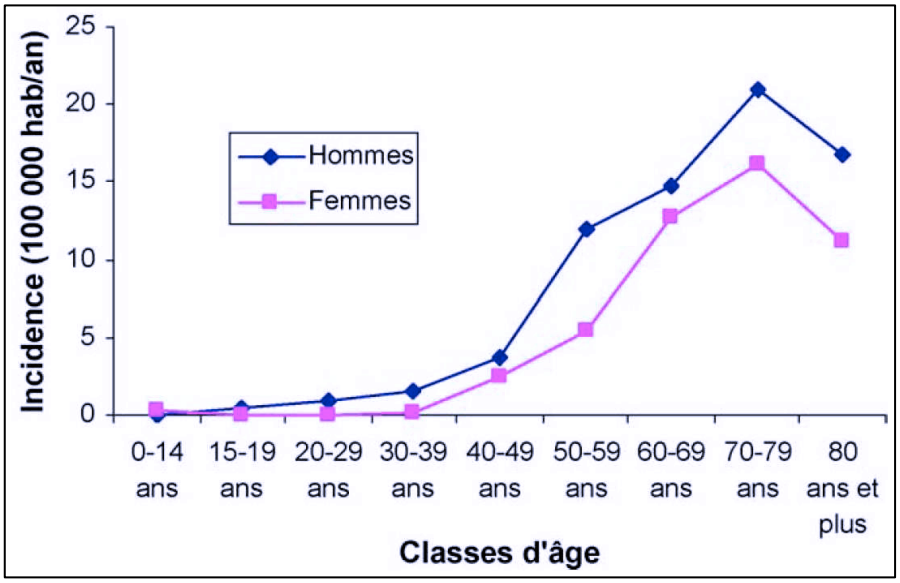

Figure 1. Incidence des glioblastomes selon l'âge et le sexe (d'après Baldi et al.) (7). L'incidence augmente de manière linéaire chez l'adulte jusqu'à 75 ans. Les GBM sont plus fréquents chez l'homme dans un rapport de 1,5 à 1,8/1.

1.2.2 Classifications génomique et moléculaire des GBM

- Classification génomique : différentes mutations ont été identifiées au sein des GBM

La présence ou non de la mutation du gène isocitrate dehydrogenase (IDH) enzyme du cycle de Krebs IDH1 ou IDH2

Cette mutation a été retrouvée dans les gliomes grade II et III principalement. Elle n'est présente que dans 5% des GBM primaires et par l'évolution des gliomes II et III dans 90% des GBM secondaires. Un GBM cliniquement diagnostiqué comme primaire mais possédant la mutation IDH1 doit être considéré comme un GBM secondaire à un gliome de grade moins élevé (le plus souvent anaplasique) cliniquement silencieux. Cette mutation constitue un marqueur pronostique majeur (3) (8) (9).

La présence ou non de la méthylation de la O6-methylguanine methyl transférase (MGMT)

La méthylation de la MGMT contribue à la réponse au traitement. La principale cible de la chimiothérapie par témozolomide (TMZ) (chimiothérapie de référence actuellement) est la position O6 de la guanine, à laquelle elle ajoute un groupe méthylé rendant impossible la réplication de l'ADN; celui-ci peut être retiré par une enzyme, la MGMT. Les patients présentant donc la méthylation inactivant le promoteur du gène codant pour la MGMT ont une meilleure réponse au TMZ (10).

Mutations identifiées par le Cancer Genome Atlas Consortium

Le Cancer Genome Atlas Consortium (TCGA) a identifié de nombreuses mutations de gènes, les plus fréquentes sont *TP53, EGFR, IDH1* and *PTEN.* Le TCGA a également identifié la présence simultanée d'anomalies au sein des voies p53, RB and receptor tyrosine kinase (11).

- Classification moléculaire des GBM :

Auparavant étaient décrits *4 sous-types moléculaires* de GBM :les sous-types proneural, classique, mésenchymateux et neural (Figure 2) (12) (13).
Cependant, Wang et al. à partir de l'analyse de l'expression de gènes de 37 GBM ont démontré que le sous-type neural n'était pas un sous-type à part entière mais représentait

plutôt le tissu en périphérie du GBM (14). Les aberrations et l'expression des gènes EGFR, NF1, et PDGFRA/IDH1 définissent ces sous-types en classique, mésenchymateux et proneural respectivement. La réponse au traitement actuel du GBM est différente en fonction du sous-type. Il existe une meilleure réponse au traitement pour le sous-type classique et aucun bénéfice pour le sous-type proneural- chaque groupe présentant à la fois un profil moléculaire spécifique et un pronostic différent (15) (13).

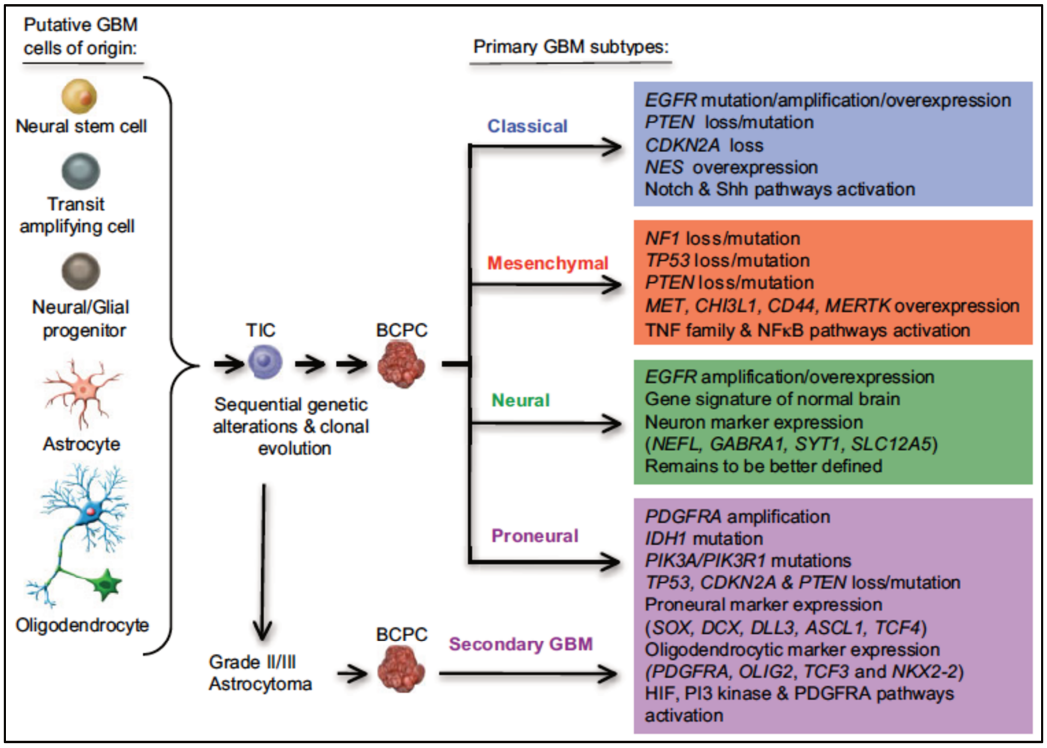

Figure 2. Classification moléculaire des GBM selon leur profil d'expression génique (d'après Van Meir et al.) (12).Modifications génétiques décrites dans les différents sous-types moléculaires des GBM avant le reclassement par Wang. Certaines cellules cérébrales présentant des altérations génétiques deviennent des TIC (Tumor initiating cells) (autrement nommées des CSC) cellules initiatrices de tumeur. Ces TICs accumulent des modifications génétiques et épigénétiques et deviennent des BCPC (Brain cancer-propagating cells) cellules cérébrales procancéreuses. Ensuite ces cellules seront à l'origine des GBM et de leurs sous-types.

1.2.3 Présentation clinique des GBM

En neurochirurgie, nous prenons en charge ces patients. Ils se présentent le plus souvent avec un tableau clinique témoignant du développement déjà important du GBM. Le mode d'entrée clinique dans la pathologie peut se révéler de trois façons, isolées ou associées. Le patient peut présenter une comitialité (épilepsie généralisée ou partielle), un déficit neurologique (en lien avec l'infiltrat tumoral ou secondaire à l'effet de masse sur des

structures neurologiques adjacentes) ou des signes d'hypertension intracrânienne. Dans ce dernier cas, le pronostic vital du patient est rapidement mis en jeu.

Quel que soit le mode de révélation, il est capital de poser un diagnostic de certitude le plus rapidement possible, par une exérèse ou en cas d'impossibilité par une biopsie.

1.3 TRAITEMENT DES GLIOBLASTOMES

Le traitement de référence des GBM est inchangé depuis 2005, aucun progrès significatif dans leur prise en charge n'a été fait depuis presque 20 ans. Il repose sur l'exérèse chirurgicale la plus complète possible (avec le moins de risque) suivie d'une radio-chimiothérapie adjuvante (protocole STUPP) (16). En raison de la capacité des gliomes à infiltrer le parenchyme sain, d'autant plus s'il s'agit d'un GBM, leur exérèse complète est impossible. En effet, les cellules cancéreuses de GBM semblent migrer préférentiellement le long des structures préexistantes comme les tractus de fibres blanches ou le long des vaisseaux (17). Après l'intervention, la radiothérapie est quotidienne (5/7jours, dose d'irradiation quotidienne entre 1,8 à 2,0 Gy par séance), associée à la chimiothérapie par TMZ. La durée totale du traitement concomitant est de 6 semaines (16). Ensuite le patient, si la tolérance au TMZ est bonne, bénéficie d'une chimiothérapie d'entretien par TMZ entre 6 et 12 mois.

Cependant, il existe une certaine variabilité dans la décision du type de traitement des patients atteints de GBM. En effet, il diffère selon l'âge et l'état général du patient (18). La décision du traitement et de ses modalités découle d'une discussion pluridisciplinaire et parfois d'un avis oncogériatrique (18). Pour des patients très âgés et/ou ayant un état général affaibli, il peut être proposé un schéma en « hypofractionné » de la radiothérapie diminuant la fréquence et la dose totale d'irradiation. Pour certains patients, si l'autonomie, l'état général ainsi que la localisation du GBM sont défavorables, une abstention thérapeutique peut être retenue (19).

Malgré cette prise en charge, la maladie progresse très vite et conduit à une rechute à 8 mois après le diagnostic et permet une médiane de survie entre 12 et 15 mois contre 3 mois en l'absence de prise en charge (20) (16). La survie des patients à deux ans est de 27% et à 5 ans entre 3 et 5% (Figure 3).

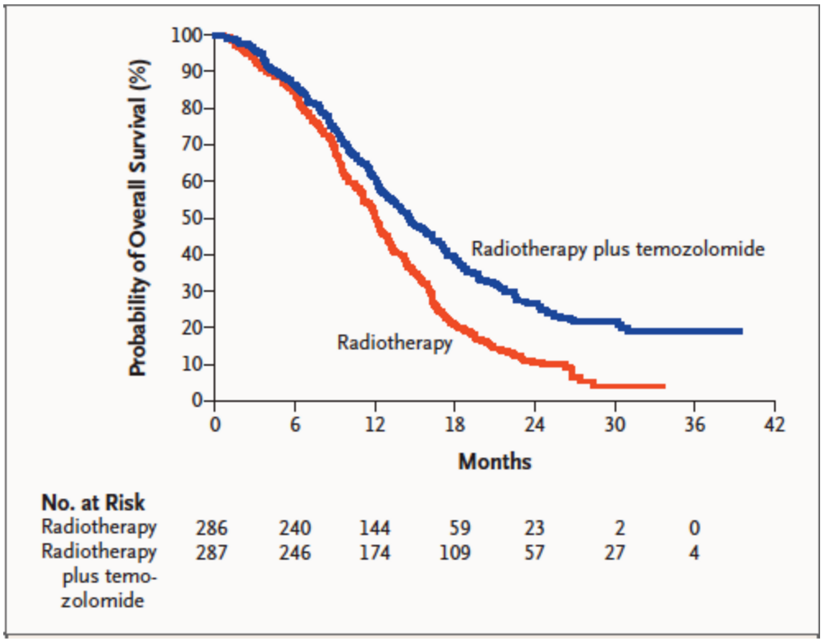

Figure 3. Courbe de Kaplan-Meier estimant la survie des patients atteints de GBM traités par protocole STUPP (d'après Stupp et al.) (16). Stupp et al ont démontré une meilleure survie pour les patients traités par radiothérapie et chimiothérapie concomitante en comparaison aux patients traités par radiothérapie seule.

Il existe, comme on l'a décrit précédemment, des facteurs pronostiques identifiés. La mutation IDH1 (rare dans les GBM primaires) augmente la survie globale et est le plus souvent pour des patients de plus jeune âge (15) (21) (10). Le statut méthylé du promoteur MGMT permet une meilleure survie globale car la méthylation de ce promoteur assure une meilleure réponse aux agents alkylants présents (TMZ) dans le protocole du traitement (10).

2 RESISTANCE DES GLIOBLASTOMES

2.1 MECANISMES IDENTIFIES DANS LA RESISTANCE

Les GBM font partie des cancers les plus difficiles à traiter. Le traitement actuel est limité et rapidement inefficace. Les difficultés dans le développement de nouveaux traitements sont dues aux différentes caractéristiques des GBM comme la présence de la barrière hémato-encéphalique (BHE), l'hétérogénéité tumorale, l'augmentation des ROS et le caractère infiltrant de cette tumeur dans le parenchyme sain.

2.1.1 La Barrière Hémato-Encéphalique

Tout d'abord, les GBM sont protégés par la barrière anatomique physiologique qu'est la BHE. Seules quelques molécules thérapeutiques sont capables de la franchir limitant d'emblée le nombre de chimiothérapies possibles efficaces (22).

2.1.2 Hétérogénéité intratumorale et interindividuelle

Il existe une très forte hétérogénéité pour chaque GBM avant et pendant le traitement ainsi qu'à la récidive. Il n'existe pas un seul type de GBM mais plusieurs.

Cette hétérogénéité s'explique par des modifications génétiques, épigénétiques et par la présence de populations multiples de cellules cancéreuses et non cancéreuses composant le microenvironnement tumoral (MET). Il est démontré dans de nombreux cancers, comme pour les GBM, le rôle incontournable du MET dans la résistance au traitement (15) (23) (22). De plus, les mutations impliquées dans les mécanismes de récidive ne sont pas bien identifiées, il est possible que la plupart de ces mutations ne correspondent pas à celles mises en évidence dans les GBM au stade initial (24).

Tout cela contribue à l'hétérogénéité dans l'espace et dans le temps de chaque GBM et de ce fait rend impossible de prédire la réponse ou la résistance au traitement (20) (25) (26) (27).

2.1.3 L'augmentation des ROS

Une grande partie des cellules composant le microenvironnement tumoral (MET) est responsable de l'augmentation significative des Reactive Oxygen Species (ROS) au sein de la tumeur. Les cancers en général, dont les GBM, s'accompagnent d'un stress oxydatif qui est la conséquence d'un déséquilibre entre la production de radicaux libres ROS et les mécanismes anti-oxydants les éliminant (28). Ces ROS jouent normalement un rôle important dans de nombreux mécanismes physiologiques.

Dans les cancers, les ROS sont produits en excès par les cellules du MET (principalement par l'intermédiaire des mitochondries). Ce stress oxydatif entraine des modifications membranaires et des dommages d'ADN qui favorisent les processus tumoraux. Les ROS participent à l'activation des mécanismes d'apoptose et d'autophagie (28). L'autophagie est assimilable à un mécanisme protumoral en permettant la survie prolongée de la cellule, phénomène favorisé par les ROS. En plus de leurs actions spécifiques, le TMZ et

l'irradiation ont pour conséquences d'augmenter l'expression des ROS et donc d'augmenter la résistance des cellules à leurs effets (28).

L'augmentation de l'expression des ROS dans les GBM contribue donc à la sélection de sous-populations tumorales encore plus résistantes au traitement et capables de survivre dans un environnement hypoxique.

2.1.4 Nature infiltrante des GBM

La nature infiltrante des GBM explique en partie leur récidive. Lors de l'exérèse d'un GBM, l'objectif est d'assurer une exérèse la plus large possible. En effet, nous savons dès le début que l'exérèse sera incomplète en raison de sa nature infiltrante (Figure 4). Ces cellules, en périphérie d'exérèse infiltrées dans le parenchyme sain, développent très vite un très haut niveau de résistance à la chimiothérapie grâce leur plasticité et leur hétérogénéité.

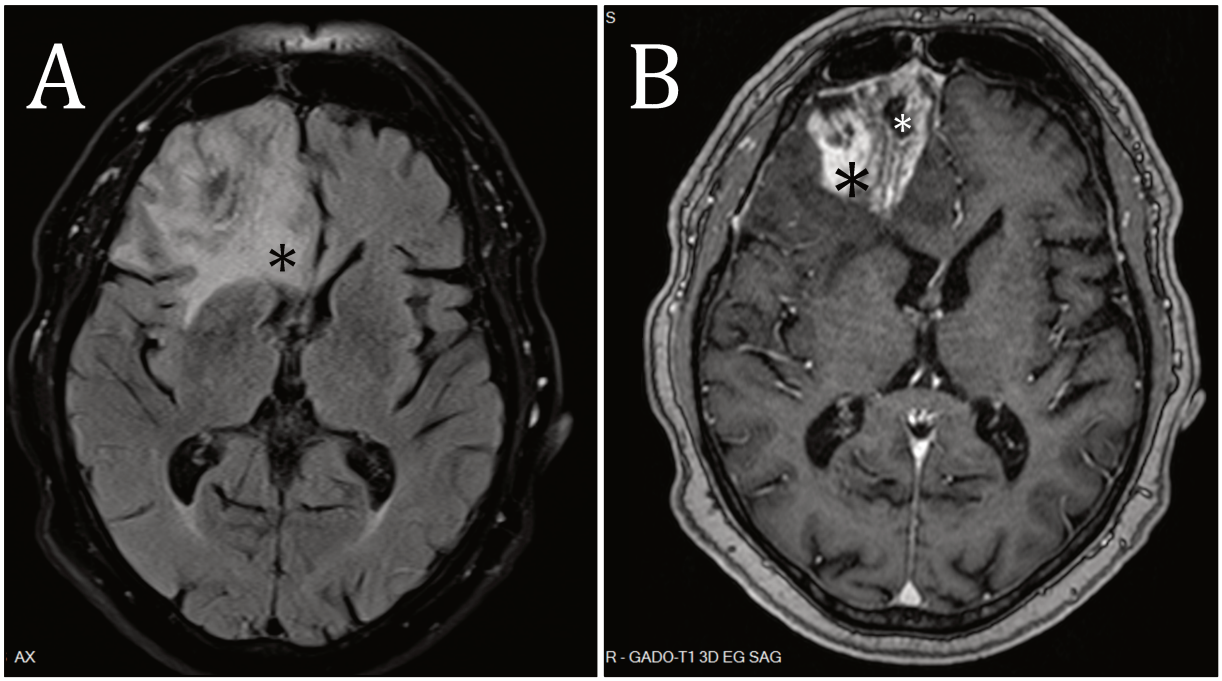

Figure 4. IRM Cérébrale en coupe axiale. Glioblastome frontal droit et infiltration péritumorale
A. Séquence Flair, hypersignal (étoile noire) témoignant de l'infiltrat tumoral au sein du parenchyme sain au-delà de la prise de contraste.
B. Séquence T1 avec injection de Gadolinium: GBM frontal droit, centre nécrotique (étoile blanche) et berges se rehaussant après injection (étoile noire) témoignant de la périphérie tumorale proliférative.

2.1.5 Expression de la MGMT

Comme nous l'avons évoqué plus haut, la MGMT est une enzyme permettant la réparation de l'ADN en cas de dommage induit par un traitement et a pour conséquence dans ce cas, l'augmentation de la résistance au TMZ. Il est démontré que pour les GBM au stade de récidive, son expression était plus importante et favorisait donc la résistance au traitement (29).

2.2 LE ROLE DU MICROENVIRONNEMENT TUMORAL DANS LA RESISTANCE

Le MET est composé de cellules cancéreuses, de cellules non cancéreuses et de sa matrice extra-cellulaire (MEC) (figure 5) (30) (31) (32). Son rôle est primordial à comprendre car il fait partie intégrante du processus d'évolution tumorale, dans sa progression locale et à distance et dans sa résistance. Il permet l'interaction intercellulaire dans les 3 plans de l'espace, l'interaction entre les cellules et la matrice. Ces interactions sont multiples et évolutives dans le temps. Le MET contient des astrocytes, des cellules de la microglie, des cellules endothéliales, des cellules souches mésenchymateuses, des fibroblastes associés au cancer, des cellules souches cancéreuses et quelques cellules immunitaires. De nombreuses cellules sont capables de modifier les fonctions des autres cellules toujours dans un seul but : promouvoir la progression et la résistance tumorale. Wang et al. ont démontré que le MET se modifie dans sa composition également entre le diagnostic initial et la récidive (14).

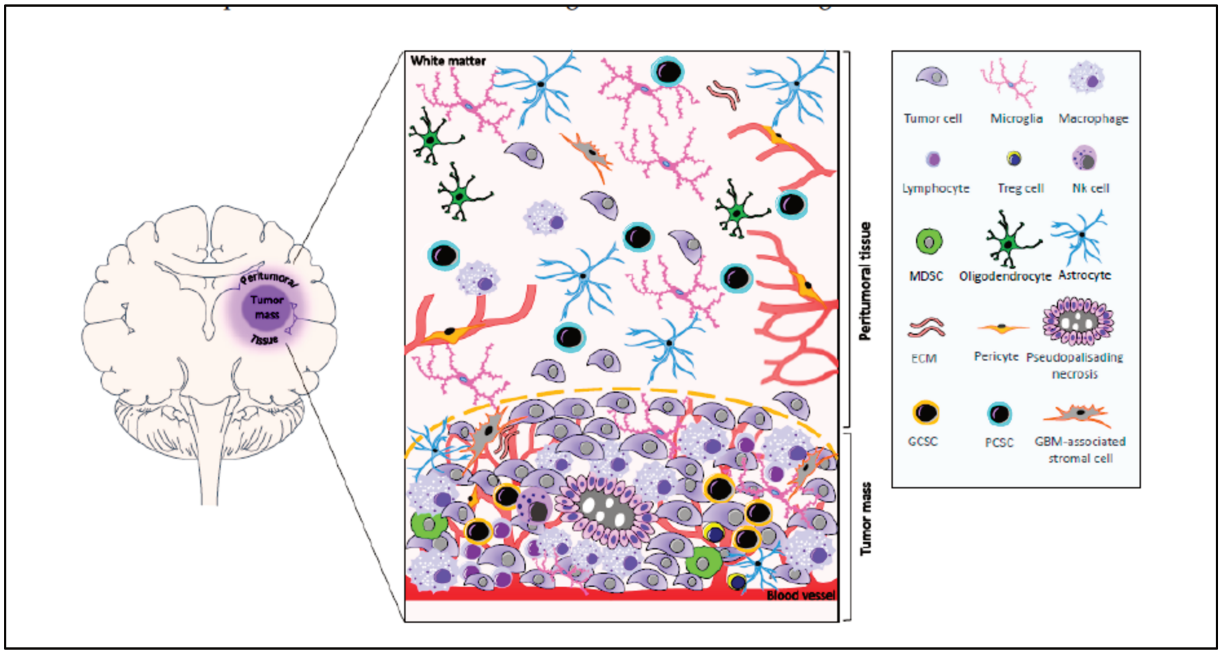

Figure 5. Représentation des principaux types cellulaires présents dans le microenvironnement tumoral (d'après D'Alessio et al.) (32). Au sein du MET, existent de larges plage de nécroses, de néoangigénèses et d'organisations prolifératives en palissade. Les cellules présentes sont les péricytes, les astrocytes, les GASCS (GBM- assiated stromal cell ou CAF), l'infiltrat immunitaire par Lymphocytes T, cellules NK, myeloide-derived suppressor cells (MDSC), macrophages des cellules souches péritumorales (PCSC) et cellules souches cancéreuses (GCSC).

2.2.1 La matrice extra-cellulaire

La MEC cérébrale est très différente des autres organes dans de nombreux aspects (33). Le composant principal de la MEC du parenchyme cérébral sain comprend des protéoglycanes, des glycoprotéines and des glycosaminoglycanes (tels que des proteoglycanes et de l'acide hyaluronique (HA)) (34). La composition de la MEC des GBM diffère du parenchyme cérébral sain, il existe beaucoup plus d'acide hyaluronique (35).

Pendant la transformation maligne des cancers dont les GBM, les cellules du MET développent la capacité d'infiltrer l'environnement de proximité ainsi que les vaisseaux sanguins. L'infiltration se déroule comme un processus complexe à plusieurs étapes dans laquelle la composition de la MEC joue un rôle majeur pour l'invasion des cellules cancéreuses (35). Les métalloprotéases, telles que les MMP2 qui sont sécrétées par les cellules cancéreuses, détruisent l'organisation de la MEC puis la réorganisent pour faciliter la propagation tumorale (36).

2.2.2 Infiltrat immunitaire

En condition physiologique, par l'intermédiaire de la BHE, le système nerveux central possède peu de cellules immunitaires (cellules présentatrices d'antigènes (CPA), moins d'expression de CMH). Cependant dans les GBM, il existe un infiltrat inflammatoire péritumoral manifeste. Différentes cellules immunitaires sont présentes comme les lymphocytes T, les cellules Natural Killer (NK) et les macrophages (15)(14).

Normalement ces cellules immunitaires permettent de lutter contre les cellules cancéreuses, mais dans le cas du GBM, il existe une immunotolérance. Les cellules immunitaires sont détournées de leur fonction protectrice et deviennent procancéreuses en sécrétant différents facteurs de prolifération, de survie et de messages anti-inflammatoires comme TGF-ß, ARG1 and IL-10 et des facteurs favorisent l'angiogenèse comme VEGF, MMP2, MMP9 (37) (38).

Le MET possédant ces cellules immunitaires protumorales permet donc la protection face à la chimiothérapie (39). Cependant dans les GBM, Wang et al. ont démontré que cette résistance est variable en fonction de leur sous-type moléculaire des GBM, l'infiltrat immunitaire est plus important pour le sous-type proneural (15).

2.2.3 Les cellules souches cancéreuses

Les cellules souches en condition physiologique permettent le développement, l'entretien et la réparation des tissus. En cas de cancer, celles-ci sont détournées, deviennent des cellules souches cancéreuses (CSC) et contribuent à sa progression et à sa résistance (40).

Dans les GBM, les CSC se situent au sein des « niches » qui ont deux sites préférentiels, en périvasculaires et au sein de l'hypoxie. Ces niches sont composées de plusieurs cellules telles que les cellules endothéliales, les péricytes, les astrocytes, les cellules immunitaires, les cellules souches cancéreuses et la MEC. Elles génèrent de nombreux signaux induisant un contrôle de l'auto-renouvellement et de la différentiation des cellules souches (Figure 6) (41) (42) (43). Bao et al ont démontré que les CSC possèdent la capacité de réparer les lésions d'ADN causées par la radiothérapie (44).

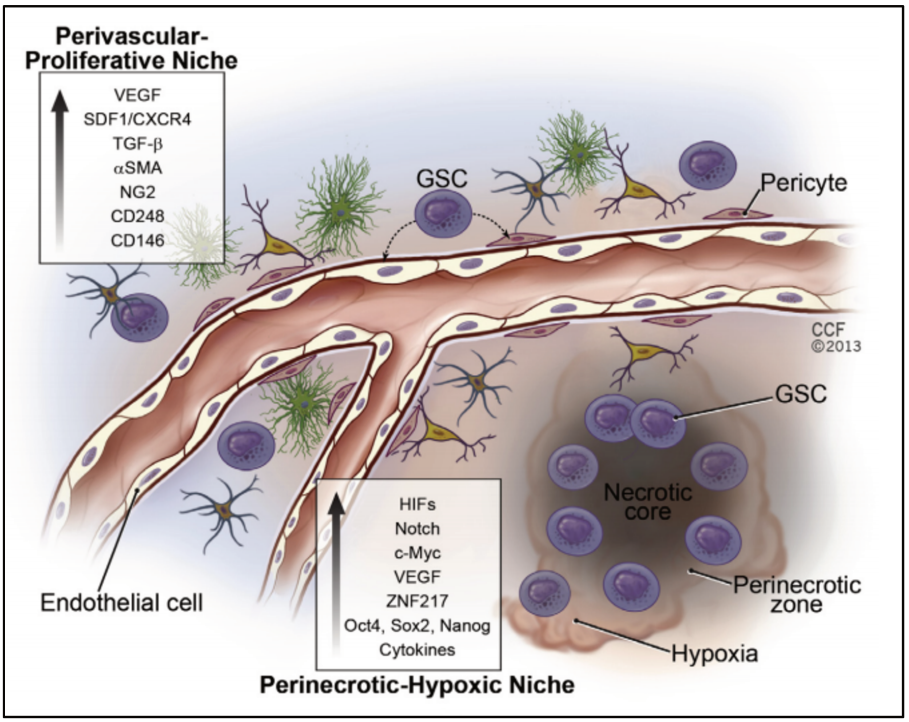

Figure 6. Localisation des cellules souches cancéreuses de GBM (d'après Schonberg et al.) (41). Les glioblastoma stem cell (GSC : cellules souches cancéreuses de GBM) se situent principalement dans des niches hypoxiques ou périvasculaires. Ces cellules interviennent dans l'augmentation de l'expression de nombreuses molécules impliquées dans la progression et la résistance tumorale et elles interagissent avec les autres cellules.

2.2.4 Cellules souches mésenchymateuses

Les cellules souches mésenchymateuses (CSM) sont présentes dans de nombreux tissus. Elles sont connues pour migrer vers les sites traumatisés en participant à leur réparation (39). Ce sont des cellules souches non hématopoïétiques caractérisées par un auto-renouvellement et des propriétés multipotentes (25).

Cependant, les CSM ne permettent pas toujours la guérison et leurs propriétés peuvent changer en fonction du statut physiopathologique du tissu dans lequel elles se trouvent. En cas de processus tumoral, ces CSM sont recrutées. Elles migrent vers le site tumoral et peuvent se différencier par exemple en CAF (39). Whiteside et al ont démontré que les cellules cancéreuses utilisent des exosomes (vésicules extra-cellulaires de petite taille) pour détourner les CSM de leurs fonctions physiologiques en fonctions pro-cancéreuses. Ces CSM une fois converties produisent elles-mêmes des exosomes (contenant mARN et miARN et des protéines protumorales) destinés aux cellules tumorales et non tumorales du MET et permettent ainsi une communication intercellulaire pro-tumorale (45). Les CSM permettent

l'auto-renouvellement et la différenciation (15). Elles activent les mécanismes d'angiogenèse et influencent les cellules du système immunitaire. Les CSM peuvent ainsi conditionner le microenvironnement pour faciliter la croissance, la progression tumorale et la récidive des cancers (39) (46).

Dans le GBM, les propriétés protumorales des CSM sont confirmées. Appaix et al. ont démontré que les CSM ont pour origine les péricytes (47). Hossain et al. ont démontré que les CSM augmentent la prolifération et l'autorenouvellement des cellules souches gliales (48). Shahar et al. ont démontré que le pourcentage de CSM était inversement proportionnel à la survie des patients, le sous-type mésenchymateux des GBM est donc plus agressif (49).

2.2.5 Importance Cancer Associated Fibroblasts (CAF)

- Fonctions des CAF dans la tumorigenèse et la résistance

Dans une très large proportion de cancers solides, les CAF sont retrouvés et connus pour intervenir dans la progression et la résistance de nombreuses tumeurs (50) (51) (52). Les CAF font partie des acteurs les plus importants dans la synthèse de la MEC, dans son organisation et sa composition (53) (51). Les CAF influencent également les communications intercellulaires. Ils interagissent avec les cellules immunitaires et cancéreuses (54) (55). Ils favorisent la néoangiogenèse et l'apoptose (56).

Dans les GBM, ils réduisent l'infiltrat immunitaire au sein de la tumeur en diminuant principalement l'action des lymphocytes T CD8+ (37). Ce mécanisme explique en partie la résistance des GBM aux immunothérapies. Cependant, la proportion des CAF diffère entre les sous-types de GBM. Le sous-type mésenchymateux qui possède peu de CAF semble plus sensible aux immunothérapies que le sous-type proneural, riche en CAF (14).

Les CAF interagissent avec les cellules cancéreuses de façon directe par contact intercellulaire (contact se faisant par les complexes E-cadherine/N-cadherine, ou par des expansions de cytoplasmes vers les cellules adjacentes (TNT tunneling nanotubes)) ou de façon indirecte par communication paracrine (en sécrétant par exemple des facteurs de croissance) (53). Ils sont capables de générer, au sein d'un environnement hypoxique, des ROS qui entrainent directement des mutations au sein des cellules environnantes (Figure 7) (52) (57).

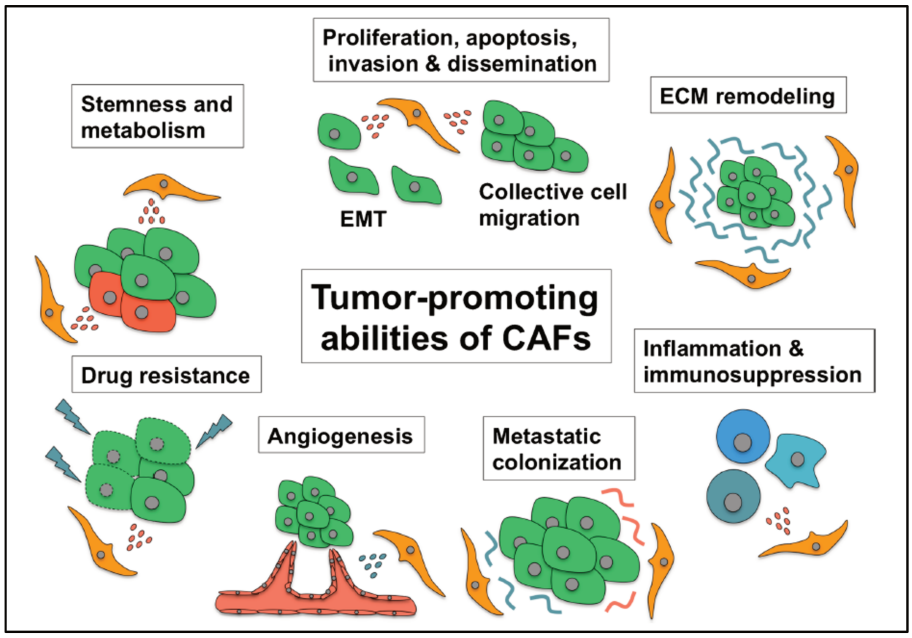

Figure 7. Les différentes actions pro-cancéreuses des CAF (d'après Mezawa et al.) (57). Les CAF favorisent l'invasion, la prolifération, le remodelage de la MEC, l'inflammation, la néoangiogenèse, la résistance au traitement. (ECM : Extracellulaire Matrix, EMT : Epithelial Mesenchymal Transition),

- Origine des CAF

Il est difficile d'affirmer l'origine des ces CAF : elle semble varier en fonction du type de cancer. Ils peuvent provenir de l'activation et du recrutement de fibroblastes présents dans le site tumoral de façon physiologique. Ils peuvent également provenir de cellules épithéliales, endothéliales, de péricytes, de macrophages voire même de CSM (47) (57). Ils sont activés en périphérie de la tumeur leur permettant d'interagir avec les cellules cancéreuses (39). Les CAF sont caractérisés par l'expression de alpha smooth muscle actin (alpha-SMA) ou par le marqueur vimentine TE-7 (58).

- CAF et glioblastomes

La fonction des CAF dans le GBM est moins bien étudiée. Il a été démontré par des biopsies cérébrales étagées au sein d'un GBM que ces CAF se situaient principalement en périphérie de la tumeur et à proximité des vaisseaux sanguins donc dans le MET. Ils se trouvent probablement dans ces niches vasculaires précédemment décrites (31).

Le rôle des CAF dans le GBM a été étudié par plusieurs équipes : Mishra et al. ont démontré en 2008 que les CSM cultivées pendant une longue période dans le milieu de culture tumoral sont capables d'acquérir le phénotype des CAF (56). Clavreul et al. ont

identifié dans le MET des cellules intervenant dans les processus du GBM. Ils ont nommé ces cellules les Glioblastoma-associated stroma cells (GASCs) ; les cellules stromales associées au GBM. Ces GASCs ont les mêmes caractéristiques que les CAF décrits dans les autres types de cancers. Ils ont démontré que ces CAF intervenaient dans la promotion des cellules cancéreuses gliales (50) (59). Trylcova et al. ont démontré in vitro en 2D que les CAF augmentaient la migration des cellules cancéreuses de GBM (58). Notre équipe a également étudié le rôle des CAF dans le GBM. Nous exposerons les techniques de culture des CAF ainsi que leur rôle dans le chapitre résultat.

3 NECESSITE D'UN MODELE PRECLINIQUE « AU PLUS PRES DE LA REALITE »

Il est primordial et indispensable de développer de nouvelles stratégies thérapeutiques. Pour cela il faut travailler sur des modèles précliniques se rapprochant le plus des conditions réelles et donc comme nous l'avons vu, ces modèles doivent en plus des cellules cancéreuses de GBM inclurent le MET (MEC, CSM, CAF, vaisseaux) et tout cela en interaction dans les 3 plans de l'espace. Depuis les années 60, différents modèles précliniques ont été créés (Figure 8) (60).

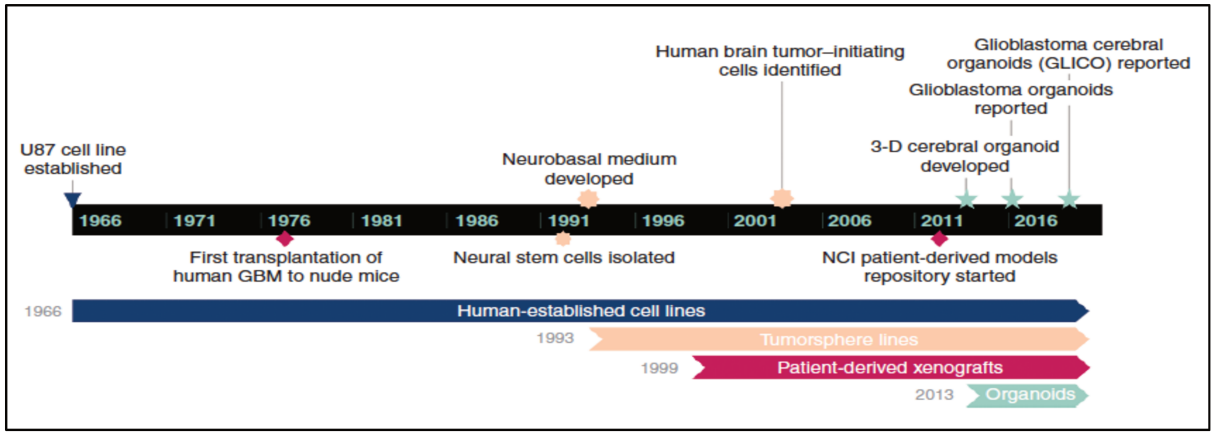

Figure 8. Évolution et amélioration des modèles précliniques de glioblastomes (d'après Luo et al.) (60)

3.1 SUPERIORITE DES CULTURES PRIMAIRES

Pendant de nombreuses années, et même encore aujourd'hui, sont utilisées des lignées cellulaires de cellules cancéreuses de GBM. Cependant, ces lignées avec le temps peuvent « s'éloigner » de la cellule cancéreuse initiale. Parmi ces cellules, une partie d'elles seulement survivent aux conditions de culture prolongée et peuvent présenter des modifications génétiques. Elles sont, de ce fait, moins pertinentes que les primo-cultures (61).

C'est pourquoi, il est beaucoup plus intéressant d'étudier les cellules cancéreuses de GBM à partir de primo-cultures prélevées lors des chirurgies des patients. Les cultures primaires permettent de meilleures conditions pour étudier les propriétés morphologiques et génétiques des cellules cancéreuses.

3.2 LIMITES DES MODELES IN VITRO 2D

Les cultures en 2 dimensions sont souvent critiquées en raison de leurs limites techniques les rendant moins proches de la réalité (30). Ces modèles représentent encore aujourd'hui le type de modèle de culture cellulaire le plus souvent utilisé, entre autres, pour tester la réponse cellulaire à de nouveaux traitements. Cependant, ils sont le plus souvent mis en défaut car ils ne permettent pas de recréer le MET indispensable pour évaluer la réponse au traitement (62).

3.3 LIMITES DES MODELES IN VIVO

De nombreuses études ont été faites à partir de modèles murins en oncologie. Les modèles murins tentent par injections orthotopiques (dans le site correspondant à la tumeur) de lignées cellulaires ou de primocultures (xenogreffes), de se rapprocher des conditions humaines, de tester de nouvelles thérapeutiques et de comprendre les mécanismes de la tumorigenèse. Les avantages de ces modèles sont leur capacité à recréer les interactions cellulaires dans les 3 plans de l'espace ainsi que la possibilité de recréer une microangioarchitecture.

Il est rapporté dans la littérature des avancées intéressantes dans la compréhension du GBM à partie de modèles murins. Certains modèles murins de GBM permettent de voir l'évolution de la tumeur par un système permettant de regarder au microscope à fluorescence la tumeur in situ après avoir rendu transparent le cerveau (intravital confocal microscopy CLARITY). Ce mécanisme est intéressant mais invasif pour la souris car il nécessite

d'implanter à la place d'une partie du crâne de la souris une « fenêtre » (17) (63). Clavreul et al. en 2014, ont réalisé l'étude chez la souris du rôle des GASC (CAF dans le GBM) associés à des cellules cancéreuses dérivées de lignées de GBM en les injectant en intracérébral. Ils ont démontré que les GASC augmentaient la néoangiogénèse tumorale (31).

Cependant ce modèle possède par définition des biais intrinsèques non modifiables. Certaines molécules anticancéreuses ayant une bonne action dans ces modèles murins sont mis en défaut chez l'Homme lors des essais cliniques (64). Les différences intrinsèques entre l'Homme et la souris font de ce modèle un modèle imparfait. Le MET péri-tumoral est différent de celui de l'Homme, or nous avons démontré son importance dans les mécanismes de prolifération et de résistance des tumeurs. De plus, les injections orthotopiques de cellules tumorales se font sur des modèles immunodéficients afin d'éviter les phénomènes de rejet. Or, il est connu que le système immunitaire interagit avec la tumeur de nombreuses façons (64). Pour finir, les règles de bioéthiques vont dans le sens du bien-être animal et de leur protection. Il paraît important de rechercher d'autres modèles précliniques d'autant plus s'ils sont plus pertinents.

3.4 IMPORTANCE D'UN MODELE 3D IN VITRO

La technique de culture en 3D a été initiée dès les années 80. Le principe des cultures 3D est donc de cultiver un ou plusieurs types cellulaires choisis dans une matrice prédéterminée afin de reproduire le MET en 3D. Ce modèle permet aux cellules de proliférer, d'interagir entre elles et avec la MEC dans les 3 plans de l'espace (Figure 9) (30) (65) (66).

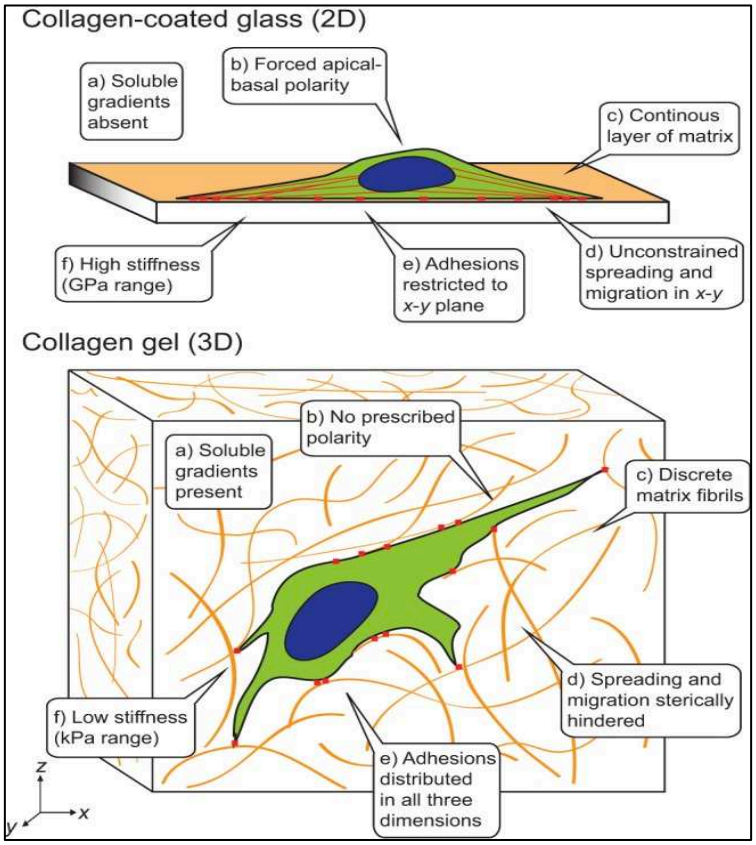

Figure 9. Avantages de la culture cellulaire en 3D versus 2D. (d'après Baker et al) (65)**.** La culture en 3D permet à la cellule d'interagir dans les 3 plans de l'espace. Par cette technique la cellule a un comportement proche de la réalité contrairement à la culture en 2D. En 3D la cellule n'a pas de polarité contrainte, pas de contrainte mécanique, elle n'est pas restreinte dans ses déplacements. Elle est exposée dans les 3 plans aux gradients solubles et peut adhérer et communiquer dans les 3 plans de l'espace.

Cette technique de culture 3D in vitro a fait émerger de nouveaux termes : organoculture, organoïdes, tumoroïdes et bioprinting, qu'il nous paraît important de préciser.

L'organoculture est la mise en culture d'un segment d'organe prélevé mis dans son intégralité en culture. Ce modèle est très limité dans son exploitation car la durée de survie n'est que de quelques jours.

La culture d'organoïdes est la mise en culture en 3D de cellules souches pluripotentes au sein d'un support qu'est la MEC spécifiquement créée et d'un milieu de culture prédéterminé contenant les facteurs stimulant la formation de l'organe (30) (67) (68). Les organoïdes s'auto-régulent et s'auto-répartissent en types cellulaires plus ou moins différentiés (69). Ils forment un « organ-like », capable de reproduire les propriétés de l'organe d'origine (66). Cet outil permet d'utiliser et de conserver un exemplaire de la tumeur du patient, d'analyser les différents biomarqueurs tumoraux spécifiques à la pathologie

étudiée et de rechercher un traitement personnalisé en sélectionnant les thérapeutiques les plus adaptées à la tumeur du patient (70).

Le Bioprinting est défini comme l'utilisation d'une technique d'impression 3D (manuelle ou automatisée) au sein d'un matériel comportant des cellules vivantes (71). Il permet la reconstruction en 3D de cellules dérivées d'un organe ou d'une tumeur (donc d'un organoïde ou d'un tumoroïde) en déposant par superposition des couches de biomatériel apparenté à la matrice extra-cellulaire (autrement appelé Bioink) (30). Il permet très facilement de recréer des tissus avec les caractéristiques volumétriques et structurelles pertinentes. Cela permet la maitrise de la composition, de la distribution spatiale et de l'architecture se rapprochant de l'organisation de l'organe ou du tissu étudié (71).

Le bioink (appelé avant « biopaper ») représente la colonne vertébrale de la construction. Le bioink doit être biocompatible non-cytotoxique. ». Il doit maintenir la structure bioimprimée en 3D et permettre la croissance, la migration et les interactions cellulaires en son sein. L'alginate est probablement le bioink le plus utilisé en technique de bioprinting appliquée à la recherche médicale. Ses propriétés mécaniques (viscosité, rhéologie), sa facilité de dissociation fait de lui un hydrogel très maniable (71). En fonction du tissu désiré, les cellules doivent être en concordance avec le microenvironnement afin de proliférer, de se différentier et de migrer si nécessaire (Figure 11).

Les tumoroïdes sont obtenus par technique de bioprinting. Ils sont composés de cellules provenant de la tumeur d'origine dans lesquels un seul ou plusieurs types cellulaires sont cultivés et s'organisent spontanément dans le temps et l'espace comme la tumeur d'origine. Ces tumoroïdes sont cultivés dans des biosphères créées manuellement ou dans des scaffolds créés par technique de bioimpression automatisée Ces deux techniques possèdent des avantages et inconvénients différents. Les biosphères se cultivent pendant environ un mois, sont peu consommatrices de cellules et utilisables dès la deuxième semaine en raison de leur petite taille. Les scaffolds peuvent se cultiver pendant plusieurs mois, utilisent un nombre important de cellules, permettent donc la création d'un réseau cellulaire important, mais ne permettent pas d'analyse en cours de culture contrairement aux biosphères. Ces deux techniques sont donc complémentaires (Figure 10).

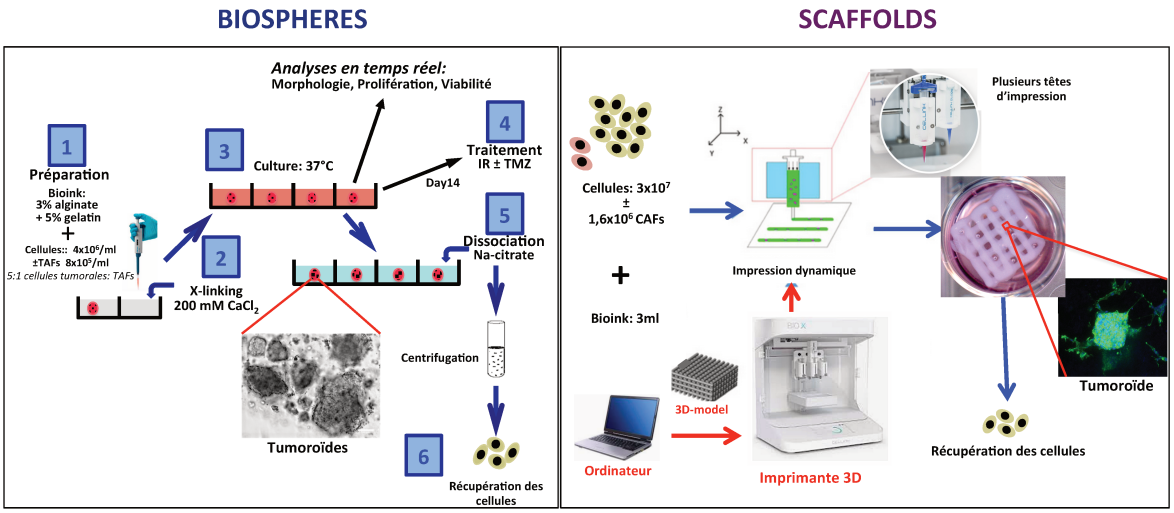

Figure 10. Techniques de création des tumoroïdes (d'après L. Oliver). Deux techniques de bioprinting permettent de créer des tumoroïdes : une technique manuelle par BIOSPHÈRES et une technique automatisée par SCAFFOLDS.

L'intérêt des tumoroïdes est qu'ils permettent de créer pour la tumeur de chaque patient, un modèle personnalisé rendant possible l'étude des caractéristiques intrinsèques de la tumeur. Ils permettent également de tester de nouvelles thérapeutiques in vitro et in vivo en fonction des besoins. Ils peuvent en théorie permettre de créer un modèle tumoral pour chaque patient afin de tester en amont le meilleur traitement pour le patient étudié. C'est le principe d'un traitement personnalisé (Figure 11).

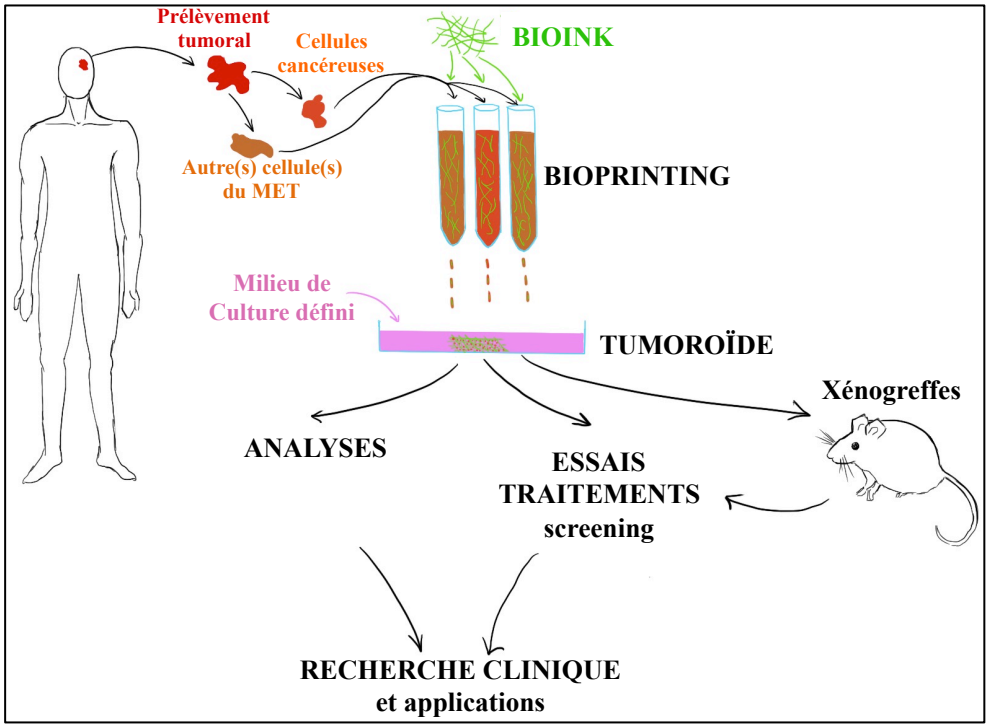

Figure 11. Principes de création et d'utilisation d'un tumoroïde par bioprinting (d'après C. Salaud). Les cellules cancéreuses et éventuellement d'autres cellules du microenvironnement tumoral sont récupérées. Elles sont ensuite mélangées avec le Bionink qui permet de recréer la MEC. Le tumoroïde est créé par la technique de bioprinting puis cultivé en milieu de culture conditionné. Ce tumoroïde permet d'analyser les caractéristiques de la tumeur, de tester des nouveaux traitements et de réaliser au besoin de xénogreffes.

4 LES MODELES 3D IN VITRO DE GLIOBLASTOMES

Pour certains cancers, il existe de nombreux modèles 3D in vitro très élaborés permettant des essais précliniques. Cependant, peu d'articles dans la littérature rapportent la création d'un modèle de culture 3D de GBM (72) (73).

4.1 CULTURES SIMPLES DE CELLULES DE GBM

Lee et al. ont développé un modèle 3D fibrin-based 3D printed (via RX1 bioprinter) en utilisant une lignée cellulaire de cellules de GBM (U87MG). Ils ont étudié la caractérisation cellulaire et la résistance au traitement (62). Ils ont testé différentes chimiothérapies et ont démontré qu'il existait plus de résistance dans les modèles 3D que 2D, laissant penser que les modèles 3D se rapprochaient plus de la réalité.

Gomez-Roman et al. ont développé un modèle de monoculture de cellules de GBM en 3D à partir d'un scaffold de polystyrene (Alvatex) qu'ils ont comparé à leur modèle 2D. Ils

n'ont pas démontré de différence pour la radiorésistance des cellules cancéreuses entre leur modèle 2D et 3D mais une résistance plus grande à la chimiothérapie (TMZ) (74).

Dai et al. ont mis ont point une culture 3D de lignées de cellules cancéreuses gliales dans des scaffolds (Tissform III) contenant de l'alginate, de la gélatine et du fibrinogène. Ils ont démontré que la résistance au TMZ était plus importante dans les cultures 3D que 2D (75).

Hubert et al. ont utilisé des cultures primaires de cellules de GBM cultivées dans Matrigel (SD San Jose). Ils nomment cette culture 3D « organoïde » mais en réalité ne correspond pas à la définition précédemment expliquée (76).

4.2 CO-CULTURES CAF/GBM

Hermida et al. ont été capables de reproduire une partie du MET en co-cultivant en 3D des fibroblastes et macrophages-like (dérivés de lignées cellulaires) et des cellules de GBM. Ils ont présenté une méthode de bioprinting utilisant un bioink à partir d'alginate modifié et de cellules tumorales et stromales dérivant de GBM. Ils ont démontré que leur modèle de co-culture était plus chimioresistant que leur modèle de culture en 2D (30).

Heinrich et al ont étudié l'interaction entre des macrophages et des cellules cancéreuses de GBM dérivés de souris dans un modèle 3D de matrice à base de gélatine qu'ils ont nommé « mini-brain ».Ils ont mis en évidence l'interaction cellulaire et le rôle dans la progression et l'invasion des cellules cancéreuses grâce aux macrophages (77).

4.3 CO-CULTURES CAF/GBM ET MEC CEREBRALE

Hee-Gyeong Yi et al. rapportent avoir recréer une fragment de GBM par technique de bioprinting à partir des cellules cancéreuses dérivées du patient associées à des cellules endothéliales, et de MEC issue de tissu cérébral. Ils ont reproduit la résistance au traitement par radiochimiothérapie (78).

4.4 LES MODELES D'ORGANOÏDES

Lancaster et al. ont développé un organoïde à partir de cellules souches pluripotentes humaines dans lequel se sont développées des régions cérébrales interdépendantes (79).

Linkous et al. ont mis au point leur modèle « GLICO » (GBM cerebral organoid).Ils ont créé un organoïde cérébral à partir de cellules souches pluripotentes puis y cultivent des

cellules souches gliales. Ils ont mis en évidence les propriétés infiltrantes et prolifératives des cellules souches gliales et ont démontré une sensibilité différente de leur modèle GLICO en comparaison aux cultures 2D à la chimiothérapie (TMZ et bis-chloroethylnitrosourea (BCNU)) (80).

Il reste des éléments encore non représentés dans ces modèles 3D de GBM. La BHE, la présence de l'ensemble des cellules du MET comme l'infiltrat immunitaire, la vascularisation.

Nous pensons que les modèles précliniques 3D in vitro de primocultures de GBM réunissent le plus de critères et le moins de biais. Ils permettent de recréer les interactions cellulaires dans les 3 plans de l'espace, ils recréent les contraintes mécaniques proches de la MEC et ils permettent de co-cultiver plusieurs types cellulaires afin de se rapprocher le plus de la tumeur initiale.

OBJECTIFS

II. OBJECTIFS

Les glioblastomes sont les tumeurs cérébrales pouvant toucher tous les âges, ils représentent les tumeurs cérébrales les plus agressives, leur médiane de survie est très faible.
Aucun progrès significatif dans la prise en charge thérapeutique depuis presque 20 ans n'a été fait. Une des caractéristiques du GBM est son hétérogénéité intratumorale dans l'espace et dans le temps et son hétérogénéité interindividuelle rendant encore plus difficile sa prise en charge à l'échelle individuelle.

Afin d'améliorer le pronostic des patients atteints de GBM et d'avoir un traitement plus efficace, dans l'idéal personnalisé, il est nécessaire de mieux comprendre les mécanismes de la tumorigenèse des GBM et leur résistance au traitement.

Il est connu et décrit depuis plusieurs années dans de nombreux cancers, les modèles in vitro en 3D (tumoroïdes et organoïdes) qui permettent de recréer le MET composé des cellules et de la MEC. Le MET est connu pour jouer un rôle important dans les mécanismes tumorigenèse et de résistance. Cependant, assez peu de modèles existent pour le GBM.

Notre objectif à moyen terme est de créer une **plateforme de criblage par tumoroïdes de chaque GBM des patients opérés**. Cette plateforme permettra de créer des tumoroïdes pour chaque patient dans le but d'analyser au mieux chaque tumeur et de proposer un traitement le plus « personnalisé » possible.
Cette approche et ce projet nécessitent de nombreuses étapes en amont mais permettent d'espérer une meilleure survie des patients atteints de GBM.

C'est pourquoi, nous nous sommes tournés vers les modèles 3D de GBM. Cette thèse s'est organisée en quatre étapes que nous allons exposer dans les résultats. Il est évidemment nécessaire de poursuivre ces recherches pour arriver à la création de cette plateforme de criblage de chaque GBM par tumoroïdes.

Première étape :

Faire un état des lieux des mécanismes de résistance des cancers et plus particulièrement des GBM afin d'identifier de nouvelles pistes de recherche et des nouvelles cibles thérapeutiques (Article 1 publié).

Deuxième étape :

Créer un modèle en 3D in vitro de GBM à partir de primocultures, modèle ayant pour objectif d'être reproductible, maniable et de recréer le MET (matrice et environnement cellulaire) (Article 2 soumis).

Troisième étape :

A partir des modèles de co-cultures de tumoroïdes validés, étudier le rôle des CAF dans les mécanismes de résistance au traitement par radiothérapie et chimiothérapie (Article 3 en cours d'écriture).

Quatrième étape :

Étudier les mécanismes par lesquels interviennent les CAF dans la résistance et la prolifération des GBM. En identifiant un ou plusieurs de ces mécanismes, cela permettrait d'envisager des nouvelles cibles thérapeutiques (Article 4 publié).

RÉSULTATS

III. RÉSULTATS

1. DRUG RESISTANCE IN GLIOBLASTOMA : ARE PERSISTERS THE KEY TO THERAPY?

Les GBM sont des tumeurs très agressives. Quelle que soit la prise en charge thérapeutique, l'évolution se fera inéluctablement vers la récidive avec une survie à 5 ans entre 3 et 5%.

Il nous paraissait important de réétudier et de rassembler les données de la littérature sur les mécanismes de résistance des cancers et en particulier des GBM. Existe-t-il des pistes de recherche innovantes dans les mécanismes de tumorigenèse et de résistance au traitement ? Peuvent-elles s'appliquer au GBM ? Sont-elles des potentielles cibles thérapeutiques ?
Cette revue de la littérature a tenté de répondre à ces questions en ciblant la discussion sur les problématiques de résistance des GBM.

1.1 PRINCIPAUX RESULTATS :

Il est décrit dans de nombreux cancers et dans le GBM la présence dans le MET de cellules peu actives (cellules souches cancéreuses quiescentes). Ces cellules, par leur activité réduite, ne sont pas altérées par les traitements anti-cancéreux. Ces cellules quiescentes peuvent de ce fait acquérir une résistance au traitement et participer à la récidive du cancer.

ARTICLE 1

Oliver *et al. Cancer Drug Resist* 2020;3:[Online First]
DOI: 10.20517/cdr.2020.29

Cancer Drug Resistance

Review

Open Access

Drug resistance in glioblastoma: are persisters the key to therapy?

Lisa Oliver[1,2], Lisenn Lalier[1,3], Céline Salaud[1,2], Dominique Heymann[1,3], Pierre François Cartron[1,3], François M. Vallette[1,3]

[1]Université de Nantes, INSERM, CRCINA, Nantes 44007, France.
[2]CHU de Nantes, Nantes 44093, France.
[3]LaBCT, ICO, Saint Herblain 44805, France.

Correspondence to: Dr. Lisa Oliver and Dr. François M. Vallette, Université de Nantes, INSERM, CRCINA, CHU de Nantes, Nantes 44007, France. E-mails: lisa.oliver@univ-nantes.fr; francois.vallette@inserm.fr

How to cite this article: Oliver L, Lalier L, Salaud C, Heymann D, Carton PF, Vallette FM. Drug resistance in glioblastoma: are persisters the key to therapy? *Cancer Drug Resist* 2020;3:[Online First]. http://dx.doi.org/10.20517/cdr.2020.29

Received: 28 Apr 2020 **First Decision**: 29 May 2020 **Revised**: 1 Jul 2020 **Accepted**: 13 Jul 2020 **Available online**: 7 Aug 2020

Academic Editor: Chiara Riganti, Joanna Kopecka **Copy Editor**: Cai-Hong Wang **Production Editor**: Jing Yu

Abstract

Glioblastoma (GBM) represents the main form of brain tumors in adults, and one of the most aggressive cancers overall. The treatment of GBM is a combination of surgery (when possible), chemotherapy (usually Temozolomide, TMZ) and radiotherapy (RT). However, despite this heavy treatment, GBM invariably recur and the median length of survival following diagnosis is 12 to 15 months, with less than 10% of people surviving longer than five years. GBM is extremely resistant to most treatments because of its heterogeneous nature, which is associated with extreme clonal plasticity and the presence of cancer stem cells, refractory to TMZ- and RT-induced cell death. In this review, we explore the mechanisms by which cancer cells, and especially GBM, can acquire resistance to treatment. We describe and discuss the concept of persister/tolerant cells that precede and/or accompany the acquisition of resistance. Persister/tolerant cells are cancer cells that are not eliminated by treatment(s) because of different mechanisms ranging from dormancy/quiescence to senescence. We discuss the possibility of targeting these mechanisms in new therapeutic regimen.

Keywords: Drug resistance, persisters, tolerance, chromatin remodeling, metabolism, tumor environment

INTRODUCTION

Cancer happens unexpectedly for the most part and by the time it is detected it has already gone through numerous "stop or go" cycles. Although not very well documented, it is assumed that most precancerous

cells are eliminated from the body through processes implicating cellular mechanisms (e.g., activation of cell death programs) or global reaction (e.g., immune system control). Hence, at diagnosis, cancer cells are likely to have acquired several mechanisms reinforcing cell survival and/or escaping from immune surveillance. Cellular heterogeneity, a common landmark in many cancers, could be the direct consequence of a pre-diagnosis selection/adaptation process. Most current treatments target proliferation and/or survival pathways in cancer cells and as such could trigger another level of selection and/or adaptation. Therefore, in some cancers, after an initial reduction in tumor mass, surviving resistant cells are detected. Understanding the mechanisms, which lead to the acquisition of resistance by tumor cells is one of the major challenges that the medical and scientific research community need to address to eradicate cancers.

Glioblastoma (GBM) represent the most frequent primitive brain tumors in adults. Their current treatment - generally described as the protocol "Stupp" - is a combination of complete surgical resection, followed by radiotherapy and concomitant chemotherapy with the methylating agent Temozolomide (TMZ)[1]. Since its introduction, this regimen has had a deep impact both on overall survival and on progression-free survival[1]. However, since then, no new treatment has been discovered and the median survival time (circa 15 month) has not been increased over past 20 years. The quest for a more effective therapy remains a primary aim in the GBM community. The reason of this lack of progress is linked to the complexity of GBM, which is extremely heterogeneous by nature (the original name of GBM was Glioblastoma Multiforme, a name that speaks for itself) and/or with an extraordinary plasticity. In addition, evidence suggests that GBM contains a population of cancer stem cells that are highly resistant to current therapies.

GENERALCONSIDERATIONONCANCERRESISTANCETOTREATMENT

Most common cellular mechanisms

Several excellent reviews have recently described the current mechanisms of resistance in cancers[2-8]. Figure 1 provides an overview of the main mechanisms responsible for the acquisition of resistance to drugs by tumors.

Cell death in drug resistance

Regulated cell death programs play a central role in the elimination of tumor cells. Figure 2 illustrates the importance of cell death in treatment resistance: the first response of cancer cells to most treatments is usually cell cycle arrest followed by cell death[9]. Failure to induce apoptosis, the most common form of the cell death programs, has been observed in many cancers and seems to be co-substantial to this disease[10]. Several drugs designed to re-activate cell death are now increasingly used in new regimens in combination with conventional treatments[9]. However, due to the complexity of drug resistance and possible side effects, the effectiveness of these treatments is still restricted to only few, mostly hematologic, malignancies. In addition, several forms of cell death can be engaged by tumors and other programs such as autophagy and senescence have also been reported to stop or slow down cancer progression. However, there is a major caveat in the induction of massive cell death as dead cells can produce signals that either protect other cancer cells or trigger the activation of cancer stem cells. Factors implicated in these processes are numerous and not well defined. However, several studies have pointed out that prostaglandin E2 could be an important survival signal for neighboring cancer cells[11]. Again, the implication of TME in this process is not well known but it could be decisive for the survival of cancer cells[12]. As illustrated in Figure 2, the balance between death and growth in untreated cancer (at diagnosis) is in favor of growth. Treatment is usually designed to kill cancer cells and often, massive cell death occurs shortly after the treatment. A lag period during which it is likely that cells are neither dying nor proliferating follows and precedes the reappearance of fast-growing tumors resistant to the treatment.

A new population implicated in resistance, the drug-tolerant persister cells

Recently, many groups have identified a subpopulation of cancer cells called "persisters", which share common properties of drug tolerance with persisters observed in bacteria population that are produced

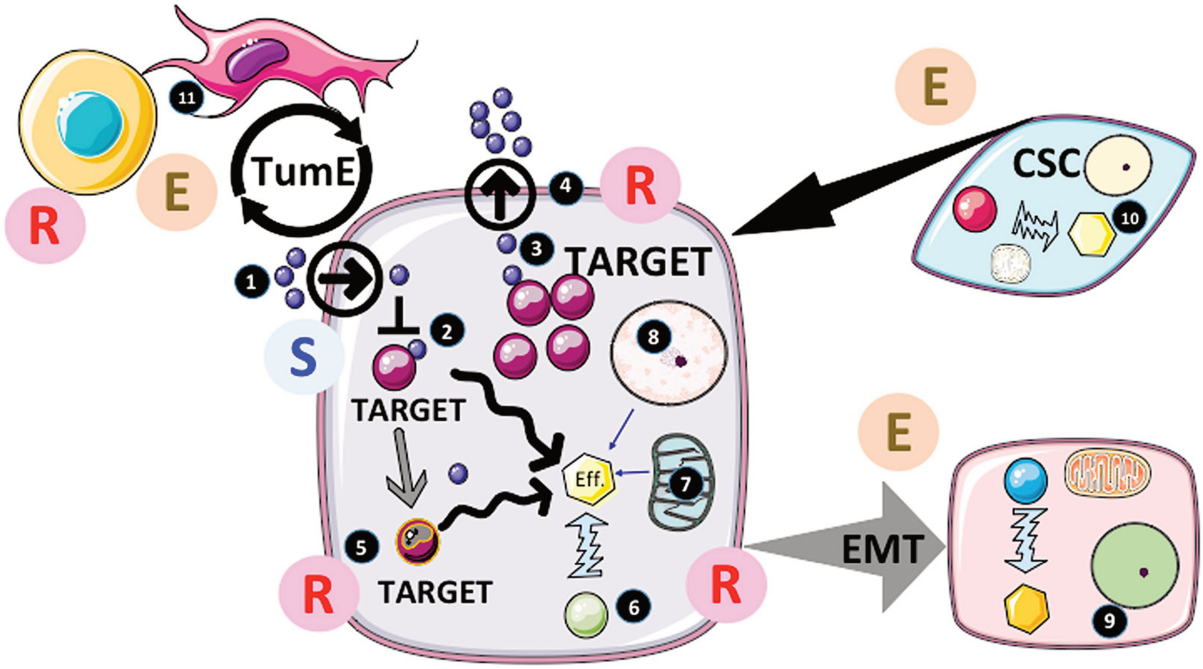

Figure 1. Actors and factors implicated in cancer resistance to treatments. 1. The accessibility of the drug to cancer cells is usually determined during clinical assays (pharmacokinetics, pharmacodynamics...). In the case of intracellular targeting, the transit of the drug across the plasma membrane can also be critical and is usually tested during pre-clinical studies. However, the drug distribution can be affected by both elements in the tumor microenvironment (TME) as well as by changes in the body response, which will result in resistance by forfeit; 2. If the drug is delivered and affects the activity of the target, several factors could intervene modifying the structure of the drug and/or its delivery to another compartment (e.g., endosomes) thereby decreasing its efficiency. If the target is upstream of a major cellular effector (Eff.) responsible for cancer progression, other pathways can be activated to sustain this activity. This would result in circumventing the treatment efficacy and induce escape; 3. Overexpression of the target would also limit the efficiency of the inhibitor and trigger resistance if an increased dose (due to side-effects) is not possible; 4. If the drugs were substrates of the multidrug resistance (MDR) pumps, activation of MDR would limit the intracellular concentration and impede its therapeutic activity; 5. One of the most-documented resistance mechanisms is mutation of the target as often observed with tyrosine kinase inhibitors (TKI) such as EGFRi or BRAFi. *Per se*, mutated cells insensitive to treatment slowly emerge from the treated tumor mass and become predominant after an initial tumor regression. Of note, the process implicated is still not completely understood (preexisting clones, induced mutations or selected random mutations); 6. Another common process observed with TKI is the bypassing of the target for the activation of the effector. Often another tyrosine kinase pathway can be amplified to compensate for the inhibition of the target. In addition, deep modifications of the cellular phenotype/genotype induced by the treatment directly or indirectly can also contribute to resistance; 7. Mitochondria are central to resistance through two distinct processes. First by rewiring metabolism; cancer cells can adapt to the inhibitory effects on target under many circumstances (providing alternative sources of core elements for the cells to proliferate such as nucleic acids, amino acids, ATP sources...) or epigenetic modifiers (see below). Secondly, mitochondria are central to apoptosis and other cell death programs[44]. Consequently, modification of mitochondrial activity can also play an active role in cancer cell survival through the life/death response following the inhibition/modulation of target. In fact, resistance to apoptosis is one of the hallmarks of cancer and plays an important role in in the escape by cancer cell to immune-surveillance; 8. Cancer genome modifications can occur through DNA mutations as mentioned but also through changes in epigenetic regulation such as miRNA production, DNA methylation and histone modifications. In this respect the metabolic input is of major importance providing key co-factors called oncometabolites, which includes alpha keto-glutarate or succinate necessary for the function of epigenetic enzymes. These oncometabolites participate in the cellular reprogramming often observed under the selective pressure induced by treatments[93]; 9. Another phenomenon triggered by the treatment is the epithelial-mesenchymal transition (EMT). EMT is a well-known process in the context of pathophysiological conditions, such as repair of injured tissue. EMT leads to the dissolution of cell-cell contacts, morphogenetic changes, increased motility and invasiveness. In cancer, EMT is accompanied by metabolic, epigenetic, and differentiation reprograming, all of which participate in drug resistance[94]. In GBM, a transition to mesenchymal phenotype is often observed[95]. This EMT-like process provides a selective advantage to cancer cells culminating in an escape from treatment[96]; 10. In many tumors (but not all), the existence of cells with some "stem cell" properties (such as stem cells markers, self-renewal, high DNA repair capacity, resistance to cell death) has been shown. Because of the aforementioned properties, cancer stem cells (CSC) have been proposed to be the cornerstone of both cancer heterogeneity and treatment resistance and the main culprit responsible for recurrence[87]; 11. Tumor microenvironment (TME) is an essential component of cancer growth and survival. The implication of TME in cancer resistance as well as sensitivity to treatment has been proposed[96]. Non-tumor cells present in the microenvironment are multiple and thus a change in TME composition is likely to influence cancer response to therapy in both ways (i.e., escape and resistance). TME can secrete factors or directly provide elements by cell-cell interactions that could participate in tumor growth and acquisition/selection of resistant cells[96]. In addition, it should be kept in mind that immune cells are part of TME and that cancer cells usually inhibit their function. The actual importance and role of TME still needs more evaluation but it is clear that it represents a major axis of research for new therapies. E: escape; R: resistance; S: sensitivity to treatment

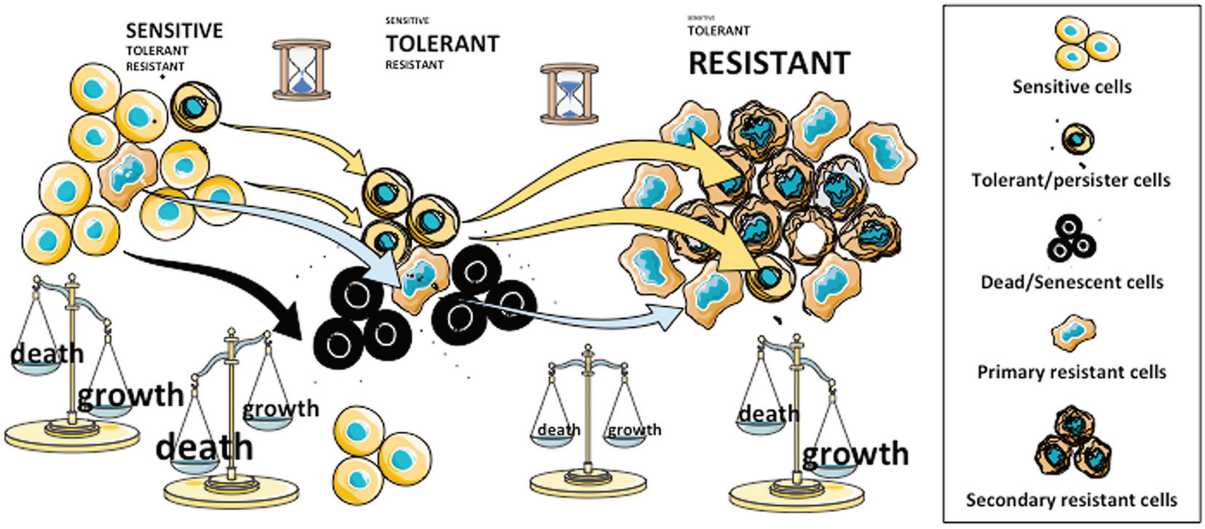

Figure 2. Cell Death and resistance to treatment in cancer. Distinct cell populations and states underline the dynamic and plasticity of emergence of resistant cancer cells. Black dots surrounding dead/senescent cells are death-inducing factors that could support the survival in surrounding cells. Treatments could trigger cell death (or senescence) in tumor cells, subsequently called "sensitive" while the same treatment could be ineffective, not only in the resistant population, be present at a low level but also in persisters (left). In the first stage of treatment when the wave of cell death is over, persisters would be predominant (middle). Resistant clones would arise from the viable pool and with time acquire high proliferation rates (right). Whether or not, some resistant cells will derive from persisters, as a secondary resistant population, is not known. At the end of this process, resistant cells might encompass multiple mechanisms of resistance, which will prevail along with persisters or persister-derived "sensitive" cells (right)

with antibiotic resistance[13]. Persisters are normal cells rendered drug-tolerant through reversible, non-mutational mechanisms such as chromatin or metabolic remodeling[13]. The putative role of these persisters in drug resistance and tumor progression is described in Figure 2. It has been shown in lung cancer that the drug-tolerant persisters exhibit a repressed chromatin state characterized by increased methylation of histone H3 lysine 9 and 27 (H3K9 and H3K27)[14]. Indeed, modifiers of chromatin such as histone lysine demethylase genes (KDM) appear to be the best persister biomarkers to date[15]. In the clinical field, however, the description of persisters is still an open question as it is also their relationship with other types of slow cycling minor cancer cell populations such as dormant, quiescent or cancer stem cells[16]. However, the distinction between persisters and resistant cells may be their capacity to proliferate under treatment. The origin of persisters is unclear and could be linked to stress, phenotypic plasticity or stochastic cell-to-cell[15,17]. Ramirez *et al.*[18] have shown that resistance can arise from gene mutations and slow-growing persisters after long-term treatment.

Persisters were found in many solid tumors originating from different organs (lung, skin, brain, colon…) and under different treatments[16]. These findings suggest that persisters with drug-tolerant phenotypes could be a common feature in cancer. Nevertheless, even if the phenotypes of these cells share common traits it is possible that distinct characteristics are conditioned by both the nature of the tumor and the treatment applied; and as such could trigger distinct types of persisters. Despite that, the reversibility of the persister phenotype has been shown in most but not all persisters.

The essential question now is to characterize persisters in cancers and to compare with persisters in bacteria, which could provide some clues. The origin of persisters in bacteria is still under discussion but could be linked to mechanisms ranging from stochastic regulation to an active induced state[13].

1. Persisters could be present in the non-treated population. It has been established that in normal growing bacterial biofilms, persisters might account for about 1% of the population[19]. The percentage of persisters is currently not known in most cancers.

2. If persisters were generated through phenotypic fluctuation, they would be generated at each generation and not necessarily immediately eliminated by selection due to their low metabolism, slow cycling, and resistance to cell death. Of note, in bacteria, persisters have been shown to evade immune surveillance, which could provide another selective advantage to them. Whether or not this process is specific to bacteria or a feature of all growing tissues (including cancer) is a pending question. Cancer persisters could be a minor subpopulation present in untreated cancers, possibly exhibiting slow cycling and death [Figure 2].

3. In bacteria, persisters can also be induced by the environment and/or specific signals[13]. Indeed, the introduction of antibiotics could be an amplifying signal for the genesis of persisters by a simple selective process (to die or not). Several mechanisms responsible for the induction of persisters have been proposed including change in specific death signals, metabolism, and stress response in bacteria[20]. Since cancer treatments trigger numerous stresses one can postulate that they could cause a significant increase in persisters.

4. The antibiotic tolerance of persisters in bacteria has been shown to depend on the amplification of certain proteins that otherwise would trigger cell death[13]. It is thus possible that conditions under which certain proteins are produced lead to an increased in persisters through reduction of cell cycling and/or induction of dormancy. Alternatively, it has been proposed that persisters do not rely on any specific mechanisms but are simply the consequences of growth reduction[20]. Studies on cancer persisters have shown that metabolic; cell survival and epigenetic changes in persisters are often accompanied by slow cell growth[16].

At this stage, one can hypothesize that persistence and resistance could be two independent responses to treatment and that the cross talk between persisters and resistant cells is necessary to produce the fast-growing resistant populations. Alternatively, it is possible that resistant cells could derive from persisters through transformation/mutation induced by the treatments. However, although a complete and thorough characterization of persisters are still underway: there is evidence of the probability of genetic heterogeneity, which would require the induction of a key number of limited mechanisms to survive. This "bottleneck" might represent a new target for the rational design of efficient lines of therapy to overcome treatment resistance.

GBM ANDRESISTANCETOTREATMENT

Mechanisms of resistance specific to TMZ

The resistance to TMZ in GBM has been reviewed in detail by Lee[21]. The DNA alkylating drug TMZ is the only drug with therapeutic activity against high-grade GBM and has become a part of the standard treatment of these tumors in combination with radiotherapy[1]. TMZ is 100% bioavailable when taken orally and, because of its small size and lipophilic properties, it can cross the blood-brain barrier[22]. In cancer cells, TMZ induces a cell cycle arrest at G2/M, which is followed by the induction of apoptosis. At the DNA level, TMZ adds methyl groups at N^7 and O^6 on guanine and O^3 sites on adenine, which trigger different DNA repair pathways. However, The extent of methylation at the O^6 position of guanine in DNA correlates well with the therapeutic activity as well as the toxicity of TMZ[23]. One of the consequences of the guanine methylation is an abnormal pairing with thymine instead of cytosine, which leads to mutations in the absence of efficient base exchange repair and DNA mismatch repair[23]. O^6-methylguanine DNA methyltransferase (MGMT) is a suicide DNA repair enzyme, which demethylates the O^6 position of guanine and thus counteracts the TMZ effect. About 50% GBM patients benefit from multiple administrations of TMZ and this efficiency correlates with the silencing of MGMT by DNA methylation on its promoter[24]. The methylation of the MGMT promoter by small methyl donors such as folate has been shown to silence its expression and consequently to enhance TMZ efficacy in MGMT-expressing GBM[25-27]. However, the expression of MGMT can be induced in MGMT negative tumors upon TMZ treatment[28,29].

As such, MGMT appears to be the main modulator of TMZ resistance in GBM as expected from its biochemical role.

Another important factor, which has been implicated in TMZ resistance, is p53 but its function has not been clearly established. Most mutations of p53 in GBM are gain of function[30]. Indeed, GBM cell lines with non-functional p53 were significantly more sensitive to TMZ[31] while small molecule activators of p53 have been shown to effectively enhanced TMZ effects in GBM xenografts *in vivo*[32]. In p53 wild-type cells, TMZ promoted the phosphorylation of p53 at Ser15 and Ser46. Since these two post-translational modifications have opposed functions in survival and death[33], however, their role in TMZ resistance is unclear. Consequently, the implication of p53 in the action of TMZ could be related to its post-translational modification ratio.

Due to its plasticity, epigenetic alterations have been described as crucial drivers in acquired chemo-resistance. The acquired resistance seen during TMZ administration in GBM patients is no exception to this rule. The study of MGMT methylation level in untreated GBM patients is considered as the most relevant epigenetic biomarker associated with the predictive response to conventional treatment[34]. Analyses of the MGMT methylation status in primary vs. recurrent GBM showed that TMZ induced modifications in the MGMT gene methylation that promoted MGMT expression in recurrent GBM[35]. In addition to methylation of its promoter region, the epigenetic regulation of a MGMT enhancer was also reported as a regulator of treatment resistance in GBM[36]. de Souza *et al*.[37] suggested that CpG Island Methylator Phenotypes (CIMP) could be used as predictive biomarkers for recurrence in GBM after TMZ treatment. Belter *et al*.[31] observed a global DNA hypomethylation in the range of therapeutically achieved TMZ concentrations over longer exposure times. Lu *et al*.[38] report that the hypomethylation of promoter region of SNHG12 occurs in TMZ-resistant cells and that this contributed to lnc-RNA-SNHG12 activation resulting in TMZ resistance. Thus, TMZ effect on DNA methylation could be responsible for the increase expression of MGMT in GBM.

Other studies have identified other epigenetic players associated with the TMZ resistance and/or GBM recurrence. For example, Briand *et al*.[39] reported that the TET2 expression increased the between primary and secondary resection in patients treated with the Stupp protocol. Banelli *et al*.[40] reported that the expression of KDM was increased in TMZ-resistant cells compared to TMZ-sensitive cells, and that TMZ-resistance was mimicked by over-expression of KDM5A while TMZ-sensitivity was mimicked by inactivation of KDM5A. These results are interesting, as KDM have been implicated in the persister state in GBM[41].

In addition to the use of tumor resection samples, the use of liquid biopsies appears as a promising alternative to perform longitudinal studies of epigenetic signatures associated with the acquisition of resistance. The MGMT methylation level in blood and cerebrospinal fluid has been shown to be promising[42]. In addition, several studies such as that published by Nadaradjane *et al*.[43] suggested that the monitoring of cell-free miRNA in blood could be a real time biomarker associated with acquired TMZ-resistance.

Death and survival mechanisms in GBM as resistance mechanisms

Apoptosis is the central cell death program regulating cellular homeostasis and much pathology in eukaryotes[44,45]. Numerous recent reviews have shown the importance of cell death in GBM and its potential use in clinic[9,46]. Apoptosis is the main cell death program and the B-cell Lymphoma-2 (BCL-2) family of proteins is instrumental in the completion of apoptosis (and probably other forms of cell death)[10]. The balance between pro- and anti-apoptotic members of the BCL-2 family is the key element in the control of apoptosis[44]. This balance between pro- and anti-apoptotic proteins is a landmark of GBM progression[47,48].

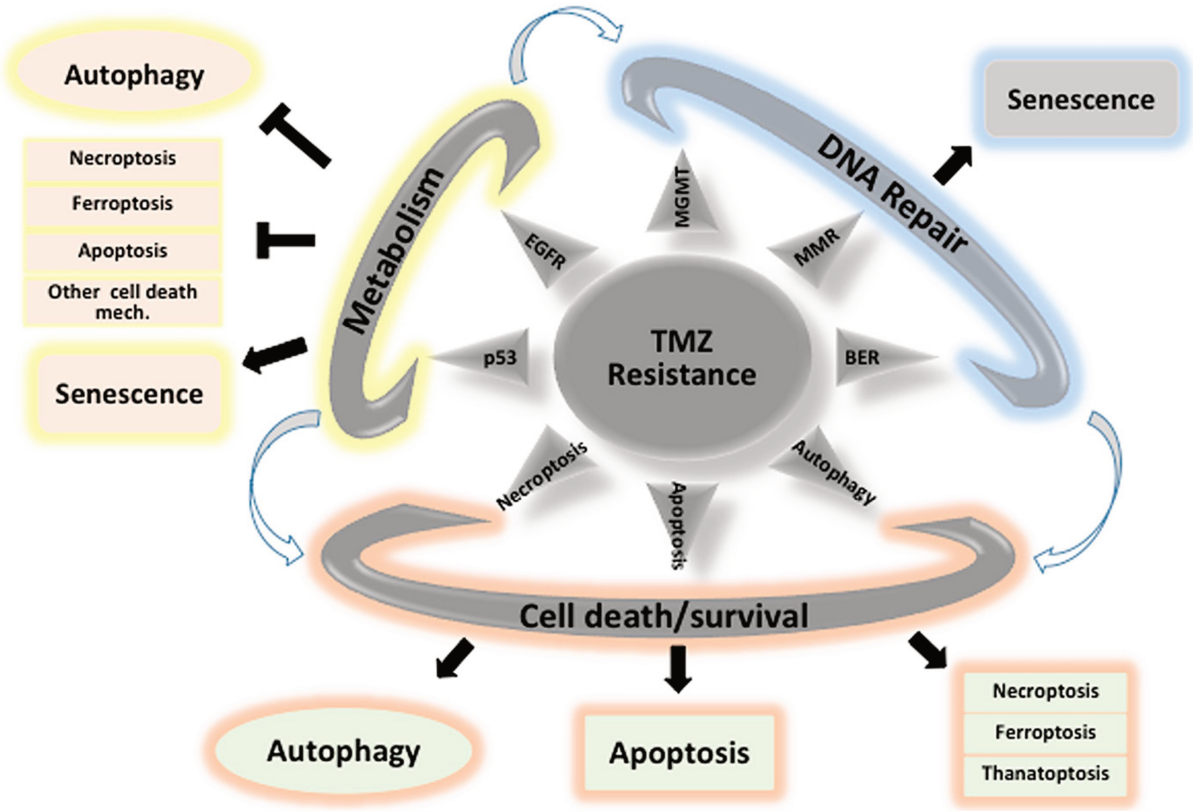

Figure 3. Major mechanisms implicated in TMZ resistance: impact of cell death/survival mechanisms. TMZ: Temozolomide

In vitro studies have shown that the inhibition of the protein Bcl-2 sensitized GBM cells to apoptotic inducers[49]. Our group has shown that TMZ induced a rapid shift in the dependency of anti-apoptotic members by promoting the degradation of Mcl-1 thereby promoting Bcl-2/Bcl-Xl-induced resistance to apoptosis in GBM cell-lines[50,51]. Subsequently, the pharmacological inhibition of anti-apoptotic members of the BCL-2 family could represent a novel strategy for in the treatment of cancer; and small-molecules targeting the BCL-2 family, including ABT-263, can augment GBM elimination when combined with other chemotherapeutic agents[49]. Of note, the use of ABT-263 should be evaluated in combination with radiotherapy as it selectively kills senescent cells[50,51]. Also, the question of the capacity of inhibitors such as ABT-263 to efficiently cross the blood brain barrier has still to be firmly established[52]. Furthermore, the side effects of these drugs on normal cells as well as the use of the proper target (Bcl-2, Bcl-Xl, Mcl-1…) at the appropriate time are also major problems that have to be solved before their therapeutic use.

The mechanisms by which TMZ eliminates GBM cells are still not universally accepted and several mechanisms including apoptosis, senescence and autophagy have been proposed to be associated with TMZ cytotoxicity[53]. Autophagy, apoptosis, and senescence could co-exist as stress-induced processes and could probably operate together in a cell autonomous or non-autonomous manner. As described in Figure 3, a failure to induce apoptosis or autophagy might unmask other cell death mechanisms such as necroptosis or ferroptosis[54,55]. The level of autophagy induced by TMZ could also depend upon different factors such as the concentration of TMZ, the degree of DNA damage, hypoxic or metabolic conditions or clonal variations[56]. The degree of autophagy could lead to adverse situations: too much or too little autophagy leading to death or an intermediate "goldilocks zone" that could promote survival. The complexity of autophagy induction and the role(s) in the GBM could be the reason of this controversial role in GBM and as such hamper therapeutic intervention[56].

Senescence, which can be induced by TMZ[57] and irradiation[58], has become an attractive feature in GBM therapy. Of note, TMZ-induced senescence depends on p21 activation and thus on the presence of wild type p53. In p53-deficient cells, which cannot activate p21, TMZ would not induce senescence[59], which nonetheless can be revealed in case of autophagy deficiency[60].

TMZ-induced senescence was accompanied by an abrogated (suppressed) DNA repair, which included mismatch repair and homologous recombination. Pro-senescence drugs such as inhibitors of CDK4/CDK6, alone or in combination with other treatments are currently under evaluation in clinical trials but the results have not been conclusive so far[61]. On the other hand, the impact of senolytic drugs on GBM has not yet been published. TMZ could under certain circumstances activate directly or indirectly cell death mechanisms and/or modify the fine balance between the many mechanisms controlling survival pathways [Figure 3].

METABOLISM AND GBM RESISTANCE TO TREATMENT

GBM cells are highly proliferative and strongly depend on aerobic glycolysis for their survival, which would result in an increase in basal levels of reactive oxygen species (ROS)[62]. Both TMZ and radiotherapy induce DNA damage and cell cycle arrest, ROS production and activation of kinase signaling pathways. Aside from the preponderant role of MGMT expression in cell survival, the relationship between GBM cell sensitivity to treatment and metabolism has been demonstrated in several studies[63,64]. Specific metabolic alterations may occur naturally (IDH mutation for example), while others occur as adapting processes during the acquisition of resistance[64].

ROS production is instrumental in cell death induced either by TMZ or radiotherapy[65]. The ability of the cells to resist to TMZ treatment depends on the endogenous capacity of the cells to maintain a redox homeostasis[66]. The antioxidant apparatus and endogenous levels of ROS in the GBM cells, therefore, condition their ability to resist to treatment[65]. A study by Lo Dico *et al*.[67] showed that TMZ caused fluctuations in cytoplasmic ROS levels inducing cytotoxic effects in TMZ-sensitive GBM cells while in TMZ-resistant GBM cells, no increase in cytoplasmic ROS levels were observed thus preventing cytotoxicity.

As GBM cells largely depend on glycolysis for their growth, several attempts have been made to inhibit glycolysis and induce cell death, by using 2-deoxy-D-glucose (2DG), 3-bromopyruvate or dichloroacetate (DCA)[68-71]. These strategies demonstrated a modest effect by when used individually but was more efficient as an adjuvant therapy to radio- or chemotherapy.

The acquisition of resistance relies on a transitory drug-tolerant cell population, related to the cancer stem-like cells, often exhibiting stem-like characteristics[16]. These slow-dividing, CD133+ cells demonstrate the highest dependency on glucose and are unable to shift their metabolism toward the use of glutamine during glucose deprivation[72]. Certainly, the dependence on glucose is higher in GCSC than in neural stem cells[69], suggesting that glucose metabolism may be an interesting target for GBM cancer stem cells (GCSC). In this endeavor, DCA would be a better candidate than 2DG since 2DG inhibits the stem cell characteristics of both neural and GCSC[69]. Indeed, low-doses DCA induce a shift of GCSC toward oxidative metabolism, although no ROS production. This was sufficient to induce the loss of some stem cells characteristics, including the initiating cell capacity[69], stem cell marker expression and triggered the induction of the expression of differentiated cell markers[70]. This resulted in an increase in the response to chemotherapy by GBM, through the p53-dependent on BH3-only proteins[69] and the cytosolic sequestration and inactivation of Oct4 by PKM2[70].

Aside from glycolysis, slow-cycling GCSC also rely on the oxidation of fatty acids for their survival[73]. Inhibiting fatty acid oxidation (for example with etoxomir[73]) is thus a possible alternative metabolic adjuvant strategy to overcome the resistance of GBM cells to therapy.

The role of microenvironment in TMZ resistance

Tumorigenesis is a complex and dynamic process, which involves different cellular and non-cellular elements in the tumor microenvironment (TME). The interaction of the TME with cancer cells is responsible for tumor development, progression, and drug resistance. TME consists of non-malignant cells present in the tumor mass including cancer associated fibroblasts, endothelial cells and pericytes composing the tumor vasculature, immune and inflammatory cells, bone marrow-derived cells; and the extracellular matrix establishing a complex cross-talk within tumor mass. Tumor cells exclude extracellular vesicles (EV) to engage non-tumor cells in the TME and reprogram these cells from their normal activity to a more pro-tumorigenic. These EV contain and transport protein and nucleic acid cargoes to the non-tumor cells resulting in molecular, transcriptional and translational modifications that cause these cells to fabricate factors required for tumor growth and at the same time, alters the function of these cells. These cells could in turn generate their own EV containing and transferring molecules not only to the tumor but also to other cells in the TME enhancing their pro-tumorigenic activity. The EV represent a heterogeneous population of vesicles that can be divided into three large groups.

Exosomes are the smallest subset (50-100 nm) originating from the endocytic compartment of cells through a series of intraluminal invaginations occurring in multi-vesicular bodies.

Microvesicles are larger than exosomes (500-1000 nm) and are formed cell surface membrane blebbing and contain a random assortment of cell content.

Apoptotic bodies (800-5000 nm) represent cellular remains after apoptosis, containing an array of cellular debris.

Tumor-derived exosomes also contribute to the development of drug resistance. This can be achieved either by concentrating and removing the drug from the cytoplasm by exosomes or by packaging into exosomes to protect cells from the cytotoxic effects. Several studies have shown that drug resistance could be partially attributable to the intercellular transfer by exosomes of transporter proteins[74,75] or miRNA[76,77] from drug-resistant cells to sensitive cells.

An important step in anticancer treatment is the identification of the biological alterations present in TME to target these key molecular players. Multi-targeted approaches that providing a simultaneous inhibition of TME components have been shown to offer a more efficient way to treat certain cancers.

Immunotherapy and TMZ

Clinical trials in GBM with checkpoint inhibitors and vaccination strategies have been so far very disappointing, probably because of the highly immunosuppressive environment of GBM. Another reason could be that most of these trials have targeted single components of an anti-tumor immune response without considering the heterogeneity of the GBM[78]. We recently showed that GBM cells with a mesenchymal signature are spontaneously eliminated by allogeneic human Vγ9Vδ2 T lymphocytes, through the cellular stress associated NKG2D pathway while other GBM subtypes were exempted from such reactivity[79].

The relationship between TMZ and immune response in GBM has not been extensively studied[80]. However, contradictory TMZ immune-modulating effects have been reported and seem to depend on its

time and the mode of delivery of the dose of TMZ[81,82]. On the other hand, quite promising results have shown that adjuvant immunotherapy against specific antigens, can efficiently eliminate TMZ-resistant GBM[83,84]. It is thus obvious that the immunotherapy regimen should be considered in combination with the effect of TMZ on the immune system[85].

Resident brain macrophages and microglia are the main innate immune against central nervous system pathogens and insults. Indeed, these cells are an important component of GBM and may constitute up to 30%-50% of the total cell populations[86]. However, despite many recent advances, there are still numerous questions that remain to be answered about the identity, molecular drivers of recruitment, cancer induced reprogramming, polarization strategies and therapeutic modulation of GBM-associated macrophage and microglia immune biology.

In conclusion, the implication of the mechanisms of therapy resistance in the mutational burden, immunosuppression, and local immune dysfunction has still to be fully investigated in the context of combination therapy in a more personalized treatment in GBM.

Persisters, stem cells and quiescence: the slow cycling connection

Since the original finding of slow cycling cells with stemness markers and high levels of DNA repair activity[87], GCSC have been extensively studied. The role of GCSC in the resistance to therapy has been described in this review, as well as by other groups[88]. One of the current major questions regarding GCSC is the function of niche in their maintenance and resistance to treatment[89]. However, it seems that several types of GCSC can be found which are related to the different subtypes of GBM[90]. The characteristics of different GCSC subtypes remain to be identified to develop potential efficient and specific therapies. However, one well-known and common characteristic of GCSC is their slow cycling and quiescence activity. Indeed, several other types of cancer cells exhibit similar low proliferative activities and thus may represent new targets in cancer[16]. The existence of a class of drug tolerance with characteristics like persister cells described above has been recently identified in GBM. The work from the laboratory of Engelman showed that GCSC could reversibly transit to a slow-cycling, persister-like state in response to tyrosine kinase inhibitors (TKI)[41]. More interestingly, this adaptation to TKI was due to chromatin changes linked to an increased activity of histone demethylases KDM6A/B. Similarly, Banelli *et al.*[40] identified histone demethylases as targets to overcome TMZ resistance. A transcriptomic study of the development of resistance to TMZ in the GBM cell line U251 identified a transient persister-like stage during which the cells were sensitive to histone deacetylase inhibitors[91]. In lung cancer cell line, Guler *et al.*[14] showed that survival of persister cells was controlled by H3K9me3-mediated heterochromatin formation and that the disruption of the repressive chromatin over LINE-1 elements resulted in their eradication. Thus, chromatin states and its evolution under treatment might represent a new biomarkers and target in TMZ resistance in GBM.

The drug-tolerant cells appear also to be associate with a particular metabolic state with a marked increase in mitochondrial oxidative phosphorylation[91], a characteristic of slow cycling cells in GBM[92].

CONCLUSION: IS TARGETING PERSISTERS A FUTURE THERAPEUTIC OPTION?

The heterogeneity of cancer cell populations increases with treatment-induced stress, causing resistance to emerge[5]. This is probably the main reason there are a multitude of mechanisms implicated in TMZ resistance. These mechanisms operate at different levels and probably cooperate within the tumor. It is thus difficult to envisage a treatment, which will target all mechanisms at the same time.

From the discussions above we can propose that a reduction in cellular heterogeneity and the elimination of persisters, which are the precursors of drug resistance, might be interesting strategies. The first response

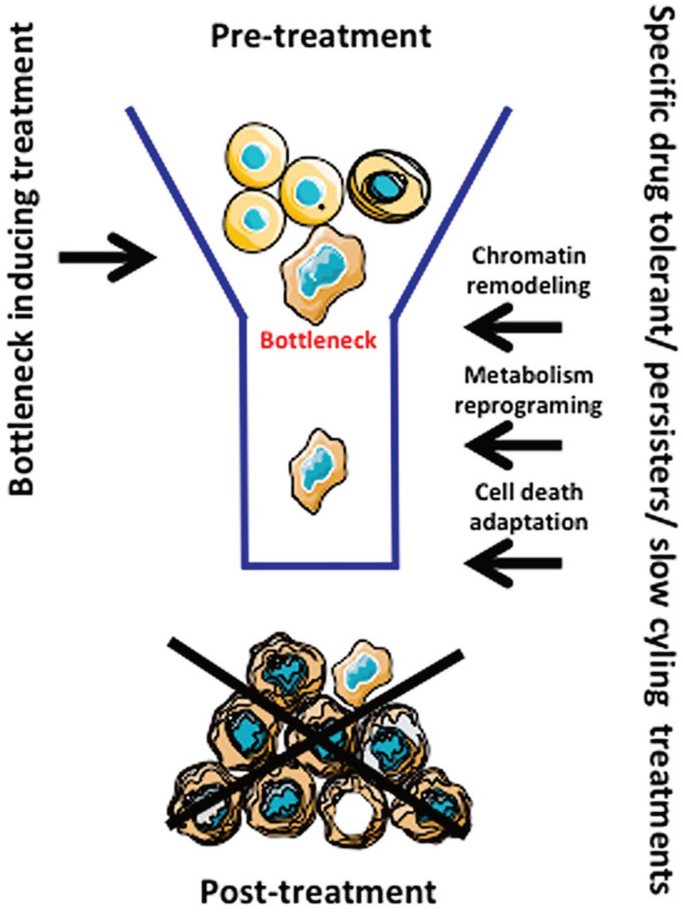

Figure 4. Formation of the bottleneck and resistance by treatment. The treatment (i.e., TMZ in GBM) induces a population restriction (bottleneck) and elicits an evolution/adaptation to treatment through cellular reprogramming. TMZ: Temozolomide; GBM: Glioblastoma

associated with the stress induced by treatment is a reduction in the population and heterogeneity of the cells leading to a "bottleneck" situation. This is followed by the emergence of a resistant cell population, which is also highly heterogeneous. An eradication strategy in GBM would thus involve sequential strategies: the first treatment should homogenize the population via adaptation to the induced stress, and the second treatment would specifically target the resulting bottleneck population. The literature points out a few dominant processes linked to this drug tolerant stage: chromatin remodeling, metabolism reprogramming and cell death adaptation [Figure 4]. It is noteworthy that therapies targeting these different mechanisms exist and could be easily evaluated in preclinical studies.

In some cases, a dominant resistant clone emerges, which could be sensitive to a second line of treatment. Recently, it appeared that resistance is linked to persisters, which undergo extensive reprogramming upon treatment. The resistant population might exhibit a few dominant clones, which in turn could be targeted by a combination of therapies. However, these resistant populations are often highly heterogeneous, impeding treatments; thus, targeting the persister population could efficiently reduce the therapeutic tools required and prevent the apparition of resistance.

DECLARATIONS

Acknowledgments

Thank all our collaborators who have helped in this project. We apologized for not citing numerous important studies in the field because of space limitations.

Authors' contributions

Made substantial contributions to the conception and writing of this review: Oliver L, Lalier L, Salaud C, Heymann D, Cartron PF, Vallette FM

Availability of data and material

Not applicable.

Financial support and sponsorship

This work was supported by INSERM/University of Nantes.

Conflicts of interest

All authors declared that there are no conflicts of interest.

Ethical approval and consent to participate

Not applicable.

Consent for publication

Not applicable.

REFERENCES

1. Stupp R, Mason WP, van den Bent MJ, Weller M, Fisher B, et al. Radiotherapy plus concomitant and adjuvant temozolomide for glioblastoma. N Engl J Med 2005;352:987-96.
2. Assaraf YG, Brozovic A, Gonçalves AC, Jurkovicova D, Linē A, et al. The multi-factorial nature of clinical multidrug resistance in cancer. Drug Resist Updat 2019;46:100645.
3. Yang J, Antin P, Berx G, Blanpain C, Brabletz T, et al. Guidelines and definitions for research on epithelial-mesenchymal transition. Nat Rev Mol Cell Biol 2020;21:341-52.
4. Gupta PB, Pastushenko I, Skibinski A, Blanpain C, Kuperwasser C. Phenotypic Plasticity: driver of cancer initiation, progression, and therapy resistance. Cell Stem Cell 2019;24:65-78.
5. Marusyk A, Janiszewska M, Polyak K. Intratumor heterogeneity: the rosetta stone of therapy resistance. Cancer Cell 2020;37:471-84.
6. Pastushenko I, Blanpain C. EMT transition states during tumor progression and metastasis. Trends Cell Biol 2019;29:212-26.
7. Saygin C, Matei D, Majeti R, Reizes O, Lathia JD. Targeting cancer stemness in the clinic: from hype to hope. Cell Stem Cell 2019;24:25-40.
8. Vasan N, Baselga J, Hyman DM. A view on drug resistance in cancer. Nature 2019;575:299-309.
9. Fulda S. Cell death-based treatment of glioblastoma. Cell Death Dis 2018;9:121.
10. Juin P, Geneste O, Gautier F, Depil S, Campone M. Decoding and unlocking the BCL-2 dependency of cancer cells. Nat Rev Cancer 2013;13:455-65.
11. Brocard E, Oizel K, Lalier L, Pecqueur C, Paris F, et al. Radiation-induced PGE2 sustains human glioma cells growth and survival through EGF signaling. Oncotarget 2015;6:6840-9.
12. Valès S, Bacola G, Biraud M, Touvron M, Bessard A, et al. Tumor cells hijack enteric glia to activate colon cancer stem cells and stimulate tumorigenesis. EBioMedicine 2019;49:172-88.
13. Balaban NQ, Helaine S, Lewis K, Ackermann M, Aldridge B, et al. Definitions and guidelines for research on antibiotic persistence. Nat Rev Microbiol 2019;17:441-8.
14. Guler GD, Tindell CA, Pitti R, Wilson C, Nichols K, et al. Repression of stress-induced LINE-1 expression protects cancer cell subpopulations from lethal drug exposure. Cancer Cell 2017;32:221-37.e13.
15. Ravindran Menon D, Hammerlindl H, Torrano J, Schaider H, Fujita M. Epigenetics and metabolism at the crossroads of stress-induced plasticity, stemness and therapeutic resistance in cancer. Theranostics 2020;10:6261-77.
16. Vallette FM, Olivier C, Lézot F, Oliver L, Cochonneau D, et al. Dormant, quiescent, tolerant and persister cells: four synonyms for the same target in cancer. Biochem Pharmacol 2019;162:169-76.
17. Hammerlindl H, Schaider H. Tumor cell-intrinsic phenotypic plasticity facilitates adaptive cellular reprogramming driving acquired drug resistance. J Cell Commun Signal 2018;12:133-41.
18. Ramirez M, Rajaram S, Steininger RJ, Osipchuk D, Roth MA, et al. Diverse drug-resistance mechanisms can emerge from drug-tolerant cancer persister cells. Nat Commun 2016;7:10690.

19. Lewis K. Persister cells. Annu Rev Microbiol 2010;64:357-72.
20. Kaldalu N, Tenson T. Slow growth causes bacterial persistence. Sci Signal 2019;12:aay1167.
21. Lee SY. Temozolomide resistance in Glioblastoma Multiforme. Genes Dis 2016;3:198-210.
22. Danson SJ, Middleton MR. Temozolomide: a novel oral alkylating agent. Expert Rev Anticancer Ther 2001;1:13-9.
23. Talhaoui I, Matkarimov BT, Tchenio T, Zharkov DO, Saparbaev MK. Aberrant base excision repair pathway of oxidatively damaged DNA: implications for degenerative diseases. Free Radic Biol Med 2017;107:266-77.
24. Karayan-Tapon L, Quillien V, Guilhot J, Wager M, Fromont G, et al. Prognostic value of O6-methylguanine-DNA methyltransferase status in glioblastoma patients, assessed by five different methods. J Neurooncol 2010;97:311-22.
25. Cartron PF, Hervouet E, Debien E, Olivier C, Pouliquen D, et al. Folate supplementation limits the tumourigenesis in rodent models of gliomagenesis. Eur J Cancer 2012;48:2431-41.
26. Esteller M, Garcia-Foncillas J, Andion E, Goodman SN, Hidalgo OF, et al. Inactivation of the DNA-repair gene MGMT and the clinical response of gliomas to alkylating agents. N Engl J Med 2000;343:1350-4.
27. Hervouet E, Debien E, Campion L, Charbord J, Menanteau J, et al. Folate supplementation limits the aggressiveness of glioma via the remethylation of DNA repeats element and genes governing apoptosis and proliferation. Clin Cancer Res 2009;15:3519-29.
28. Christmann M, Nagel G, Horn S, Krahn U, Wiewrodt D, et al. MGMT activity, promoter methylation and immunohistochemistry of pretreatment and recurrent malignant gliomas: a comparative study on astrocytoma and glioblastoma. Int J Cancer 2010;127:2106-18.
29. Wiewrodt D, Nagel G, Dreimüller N, Hundsberger T, Perneczky A, et al. MGMT in primary and recurrent human glioblastomas after radiation and chemotherapy and comparison with p53 status and clinical outcome. Int J Cancer 2008;122:1391-9.
30. Zhang Y, Dube C, Gibert M Jr, Cruickshanks N, Wang B, et al. The p53 pathway in glioblastoma. Cancers (Basel) 2018;10:297.
31. Belter A, Barciszewski J, Barciszewska AM. Revealing the epigenetic effect of temozolomide on glioblastoma cell lines in therapeutic conditions. PLoS One 2020;15:e0229534.
32. Dinca EB, Lu KV, Sarkaria JN, Pieper RO, Prados MD, et al. p53 small molecule inhibitor enhances temozolomide cytotoxic activity against intracranial glioblastoma xenografts. Cancer Res 2008;68:10034-9.
33. He F, Borcherds W, Song T, Wei X, Das M, et al. Interaction between p53 N terminus and core domain regulates specific and nonspecific DNA binding. Proc Natl Acad Sci U S A 2019;116:8859-68.
34. Hegi ME, Diserens AC, Gorlia T, Hamou MF, de Tribolet N, et al. MGMT gene silencing and benefit from temozolomide in glioblastoma. N Engl J Med 2005;352:997-1003.
35. O'Regan CJ, Kearney H, Beausang A, Farrell MA, Brett FM, et al. Temporal stability of MGMT promoter methylation in glioblastoma patients undergoing STUPP protocol. J Neurooncol 2018;137:233-40.
36. Chen X, Zhang M, Gan H, Wang H, Lee JH, et al. A novel enhancer regulates MGMT expression and promotes temozolomide resistance in glioblastoma. Nat Commun 2018;9:2949.
37. de Souza CF, Sabedot TS, Malta TM, Stetson L, Morozova O, et al. A distinct DNA methylation shift in a subset of glioma CpG island methylator phenotypes during tumor recurrence. Cell Rep 2018;23:637-51.
38. Lu C, Wei Y, Wang X, Zhang Z, Yin J, et al. DNA-methylation-mediated activating of lncRNA SNHG12 promotes temozolomide resistance in glioblastoma. Mol Cancer 2020;19:28.
39. Briand J, Nadaradjane A, Bougras-Cartron G, Olivier C, Vallette FM, et al. Diuron exposure and Akt overexpression promote glioma formation through DNA hypomethylation. Clin Epigenetics 2019;11:159.
40. Banelli B, Daga A, Forlani A, Allemanni G, Marubbi D, et al. Small molecules targeting histone demethylase genes (KDMs) inhibit growth of temozolomide-resistant glioblastoma cells. Oncotarget 2017;8:34896-910.
41. Liau BB, Sievers C, Donohue LK, Gillespie SM, Flavahan WA, et al. Adaptive chromatin remodeling drives glioblastoma stem cell plasticity and drug tolerance. Cell Stem Cell 2017;20:233-46.e7.
42. Wang Z, Jiang W, Wang Y, Guo Y, Cong Z, et al. MGMT promoter methylation in serum and cerebrospinal fluid as a tumor-specific biomarker of glioma. Biomed Rep 2015;3:543-8.
43. Nadaradjane A, Briand J, Bougras-Cartron G, Disdero V, Vallette FM, et al. MiR-370-3p is a therapeutic tool in anti-glioblastoma therapy but is not an intratumoral or cell-free circulating biomarker. Mol Ther Nucleic Acids 2018;13:642-50.
44. Estaquier J, Vallette F, Vayssiere JL, Mignotte B. The mitochondrial pathways of apoptosis. Adv Exp Med Biol 2012;942:157-83.
45. Rossin A, Miloro G, Hueber AO. TRAIL and FasL functions in cancer and autoimmune diseases: towards an increasing complexity. Cancers (Basel) 2019;11:639.
46. Trejo-Solís C, Serrano-Garcia N, Escamilla-Ramírez Á, Castillo-Rodríguez RA, Jimenez-Farfan D, et al. Autophagic and apoptotic pathways as targets for chemotherapy in glioblastoma. Int J Mol Sci 2018;19:3773.
47. Cartron PF, Loussouarn D, Campone M, Martin SA, Vallette FM. Prognostic impact of the expression/phosphorylation of the BH3-only proteins of the BCL-2 family in glioblastoma multiforme. Cell Death Dis 2012;3:e421.
48. Martin S, Toquet C, Oliver L, Cartron PF, Perrin P, et al. Expression of bcl-2, bax and bcl-xl in human gliomas: a re-appraisal. J Neurooncol 2001;52:129-39.
49. Manero F, Gautier F, Gallenne T, Cauquil N, Grée D, et al. The small organic compound HA14-1 prevents Bcl-2 interaction with Bax to sensitize malignant glioma cells to induction of cell death. Cancer Res 2006;66:2757-64.
50. Gratas C, Séry Q, Rabé M, Oliver L, Vallette FM. Bak and Mcl-1 are essential for Temozolomide induced cell death in human glioma. Oncotarget 2014;5:2428-35.
51. Chang J, Wang Y, Shao L, Laberge RM, Demaria M, et al. Clearance of senescent cells by ABT263 rejuvenates aged hematopoietic stem cells in mice. Nat Med 2016;22:78-83.

52. Yamaguchi R, Perkins G. Finding a Panacea among combination cancer therapies. Cancer Res. 2012;72:18-23.
53. Taylor MA, Das BC, Ray SK. Targeting autophagy for combating chemoresistance and radioresistance in glioblastoma. Apoptosis 2018;23:563-75.
54. Buccarelli M, Marconi M, Pacioni S, De Pascalis I, D'Alessandris QG, et al. Inhibition of autophagy increases susceptibility of glioblastoma stem cells to temozolomide by igniting ferroptosis. Cell Death Dis 2018;9:841.
55. Pawlowska E, Szczepanska J, Szatkowska M, Blasiak J. An interplay between senescence, apoptosis and autophagy in glioblastoma multiforme - role in pathogenesis and therapeutic perspective. Int J Mol Sci 2018;19:889.
56. Ulasov IV, Lenz G, Lesniak MS. Autophagy in glioma cells: an identity crisis with a clinical perspective. Cancer Lett 2018;428:139-46.
57. Aasland D, Götzinger L, Hauck L, Berte N, Meyer J, et al. Temozolomide induces senescence and repression of DNA repair pathways in glioblastoma cells via activation of ATR-CHK1, p21, and NF-κB. Cancer Res 2019;79:99-113.
58. Jeon HY, Kim JK, Ham SW, Oh SY, Kim J, et al. Irradiation induces glioblastoma cell senescence and senescence-associated secretory phenotype. Tumour Biol 2016;37:5857-67.
59. Tomicic MT, Christmann M. Targeting anticancer drug-induced senescence in glioblastoma therapy. Oncotarget 2018;9:37466-7.
60. Gammoh N, Fraser J, Puente C, Syred HM, Kang H, et al. Suppression of autophagy impedes glioblastoma development and induces senescence. Autophagy 2016;12:1431-9.
61. Tien AC, Li J, Bao X, Derogatis A, Kim S, et al. A phase 0 trial of Ribociclib in recurrent glioblastoma patients incorporating a tumor pharmacodynamic- andpharmacokinetic-guided expansion cohort. Clin Cancer Res 2019;25:5777-86.
62. Nagy A, Eder K, Selak MA, Kalman B. Mitochondrial energy metabolism and apoptosis regulation in glioblastoma. Brain Res 2015;1595:127-42.
63. Oizel K, Chauvin C, Oliver L, Gratas C, Geraldo F, et al. Efficient mitochondrial glutamine targeting prevails over glioblastoma metabolic plasticity. Clin Cancer Res 2017;23:6292-304.
64. Lee JH, Lee JE, Kahng JY, Kim SH, Park JS, et al. Human glioblastoma arises from subventricular zone cells with low-level driver mutations. Nature 2018;560:243-7.
65. Zhu Z, Du S, Du Y, Ren J, Ying G, et al. Glutathione reductase mediates drug resistance in glioblastoma cells by regulating redox homeostasis. J Neurochem 2018;144:93-104.
66. Singer E, Judkins J, Salomonis N, Matlaf L, Soteropoulos P, et al. Reactive oxygen species-mediated therapeutic response and resistance in glioblastoma. Cell Death Dis 2015;6:e1601.
67. Lo Dico A, Salvatore A, Martelli C, Ronchi D, Diceglie C, et al. Intracellular redox-balance involvement in temozolomide resistance-related molecular mechanisms in glioblastoma. Cells 2019;8:1315.
68. Michelakis ED, Sutendra G, Dromparis P, Webster L, Haromy A, et al. Metabolic modulation of glioblastoma with dichloroacetate. Sci Transl Med 2010;2:31ra34.
69. Morfouace M, Lalier L, Bahut M, Bonnamain V, Naveilhan P, et al. Comparison of spheroids formed by rat glioma stem cells and neural stem cells reveals differences in glucose metabolism and promising therapeutic applications. J Biol Chem 2012;287:33664-74.
70. Morfouace M, Lalier L, Oliver L, Cheray M, Pecqueur C, et al. Control of glioma cell death and differentiation by PKM2-Oct4 interaction. Cell Death Dis 2014;5:e1036.
71. Shen L, Zhu J, Chen F, Lin W, Cai J, et al. RUNX1-Evi-1 fusion gene inhibited differentiation and apoptosis in myelopoiesis: an in vivo study. BMC Cancer 2015;15:970.
72. Oizel K, Gratas C, Nadaradjane A, Oliver L, Vallette FM, et al. D-2-Hydroxyglutarate does not mimic all the IDH mutation effects, in particular the reduced etoposide-triggered apoptosis mediated by an alteration in mitochondrial NADH. Cell Death Dis 2015;6:e1704.
73. Lin H, Patel S, Affleck VS, Wilson I, Turnbull DM, et al. Fatty acid oxidation is required for the respiration and proliferation of malignant glioma cells. Neuro Oncol 2017;19:43-54.
74. Al-Nedawi K, Meehan J, Micallef V, Lhotak L, May A, et al. Intercellular transfer of the oncogenic receptor EGFRvIII by microvesicles derived from tumour cells. Nat Cell Biol 2008;10:619-24.
75. Corcoran C, Rani S, O'Brien K, O'Neill A, Prencipe M, et al. Docetaxel-resistance in prostate cancer: evaluating associated phenotypic changes and potential for resistance transfer via exosomes. PLoS One 2012;7:e50999.
76. Challagundla KB, Wise PM, Neviani P, Chava H, Murtadha M, et al. Exosome-mediated transfer of microRNAs within the tumor microenvironment and neuroblastoma resistance to chemotherapy. J Natl Cancer Inst 2015;107:djv135.
77. Mao L, Li J, Chen WX, Cai YQ, Yu DD, et al. Exosomes decrease sensitivity of breast cancer cells to adriamycin by delivering microRNAs. Tumour Biol 2016;37:5247-56.
78. Medikonda R, Dunn G, Rahman M, Fecci P, Lim M. A review of Glioblastoma immunotherapy. J Neurooncol 2020; doi: 10.1007/s11060-020-03448-1.
79. Chauvin C, Joalland N, Perroteau J, Jarry U, Lafrance L, et al. NKG2D controls natural reactivity of Vγ9Vδ2 T lymphocytes against mesenchymal glioblastoma cells. Clin Cancer Res 2019;25:7218-28.
80. Sengupta S, Marrinan J, Frishman C, Sampath P. Impact of temozolomide on immune response during malignant glioma chemotherapy. Clin Dev Immunol 2012;2012:831090.
81. Candolfi M, Yagiz K, Wibowo M, Ahlzadeh GE, Puntel M, et al. Temozolomide does not impair gene therapy-mediated antitumor immunity in syngeneic brain tumor models. Clin Cancer Res 2014;20:1555-65.
82. Karachi A, Dastmalchi F, Mitchell DA, Rahman M. Temozolomide for immunomodulation in the treatment of glioblastoma. Neuro Oncol 2018;20:1566-72.
83. Noh H, Zhao Q, Yan J, Kong LY, Gabrusiewicz K, et al. Cell surface vimentin-targeted monoclonal antibody 86C increases sensitivity to

temozolomide in glioma stem cells. Cancer Lett 2018;433:176-85.
84. Fleurence J, Bahri M, Fougeray S, Faraj S, Vermeulen S, et al. Impairing temozolomide resistance driven by glioma stem-like cells with adjuvant immunotherapy targeting O-acetyl GD2 ganglioside. Int J Cancer 2020;146:424-38.
85. Karachi A, Yang C, Dastmalchi F, Sayour EJ, Huang J, et al. Modulation of temozolomide dose differentially affects T-cell response to immune checkpoint inhibition. Neuro Oncol 2019;21:730-41.
86. Wei J, Chen P, Gupta P, Ott M, Zamler D, et al. Immune biology of glioma-associated macrophages and microglia: functional and therapeutic implications. Neuro Oncol 2020;22:180-94.
87. Bao S, Wu Q, McLendon RE, Hao Y, Shi Q, et al. Glioma stem cells promote radioresistance by preferential activation of the DNA damage response. Nature 2006;444:756-60.
88. Gimple RC, Bhargava S, Dixit D, Rich JN. Glioblastoma stem cells: lessons from the tumor hierarchy in a lethal cancer. Genes Dev 2019;33:591-609.
89. Aderetti DA, Hira VVV, Molenaar RJ, van Noorden CJF. The hypoxic peri-arteriolar glioma stem cell niche, an integrated concept of five types of niches in human glioblastoma. Biochim Biophys Acta Rev Cancer 2018;1869:346-54.
90. Verhaak RG, Hoadley KA, Purdom E, Wang V, Qi Y, et al. Integrated genomic analysis identifies clinically relevant subtypes of glioblastoma characterized by abnormalities in PDGFRA, IDH1, EGFR, and NF1. Cancer Cell 2010;17:98-110.
91. Rabé M, Dumont S, Álvarez-Arenas A, Janati H, Belmonte-Beitia J, et al. Identification of a transient state during the acquisition of temozolomide resistance in glioblastoma. Cell Death Dis 2020;11:19.
92. Hoang-Minh LB, Siebzehnrubl FA, Yang C, Suzuki-Hatano S, Dajac K, et al. Infiltrative and drug-resistant slow-cycling cells support metabolic heterogeneity in glioblastoma. EMBO J 2018;37:e98772.
93. Quinones A, Le A. The multifaceted metabolism of glioblastoma. Adv Exp Med Biol 2018;1063:59-72.
94. Dongre A, Weinberg RA. New insights into the mechanisms of epithelial-mesenchymal transition and implications for cancer. Nat Rev Mol Cell Biol 2019;20:69-84.
95. Fedele M, Cerchia L, Pegoraro S, Sgarra R, Manfioletti G. Proneural-mesenchymal transition: phenotypic plasticity to acquire multitherapy resistance in glioblastoma. Int J Mol Sci 2019;20:2746.
96. Broekman ML, Maas SLN, Abels ER, Mempel TR, Krichevsky AM, et al. Multidimensional communication in the microenvirons of glioblastoma. Nat Rev Neurol 2018;14:482-95.

1.2 PERSPECTIVES :

Cette population cellulaire fait donc partie du MET et joue un rôle important dans l'évolution la résistance des GBM. Notre équipe a réussi à les identifier à partir de prélèvements tumoraux de GBM. Les CSC quiescentes se situent en majeure partie dans les régions nécrotiques donc hypoxiques juste à la jonction (zone palissadique) avec la périphérie tumorale proliférative. Les CSC actives se situent elles, dans les zones hypervascularisées prolifératives (résultats non publiés de l'équipe).

Dans notre projet de plateforme de criblage, il est nécessaire de réussir à les cultiver dès le début de la création des modèles 3D afin d'analyser leur action initiale et leur évolution après traitement. Elles représentent une cible thérapeutique potentielle.

2 A SIMPLE 3D CELL CULTURE METHOD FOR STUDYING THE INTERACTIONS BETWEEN PRIMARY GLIOBLASTOMA CELLS AND TUMOR-ACTIVATED FIBROBLASTS

Afin de rechercher de nouvelles cibles thérapeutiques et de mieux comprendre les mécanismes de tumorigenèse, le choix du modèle tumoral est déterminant.
Comme nous l'avons décrit dans l'introduction, les modèles 3D in vitro de primocultures de GBM semblent les modèles les plus pertinents.

Notre équipe a travaillé à mettre au point la technique de primoculture en 3D en créant des tumoroïdes. Il a fallu déterminer la composition la plus adéquate du Bioink et définir la meilleure concentration cellulaire des cellules cancéreuses de GBM et de CAF permettant leur co-culture en 3 dimensions. Nous avons décrit dans cet article la méthodologie de création de ces tumoroïdes ainsi que les premiers constats de prolifération et de réponse au traitement par TMZ.

2.1 PRINCIPAUX RESULTATS :

-Le bioink le plus pertinent utilisé dans les tumoroïdes créé par technique de bioimpression est un mélange de 5% de gélatine et de 2% d'alginate.

-La concentration de cellules cancéreuses la plus pertinente est de $4x10^6$/mL et $4x10^5$/mL de CAF.

-La présence des CAF semble augmenter la résistance à la chimiothérapie par TMZ qui pénètre moins dans la biosphère.

-Il existe au sein des tumoroïdes une architecture proche de la réalité. Ils possèdent un centre nécrotique, une périphérie prolifératives et une MEC contenant du collagène et des GAG synthétisés par les cellules présentes (cf résultats non présentés dans l'article).

- Grâce à l'analyse mathématique, nous avons validé le modèle et nous avons mis en évidence l'existence d'une structure différente des tumoroïdes en fonction des sous-types de GBM. Le sous-type mésenchymateux est beaucoup plus compact que le sous-type proneural.

ARTICLE 2

A simple 3D cell culture method for studying the interactions between primary Glioblastoma cells and tumor-activated fibroblasts

Lisa Oliver[1,2*], Arturo Álvarez-Arenas[3], Céline Salaud[1,2], Juan Jiménez-Sanchez[3], Fanny Geraldo[1], Gabriel F. Calvo[3], Juan Belmonte-Beitia[3], Stéphanie Blandin[1,4], Pierre Layrolle[5], Luciano Vidal[5], Victor Pérez[3], Dominique Heymann[1,6], François M. Vallette[1,6*]

Abstract

One of the main tasks GBM research, is the development of culture conditions that maintain the molecular genotype and phenotype as well as heterogeneity of the original tumor *in vitro*. The current gold standard method for studying cancer biology includes using two-dimensional (2D) monocultures, organotypic culture or animal models. However, none of these different methods fully recapitulate the key aspects of tumors such as three-dimensional (3D) architecture, the presence of the extracellular matrix (ECM) and the interplay between cancer cells and the tumor microenvironment (TME). Thus, it is important to develop models representative of the complex and dynamic tumoral system in which heterogeneous cancer cells interplay with the TME.

We have developed a 3D biosphere model using patient-derived cells (PDCs) from Glioblastoma (GBM), the major form of primary brain tumors in adult, plus cancer-associated fibroblasts (CAFs) or tumor-activated fibroblasts (TAFs), obtained by culturing fibroblasts with conditioned media from the PDCs. The effect of CAFs and TAFs on the proliferation, cell-cell interactions and response to treatment of PDCs was evaluated. Proliferation in the presence of TAFs was statistically lower but the spheroids formed within the 3D-biosphere were larger. A treatment for 5 days with 100 µM Temozolomide (TMZ), the standard chemotherapy for GBM, had a marked effect on cell number in monocultures compared to co-cultures. Here we provide a simple and reproducible method to obtain tumoroids from patient-derived biopsies with a near 100% success. This method provides the basis for relevant in vitro functional models for predicting the response to treatments and the potential use in precision and/or personalized medicine.

A simple 3D cell culture method for studying the interactions between primary Glioblastoma cells and tumor-activated fibroblasts

Lisa Oliver[1,2*], Arturo Álvarez-Arenas[3], Céline Salaud[1,2], Juan Jiménez-Sanchez[3], Fanny Geraldo[1], Gabriel F. Calvo[3], Juan Belmonte-Beitia[3], Stéphanie Blandin[1,4], Pierre Layrolle[5], Luciano Vidal[5], Victor Pérez[3], Dominique Heymann[1,6], François M. Vallette[1,6*]

[1] Université de Nantes, INSERM, CRCINA - INSERM U1232

[2] Centre Hospitalier-Universitaire (CHU) de Nantes, Nantes 44007 France

[3] Department of Mathematics & MOLAB-Mathematical Oncology Laboratory, University of Castilla-La Mancha, 13071, Ciudad Real, Spain

[4] Micropicell Facility-INSERM UMS 016, CNRS 3556, Structure Fédérative de Recherche François Bonamy

[5] Université de Nantes, INSERM, PHYOS UMR 1238

[6] LaBCT- Institut de Cancérologie de l'Ouest, St Herblain

Corresponding authors: lisa.oliver@univ-nantes.fr
francois.vallette@inserm.fr

CRCINA INSERM U1232 Université de Nantes

8 quai Moncousu, 44007 Nantes, France

Tel: +(33)2 2808 0325; Fax: +(33)2 2808 0204

Keywords: Bioprinting, Glioma and TAFs

Running title: A 3D method for culturing Glioma cells

Abbreviations: two-dimensional (2D); cancer-associated fibroblasts (CAFs); collagen (Coll); extracellular matrix (ECM); formaldehyde fixed paraffin-embedded (FFPE); glycosaminoglycan (GAGs); Glioblastoma (GBM); gelatin (Gel); glial fibrillary acidic protein (GFAP); green fluorescent protein (GFP); Glioma stem cells (GSCs); Hank's buffered saline solution (HBSS); laminin (Lam); Patient-Derived Cells (PDCs); Patients-Derived Xenografts (PDX); Arg-Gly-Asp (RGD); tumor-activated fibroblasts (TAFs); tumor microenvironment (TME); Temozolomide (TMZ).

Abstract

One of the main tasks GBM research, is the development of culture conditions that maintain the molecular genotype and phenotype as well as heterogeneity of the original tumor *in vitro*. The current gold standard method for studying cancer biology includes using two-dimensional (2D) monocultures, organotypic culture or animal models. However, none of these different methods fully recapitulate the key aspects of tumors such as three-dimensional (3D) architecture, the presence of the extracellular matrix (ECM) and the interplay between cancer cells and the tumor microenvironment (TME). Thus, it is important to develop models representative of the complex and dynamic tumoral system in which heterogeneous cancer cells interplay with the TME.

We have developed a 3D biosphere model using patient-derived cells (PDCs) from Glioblastoma (GBM), the major form of primary brain tumors in adult, plus cancer-associated fibroblasts (CAFs) or tumor-activated fibroblasts (TAFs), obtained by culturing fibroblasts with conditioned media from the PDCs. The effect of CAFs and TAFs on the proliferation, cell-cell interactions and response to treatment of PDCs was evaluated. Proliferation in the presence of TAFs was statistically lower but the spheroids formed within the 3D-biosphere were larger. A treatment for 5 days with 100 µM Temozolomide (TMZ), the standard chemotherapy for GBM, had a marked effect on cell number in monocultures compared to co-cultures. Here we provide a simple and reproducible method to obtain tumoroids from patient-derived biopsies with a near 100% success. This method provides the basis for relevant in vitro functional models for predicting the response to treatments and the potential use in precision and/or personalized medicine.

1. Introduction

Glioblastoma (GBM) is the most deadly brain tumor and the outcome for these patients is dismal. The standard treatment includes surgical resection followed by a combination of radio- and chemotherapy (**Stupp *et al*., 2005; 2009**). The poor prognosis with a median survival of about 15 months is due to the presence of treatment-resistant tumor-initiating cells or Glioblastoma stem cells (GSCs) (**Singh *et al*., 2004**) and inter- and intra-tumoral heterogeneity (**Qazi et al., 2017**). These features are the main reasons for therapeutic failures, as specificity and efficacy of the treatments are not achievable throughout the total population (**Fallica *et al*., 2011; Fong *et al*., 2012**). Transcriptomic analyses on single cells profiled three defined intrinsic gene expressions that have been designated as proneural, mesenchymal and classical (Wang et al., 2017)

It has been shown that in two-dimensional (2D) cell culture systems, which are most common form of cell culture, cells adapt to the new environment by inducing changes at the genetic, transcriptional and protein levels. Recently, patient-derived cells (PDCs) cultured in 3D systems as tumoroids behave more like the native tumor, retaining their intra-tumor heterogeneity (**Fallica *et al*., 2011; Griffith and Swartz, 2006; Pine et al., 2020**). Animal models such as the Patients-Derived Xenografts (PDXs) display some important limitations due to cell selection and a non-natural microenvironment, which often constitutes the major part of the tumor (**William *et al*., 2017**). Thus, an interesting alternative would be a simple and reliable culture method that will retain the heterogeneity of the tumor precluding the selection of cells and that could be maintained *in vitro* with and/or without cells from the tumor microenvironment (TME) for treatment screening purposes.

Hierarchical clustering of gene expression profiles of both cell lines and tissue samples has shown that the gene expression profile of cell lines is different from tissue samples (**Birgersdotter *et al*., 2005**). It has become increasingly evident that cell lines only approximate properties of the tumor. In fact, it is now apparent that the deregulation within the tumor can be best explained when the contributions of and interactions with the microenvironment are taken into account (**Hirschhaeuser *et al*., 2010; Hanahan and Weinberg, 2011; Pine et al., 2020**). In tissues, tumor cells interact with the extracellular matrix (ECM), non-tumor cells and soluble factors all present in the TME; and these interactions would both be responsible for the mechanical properties of the cells and contribute to communication between cells. Given this complex mechanical and biochemical interplay, many important biological properties are absent when cells are cultured in 2D cell

cultures. It would be more appropriate to use tissue specific matrices, however, preparation of these matrices show large variations, are time consuming to prepare and costly. It is probable that the development of *in vitro* models, which include the TME could lead to a better understanding of the effects of drugs on tumor cells since there are now many indications that the biomechanical properties as well as components of the extracellular matrix (ECM) as well as the matrix rigidity can influence the proliferation and migration of GBM cells (**Ulrich et *al*., 2009**; **Ruiz-Ontañon *et al*., 2013**).

The principal component of normal brain ECM is hyaluronic acid and a variety of proteoglycans (**Bonneh-Barkay and Wiley, 2009**). On the other hand, the composition of the ECM of GBM is different from normal brain consisting of many fibrous collagens (**Huijbers *et al*., 2010; Virga *et al*., 2017**) and essential for the activation of signal transduction (**Leitinger, 2011**).

The aim of this study was to develop a simple easy technique to construct a three-dimensional (3D) patient-derived cell (PDC) model, which could easily support co-cultures of PDCs and stromal cells of the TME to phenocopy the *in vivo* tumors. This has been performed for more than 20 patients in our laboratory with a near 100% success rate. This method can thus be used to develop/adapt treatment to the individual characteristics of each GBM patient.

2. Results

2.1 Composition of biospheres

To determine the optimal cell-free structural material or biopaper, 3D biospheres were prepared with PDCs using various different matrices using the protocol described in **Figure 1A**. Initially laminin and gelatin were tested and the cell proliferation and the capacity of the cells to form a cellular network were used to validate the biopaper. The results presented in **Figure 1B** illustrate that cells proliferated more rapidly in the gelatin than in the laminin-containing matrix. This was observed for two concentrations (0.3 - 0.6 mg/ml) of laminin while cells proliferated more rapidly at in 2% gelatin as compared to 1% gelatin. Microscopic analyses of the cell networks represented in **Figure 1C,** show virtually single cell suspensions at both concentrations of laminin-containing biopapers as compared to gelatin where a network of cell-cell interconnections or neurospheres could be distinguished. In addition, PDCs cultured in the presence of gelatin displayed heterogeneous growth both in size and shape. Thus, proliferation rate and the formation of neurospheres suggested that gelatin was a

better biopaper for PDCs than laminin. Further experiments showed that increasing the concentration of gelatin from 1.25 to 5% also increased the proliferation of the cells (**Figure 1C**) without having any effect of the formation of neurospheres (**data not shown**).

Next we analyzed the proliferation of PDCs in collagen-containing 3D biospheres at final concentrations of 0.25, 0.5 or 2 mg/ml (**Figure 1D**). As shown in **Figure 1E,** cells only proliferated in biospheres containing 2 mg/ml collagen and with similar proliferation rates as observed for gelatin-containing biospheres.

2.2 Proliferation and cellular network in 3D biosphere

Next, we determined the optimal initial cell concentration required to obtain the most advantageous growth. The data in **Figure 2A** suggest that the initial cell number required to support proliferation of the PDCs in the biospheres was important. The results show that an initial cell concentration of $4x10^4$ cells/biosphere gave an optimal growth over 21 days compared to $2x10^4$ or $5x10^5$ cells/biosphere. Actually, having too few cells ($2x10^4$ cells) appeared to delayed proliferation and the resulting neurospheres formed were of inadequate size to render sufficient cells for detailed post-biosphere analyses before day 21, while having too many ($5x10^5$ cells) resulted in no cell growth (**Figure 2A**). To validate these results, biospheres representing a volume of approximately 10 μl, were prepared having a final concentration of 2 mg/ml collagen or 5% gelatin, both containing an initial cell concentration of approximately $4x10^4$ cells/biosphere were performed and the data in **Figure 2B** show that the proliferation of the PDCs in the two types of biospheres was quite similar. Comparisons were performed with 5 additional PDC cultures and all gave similar results (**data not shown**).

Subsequently cellular networks developed by PDCs in gelatin vs. collagen containing biospheres were assessed over a 3-week period. As depicted in **Figure 2C**, a unicellular cell suspension was present on day 1 in both types of biospheres. These cells evolved over time into compact oval neurospheres. These structures are different from the neurospheres observed in 2D-cultures, which were much less compact (**Figure S1**). To further analyze the cellular structures in the biospheres, the diameters of these neurospheres were measured (**see** experimental section) and as shown in **Figure 2D** there was no statistical difference in neurosphere size between gelatin and collagen biopapers.

2.3 Cellular heterogeneity and interaction cell-cell

To determine if there is a change in the phenotype of the cells after 3D biosphere culture, the cells were recuperated after day 36 and phenotypic analyses were carried out by

FACS analyses (see experimental section). GBMA1 PDCs (subtype: mesenchymal) grew as loosely associated neurospheres in 2D culture (**Figure S1**). As showed in **Figure 3A**, the percentage of cells positive for stemness markers CD133 (proneural), CD90 (mesenchymal) and CD44 (mesenchymal) was similar in 2D culture vs. 3D biospheres with either a gelatin or collagen biopaper. GBM8 PDC (subtype: proneural) grew as semi-adherent cells in 2D cultures (**Table S1**, **Figure S2**) and showed marked differences in their phenotype in 2D vs. 3D cultures. The data presented in **Figure 3B** indicated a complete absence of CD90 positive cells and an increase in the number of CD133 positive cells in GBM8 cultured in 3D biospheres. Thus, our 3D model favored the expansion of the proneural subtype but did not alter the mesenchymal subtype determined by genomic analyses on the resected tumors (**Table S1**).

We also performed colony-forming assays to determine the number of single cells capable of instigating the formation of cell colonies. These colony-initiating cells are considered to be the "cancer initiating cells" or Glioma stem cells (GSCs). For these experiments GBMA1 cells from 2D and biospheres were plated on micro-raft plates and then rafts containing single cells were recuperated and transferred into wells of 96-well plates. After 20 days the 198 wells for each condition were scored and the percentage of colonies (+10 cells) determined. The data in **Figure 3C** show that the percentage of colonies formed from cells obtained from 2D was similar to that obtained with cells obtained from 3D biospheres with GBM A1 and GBM 10. These results suggested that there is no modification of the number of GSC under our 3D culture conditions.

In addition to the ECM, the tumor consists of a heterogeneous cell population that interacts in multiple different ways. It is thus important that we could mimic cellular interactions similar to those observed *in vivo*, imitating the high degree of structural complexity. For this we analyzed the cell-cell interactions as well as the cellular heterogeneity in biospheres. Whole biospheres prepared with GBM69 PDCs (subtype: heterogeneous) were recuperated after day 21, fixed and labeled for nestin (a marker of neural stem cells) and GFAP (a marker of glial cells). As seen in **Figure 3D** cells were labeled with nestin or GFAP and some were even labeled with both nestin and GFAP signifying the presence of a heterogeneous population of cells. Furthermore, the cells appeared elongated with numerous interconnections among the cells inferring an interaction between the cells.

Next we investigate whether the cells in the neuropheres were able to synthesize and secrete an ECM. For this, fixed biospheres embedded in paraffin were sectioned and then stained with Masson's trichrome to reveal collagen and Alcian blue to stain for

glycosaminoglycan (GAGs). The presence of both collagen and GAGs were detected inside and around the spheroids formed in the biospheres (**Figure 3E**).

2.4 Mathematical analysis of neurosphere growth and morphology

Several studies have suggested that morphological measures may help to classify and characterize brain tumors (**Hevia-Montiel et al., 2015; Jubran et al., 2020**). To quantify the morphology of the neurospheres in the 3D cultures, we determined the circularity of the cellular structures formed in the biospheres. It is known that GBM tumors of patients have different GBM molecular subtypes, which display quite different behaviors. To study whether those differences are also observed in 3D cultures, we have used mathematical techniques to analyze each case.

The number of cells was quantified in a single biosphere at different time points, and to avoid other possible factors, the doubling time was estimated over the period during which the cells grew exponentially; consequently, fits were done using the exponential function Eq. (2) given below. The resulting doubling times of the different primary cultures can be seen in **Figure 4A**. Note that the primary cultures GBM3 and GBM8, classified as proneural subtype, proliferated more slowly compared to the mesenchymal primary cultures GBM22 and GBMA1.

At each time point the diameter (μm) and the area (μm^2) of about 200 neurospheres within the biospheres were assessed directly from the images, as shown in **Figure 4B**. With the measurements obtained, the corresponding distribution was reconstructed, and its temporal variation was analyzed in **Figure 4C**. Our analyses on the dynamics of the diameter and area distributions were based on the following considerations. Let v_c denotes the characteristic volume of a single cell. The volume of one multicellular spheroid consisting of $n(t)$ cells at time t is thus given by:

$$V_{Tot}(t) = v_c n(t) \qquad \textbf{(Eq. 1)}$$

If the cells exhibit an exponential growth, then their number at time t would be given by:

$$n(t) = n(0)e^{\frac{t-t_0}{\tau}} \qquad \textbf{(Eq. 2)}$$

where $n(0)$ is the number of cells at the initial time t_0 and τ denotes the cell proliferation time. Substituting expression Eq. (2) for $n(t)$ into Eq. (1), and taking into account that the initial volume is $V(0) = v_c n(0)$, we obtain the total spheroid volume:

$$V_{Tot}(t) = V(0)e^{\frac{t-t_0}{\tau}} \qquad \textbf{(Eq. 3)}$$

If during growth, the cells adopt a spherical shape then, since the volume of a sphere with diameter d is: $V = \frac{\pi}{6}d^3$, substituting into Eq. (3), the diameter and the area would evolve according to the following laws:

$$d(t) = d(0)e^{\frac{t-t_0}{3\tau}} \qquad \textbf{(Eq. 4)}$$

$$A(t) = A(0)e^{\frac{2(t-t_0)}{3\tau}} \qquad \textbf{(Eq. 5)}$$

where d_0 and A_0 are respectively the inital diameter and area of the multicellular structure.

From the estimated proliferation time τ (**Figure 5A**) and the initial diameters $d(0)$ and areas $A(0)$, measured from the recorded images (see **Figure 2D),** it is straightforward to compare the experimental diameters and areas at the different time t with the expression for the diameter $d(t)$ and the area $A(t)$ that the structures would have if they grew spherically. With this comparison, we determined which primary cultures give rise to structures with different compactness during growth. In **Figure 5B, C,** we show that mesenchymal PDC (GBM 22), formed compact structures, while proneural PDC (GBM8), formed less compact structures. Similar comparisons were made on several PDCs (**data not shown**) and the overall results suggest that cells from mesenchymal tumors form more compact cell structures in our biospheres when compared to cell structures observed in proneural tumors under our culture conditions. These results suggest that proneural tumors can adopt very different shapes, while mesenchymal tumors tend to form more uniform spherical structures.

Circularity and sphericity both refer to the same concept but applied in different dimensions. Circularity (or roundness) measures how close a geometric shape is to a perfect circle in 2D, while sphericity measures how close a 3D volume is to a perfect sphere. Sphericity is calculated as the ratio between the surface of a sphere with the same volume as our 3D volume, and the surface of our 3D volume. Circularity of four different primary cultures was compared among each other showing no significant differences. However, when we compared the circularity of the larger neurospheres (in terms of area) to the smaller

neurospheres in each primary culture, we observed some differences. The variance in the circularity was much larger in the bigger structures in the proneural tumors (**Figure 6A, B**), with a very high statistical significance ($5.7396x10^{-6}$ and 0.00047661) while with mesenchymal tumors (**Figure 6C, D**), the significance of the differences in variance was much smaller or not significant (0.037342 and 0.38142). These results suggest that proneural tumors can adopt very different shapes, while mesenchymal tumors tend to form more uniform spherical structures.

In order to further analyze tumor compactness, a bigger sample size of a cohort of 340 tumors from the GLIOMAT project was analyzed, using the protocol in **Pérez-Beteta *et al*., 2018**. Using the concept of sphericity MRI images from the GLIOMAT was analyzed (**Figure 6E**). Sphericity was calculated as an approach to estimate their compactness. The cohort was divided in two groups, according to median volume, in order to separate between small and large tumors (threshold volume = 29.09 cm^3). The sphericity of the two groups was compared using the Mann-Whitney non-parametric test, to determine the difference. Mann-Whitney test revealed significant differences between the two groups ($p = 0.000228$), with a median sphericity of 0.5892 for the small tumors, and a median sphericity of 0.5455 for the large tumors. Although the magnitude of differences is small, due to big sample size it is possible to assert that large tumors usually have a significantly smaller sphericity than small tumors. The overall conclusion is that, as tumors grow in size, it is expected that their surface regularity will decrease. These results are in accordance with spheroids in biospheres; as spheroids increase in size, their compactness decreases compared to that of a perfect circle growing at the same rate. This result is in agreement with data obtained by **Griveau et al**. (**2018**).

2.5 Influence of the tumor microenvironment cells on biospheres

Numerous reports have shown that the non-tumor cells in the TME play an important role in the survival and aggressiveness of tumor cells (**Hashimoto *et al*., 2016; Bergfeld and DeClerck, 2010; Mishra *et al*., 2008; Borriello *et al*., 2017**). To determine whether we could use our model to analyze these intercommunications, CAFs isolated from GBM tumors or TAFs obtained by culturing normal fibroblasts with conditioned media from GBM primary cultures for 7 days were co-cultured with PDCs at a ratio of 1:5. Neither the CAFs nor the TAFs cultured in 3D biospheres proliferated (**Figure 7A, B**). In addition, these cells did not form spheroids in biospheres under our culture conditions, even when cultured at high cell numbers (**Figure 7B**, **data not shown**). To evaluate the effect of the TME on tumor cell

growth in biospheres, GFP-labeled TAFs were cultured with tumor cells in biospheres and the proliferation was assessed over 3 weeks. GFP-labeled TAFs were visible until day 14 within the biospheres after which no labeled cells were observed, however, GFP-labeled fragments could be observed within spheroids (**Figure 7C**). The co-culture of TAFs and PDCs resulted in a significant reduction in overall cell proliferation after day 7 (**Figure 7D**). However, the mean size of the tumoroids within the biosphere was significantly larger in co-cultures and compared to monocultures (**Figure 7E**) suggesting that there was more cell clustering resulting in larger tumoroids in co-cultures. Treatment of these biospheres with TMZ for 96 h significantly reduced the number of cells in monoculture biospheres compared to the co-cultures (**Figure 7F**). These data suggest that the TAFs protected the tumor cells from cell death.

3. Discussion

Many cancers feature cellular hierarchies that are driven by tumor-initiating cancer stem cells (CSC) and rely on complex interactions with the TME. Traditional 2D culture systems are very restrictive and fail to recapitulate the original tumor architecture and the TME and do not retain the cellular heterogeneity. The consequences of these systems generate a mediocre consistency in assays because *in vivo* molecular targets are modulated by exchanges with TME. These exchanges could include communication cell-cell, cell-stroma as well as cell-matrix. Furthermore, other processes related to the tumor construction including gradient of O_2 (formation of hypoxic regions) or nutrients are all lacking in the 2D culture models. Matrix-based 3D culture models are becoming increasingly important tools. 3D tumoroid culture systems permit the development of a complex structure, mimicking the tumor architecture. Indeed, these systems offer the possibility to generate a TME that more closely reproduces that present in the *in vivo* tumor than the stiff 2D petri dish. The 3D tumor models are crucial to study the influence of the spatial configuration of the cell surface receptors involved in cell-cell as well as cell-TME exchanges. Exploiting a simple 3D biosphere we have developed a method to embed GBM cells within a cross-linked alginate-gelatin matrix. We have observed that after 7 days of culture PDCs begin to form multicellular neurospheres that increase in size over time. Alginate and gelatin combination has been used as a biocompatible hydrogel bioink to embed cells for the use in 3D bioprinting. The alginate would give the viscosity and when cross-linked will afford mechanical support, while gelatin would give elasticity as well as bioactive would that

promote cell adhesion. Other 3D methods have been used to create multicellular neurospheres that use either physical confinement to force to form aggregation or the addition of Arg-Gly-Asp (RGD) peptide. The RGD motif is important for the interactions between cells and the ECM and is mediated by cell receptors called integrins thus the RGD peptide would act as integrin ligands. It should be noted that RGD motif is present in gelatin. The composite hydrogel created a biomimetic environment that facilitates the formation of neurospheres without the use of external stresses (**Jiang et al., 2017**).

It has been previously shown that chitosan-alginate 3D scaffolds could be used as a mimic of glioma microenvironment (**Kievit *et al*., 2010).** We show that our system constitutes an *in vitro* platform, which more accurately represents the tumor microenvironment for PDC, as the addition of CAFs, a constituent of tumors, is possible and had an influence to the cancer cells responses to treatments. This simple system can be used to understand the tumors components interactions and thus to develop new cancer therapeutics.

In addition, the mathematical analysis showed that some of the pathophysiological differences between the molecular subtypes that have been observed in GBM patients are also seen in these scaffolds. Mesenchymal tumors are known to have a more proliferative behavior and a worse prognosis, while proneural tumors are more related with an infiltrative or diffusive character. Our 3D biospheres has been able to mimic a very similar behavior, with mesenchymal tumors growing faster and forming compact and spherical structures, while proneural tumors give rise to both less compact and spherical structures, which could be explained due to their diffusive behavior and the tendency to form less cell clustering. To complete the analysis of how fast the different primary cultures grow and how compact of the resulting neurospheres are; the roundness or circularity of the different neurospheres was also studied. Circularity of four different primary cultures was compared among each other showing no significant differences. However, when we compared the circularity of the larger spheroids (in terms of area) to the smaller spheroids in each primary culture, we observed some differences. The variance in the circularity was much larger in the bigger structures in the proneural tumors (GBM3 and 8), with a very high statistical significance (5.7396×10^{-6} and 0.00047661), as shown in **Figure 4**. On the other hand, in the mesenchymal tumors (GBMA1 and 22), the significance of the differences in variance was much smaller or not significant (0.037342 and 0.38142).

Our results are in complete agreement with data presented in **De Witt Hamer *et al*. (2008)** suggesting that the cells cultured in 3D recapitulate a phenotype similar to that observed in the original tumor.

The development of tumoroid technology holds great promises for efficient and easy in vitro testing of new drugs and of new therapeutic approaches. Tumor-derived organoids are 3D structures that closely recapitulate tissue architecture and cancer cells composition (**Blue et al., 2020**). This has been established in several recent publications, which used for the most part cell line and rarely patient-derived primary cultures (**Dai et al., 2016; Herrera-Perez et al., 2018; Hubert et al., 2016; Ma et al., 2016**).

We have established a protocol, which has been used to generate tumoroids from GBM patients that can be co-cultivated with components of the TME with a remarkable high success (over 90%). We have found that these cultures exhibit gross morphologies and responses to TMZ, which is predictive for patient response to therapy.

The protocol and culture conditions described herein have been made simple in order to provide an easy and reliable clinically relevant model, which could be used to design personalized treatment in the vast majority of GBM patients. This constitutes a basic prerequisite for the use of tumoroids for the discovery of efficient therapies in this presently incurable tumor.

4. Materials and Methods

4.1 Materials

Unless stated otherwise, all cell culture material was obtained from Life Technologies (Cergy Pontoise, France) and chemicals were from Sigma-Aldrich (St. Louis, MO, USA).

4.2 Cell culture

After informed consent, tumor samples classified as Glioblastoma, based on the World health Organization criteria were obtained from patients undergoing surgical intervention at the "Dept. of Neurosurgery at "Centre Hospitalier Universitaire de Nantes" and the "Tumorothèque IRCNA". Within 4 h after surgical removal, Patient-Derived Cells (PDCs) were recuperated after mechanical dissociation as described in **Brocard *et al***. (2015). All procedures involving human participants were in accordance with the ethical standards of the ethic national research committee and with the 1964 Helsinki declaration and its later amendments or comparable ethical standards. At present 80 fresh samples obtained before treatment have been processed and stored in a biobank. Those used in this study are cited in **Table S1**. Primary GBM cells were cultured in defined medium (DMEM/F12 supplemented with 2 mM L-glutamine, N2 and B27 supplement, 2 μg/ml heparin, 20 ng/ml EGF, 40 ng/ml bFGF, 100 U/ml penicillin and 100 μg/ml streptomycin). All the experiments with primary GBM cells were performed at early passages. Cells were analyzed for mycoplasma regularly.

Bone marrow mesenchymal stem cells (MSCs) were obtained from the "Tumorothèque IRCNA" and cultured in DMEM complemented with 20% heat-inactivated fetal calf serum, 5 ng/ml bFGF, 100 U/mL penicillin and 100 µg/mL streptomycin in an atmosphere of 5% CO_2 and 95% humidity at 37°C. To prepare TASCs: MSCs were cultured in conditioned medium obtained from PDCs and defined medium at a ratio of 30:70 for at least 7 days.

4.3 Biosphere formation

Briefly, alginate and gelatin were dissolved in HBSS at a concentration of 8% and 10% (w/v) respectively. For the formation of the biospheres the 500 μl 8% alginate and 500 μl 10% gelatin were mixed and incubated for 1 h; after which 20 μl PDC suspension ($2x10^8$ cells) was added and the solution was mixed without forming air bubbles. Using a 200 μl pipette a single droplet of the alginate-gelatin-cell solution was added into wells of a 48-well plate containing 300 μl 200 mM $CaCl_2$. The $CaCl_2$ was replaced by 400 μl defined medium and incubated at 37°C for 30 min after which the medium was then replaced by fresh medium (**Figure S1**). The culture medium was replaced every 2-3 days over 21 days after which the cells were treated with 100 µM Temozolomide (TMZ) for 96 h.

To determine cell proliferation: a single biosphere was dissociated by incubation for 3 min incubation in 100 mM Na-Citrate. Cell counts and viability were analyzed using the Countess optics and image automated cell counter (Life Technologies). Cells were mixed with Trypan blue (1:1) and loaded into a Countess chamber slide. The image analysis software analyzed the acquired cell images to determine cell count and viability.

To analyze the morphology and to determine the length, **area and circularity of** spheroids in the biospheres; images were obtained from 5 areas in a single biosphere from a minimum of 10 biospheres per condition using a Zeiss microscope (Axio Observer and ZEN 2 program). The images obtained were analyzed using the FIJI program. Circularity, which is a measure that provides values approaching 1 when a 2D object is close to a circular shape and approaching 0 when it is highly irregular, is defined as:

$$\boldsymbol{Circ = 4\pi \frac{Area}{Perimeter^2}}$$

4.4 Determination of percentage of tumor initiating cells

Cells obtained either from biospheres or from 2D cultures were cultured in CellTak (Life Technologies) coated QIAscout 12 000-microraft plates (Qiagen, Courtaboeuf, France) for

24 h and then 200 rafts containing single cells were recuperated into 96-well plates. 20 days later the percentage of cells capable of forming colonies were determined.

4.5 Structure formation in biospheres

To analyze the formation of cell structures within the biospheres; whole biospheres were fixed for 30 min with 4% paraformaldehyde in 50 mM $CaCl_2$-HBSS then permeabilized with 0.1% Triton X-100 for 15 min at 37°C, washed with HBSS and stained with ActinGreen™ Ready Probe® reagent (Life Technologies) for 30 min at 37°C in the dark. After washing the biospheres were counterstained with Hoechst. The biospheres were analyzed using a confocal microscope.

4.6 FACS analysis, immunocytochemistry and immunohistochemistry

Biospheres were dissociated manually; cells were recuperated and washed then incubated 30 min with the primary antibody CD133-APC, CD44-APC, CD10-BV420 or CD90-PE. Data acquisition was performed on a FACS CANTO II (Becton Dickinson) and analyzed using the FlowLogic software (Miltenyi). For immunocytochemistry, biospheres were fixed with 4% paraformaldehyde for 1 h then permeabilized with 0.1% Triton X-100 for 30 min saturated with 5% BSA and then incubated with rabbit anti-human nestin (Proteintech, Rosemont, IL, USA) and mouse anti-human anti-GFAP (Proteintech). Secondary antibodies coupled to Alexafluor-488 or -568 was added and then the sections were analyzed under a confocal microscope (Nikon A1 Rsi, MicroPicell Facility).

To stain for glycoaminoglycans (GAGs) formaldehyde fixed paraffin-embedded (PPFE) sections of biospheres were colored with Alcian Blue (A5268, Sigma) and then counterstained with Kerechtrot (m00283, Diapath, Martinengo, Italy). The detection of collagen in FFPE sections was done using Masson's trichrome (F/010210, Microm Microtech, Brignais, France) and counterstained with Weigert's iron hematoxylin solution. Slides were analyzed after scanning with a Nanozoomer HAMAMATSU (MicroPicell Facility).

4.7 Statistical Analysis

Data were analyzed and statistical analyses were performed using GraphPad Prism 7.00 (GraphPad Software, San Diego, CA, USA). Data points are expressed as mean ± SD unless otherwise indicated. * $p<0.05$, ** $p<0.01$, *** $p<0.001$. To study the circularity, Levene quadratic test was performed. With this test it is possible to compare the variances for two or more groups, where the null hypothesis assumes all variances to be equal.

5. Credit author statement

Conceptualization: LO, VPG, FMV; Methodology: LO, AAA, JJS GFC, JBB, PL, LV, DH; Investigation: LO, CS, FG, AAA, JJS, SB; Writing - original draft: LO, FV; Writing - review & editing: LO, AAA, JJB, FV. Supervision: LO, FMV.

6. Funding information

This work is supported by grants from "Ligue Grand Ouest Contre le Cancer" and the "Plan Cancer/ HTE program "MoGlimaging", the Ministerio de Economía y Competitividad/FEDER, Spain [grant number MTM2015-71200-R] and James S. Mc. Donnell Foundation (USA) 21st Century Science Initiative in Mathematical and Complex Systems Approaches for Brain Cancer (Collaborative award 220020450). AAA was supported by a fellowship from UCLM [2015/4062].

7. Declaration of Competing interest

The authors declare no financial interests/personal relationships, which may be considered as potential competing interests.

8. Acknowledgements

We want to thank the members of the Department of Neurosurgery and Pathology at the CHU Nantes for providing GBM patient samples. The bio-collection used for this analysis is the Glioblastoma collection belonging to the pediatric research program of the University Hospital of Nantes (Ref MESR DC-2014-2206, having obtained a favorable opinion from CPP Ouest IV (Dossier 06/15) on 08 / 04/2015).

7. References

Bergfeld SA and DeClerck YA. Bone marrow-derived mesenchymal stem cells and the tumor microenvironment. Cancer Metastasis Rev. 2010;29(2):249-61. doi: 10.1007/s10555-010-9222-7.

Birgersdotter A, Sandberg R, Ernberg I. Gene expression perturbation in vitro - a growing case for three-dimensional (3D) culture systems. Semin Cancer Biol. 2005;15(5):405-12. doi: 10.1016/j.semcancer.2005.06.009.

Blue R, Miranda SP, Gu BJ, Chen HI. A primer on human brain organoids for the neurosurgeon. Neurosurgery. 2020;87(4):620-9. doi: 10.1093/neuros/nyaa171.

Bonneh-Barkay D and Wiley CA. Brain extracellular matrix in neurodegeneration. Brain Pathol. 2009;19(4):573-85. doi: 10.1111/j.1750-3639.2008.00195.x.

Borriello L, Nakata R, Sheard MA, Fernandez GE, Sposto R, Malvar J, et al. Cancer-associated fibroblasts share characteristics and protumorigenic activity with mesenchymal stromal cells. Cancer Res. 2017;77(18):5142-57. doi: 10.1158/0008-5472.CAN-16-2586.

Brocard E, Oizel K, Lalier L, Pecqueur C, Paris F, Vallette FM, et al. Radiation-induced PGE2 sustains human glioma cells growth and survival through EGF signaling. Oncotarget. 2015; 6(9):6840-9. doi: 10.18632/oncotarget.3160

Dai X, Ma C, Lan Q, Xu T. 3D bioprinted glioma stem cells for brain tumor model and applications of drug susceptibility. Biofabrication. 2016;8(4):045005. doi: 10.1088/1758-5090/8/4/045005.

De Witt Hamer PC, Van Tilborg AA, Eijk PP, Sminia P, Troost D, Van Noorden CJ, et al. The genomic profile of human malignant glioma is altered early in primary cell culture and preserved in spheroids. Oncogene. 2008;27(14):2091-6. doi: 10.1038/sj.onc.1210850.

Fallica B, Makin G, Zaman MH. Bioengineering approaches to study multidrug resistance in tumor cells. Integr Biol (Camb). 2011;3(5):529-39. doi: 10.1039/c0ib00142b.

Fong EL, Watson BM, Kasper FK, Mikos AG. Building bridges: leveraging interdisciplinary collaborations in the development of biomaterials to meet clinical needs. Adv Mater. 2012;24(36):4995-5013. doi: 10.1002/adma.201201762.

Gomez-Roman N, Stevenson K, Gilmour L, Hamilton G, Chalmers AJ. A novel 3D human glioblastoma cell culture system for modeling drug and radiation responses. Neuro Oncol. 2017;19(2):229-241. doi: 10.1093/neuonc/now164.

Griffith LG and Swartz MA. Capturing complex 3D tissue physiology in vitro. Nat Rev Mol Cell Biol. 2006;7(3):211-24. doi: 10.1038/nrm1858.

Griveau A, Seano G, Shelton SJ, Kupp R, Jahangiri A, Obernier K, et al. A glial signature and Wnt7 signaling regulate glioma-vascular interactions and tumor microenvironment. Cancer Cell. 2018;33(5):874-889.e7. doi: 10.1016/j.ccell.2018.03.020

Hanahan D and Weinberg RA. The hallmarks of cancer: the next generation. Cell. 2011;144(5):646-74. doi: 10.1016/j.cell.2011.02.013.

Hashimoto O, Yoshida M, Koma Y, Yanai T, Hasegawa D, Kosaka Y, et al. Collaboration of cancer-associated fibroblasts and tumour-associated macrophages for neuroblastoma development. J Pathol. 2016;240(2):211-23. doi: 10.1002/path.4769.

Herrera-Perez RM, Voytik-Harbin SL, Sarkaria JN, Pollok KE, Fishel ML, Rickus JL. Presence of stromal cells in a bioengineered tumor microenvironment alters glioblastoma migration and response to STAT3 inhibition. PLoS One. 2018;13(3):e0194183. doi: 10.1371/journal.pone.0194183.

Hevia-Montiel N, Rodriguez-Perez PI, Lamothe-Molina PJ, Arellano-Reynoso A, Bribiesca E, Alegria-Loyola MA. Neuromorphometry of primary brain tumors by magnetic resonance imaging. J Med Imaging (Bellingham). 2015;2(2):024503. doi:10.1117/1.JMI.2.2.024503.

Hirschhaeuser F, Menne H, Dittfeld C, West J, Mueller-Klieser W, Kunz-Schughart LA. Multicellular tumor spheroids: an underestimated tool is catching up again. J Biotechnol. 2010;148(1):3-15. doi: 10.1016/j.jbiotec.2010.01.012.

Hubert CG, Rivera M, Spangler LC, Wu Q, Mack SC, Prager BC, et al. A three-dimensional organoid culture system derived from human glioblastomas recapitulates the hypoxic gradients and cancer stem cell heterogeneity of tumors found in vivo. Cancer Res. 2016;76(8):2465-77. doi: 10.1158/0008-5472.CAN-15-2402.

Huijbers IJ, Iravani M, Popov S, Robertson D, Al-Sarraj S, Jones C, et al. A role for fibrillar collagen deposition and the collagen internalization receptor endo180 in glioma invasion. PLoS One. 2010;5(3):e9808. doi: 10.1371/journal.pone.0009808.

Jiang T, Munguia-Lopez JG, Flores-Torres S, Grant J, Vijayakumar S, Leon-Rodriguez A, et al. Directing the self-assembly of tumour spheroids by bioprinting cellular heterogeneous

models within alginate/gelatin hydrogels. Sci Rep. 2017;7(1):4575. doi: 10.1038/s41598-017-04691-9.

Jubran MR, Rubinstein AM, Cojocari I, Adejumobi IA, Mogilevsky M, Tibi S, et al. Dissecting the role of crosstalk between glioblastoma subpopulations in tumor cell spreading. Oncogenesis. 2020;9(2):11. doi:10.1038/s41389-020-0199-y.

Kievit FM, Florczyk SJ, Leung MC, Veiseh O, Park JO, Disis ML, et al. Chitosan-alginate 3D scaffolds as a mimic of the glioma tumor microenvironment. Biomaterials. 2010;31(22):5903-10. doi: 10.1016/j.biomaterials.2010.03.062.

Leitinger B. Transmembrane collagen receptors. Annu Rev Cell Dev Biol. 2011;27:265-90. doi: 10.1146/annurev-cellbio-092910-154013.

Lv D, Yu S-C, Ping Y-F, Wu H, Zhao X, Zhang H, et al. A three-dimensional collagen scaffold cell culture system for screening anti-glioma therapeutics. Oncotarget. 2016;7(35):56904-56914. doi: 10.18632/oncotarget.10885.

Ma NK, Lim JK, Leong MF, Sandanaraj E, Ang BT, Tang C, et al. Collaboration of 3D context and extracellular matrix in the development of glioma stemness in a 3D model. Biomaterials. 2016;78:62-73. doi: 10.1016/j.biomaterials.2015.11.031.

Mishra PJ, Mishra PJ, Humeniuk R, Medina DJ, Alexe G, Mesirov JP, et al. Carcinoma-associated fibroblast-like differentiation of human mesenchymal stem cells. Cancer Res. 2008; 68(11):4331-9. doi: 10.1158/0008-5472.CAN-08-0943.

Pérez-Beteta J, Molina-García D, Ortiz-Alhambra JA, Fernández-Romero A, Luque B, Arregui E, et al. Tumor surface regularity at MR imaging predicts survival and response to surgery in patients with glioblastoma. Radiology 2016;288(1):218-25. doi: 10.1148/radiol.2018171051.

Pine AR, Cirigliano SM, Nicholson JG, Hu Y, Linkous A, Miyaguchi K, et al. Tumor microenvironment is critical for the maintenance of cellular states found in primary Glioblastomas. Cancer Discov 2020;10(7):964-79; doi: 10.1158/2159-8290.CD-20-0057.

Qazi MA, Vora P, Venugopal C, Sidhu SS, Moffat J, Swanton C, et al. Intratumoral heterogeneity: pathways to treatment resistance and relapse in human glioblastoma. Ann Oncol. 2017;28(7):1448-56. doi: 10.1093/annonc/mdx169.

Ruiz-Ontañon P, Orgaz JL, Aldaz B, Elosegui-Artola A, Martino J, Berciano MT, et al. Cellular plasticity confers migratory and invasive advantages to a population of glioblastoma-initiating cells that infiltrate peritumoral tissue. Stem Cells. 2013;31(6):1075-85. doi: 10.1002/stem.1349.

Singh SK, Hawkins C, Clarke ID, Squire JA, Bayani J, Hide T, et al. Identification of human brain tumour initiating cells. Nature. 2004;432(7015):396-401. doi: 10.1038/nature03128.

Stupp R, Hegi ME, Mason WP, van den Bent MJ, Taphoorn MJ, Janzer RC, et al. Effects of radiotherapy with concomitant and adjuvant temozolomide versus radiotherapy alone on survival in glioblastoma in a randomised phase III study: 5-year analysis of the EORTC-NCIC trial. Lancet Oncol. 2009;10(5):459-66. doi: 10.1016/S1470-2045(09)70025-7.

Stupp R, Mason WP, van den Bent MJ, Weller M, Fisher B, Taphoorn MJ, et al. Radiotherapy plus concomitant and adjuvant temozolomide for glioblastoma. N Engl J Med. 2005; 352(10):987-96. doi: 10.1056/NEJMoa043330.

Ulrich TA, de Juan Pardo EM, Kumar S. The mechanical rigidity of the extracellular matrix regulates the structure, motility, and proliferation of glioma cells. Cancer Res. 2009;69(10):4167-74. doi: 10.1158/0008-5472.CAN-08-4859.

Virga J, Szemcsák CD, Reményi-Puskár J, Tóth J, Hortobágyi T, Csősz É, et al. Differences in extracellular matrix composition and its role in invasion in primary and secondary intracerebral malignancies. Anticancer Res. 2017;37(8):4119-26. doi: 10.21873/anticanres.11799.

William D, Mullins CS, Schneider B, Orthmann A, Lamp N, Krohn M, et al. Optimized creation of glioblastoma patient derived xenografts for use in preclinical studies. J Transl Med. 2017;15(1):27. doi: 10.1186/s12967-017-1128-5.

Legends to Figures:

Figure 1: Cell proliferation in 3D biospheres. A. Protocol for the construction of 3D biospheres. **B.** PDCs (GBM69) were cultured in 3D biospheres composed of either laminin (Lam: 0.3 or 0.6 mg/ml) or gelatin (Gel: 1% or 2%) and cell number was determined over time. This experiment is representative of 3 experiment performed using different PDCs. **C.** Representative cell morphology of GBM69 cells cultured in biospheres shown in (**B**) was photographed at different times. Proliferation of PDCs (GBM71) in biospheres composed either of 1.25%, 2.5% and 5% gelatin (**D)** or 0.25, 0.5 and 2 mg/ml collagen (Coll) **(E).** Data shown are representative of 3 different primary GBM cultures.

Figure 2: Validation of the composition of bioink. A. Biospheres were made using different initial cell numbers to determine the optimal cell number required to initiate spheroid formation in 3D biospheres. The data presented is that of GBM69 cells but is representative of 3 different PDCs. **B.** The proliferation of PDCs embedded in either collagen- (Coll) or gelatin (Gel)-containing biospheres was determined over 21 days. The initial cell number was as determined in **A** (i.e. $4x10^4$). **C.** The images of the morphology of the cellular network formed with GBM22 cells cultured in gelatin (Gel) or collagen (Coll) containing biospheres over 3 weeks. 30 biospheres were prepared for each condition and 4 representative pictographs were taken of each biosphere. **D.** Analyses of the mean structure length of the spheroids present in the biospheres over time. The length of the spheroids were determined from the pictographs obtained in (**C**) using Image J, an average of 200 spheroids were measured at each time point. For **B**, **C** and **E** 4 different PDCs were used and the data presented is that of GBM22 cells.

Figure 3: Interaction cell-cell in 3D biospheres. A. FACS analyses of the expression of CD44, CD90 and CD133 in GBMA1 cells (subtype: mesenchymal) obtained from either 2D cultures or 3D biospheres composed of either 2.5% gelatin (Gel) or 2 mg/ml collagen (Coll). **B.** FACS analyses of the expression of CD44, CD90 and CD133 in GBM8 cells (subtype: proneural) obtained from either 2D cultures or 3D biospheres composed of 2.5% gelatin (Gel). The results are representative of 3 experiments. **C.** Determination of the percentage of GSCs present in GBMA1 cells obtained from either 2D cultures or 3D biospheres as expressed as the percentage of colonies formed. **D.** Whole biospheres, obtained on day 21, prepared using GBM69 cells were labeled for GFAP (green), nestin (red) and nuclei (blue). The insert is a magnification of 5x of a section of the merge shows tubular interactions

between the cells as well as the double labeling of some cells for both nestin and GFAP. **E**. Histological staining for collagen (**a**) and GAGs (**b**) in FFPE sections of biospheres using GBM3 cells collected after 21 days in culture. Data shown are representative of 3 different primary GBM cultures. Data shown are representative of 3 different PDC cultures.

Figure 4: Mathematical determination of cell proliferation and compactness. A. Boxplot of the doubling time of 4 PDC cultures (2 proneural subtypes: GBM3 and GBM8 and 2 mesenchymal subtypes: GBM22 and GBMA1). Where *n* is the number of experiments used to determine the average rate. **B.** Image from a biosphere showing spheroids and indicating the diameter (μm) and area (μm^2) of each spheroid measured. **D.** Boxplots of the distribution of the area of the spheroids measured as in **C**. for GBM22 on day 3, 8 and 16.

Figure 5: Mathematical comparison of structural shapes. A. Graph showing the experimental growth of GBM22 PDCs and the calculated exponential growth required evaluating the estimated proliferation time τ. Boxplots of two examples of PDCs in biospheres: (**B**) GBM22 cells which form dense spheroids and (**C**) GBM8 cells which form less compact spheroids. Data is presented as areas of the spheroids measured in the biospheres on day 3, 8 and 16 for GBM22 and on day 1, 7, 14 and 18 for GBM8. Two examples for the same PDC culture are represented (E and S).

Figure 6: Analysis of circularity. Boxplots of the circularity in small and large structures in biospheres in two proneural PDCs (**A**, **B**: GBM3 and GBM8) were compared to two mesenchymal PDCs (**C**, **D**: GBMA1 and GBM22). The data presented show no statistical differences between small and large spheroids in GBMA1 ($p = 0.037342$) and in GBM8 ($p = 0.38142$) biospheres, however, significant differences were present in GBM3 ($p = 5.7396 \times 10^{6}$) and GBM8 ($p = 0.00047661$) biospheres. Statistical analyses were performed using the Levene quadratic test. **E.** Boxplots of sphericity in small and large tumors. Data presented show statistical differences between small and large tumors ($p = 0.000228$). Tumor cohort extracted from GLIOMAT project. Tumor volumes were determined from MRI segmentation.

Figure 7: Intercellular exchange with the TME. A. Proliferation of monocultures of TAFs in 3D biospheres. The initial cell number was 4×10^4 cells/biospheres. **B.** Pictographs depicting the morphology of TAFs cultured in biospheres over 21 days. **C.** Pictograph on day 14 of the cells in co-cultures of GFP-labeled TAFs and PDCs (GBM8) in biospheres. Results

are representative of experiment was done with 5 different PDCs. **D.** Proliferation of GBM8 cells cultured in the absence or presence of TAFs at a ratio of 5:1 in biospheres. Statistical analyses were done using grouped 2way ANOVA. **E.** Analysis of the length of the spheroids formed in biospheres of mono- and co-cultures GBM8 cells and TAFs. Statistical analyses was performed with by grouped 2way ANOVA **F.** Quantification of the proliferation in biospheres of mono- and co-cultures GBM8 cells or GBM8 cells plus TAFs treated with 100 µM TMZ for 96 h. Data present are representative of 4 different experiments using different PDCs and/or TASCs.

Figure

Click here to download Figure: Figures Oliver et al.pptx

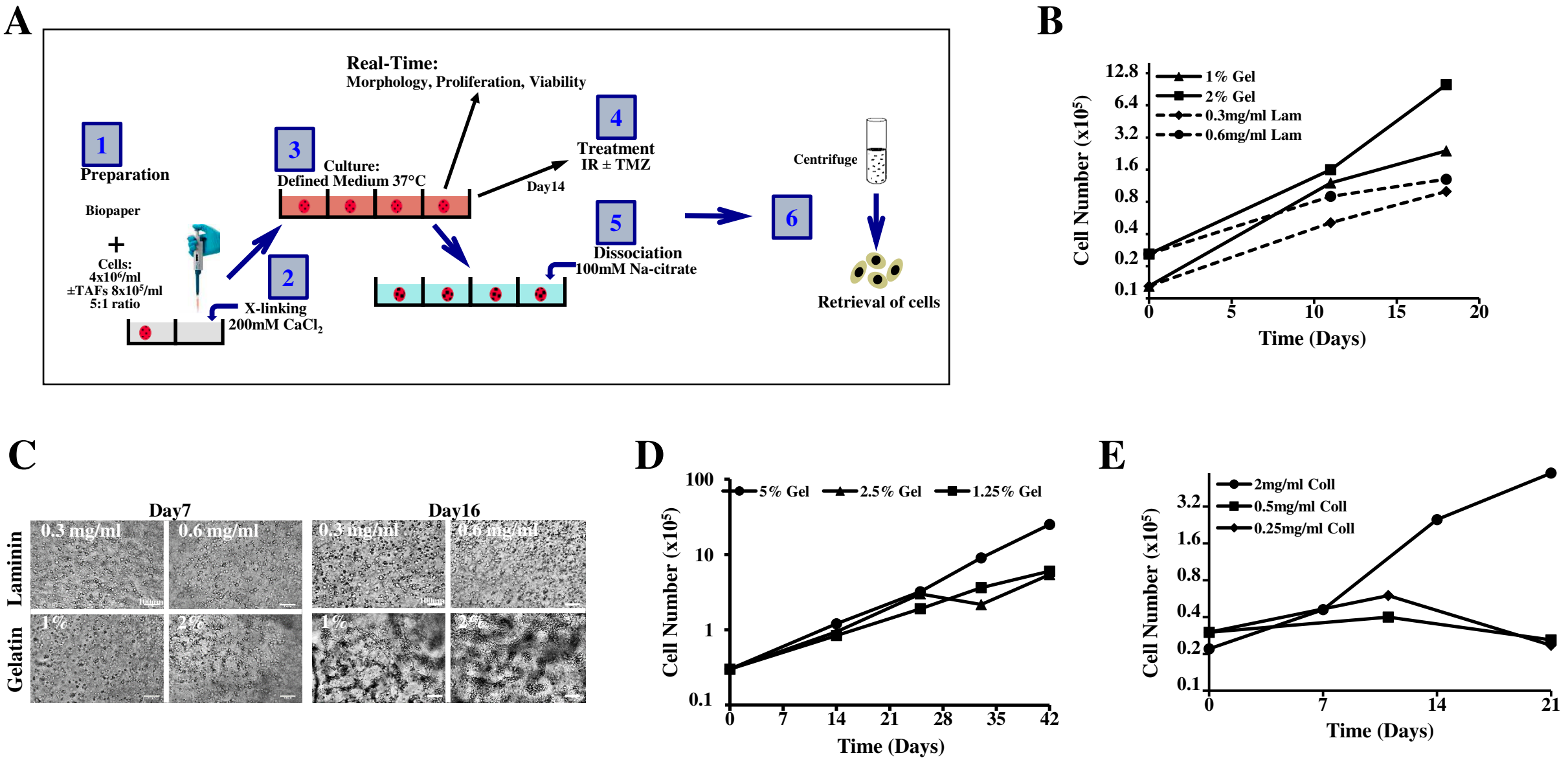

Figure 1: Oliver et al.

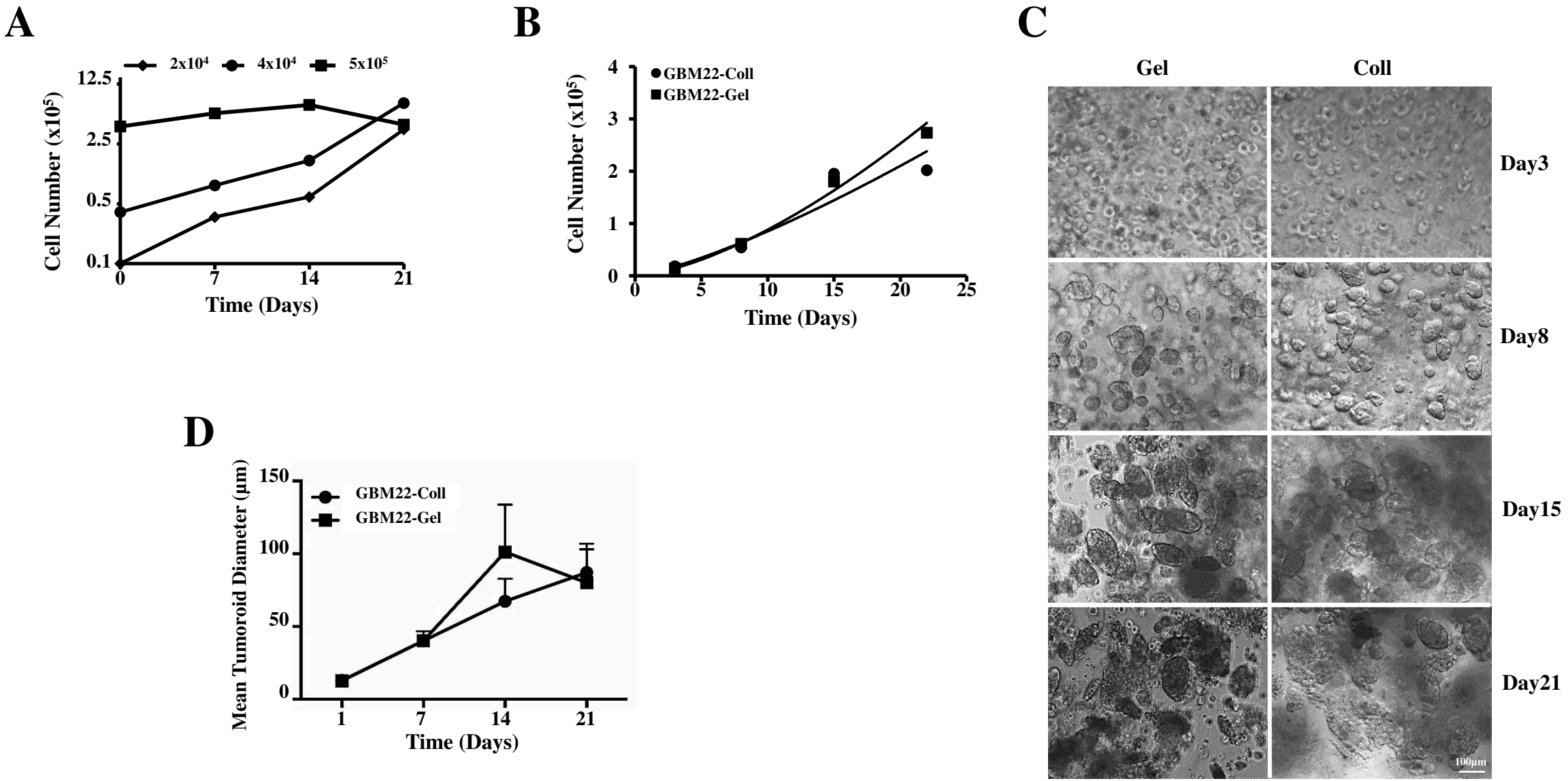

Figure 2: Oliver et al.

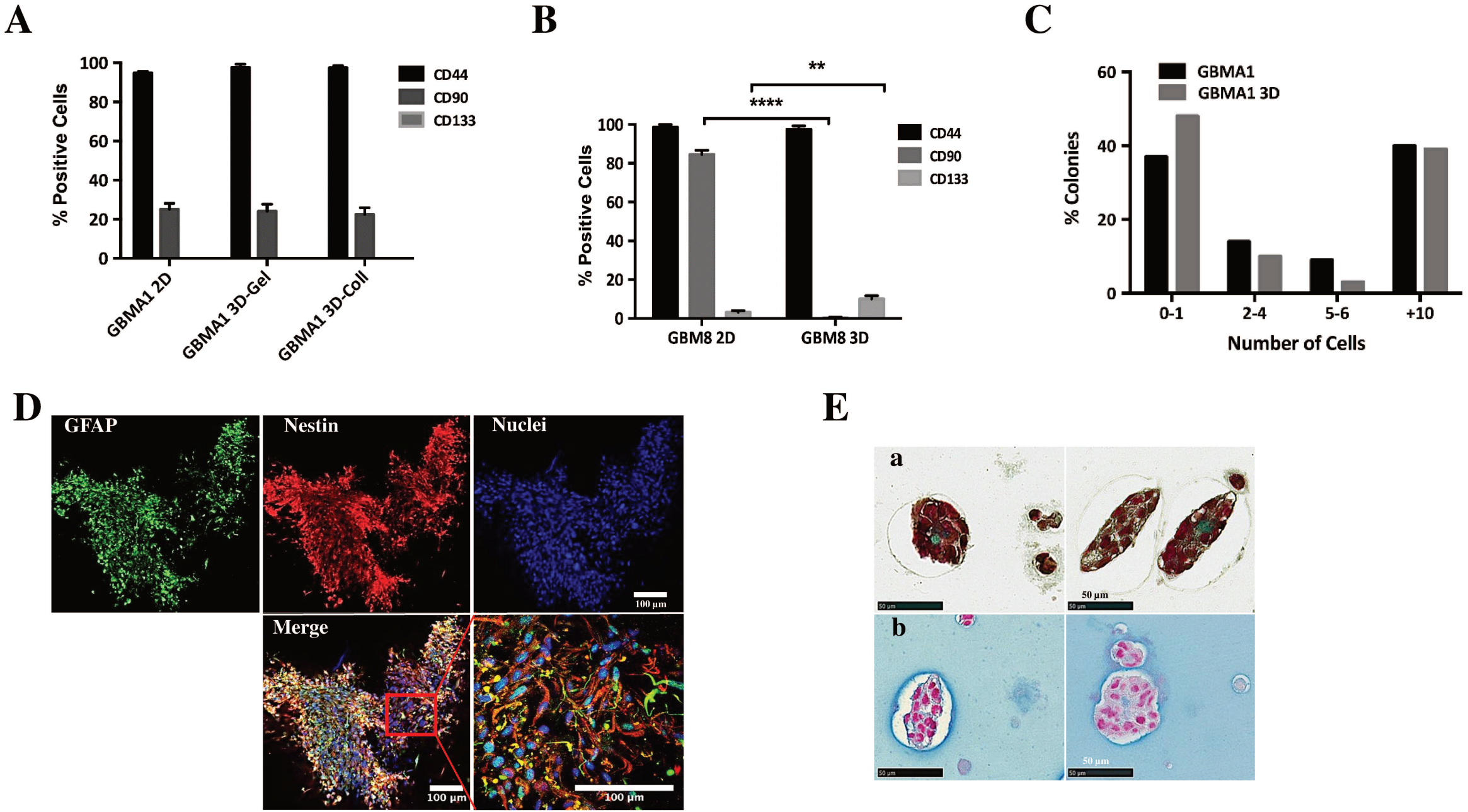

Figure 3: Oliver et al.

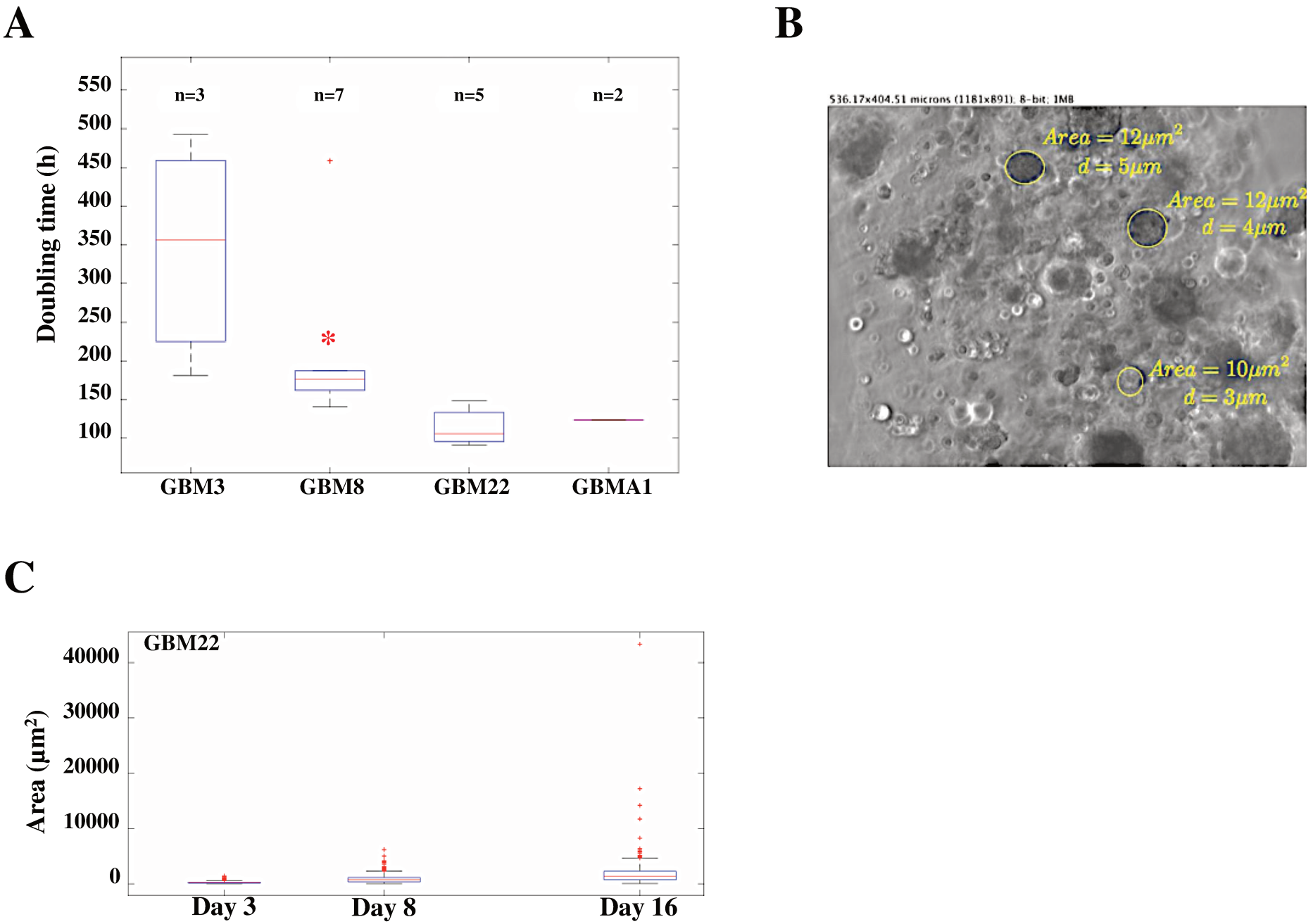

Figure 4: Oliver et al.

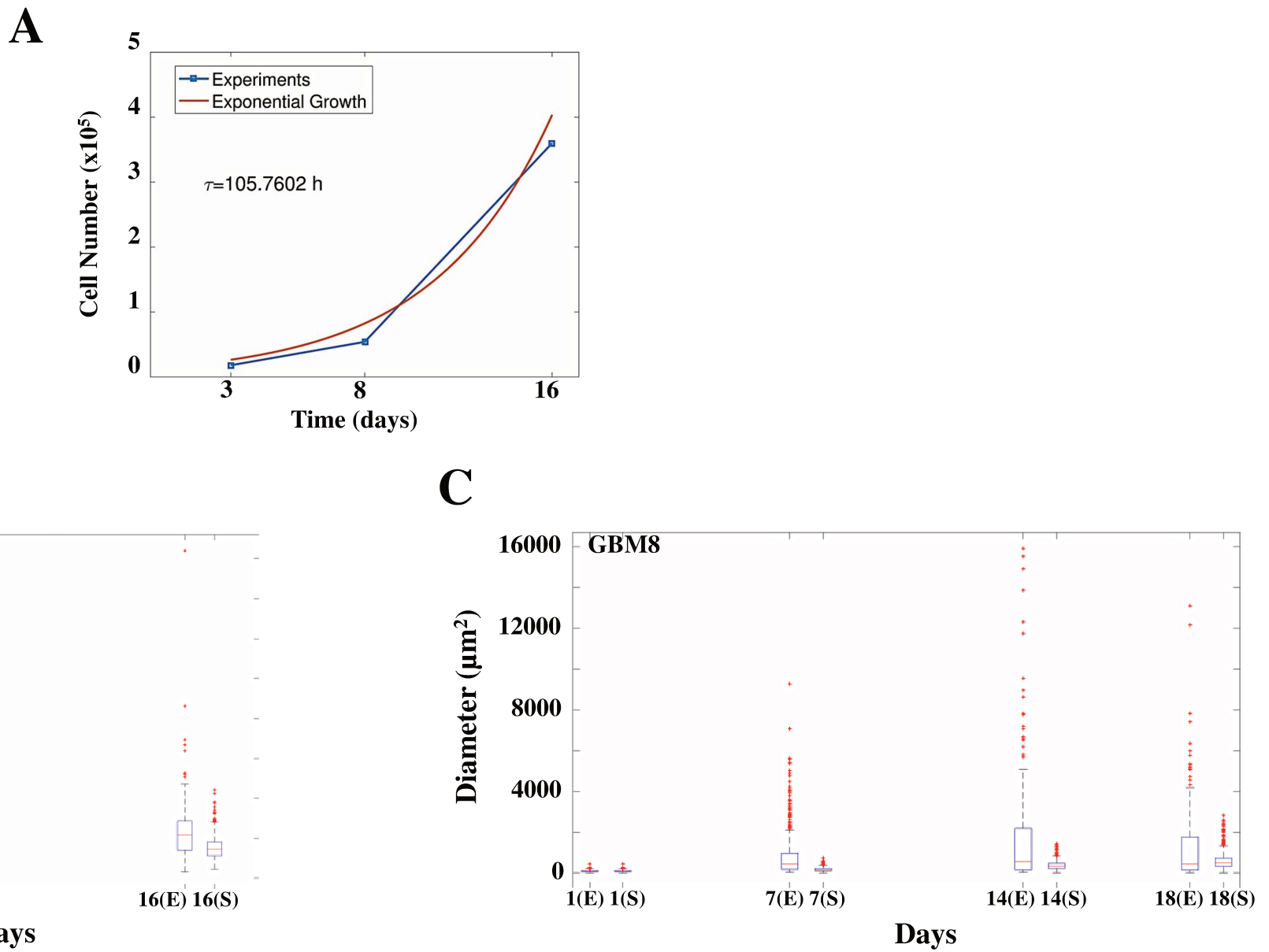

Figure 5: Oliver et al.

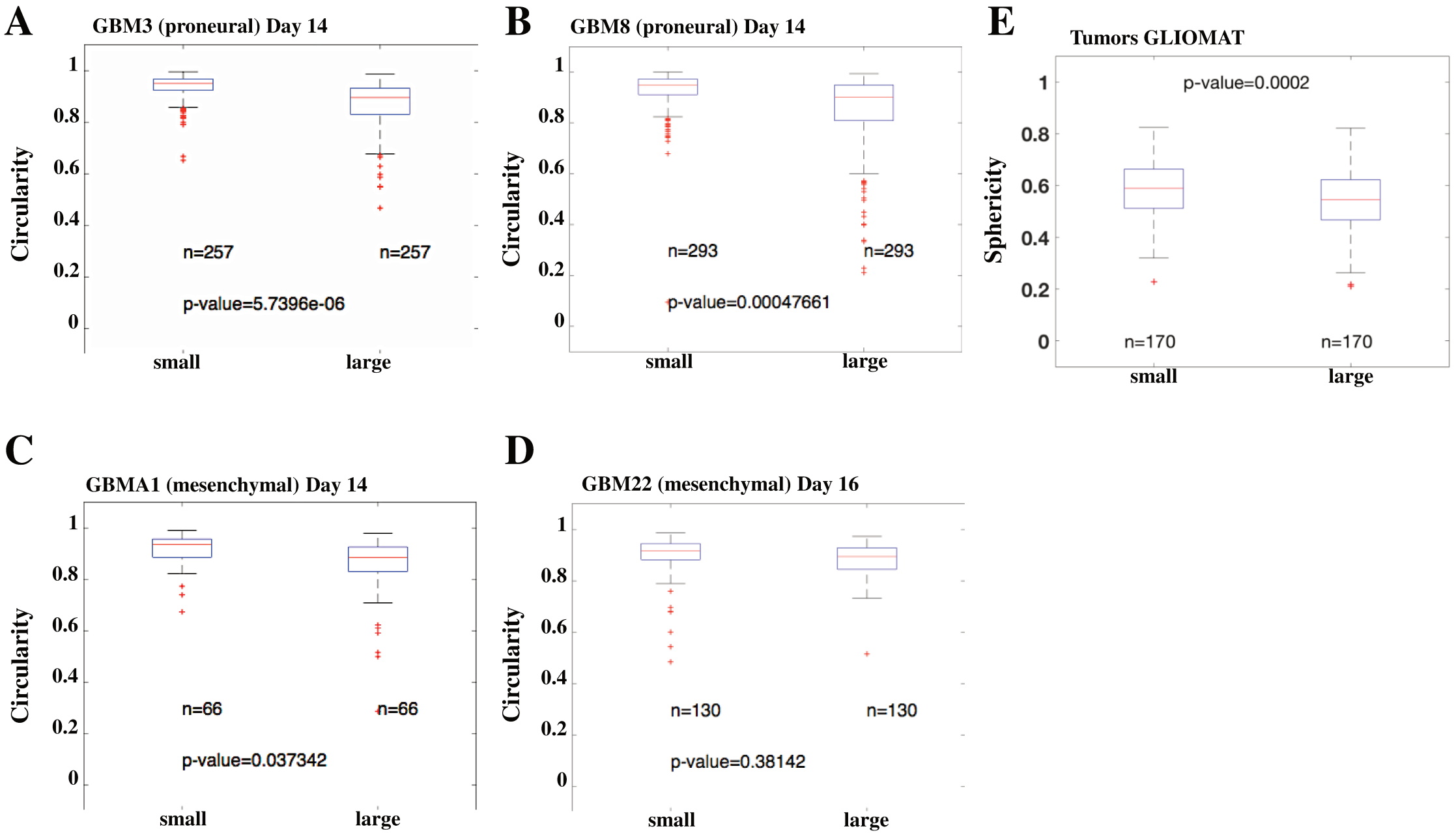

Figure 6: Oliver et al.

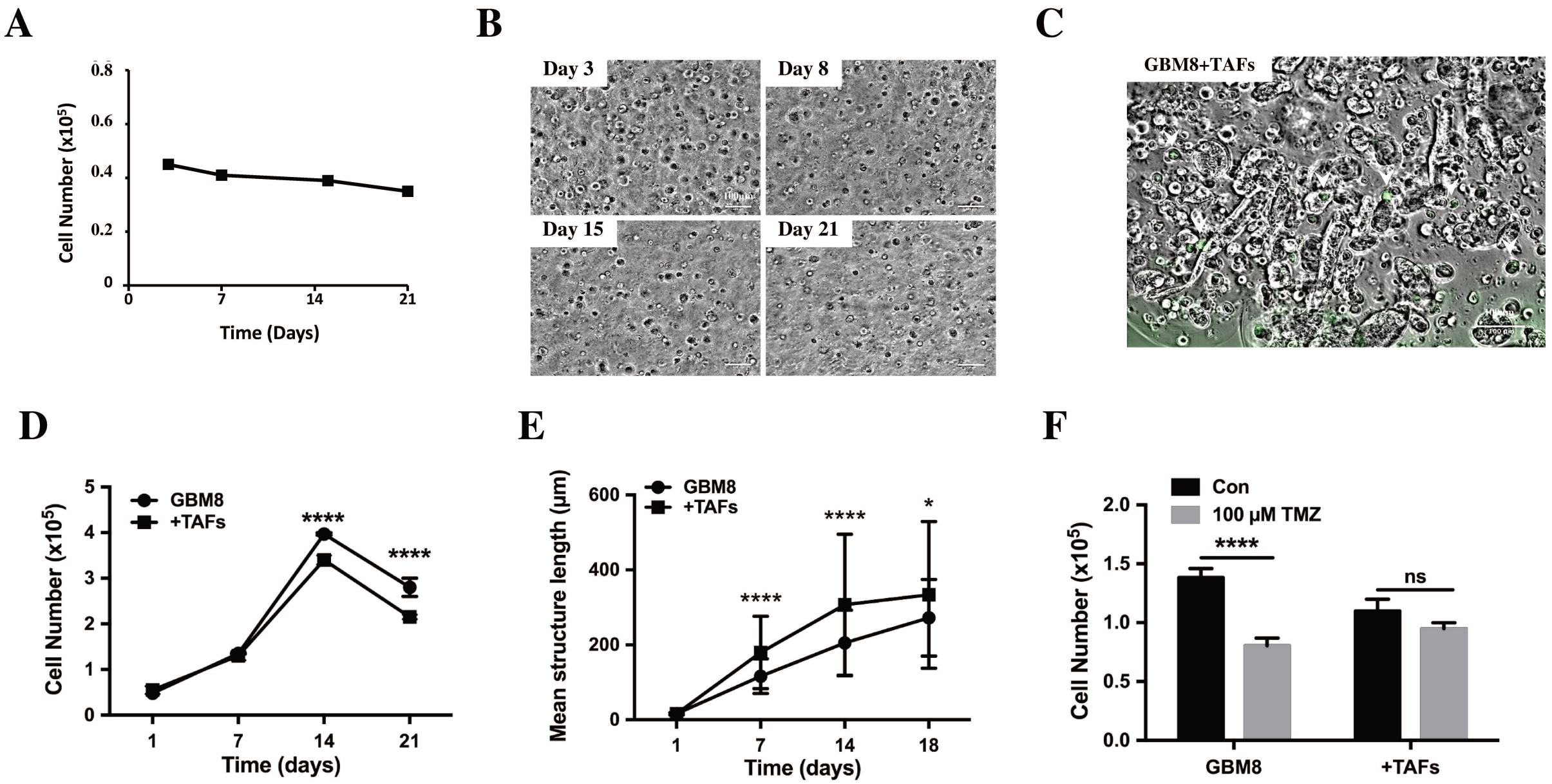

Figure 7: Oliver et al.

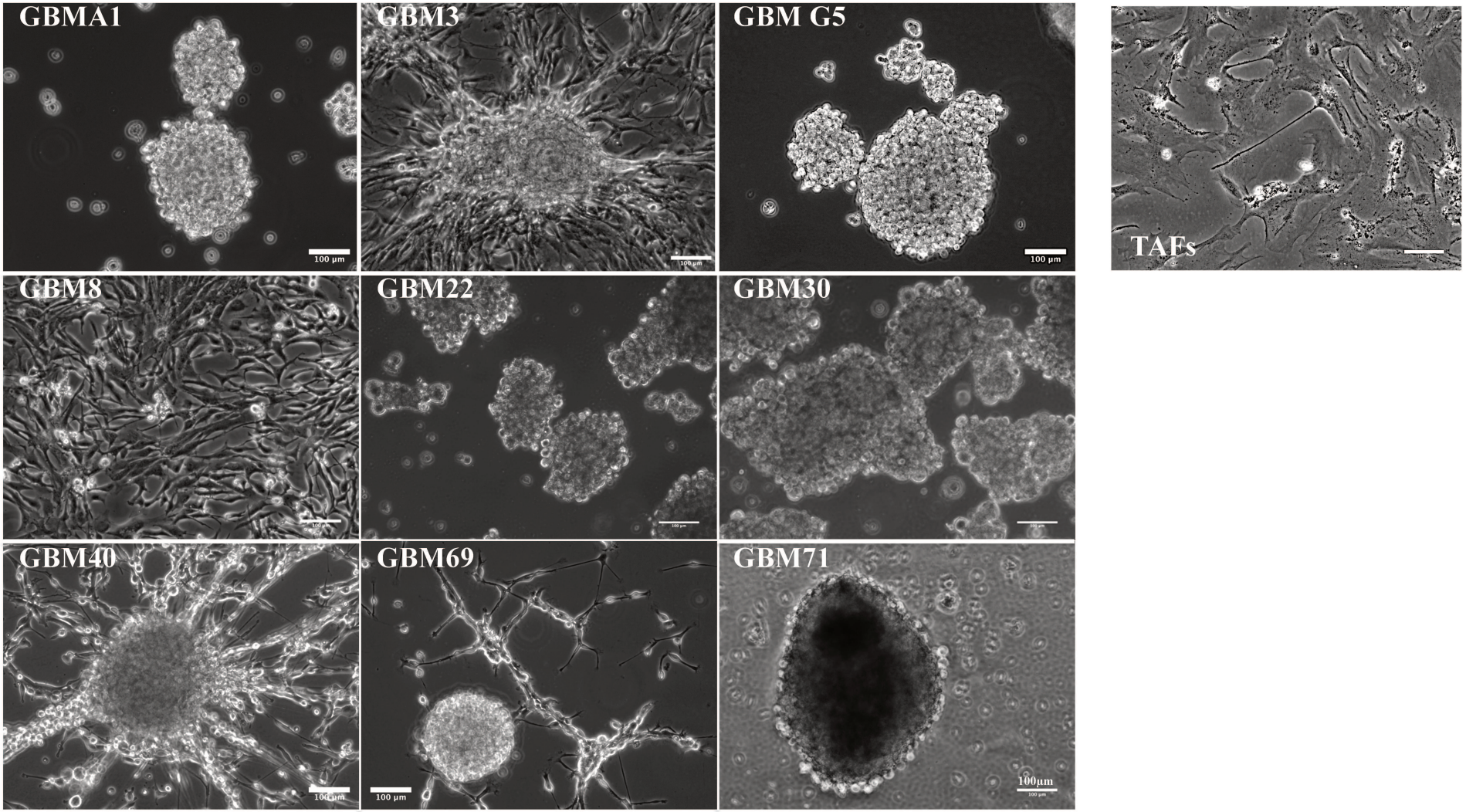

Figure S1: Oliver et al.

GBM	Type	Morphology	Subtype	Treatment	Survival (months)
GBMA1	GBM IV	neurospheres	mesenchymal	Stupp	?
GBM3	GBM IV	adherent	proneural	Stupp	13 m
GBMG5	GBM IV	neurospheres	proliferative	no	?
GBM8	GBM IV	neuro/adherent	proneural	no	7 m
GBM22	GBM IV	neurospheres	mesenchymal	Stupp	15 m
GBM30	GBM IV	neurospheres	mesenchymal	Stupp	18 m
GBM40	GBM IV	neuro/adherent	nd	Stupp	17 m
GBM69	GBM IV	neuro/adherent	mesenchymal	Stupp	16 m
GBM71	GBM IV	neurospheres	mesenchymal	Stupp	14 m

Table S1: Oliver et al.

2.2 RESULTATS NON PRESENTES DANS L'ARTICLE

Caractérisation des tumoroïdes obtenus par scaffold ou biosphères :

Nous avons démontré au sein des tumoroïdes obtenus par primoculture de cellules cancéreuses que leur organisation se rapproche de l'organisation du GBM chez le patient. En périphérie sont retrouvées les cellules actives proliférentes et au centre beaucoup moins de cellules correspondant au centre nécrotique (Figure 12).

Nous sommes en collaboration avec Alicia Martinez Gonzalez (mathématicienne espagnole). Cette collaboration permet l'analyse de la densité, de la morphologie et de l'expansion des biosphères sur une période de plusieurs mois en comparaison à la morphologie à l'IRM de la tumeur du patient duquelle dérive le tumoroïde étudié.

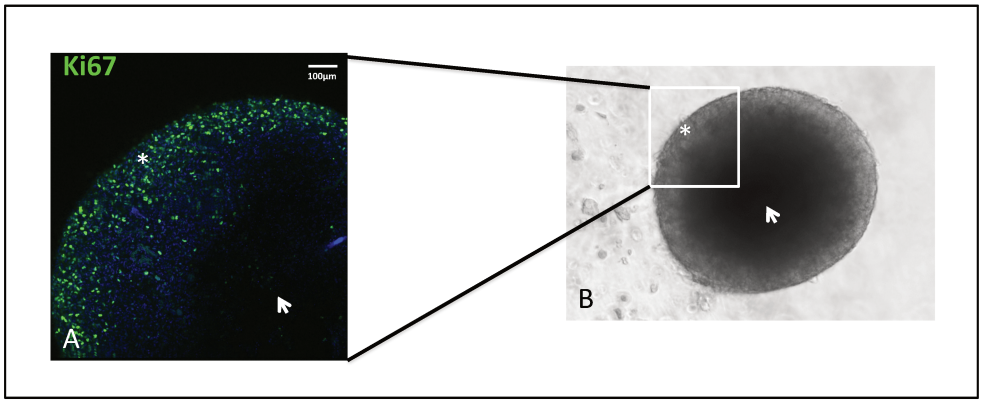

Figure 12. Architecture du tumoroïde de cultures de cellules cancéreuses de GBM au sein d'une biosphère A. Tumoroïde marqué au KI67 obtenue par microscopie confocale, **B** photographie microscopique d'un tumoroïde dans une biosphère En périphérie du tumoroïde se trouvent les cellules actives proliférantes index KI67 élevé (astérisques blanches), au centre l'index KI67 est quasi nul témoignant de l'absence de cellule proliférante dans le centre nécrotique (tête de flèche blanche).

Comme décrit dans l'article, nous avons mis en évidence la production, l'organisation et la composition de la MEC créé au sein des tumoroïdes dans les biosphères. Nous avons également mis en évidence la présence de la MEC au sein des scaffolds (Figure 13).

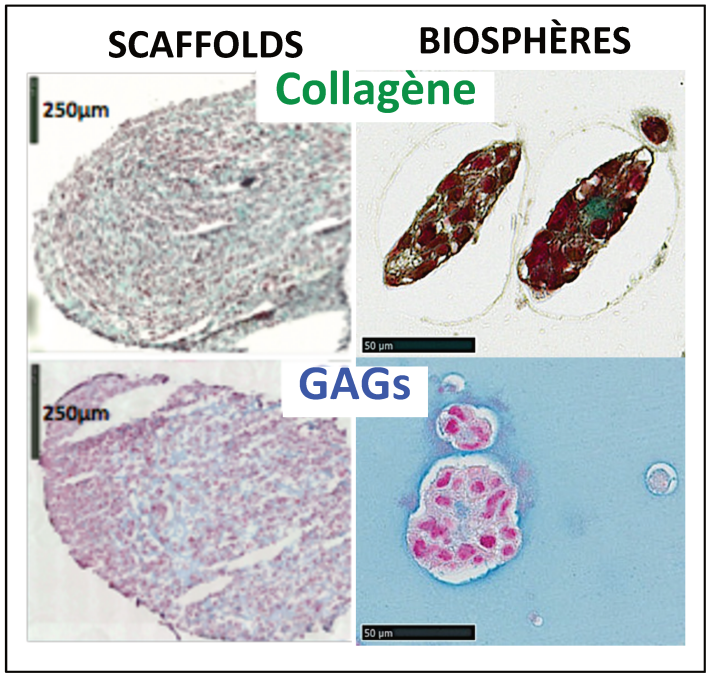

Figure 13. Caractérisation de la matrice extracellulaire présente dans les tumoroïdes. Immunohistochimies de tumoroïdes présents dans les scaffolds et biosphères, marquage de la MEC, mise en évidence de collagène et de glycoaminoglycanes (GAG).

Comme nous l'avons expliqué dans l'introduction, les deux types de bioimpression (manuelle par biosphères et automatisée par scaffolds) sont complémentaires (Tableau 2). Notre expérience nous a permis d'identifier pour chacune leurs avantages et inconvénients complémentaires. L'une ou l'autre de ces techniques est choisie en fonction du sujet étudié et de ses besoins.

	BIOSPHÈRES	SCAFFOLDS
Durée manipulation	Max 4 semaines	5 à 6 mois
Taille du réseau cellulaire	Petite	Très grande
Nombre de cellules	Raisonnable	Très consommateur
Séparation des différentes populations cellulaires	impossible	Possible dans les 3 plans
Évolution dans le temps	Cellules sortent des biosphères	Bonne tenue
Analyse pendant la manipulation	Oui (diamètre, nombre cellules) Pas de migration possible	Non pas assez de scaffolds Migration visible
Analyse morphologique	Facile à chaque étape	Difficile
Nombre	Illimité	40 max/manip
Réseau cellulaire	+	+++++
Début du traitement	Dès J14	De 1 à 4 mois

Tableau 2. Avantages et inconvénients des techniques de bioimpression par biosphères ou scaffolds

2.3 PERSPECTIVES :

Ces résultats représentent les bases techniques de création de notre modèle de tumoroïde de cultures primaires de GBM. Il recrée les caractéristiques architecturales des GBM. Il s'agit donc bien d'un tumoroïde. Ce modèle est validé en tant que tel grâce à l'analyse mathématique démontrant sa reproductibilité. Nous sommes capables de créer pour chaque tumeur de patient opéré son tumoroïde. Nous pouvons mettre en culture les cellules cancéreuses et les CAF propres à chaque patient. Ce modèle permet d'étudier les mécanisme de résistance et de tester des traitements, il faut également poursuivre l'amélioration de ce modèles en y rajoutant les autres éléments du MET.

3 A 3D MODEL TO STUDY THE ROLE OF THE TUMOR MICROENVIRONMENT IN RESPONSE TO TREATMENT IN GLIOBLASTOMAS

Le MET est déterminant dans l'initiation, l'évolution et la résistance des cancers. Comme expliqué précédemment, les CAF font partie des cellules du MET décrits comme essentiels dans la résistance au traitement entre autre pour les GBM. Un des intérêts des modèles 3D est de « décortiquer » les phénomènes et étapes de chaque cancer. La co-culture de CAF et de cellules cancéreuses permet donc d'analyser le rôle spécifique des CAF dans chaque cancer.

Grâce à la validation de notre modèle de tumoroïde de co-culture de CAF et de cellules cancéreuses de GBM, nous sommes dans la capacité d'étudier les interactions entres ces deux types de cellules. Nous avons également analysé le rôle des CAF face au traitement par radio et chimiothérapie.

3.1 PRINCIPAUX RESULTATS :

- La présence des CAF influence la croissance et l'organisation du tumoroïde.
- Les CAF permettent aux cellules cancéreuses d'augmenter leurs tight-junctions rendant le tumoroïde en périphérie plus dense.
- Cette architecture de surface permet de protéger les cellules cancéreuses des effets de la radiothérapie et de la chimiothérapie isolée ou en traitement combiné.
- Nous avons démontré qu'il existait beaucoup plus de mitochondries fonctionnelles présentes dans les cellules cancéreuses en présence des CAF.

ARTICLE 3

A 3D model to study the role of the tumor microenvironment in response to treatment in Glioblastomas

Céline Salaud[1,2,3], Juan Jimenez-Sanchez[4], Fanny Geraldo[1,2], Juan Belmonte-Beitia[4], Gabriel F. Calvo[4], Dominic Heymann[1,2,7,8], François M. Vallette[1,2,7] , Lisa Oliver[1,2,3].

[1] CRCINA - INSERM U1232, Nantes 44007 France

[2] Faculté de Médecine, Université de Nantes, Nantes 44007 France

[3] Centre Hospitalier-Universitaire (CHU) de Nantes, Nantes 44007 France

[4] Department of Mathematics & MOLAB-Mathematical Oncology Laboratory, University of Castilla-La Mancha, 13071, Ciudad Real, Spain

[7] LaBCT- Institut de Cancérologie de l'Ouest - René Gauducheau, St Herblain

[8] ICO - Institut de Cancérologie de l'Ouest - René Gauducheau, St Herblain

Corresponding authors: lisa.oliver@univ-nantes.fr

francois.vallette@inserm.fr

CRCINA INSERM U1232 Université de Nantes

8 quai Moncousu, 44007 Nantes, France

Tel: +(33)2 2808 0325; Fax: +(33)2 2808 0204

Keywords: Bioprinting, Glioma and TAFs

Running title: A 3D method for culturing Glioma cells

Abbreviations: Cancer associated fibroblasts (CAFs); cancer stem cells (CSCs); extracellular matrix (ECM); extracellular acidification rate (ECAR); Glioblastoma (GBM); glycosaminoglycans (GAGs); irradiation (IR); mesenchymal stem cells (MSCs); median fluorescence index (MFI); mitochondria (Mito); MitoTracker (MitoT); oxygen consumption rate (OCR); Reactive oxygen species (ROS); tumor microenvironment (TME); tunneling nanotubules (TNTs); tumor-activated stromal cells (TASCs); Temozolomide (TMZ).

ABSTRACT

The cellular hierarchy present in Glioblastomas (GBM) is driven by both the tumor-initiating cancer stem cells (CSCs) and intricate interactions with the tumor microenvironment (TME). The TME has increasingly been recognized as being important as a regulator of tumor development and progression. Current two-dimensional (2D) cell culture methods do not reproduce the *in vivo* tumor architecture or TME and contain none of the tumor heterogeneity present in patient tumors. In this study we have developed a three-dimensional (3D) culture model to investigate the effects of patient-derived primary cultures and cancer-activated stromal cells (TASCs). We have previously shown that this 3D-model supports long-term growth and retains the heterogeneity present the tumor *in vivo*. An analysis of mono- vs. co-cultures containing TASCs depicts the role of the stromal cells present in the TME on the proliferation of the tumor cells and the response of the tumor cells to treatment. We also show that the effect(s) of the TASCs on tumor cells is present even after the tumor cells consumed all the TASCs.

INTRODUCTION

Glioblastoma (GBM) is the most deadly malignant brain tumor, for which there is currently no cure (**Louis *et al*., 2016**). The standard treatment for GBM patients involves neurosurgical resection followed by combined radio- and chemotherapy (**Stupp *et al*., 2005, 2009**). The median survival of these patients is about 15 months. This therapeutic failure is due to the presence of treatment-resistant tumor-initiating cells or glioma stem cells (GSCs) (**Singh *et al*., 2004**). Another possible reason is the absence of a clear boundary between the tumor and the surrounding brain parenchyma, which complicates complete surgical resection and subsequently within months after surgery recurrent tumors are initiated in the resected region (**Holland *et al*., 2000**). These tumors exhibit molecular heterogeneity among patients as well as within the same tumor. Inter- and intra-tumoral heterogeneity is problematic for attaining a long-lasting therapeutic response. Heterogeneous cell populations are difficult to treat, as specificity and efficacy are not feasible throughout the population (**Fallica *et al*., 2011; Fong *et al*., 2012**).

Like all solid tumors, GBMs are an intricate amalgam of tumor cells, non-tumor cells including fibroblasts, vascular endothelial cells and immune cells, and extracellular matrix (ECM), which make up the tumor microenvironment (TME) and as such TME could be as important to the evolution of the tumor as the accumulation of genetic mutations (**Bissell *et al*., 1982**). The presence of tumor-activated stromal cells (TASCs) in the GBM microenvironment could, in part, promote tumor progression and subsequently play an important role in the resistance to the current radio- and chemotherapies observed in patients (**Ji *et al*., 2017; Li *et al*., 2015**). Recently it has been shown that the TME was able to regulate stemness in colo-rectal carcinomas suggesting that stromal cues can influence tumor cell hierarchy and subsequently would have strong effects on the tumor mass suggesting that a change in the emphasis of targeting the tumor mass to targeting the niche that maintains tumor mass (**Lenos *et al*., 2018; Su *et al*., 2018**). An important factor influencing GBM cell migration is the TME composition and the mechanical force that is determined by the components of the ECM. The rigidity of the ECM will determine the degree of mobility of the GBM cells with a more rigid ECM resulting in greater migration of GBM cells (**Ferrer *et al*., 2018**).

The microenvironment of GBM tumors have been shown to contain astrocytes, microglia and endothelial cells (**Brandao *et al*., 2019; Quail *et al*., 2016**), however, recently the presence of mesenchymal stem cells (MSCs) conscripted from the bone marrow or from local

perivascular sites within the brain have been observed in GBM tumors (**Hossain *et al*., 2015**). These MSCs have the capacity to promote the proliferation and stemness of GSCs and the number of MSCs present in the GBM tumors has an effect on patient survival (**Shakar et al., 2017**). Indeed, it has been shown that tumor-associated fibroblasts (CAFs) and MSCs share many characteristics as well as pro-tumorigenic activity (**Borriello *et al*., 2017**). Since MSCs can migrate to damaged tissue sand as the TME closely resembles damaged tissue it is logical to think that MSCs can also home to developing tumors and promote their growth (**Loebinger et al., 2009**). The MSCs would induce proliferation either by paracrine secretion of growth factors or by differentiation into CAFs, which can promote tumor growth, metastasis and therapy resistance (**Dawson et al., 2011; Arena et al., 2018, Behnan et al., 2014)**). Drug resistance could be due to genetic changes resulting in increased drug efflux or could be the result of the TME protecting the cells against treatment. The TME can promote drug resistance in a passive way by preventing penetration of drugs into the tumor cells or in an active way by secreting protective cytokines or by altering gene expression within the tumor cells to override the cytotoxic effects (**Meads et al., 2008**).

MATERIALS AND METHODS

Materials

Unless stated otherwise, all cell culture material was obtained from Life Technologies (Cergy Pontoise, France) and chemicals were from Sigma-Aldrich (St. Louis, MO, USA).

Methods

Cell culture

After informed consent, tumor samples classified as Glioblastoma type IV (GBM), based on the World health Organization criteria were obtained from patients undergoing surgical intervention at the "CHU de Nantes" and the "Tumorothèque IRCNA". Within 4 h after surgical removal, GBM cells were recuperated after mechanical dissociation as described in **Brocard *et al***. (2015). All procedures involving human participants were in accordance with the ethical standards of the ethic national research committee and with the 1964 Helsinki declaration and its later amendments or comparable ethical standards. GBM cells were cultured in defined medium (DMEM/F12 supplemented with 2 mM L-glutamine, N2 and B27 supplement, 2 μg/ml heparin, 20 ng/ml EGF, 40 ng/ml bFGF, 100 U/ml penicillin and 100 μg/ml streptomycin). All the experiments with primary GBM cells were performed at early passages. Cells were analyzed for mycoplasma regularly.

Bone marrow mesenchymal stem cells (MSCs) were obtained from the "Tumorothèque IRCNA" and cultured in DMEM complemented with 20% heat-inactivated fetal calf serum, 5 ng/ml bFGF, 2 mM L-glutamine, 100 U/mL penicillin and 100 µg/mL streptomycin in an atmosphere of 5% CO_2 and 95% humidity at 37°C. To prepare tumor-activated stromal cells (TASCs): MSCs were cultured in conditioned medium obtained from primary cultures and defined medium at a ratio of 30:70 for at least 7 days.

Scaffold / Biosphere formation

Scaffolds were made using an Incredible^{+} bioprinter (Cellink, Göteborg, Sweden). $3x10^7$ GBM cells (monoculture) or $3x10^7$ GBM cells + $1{,}6x10^6$ TASCs (co-cultures) was mixed with 3 ml Cellink Bioink (Cellink) and then bioprinted, cross-linked for 3 min in 200 mM $CaCl_2$ and then incubated in defined medium for 30 min at 37°C after which the medium was replaced by fresh medium as visualized in **Figure S1**.

Biosphere formation was done as described in **Oliver *et al.*,** (2019). Briefly, $4x10^6$ GBM cells $\pm$ $4x10^5$ TASCs were mixed in 1 ml bioink (2% alginate and 5% gelatin) and then 20 μl droplets were added to 24-well plates containing 300 μl 200 mM $CaCl_2$ for 3 min. The $CaCl_2$ was replaced by 1 ml defined medium.

To determine cell proliferation: a single biosphere was dissociated by incubation for 3 min incubation in 100 mM Na-Citrate. Cell counts and viability were analyzed using the Countess optics and image automated cell counter (Life Technologies). Cells were mixed with Trypan blue (1:1) and loaded into a Countess chamber slide. The image analysis software analyzed the acquired cell images to determine cell count and viability.

To analyze the morphology and to determine the dimensions of the spheroids in the biospheres; images were obtained from 5 areas in a single biosphere from a minimum of 10 biospheres per condition using a Zeiss microscope (Axio Observer and ZEN 2 program). The images obtained were analyzed using the FIJI program.

FACS analysis

GBM cells were dissociated washed and incubated 30 min with the primary antibodies directed against CD133 (CD133/2-APC; clone 293C3, Miltenyi Biotec, Auburn, CA, USA), CD44 (CD44-APC, clone BJ18, BioLegend San Diego, CA, USA), CD90 (CD90-PE; 130-095-400, Miltenyi Biotec.), CD10 (CD10-BV421; clone HI10a, BD Biosciences, Le Pont de Claix, France) and CD105 (CD105-BV421; clone 266, BD Biosciences). Data acquisition was performed on a FACS CANTO II (Becton Dickinson) and analyzed using the FlowLogic (Miltenyi) software.

Immunochemistry

To analyze the formation of cellular spheroids within scaffolds, 4% paraformaldehyde fixed scaffolds were clarified for 24 h with Rapiclear® 1.52, were permeabilized with 2% Triton X-100 in HBSS overnight at 4°C, washed with HBSS and then stained with ActinGreen™ Ready Probe® reagent (Life Technologies) for 30 min at 37°C in the dark. After washing the scaffolds were counterstained with Hoechst-33342. The scaffolds were mounted with Rapiclear® 1.52 between 2 glass cover slips separated by a 5 mm insert then analyzed on a confocal microscope (Nikon AIRS, Nikon, France).

For immunocytochemistry, scaffolds were fixed with 4% paraformaldehyde for 1 h then clarified for 24 h with Rapiclear® 1.52, permeabilized with 2% Triton X-100 in HBSS overnight at 4°C, washed with HBSS permeabilized with 0.1% Triton X-100 for 30 min saturated with 5% BSA and then incubated with rabbit anti-human nestin (Proteintech, Rosemont, IL, USA) and mouse anti-human anti-GFAP (Proteintech). Secondary antibodies coupled to Alexafluor-488 or -568 (Life Technologies) was added and then the sections were analyzed using a confocal microscope (Nikon).

Statistical Analysis

Data were analyzed and statistical analyses were performed using GraphPad Prism 7.00 (GraphPad Software, San Diego, CA, USA). Wilcoxon signed-rank test and bootstrap analysis were performed using R (version 3.4.4). Data points are expressed as mean ± SD unless otherwise indicated. * $p < 0.05$, ** $p < 0.01$, *** $p < 0.001$.

Bootstrap analyses were used to analyze the differential effect of radiation on small and large-sized spheroids in the biospheres. Quantiles 0.15 and 0.85 were selected to represent small and large spheroids, respectively. The difference between treated and control 0.15 quantiles was calculated to assess differences in size for small spheroids. The same difference was calculated for 0.85 quantiles (large spheroids). To determine the p-value bootstrap analyses were performed, which gave an empirical distribution of quantile differences. First, all measured spheroid sizes (both treated and control) were mixed together, as if they came from the same population. Next, two random samples were taken from previous mix: one representing control (same sample size as original control), and another representing treated spheroid sizes. The difference in corresponding quantile was calculated for these resampled groups. Finally, this process was repeated 10 000 times. In this way, the empirical quantile difference empirical distribution was retrieved, in order to compare the original quantile difference with the calculated difference. A p-value was estimated as the

number of more extreme bootstrapped cases from the original quantile difference, divided by the total number of cases.

RESULTS

Morphology of the spheroids in biospheres and scaffolds

We have previously shown that our GBM cells are capable of proliferating and forming spheroids in 3D-biospheres (**Oliver *et al.*, 2019**). To analyze the role of the TME by exploring the effects of TASCs on GBM cells cultured in 3D-scaffolds. The morphology of the co-cultured cells after ActinGreen staining on day 30 showed no difference between mono-and co-cultures; interconnecting tubules extending from cells linked up neighboring spheroids similar to that observed in monocultures containing only GBM cells. (**Figure 1A**). Hematoxylin and eosin staining of these spheroids in scaffolds revealed that these spheroids have a proliferative rim region and a necrotic core (**Figure 1B**). Analysis of the cell morphology in co-cultures of GBM cells and TASCs in 3D-scaffolds at an earlier stage (at day 10) showed the presence of TASCs joining aggregates of tumor cells. At higher magnifications we observed the presence of some cargo-carrying TNTs originating from TASCs and connecting up within GBM cells (**Figure 1C**). Note that TASCs were only visible until about day 14 after which they were no longer detectable in 3D-scaffolds (data not shown).

Effect of TASCs on the proliferation of GBM cells

GBMG5 cells were cultured in the absence and in the presence of TASCs at a ratio of 5:1 in biospheres and the morphology and the proliferation of the cells were determined. The data presented in **Figure 1D** and **1E** show that both cultures presented single cell morphology around day 2. By day 7 the cells in the co-cultures started to form small spheroid structures while in monocultures some aggregates were present but many single cells as well. It could be suggested that the cells in the co-cultures are more migratory that the cells in the monocultures, which appear more proliferative. "Go-or-Grow mechanism" Between day 7 and day 14 spheroid structures were formed in both culture types. When we determined the proliferation of the cells in the mono- and co-cultures we observed a higher proliferation in the monocultures as compared to the co-cultures over the 35 days of culture. (**Figure 1F**). This could be explained by the fact that proliferative cells tend to be present on the outer layers of the spheroid and since the surface to volume ratio is higher in small spheroids than

in larger spheroids; there will be a higher proportion of proliferative cells in small spheroids (in mono-cultures, which contained smaller aggregates) compared to larger spheroids (in co-cultures). No significant difference was observed in the viability of the cells in the different cultures over the 35 days of culture (**Figure 1G**).

Effect of radiation on mono-and co-cultures of GBM cells

GBMG5 cells cultured in the absence or in the presence of TASCs were subjected to 3 doses of 2 Gy, either daily, every 3 days or weekly as depicted in **Figure S2**. The morphology on day 26 of the spheroids present in mono- and cultures of GBMG5 cells after the different treatments are shown in **Figure 2A** and **2B**. The morphology of the spheroids in the monocultures appear ragged with what looks like shedding of the cells from the spheroids while in the co-cultures the spheroid surface appears smooth. When we look at the proliferation of the cells it would appear that the cells proliferate more in the monocultures than in the co-cultures (**Figure 2C** and **2D**) while the viability was unaffected by the irradiation (**Figure 2E** and **2F**). Next we looked at CSC markers in mono- and co-cultures of GBMG5 cells after the different regimes of irradiation (**Figure 2G** and **2H**). Irradiation appears to reduce the number of $CD133^+$ cells in the 3 day and weekly irradiated co-cultures while the number of $CD133^+$ cells appears to increase in the 3 day and weekly irradiated biospheres. The number of $CD133^+$ cells remained the same in daily-irradiated biospheres both in mono- and co-cultures. CD44 is a ligand for hyaluronic acids and contributes to mechanosensing and the invasive motility of cells **Kim and Kumar (2014).** The similar pattern to $CD133^+$ cells was observed for $CD44^+$ cells.

Next we measured the diameter of spheroids formed in mono- and co-cultures of GBMG5 cells and TASCs. Diameters were calculated directly from pictographs taken over the 34 days of culture and a minimum of 200 spheroids was evaluated at each point. In the untreated cultures we observed a significant increase in the diameter of the spheroids formed in co-cultures compared to monocultures (**Figure 3A**). The results in **Figure 3B** and **3C** using the Wilcoxon signed-rank test show the median spheroid size difference in treated versus control biospheres. The statistical significance is determined by whether the confidence interval traverses the x-axis. Taking this into account one could infer that the further the confidence interval from the x-axis, the larger the difference in magnitude. From the graphs in Figure 3B, C we can see that the size differences are positive for mono-culture biospheres under all irradiation treatments and negative for co-culture biospheres implying that the mono-culture biospheres after treatment are larger than control mono-cultures, while the

inverse is true for co-cultures after irradiation.

Effect of irradiation on the spheroids formed in mono-and co-cultures

In the co-cultured biospheres the total number of cells was similar in the control and the corresponding irradiated biospheres, but the size of spheroids was smaller in irradiated biospheres. However, in the mono-cultured biospheres while the number of cells in the treated and untreated biospheres was similar the spheroids were bigger in irradiated biospheres as compared to control. We decided to analyze why spheroid size change at two different intervals: small spheroids, which we thought would be more affected by irradiation, and large spheroids, which were expected to better survive irradiation.

To circumvent this, a representative value for both small and large spheroids was selected: quantiles 0.15 and 0.85 of empirical distribution, respectively. We wanted to see how treatment affected both small and large spheroids, by comparing control with treatment for small and large spheroids separately. But, because of quantiles follow and unknown statistical distribution, a bootstrap analysis was performed in order to assess significance in size differences (see Methods – Statistical Analysis). The data presented in **Figure 4** show the results of bootstrap analysis.

By looking at the results it can be inferred that spheroids in mono-culture show significant differences in their sizes when treated, compared to untreated spheroids. Specifically, the size of the 0.15 quantile group of spheroid is 'larger' after irradiation (**Figure 4A**), while 0.85 quantile group do not show a significant change in size (**Figure 4C**). This is in accordance with the hypothesis that as smaller spheroids have a higher surface-to-volume ratio and as proliferative cells (which are more affected by irradiation) are present on the outer layers of the spheroids, small spheroids would be more affected by irradiation than larger spheroids. As irradiation will wipe out most small spheroids, 0.15 quantile will be higher in treated biospheres.

However, for co-cultured spheroids an unexpected result was observed. Surface-to-volume ratio hypothesis should also apply here, but results show that both small and large spheroids were smaller after radiation (**Figures 4D** and **4F**, respectively). Small spheroids after irradiation are smaller than their control counterparts. This may point to a 'protective' effect of TASCs, permitting the cells in both small and large spheroids to survive irradiation.

TASCs increase survival of GBM cells in 3D culture and resistance to combined radio- and chemotherapy

In a second set of experiments to analyze the effect of TASCs on long-term survival of GBM cells after combined radio- and chemotherapy, 3D scaffolds containing GBMA1 with or without TASCs were bioprinted as described in **Figure S1**. After 4 weeks of culture when the formation of a complex interconnected cellular network was present; the 3D scaffolds of GBMA1 cells or co-culture of TASCs plus GBMA1 cells were treated with either 100 μM TMZ alone or in combination with radiotherapy (2 Gy and 5 Gy) for 4 days, after which the cells were recuperated from the scaffold and cultured for a further 30 days and then the proliferation and mitochondrial content was analyzed. The cells in the co-cultures continued to proliferate regardless of the treatment, however, the cells in monocultures only proliferated in cultures treated with 100 μM TMZ, 2 Gy and 5 Gy and no proliferation was detected in scaffolds treated with 100 μM TMZ + 2 Gy or 100 μM TMZ + 5 Gy (**Figure 5A**).

Analysis of the mitochondrial content of the different cultures showed that in the co-cultures all cell had a healthy population of mitochondria even with a treatment of 100 μM TMZ + 5 Gy. However, in the monocultures a small population of cells under the control conditions contained no functional mitochondria and this was markedly increased after a treatment of 100 μM TMZ + 2 Gy (**Figure 5B**). These data show that as in 2D cultures the presence of TASCs the survival of cell and even more protected the tumor cells against radio- and chemotherapy.

DISCUSSION

One of the most significant hallmarks of the biological identity of CAFs is that their tumor-promoting phenotype is stably maintained during *in vitro* and *ex vivo* propagation without the continued interaction with the adjacent tumor cells (**Lamprecht et al., 2018**).

We have previously shown that GBM cells in 3D-bioprinting was capable of secreting GAGs and here we show that GBM cells in 3D biospheres express more CD44 suggesting that GBM cells can regulate the stiffness of the bioink.

Irradiation causes more damage to proliferating rather than to quiescent cells. Taking into account the "Rim and core" hypothesis proliferative cells are present rim of the spheroids. Surface to volume ratio is higher in small spheroids and as such there should be proliferation in small spheroids. Thus in theory irradiation should preferably impact small spheroids.

ACKNOWLEDGEMENTS

This work is supported by grants from "Ligue Grand Ouest Contre le Cancer" and the "Plan Cancer" HTE program MoGlimaging, Ministerio de Economía y Competitividad/FEDER, Spain [grant number MTM2015-71200-R] and James S. Mc. Donnell Foundation (USA) 21st Century Science Initiative in Mathematical and Complex Systems Approaches for Brain Cancer (Collaborative award 220020450). We thank the platform MicroPicell for their aid with all the microscopic work. The bio-collection used for this analysis is the Glioblastoma collection belonging to the pediatric research program of the University Hospital of Nantes (Ref MESR DC-2014-2206, having obtained a favorable opinion from CPP Ouest IV (Dossier 06/15) on 08 / 04/2015).

REFERENCES

Allen M, Louise Jones J. *Jekyll and Hyde: the role of the microenvironment on the progression of cancer. J Pathol. 2011 Jan;223(2):162-76. doi: 10.1002/path.2803*

Arcucci A, Ruocco MR, Granato G, Sacco AM, Montagnani S. *Cancer: An oxidative crosstalk between solid tumor cells and cancer associated fibroblasts. Biomed Res Int. 2016;2016:4502846. doi: 10.1155/2016/4502846.*

Arena S, Salati M, Sorgentoni G, Barbisan F, Orciani M. Characterization of tumor-derived mesenchymal stem cells potentially differentiating into cancer-associated fibroblasts in lung cancer. Clin Transl Oncol. 2018 Dec;20(12):1582-1591. doi: 10.1007/s12094-018-1894-4.

Avagliano A, Granato G, Ruocco MR, Romano V, Belviso I, Carfora A, Montagnani S, Arcucci A. *Metabolic reprogramming of cancer associated fibroblasts: The slavery of stromal fibroblasts. Biomed Res Int. 2018 Jun 5;2018:6075403. doi: 10.1155/2018/6075403.*

Behnan J, Isakson P, Joel M, Cilio C, Langmoen IA, Vik-Mo EO, Badn W. Recruited brain tumor-derived mesenchymal stem cells contribute to brain tumor progression. Stem Cells. 2014 May;32(5):1110-23. doi: 10.1002/stem.1614.

Belli C, Trapani D, Viale G, D'Amico P, Duso BA, Della Vigna P, Orsi F, Curigliano G. *Targeting the microenvironment in solid tumors. Cancer Treat Rev. 2018 Apr;65:22-32. doi: 10.1016/j.ctrv.2018.02.004.*

Bissell MJ, Hall HG, Parry G. How does the extracellular matrix direct gene expression? J Theor Biol. 1982 Nov 7;99(1):31-68.

Borriello L, Nakata R, Sheard MA, Fernandez GE, Sposto R, Malvar J, Blavier L, Shimada H, Asgharzadeh S, Seeger RC, DeClerck YA. *Cancer-associated fibroblasts share characteristics and protumorigenic activity with mesenchymal stromal cells. Cancer Res. 2017 Sep 15;77(18):5142-5157. doi: 10.1158/0008-5472.CAN-16-2586.*

Brandao M, Simon T, Critchley G, Giamas G. Astrocytes, the rising stars of the glioblastoma microenvironment. Glia. 2019 May;67(5):779-790. doi: 10.1002/glia.23520.

Brocard E, Oizel K, Lalier L, Pecqueur C, Paris F, Vallette FM, Oliver L. Radiation-induced PGE2 sustains human glioma cells growth and survival through EGF signaling. Oncotarget. 2015; 6(9):6840-9.

Dzobo K, Senthebane DA, Thomford NE, Rowe A, Dandara C, Parker MI. *Not everyone fits the mold: Intratumor and intertumor heterogeneity and innovative cancer drug design and development. OMICS. 2018 Jan;22(1):17-34. doi: 10.1089/omi.2017.0174.*

Ferrer VP, Moura Neto V, Mentlein R. Glioma infiltration and extracellular matrix: key players and modulators. Glia. 2018 Aug;66(8):1542-1565. doi: 10.1002/glia.23309.

Figueroa J, Phillips LM, Shahar T, Hossain A, Gumin J, Kim H, Bean AJ, Calin GA, Fueyo J, Walters ET, Kalluri R, Verhaak RG, Lang FF. *Exosomes from glioma-associated Mesenchymal stem cells increase the tumorigenicity of glioma stem-like cells via transfer of miR-1587. Cancer Res. 2017 Nov 1;77(21):5808-5819. doi: 10.1158/0008-5472.CAN-16-2524*.

Furuse M, Fujita K, Hiiragi T, Fujimoto K, Tsukita S. *Claudin-1 and -2: novel integral membrane proteins localizing at tight junctions with no sequence similarity to occludin. J. Cell Biol. 1998; 141 (7): 1539–50. doi:10.1083/jcb.141.7.1539.*

Gonda TA, Varro A, Wang TC, Tycko B. *Molecular biology of cancer-associated fibroblasts: can these cells be targeted in anti-cancer therapy? Semin Cell Dev Biol. 2010 Feb;21(1):2-10. doi: 10.1016/j.semcdb.2009.10.001.*

Grinde MT, Vik J, Camilio KA, Martinez-Zubiaurre I, Hellevik T*. Ionizing radiation abrogates the pro-tumorigenic capacity of cancer-associated fibroblasts co-implanted in xenografts. Sci Rep. 2017 Apr 25;7:46714. doi: 10.1038/srep46714.*

Griveau A, Seano G, Shelton SJ, Kupp R, Jahangiri A, Obernier K, Krishnan S, Lindberg OR, Yuen TJ, Tien AC, Sabo JK, Wang N, Chen I, Kloepper J, Larrouquere L, Ghosh M, Tirosh I, Huillard E, Alvarez-Buylla A, Oldham MC, Persson AI, Weiss WA, Batchelor TT, Stemmer-Rachamimov A, Suvà ML, Phillips JJ, Aghi MK, Mehta S, Jain RK, Rowitch D*H. A glial signature and Wnt7 signaling regulate glioma-vascular interactions and tumor microenvironment. Cancer Cell. 2018 May 14;33(5):874-889.e7. doi: 10.1016/j.ccell.2018.03.020.*

Han Y, Zhang Y, Jia T, Sun Y. *Molecular mechanism underlying the tumor-promoting functions of carcinoma-associated fibroblasts. Tumour Biol. 2015 Mar;36(3):1385-94. doi: 10.1007/s13277-015-3230-8.*

Hashimoto O, Yoshida M, Koma Y, Yanai T, Hasegawa D, Kosaka Y, Nishimura N, Yokozaki H. *Collaboration of cancer-associated fibroblasts and tumour-associated macrophages for neuroblastoma development. J Pathol. 2016 Oct;240(2):211-23. doi: 10.1002/path.4769.*

Herrera-Perez RM, Voytik-Harbin SL, Sarkaria JN, Pollok KE, Fishel ML, Rickus JL. *Presence of stromal cells in a bioengineered tumor microenvironment alters glioblastoma migration and response to STAT3 inhibition. PLoS One. 2018 Mar 22;13(3):e0194183. doi: 10.1371/journal.pone.0194183.*

Holland EC, Celestino J, Dai C, Schaefer L, Sawaya RE, Fuller GN. Combined activation of Ras and Akt in neural progenitors induces glioblastoma formation in mice. Nat Genet. 2000 May;25(1):55-7.

Hubert CG, Rivera M, Spangler LC, Wu Q, Mack SC, Prager BC, Couce M, McLendon RE, Sloan AE, Rich JN. *A three-dimensional organoid culture system derived from human Glioblastomas recapitulates the hypoxic gradients and cancer stem cell heterogeneity of tumors found in vivo. Cancer Res. 2016 Apr 15;76(8):2465-77. doi: 10.1158/0008-5472.CAN-15-2402.*

Jeong SY, Lee JH, Shin Y, Chung S, Kuh HJ. *Co-Culture of Tumor Spheroids and Fibroblasts in a Collagen Matrix-Incorporated Microfluidic Chip Mimics Reciprocal Activation in Solid Tumor Microenvironment. PLoS One. 2016 Jul 8;11(7):e0159013. doi: 10.1371/journal.pone.0159013.*

Ji X, Zhu X, Lu X. Effect of cancer-associated fibroblasts on radiosensitivity of cancer cells. Future Oncol. 2017 Jul;13(17):1537-1550. doi: 10.2217/fon-2017-0054.

Kim Y, Kumar S. CD44-mediated adhesion to hyaluronic acid contributes to mechanosensing and invasive motility. Mol Cancer Res. 2014 Oct;12(10):1416-29. doi: 10.1158/1541-7786.MCR-13-0629.

Kuzet SE, Gaggioli C. *Fibroblast activation in cancer: when seed fertilizes soil. Cell Tissue Res. 2016 Sep;365(3):607-19. doi: 10.1007/s00441-016-2467-x.*

Lamprecht S, Sigal-Batikoff I, Shany S, Abu-Freha N, Ling E, Delinasios GJ, Moyal-Atias K, Delinasios JG, Fich A. Teaming Up for Trouble: Cancer Cells, Transforming Growth Factor-β1 Signaling and the Epigenetic Corruption of Stromal Naïve Fibroblasts. Cancers (Basel). 2018 Feb 27;10(3). pii: E61. doi: 10.3390/cancers10030061.

Lang FM, Hossain A, Gumin J, Momin EN, Shimizu Y, Ledbetter D, Shahar T, Yamashita S, Parker Kerrigan B, Fueyo J, Sawaya R, Lang FF. *Mesenchymal stem cells as natural biofactories for exosomes carrying miR-124a in the treatment of gliomas. Neuro Oncol. 2018 Feb 19;20(3):380-390. doi: 10.1093/neuonc/nox152.*

Lenos KJ, Miedema DM, Lodestijn SC, Nijman LE, van den Bosch T, Romero Ros X, Lourenço FC, Lecca MC, van der Heijden M, van Neerven SM, van Oort A, Leveille N, Adam RS, de Sousa E Melo F, Otten J, Veerman P, Hypolite G, Koens L, Lyons SK, Stassi G, Winton DJ, Medema JP, Morrissey E, Bijlsma MF, Vermeulen L. Stem cell functionality is microenvironmentally defined during tumour expansion and therapy response in colon cancer. Nat Cell Biol. 2018 Oct;20(10):1193-1202. doi: 10.1038/s41556-018-0179-z.

Li XY, Hu SQ, Xiao L. The cancer-associated fibroblasts and drug resistance. Eur Rev Med Pharmacol Sci. 2015;19(11):2112-9.

Louis DN, Perry A, Reifenberger G, von Deimling A, Figarella-Branger D, Cavenee WK, Ohgaki H, Wiestler OD, Kleihues P, Ellison DW. The 2016 World Health Organization Classification of tumors of the Central Nervous System: a summary. Acta Neuropathol. 2016 Jun;131(6):803-20. doi: 10.1007/s00401-016-1545-1.

Mishra PJ, Mishra PJ, Glod JW, Banerjee D. *Mesenchymal stem cells: flip side of the coin. Cancer Res. 2009 Feb 15;69(4):1255-8. doi: 10.1158/0008-5472.CAN-08-3562.*

Mishra PJ, Mishra PJ, Humeniuk R, Medina DJ, Alexe G, Mesirov JP, Ganesan S, Glod JW, Banerjee D. *Carcinoma-associated fibroblast-like differentiation of human mesenchymal stem cells. Cancer Res. 2008 Jun 1;68(11):4331-9. doi: 10.1158/0008-5472.CAN-08-0943.*

Nagle PW, Plukker JTM, Muijs CT, van Luijk P, Coppes RP. *Patient-derived tumor organoids for prediction of cancer treatment response. Semin Cancer Biol. 2018 Dec;53:258-264. doi: 10.1016/j.semcancer.2018.06.005.*

Nakod PS, Kim Y, Rao SS. *Biomimetic models to examine microenvironmental regulation of glioblastoma stem cells. Cancer Lett. 2018 Aug 10;429:41-53. doi: 10.1016/j.canlet.2018.05.007.*

Neumann CCM, von Hörschelmann E, Reutzel-Selke A, Seidel E, Sauer IM, Pratschke J, Bahra M, Schmuck RB. *Tumor-stromal cross-talk modulating the therapeutic response in pancreatic cancer. Hepatobiliary Pancreat Dis Int. 2018 Oct;17(5):461-472. doi: 10.1016/j.hbpd.2018.09.004.*

O'Brien ER, Howarth C, Sibson NR. The role of astrocytes in CNS tumors: pre-clinical models and novel imaging approaches. Front Cell Neurosci. 2013 Apr 16;7:40. doi: 10.3389/fncel.2013.00040.

Paggetti J, Haderk F, Seiffert M, Janji B, Distler U, Ammerlaan W, Kim YJ, Adam J, Lichter P, Solary E, Berchem G, Moussay E. *Exosomes released by chronic lymphocytic leukemia cells induce the transition of stromal cells into cancer-associated fibroblasts. Blood. 2015 Aug 27;126(9):1106-17. doi: 10.1182/blood-2014-12-618025.*

Puré E, Hingorani SR. *Mesenchymal cell plasticity and perfidy in epithelial malignancy. Trends Cancer. 2018 Apr;4(4):273-277. doi: 10.1016/j.trecan.2018.02.007.*

Quail DF, Bowman RL, Akkari L, Quick ML, Schuhmacher AJ, Huse JT, Holland EC, Sutton JC, Joyce JA. The tumor microenvironment underlies acquired resistance to CSF-1R inhibition in gliomas. Science. 2016 May 20;352(6288):aad3018. doi: 10.1126/science.aad3018.

Shahar T, Rozovski U, Hess KR, Hossain A, Gumin J, Gao F, Fuller GN, Goodman L, Sulman EP, Lang FF. Percentage of mesenchymal stem cells in high-grade glioma tumor samples correlates with patient survival. Neuro Oncol. 2017 May 1;19(5):660-668. doi: 10.1093/neuonc/now239.

Su S, Chen J, Yao H, Liu J, Yu S, Lao L, Wang M, Luo M, Xing Y, Chen F, Huang D, Zhao J, Yang L, Liao D, Su F, Li M, Liu Q, Song E. $CD10^{+}GPR77^{+}$ Cancer-associated fibroblasts promote cancer formation and chemoresistance by sustaining cancer stemness. Cell. 2018 Feb 8;172(4):841-856.e16. doi: 10.1016/j.cell.2018.01.009.

Zhao H, Yang L, Baddour J, Achreja A, Bernard V, Moss T, Marini JC, Tudawe T, Seviour EG, San Lucas FA, Alvarez H, Gupta S, Maiti SN, Cooper L, Peehl D, Ram PT, Maitra A, Nagrath D. *Tumor microenvironment derived exosomes pleiotropically modulate cancer cell metabolism. Elife. 2016 Feb 27;5:e10250. doi: 10.7554/eLife.10250.*

Stupp R, Mason WP, van den Bent MJ, Weller M, Fisher B, Taphoorn MJ, Belanger K, Brandes AA, Marosi C, Bogdahn U, Curschmann J, Janzer RC, Ludwin SK, Gorlia T, Allgeier A, Lacombe D, Cairncross JG, Eisenhauer E, Mirimanoff RO; European Organisation for Research and Treatment of Cancer Brain Tumor and Radiotherapy Groups;

National Cancer Institute of Canada Clinical Trials Group. Radiotherapy plus concomitant and adjuvant temozolomide for glioblastoma. N Engl J Med. 2005; 352(10):987-96.

Stupp R, Hegi ME, Mason WP, van den Bent MJ, Taphoorn MJ, Janzer RC, Ludwin SK, Allgeier A, Fisher B, Belanger K, Hau P, Brandes AA, Gijtenbeek J, Marosi C, Vecht CJ, Mokhtari K, Wesseling P, Villa S, Eisenhauer E, Gorlia T, Weller M, Lacombe D, Cairncross JG, Mirimanoff RO; European Organisation for Research and Treatment of Cancer Brain Tumour and Radiation Oncology Groups; National Cancer Institute of Canada Clinical Trials Group. Effects of radiotherapy with concomitant and adjuvant temozolomide versus radiotherapy alone on survival in glioblastoma in a randomised phase III study: 5-year analysis of the EORTC-NCIC trial. Lancet Oncol. 2009; 10(5):459-66. doi: 10.1016/S1470-2045(09)70025-7.

Griffith LG, Swartz MA. Capturing complex 3D tissue physiology in vitro. Nat Rev Mol Cell Biol. 2006; 7(3):211-24.

Fallica B, Makin G, Zaman MH. Bioengineering approaches to study multidrug resistance in tumor cells. Integr Biol (Camb). 2011; 3(5):529-39.

Fong EL, Watson BM, Kasper FK, Mikos AG. Building bridges: leveraging interdisciplinary collaborations in the development of biomaterials to meet clinical needs. Adv Mater. 2012; 24(36):4995-5013.

Singh SK, Hawkins C, Clarke ID, Squire JA, Bayani J, Hide T, Henkelman RM, Cusimano MD, Dirks PB. Identification of human brain tumour initiating cells. Nature. 2004 Nov 18;432(7015):396-401.

Hossain A, Gumin J, Gao F, Figueroa J, Shinojima N, Takezaki T, Priebe W, Villarreal D, Kang SG, Joyce C, Sulman E, Wang Q, Marini FC, Andreeff M, Colman H, Lang FF. Mesenchymal stem cells isolated from human gliomas increase proliferation and maintain stemness of glioma stem cells through the IL-6/gp130/STAT3 pathway. Stem Cells. 2015 Aug;33(8):2400-15. doi: 10.1002/stem.2053.

Dawson MR, Chae SS, Jain RK, Duda DG. Direct evidence for lineage-dependent effects of bone marrow stromal cells on tumor progression. Am J Cancer Res. 2011;1(2):144-54.

Meads MB, Hazlehurst LA, Dalton WS. The bone marrow microenvironment as a tumor sanctuary and contributor to drug resistance. Clin Cancer Res. 2008 May 1;14(9):2519-26. doi: 10.1158/1078-0432.CCR-07-2223.

Loebinger MR, Kyrtatos PG, Turmaine M, Price AN, Pankhurst Q, Lythgoe MF, Janes SM. Magnetic resonance imaging of mesenchymal stem cells homing to pulmonary metastases using biocompatible magnetic nanoparticles. Cancer Res. 2009 Dec 1;69(23):8862-7. doi: 10.1158/0008-5472.CAN-09-1912.

LEGENDS TO FIGURES

Figure 1: Comparison of mono- and co-cultures of GBM cells and TASCs. **A**. Image representing the cellular structures present in the 3D scaffold stained with ActinGreen in monoculture of GBM67 cells taken on day 35. Note the interconnection between the spheroids. Similar images were obtained for co-cultures (data not shown). **B**. Hematoxylin and eosin staining of 10 µm section of a scaffold prepared using GBMG5 cells snap-frozen in Tissue-Tek OCT medium. Note the presence of a necrotic core present in the center of the spheroids. **C**. Images of co-cultures of GBM8 cells and TASCs taken on day 10. Arrowheads indicate tunneling nanotubules (TNT) laden with cargo. Images representing the morphology of cells and spheroids in mono-cultures of GBMG5 cells (**D**) or co-cultures of GBMG5 cells and TASCs (**E**) cultivated in 3D biospheres every 7 days over 21 days. The red circles in **E** on day 7 highlight early spheroid formation in co-culture biospheres. **F**. The proliferation of GBMG5 cells in the mono- and co-culture was assessed over 31 days. **G**. The viability GBMG5 of the cells was determined in mono- and co-cultures. The data presented are representative of that obtained using 4 different primary GBM cultures.

Figure 2: Effect of irradiation on growth of mono- and co-cultures of GBM cells and TASCs in biospheres. Images representing the morphology of cells and spheroids in mono-cultures of GBMG5 cells (**A**) or co-cultures of GBMG5 cells and TASCs (**B**) grown in 3D biospheres taken on the end of the treatment regime consisting of 3 doses of irradiation either daily, every 3 days or weekly (see **Figure S2**). Note the presence of more regular surface spheroid in co-cultures compared to the rough spheroids present in monocultures. Quantification of the proliferation of the cells in mono- (**C**) and co-cultures (**D**) of GBMG5 cells treated as in **A** and **B**. The viability of the cells was assessed in mono- (**E**) and in co-cultures (**F**) of GBMG5 cells, treated as above. **G**. FACS analyses to determine the percentage of $CD133^+$ cells was determined in mono- and cultures of GBMG5 cells and TASCs after the different regimes of radiation. **H**. FACS analyses to determine the percentage of CD44+ cells was determined in mono- and co-cultures of GBMG5 and TASCs after the different regimes of radiation.

Figure 3: Analyses of the diameter of spheroids formed in biospheres. A. The median diameter of the spheroids present in mono- and co-cultures of GBMG5 cells and TASCs was determined over the 35 days of culture. At each point a minimum of 100 spheroids were

analyzed. The median diameter of the spheroids present in mono- (**B**) and co-cultures (**C**) of GBMG5 cells and TASCs was assessed during the different treatments of irradiation with 2 Gy. The vertical dashed lines correspond to the days of different radiation schedules.

Figure 4: Analyses of the density of the spheroids after irradiation.
The size of small spheroids (0.15 quantile) present in mono- (**A**) and co-cultures (**B**) after irradiation was compared to those present in control biospheres. The solid vertical line represents the original difference in size between control and treated samples measured from empirical distributions. The further this line is from bootstrapped distribution, the more significant the difference in sizes will be. The size of small spheroids present in mono-(**C**) and co-cultures (**D**) after irradiation was compared to those present in control biospheres. The p-values in mono-cultures after irradiation (IR) for weekly vs. control, 3days vs. control and daily vs. control are 0.0213, 0.1638 and 0.009 respectively while that of the co-cultures are 0.004, 0.001 and 0 respectively. The size of large spheroids (0.85 quantile) present in mono-(**E**) and co-cultures (**F**) after irradiation was compared to those present in control biospheres. The p-values in mono-cultures after IR for weekly vs. control, 3days vs. control and daily vs. control are 0.3171, 0.5236 and 0.2767 respectively while that of the co-cultures are 0.0048, 0.0086 and 0 respectively.

Figure 5: Long-term effects of radiation and TMZ-treatment. A. Scaffolds containing GBMA1 or GBMA1 plus TASCs treated with a single dose 100 μM TMZ plus or minus 2 Gy or 5 Gy for 5 days were dissociated and the cells cultured in 2D. After 30 days the morphology and proliferation of the cells was assessed. **B**. Cells obtained from the different cultures in (**A**) were labeled with MitoT Deep-Red and the mean fluorescence index of the mitochondrial mass was determined in the different mono- (**a**) and co-cultures (**b**) after FACS analyses. **C**. Cells from cultures in (**A**) were plated in 24-well plates and the oxygen consumption rate (OCR) (calculated from the difference between the basal rate and the rate after a treatment with rotenone and antimycin A (**a**), the extracellular acidification rate (ECAR) (**b**), the ratio OCR / ECAR (**c**) and the percentage of fatty acid oxidation after inhibition with etomoxir (% FAOX) (**d**) was determined using the Seahorse Technology. Each point is the mean of 3 values. The statistical analyses were done using one-way ANOVA with multiple comparisons.

LEGENDS TO SUPPLEMENTARY FIGURES:

Supplementary Figure 1: Protocol used for 3D bioprinting.

Supplementary Figure 2: Protocol used in the treatment of GBM cells ± TASCs biospheres with 2 Gy.

Supplementary Table 1: List of primary PDCs used in this study.

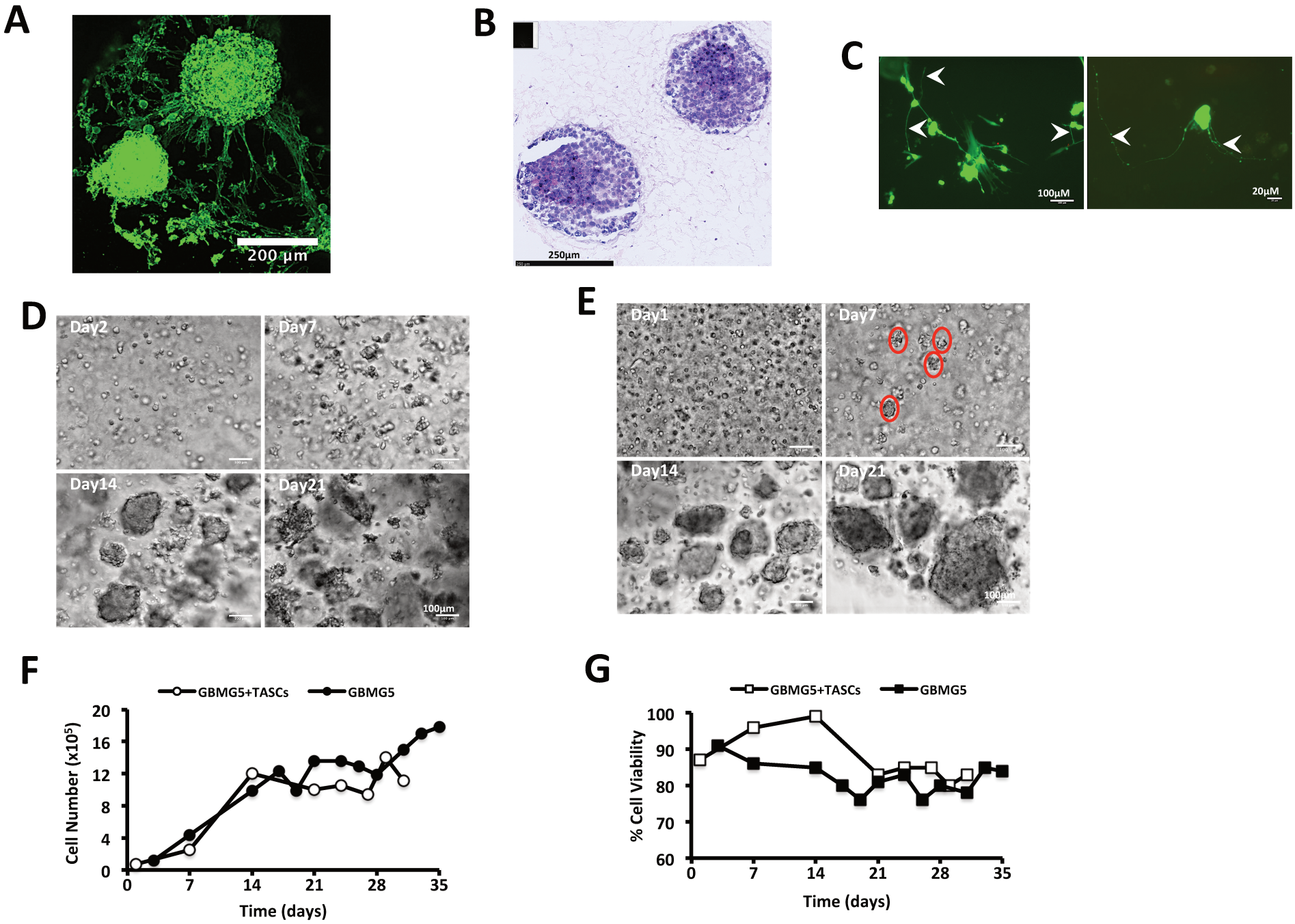

Figure 1: Mono- and co-cultures of GBM cells alone or with TASCs in 3D biospheres

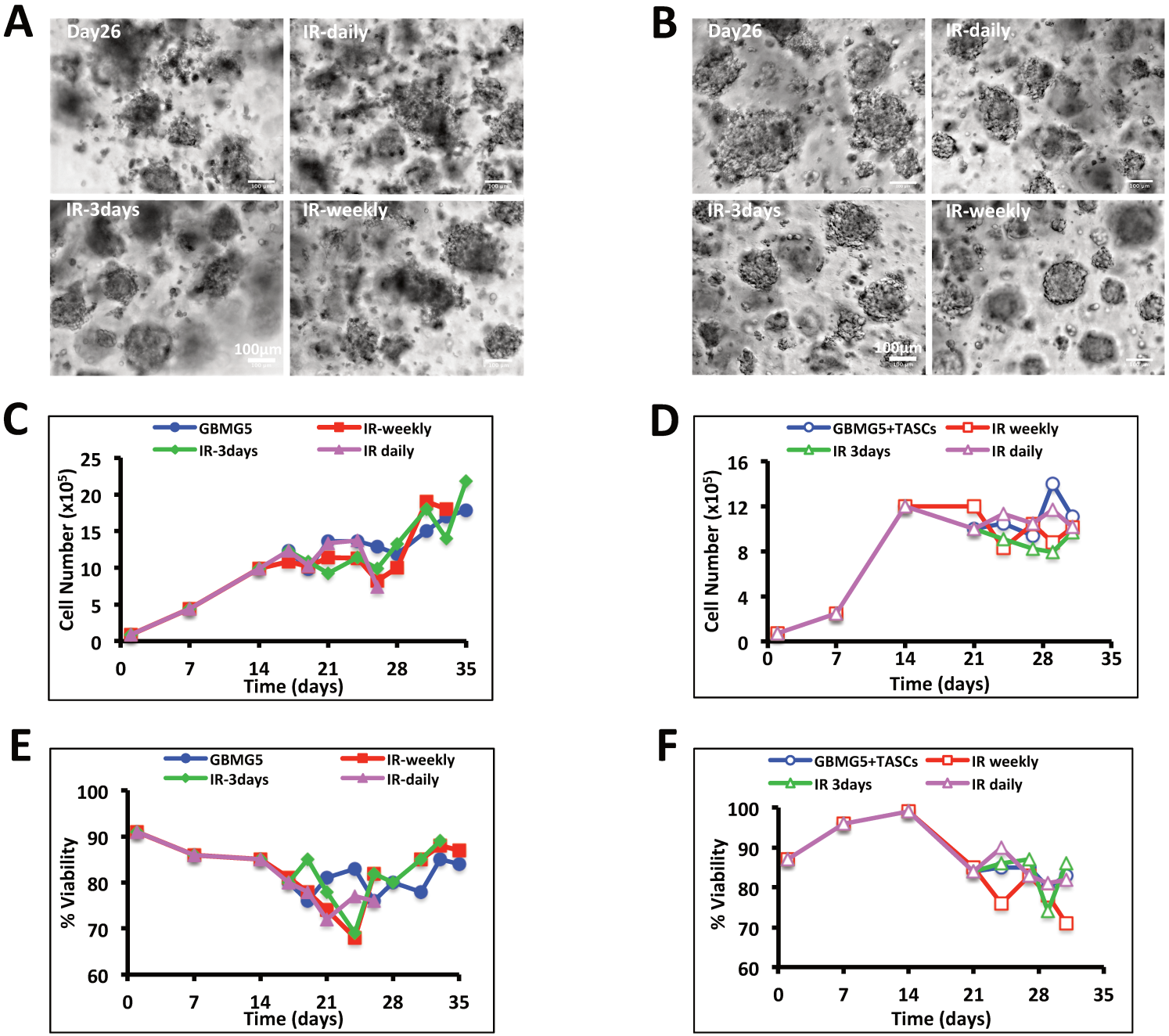

Figure 2: Effects of irradiation of proliferation and viability of cells and diameter of spheroids

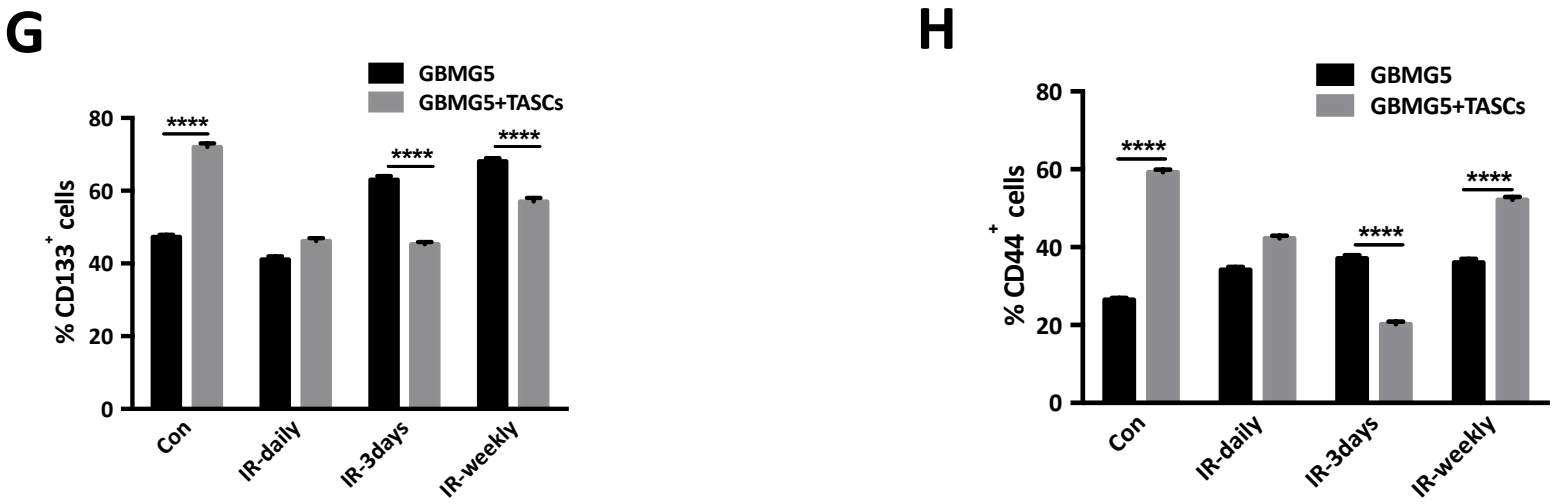

Figure 2: cont.

A

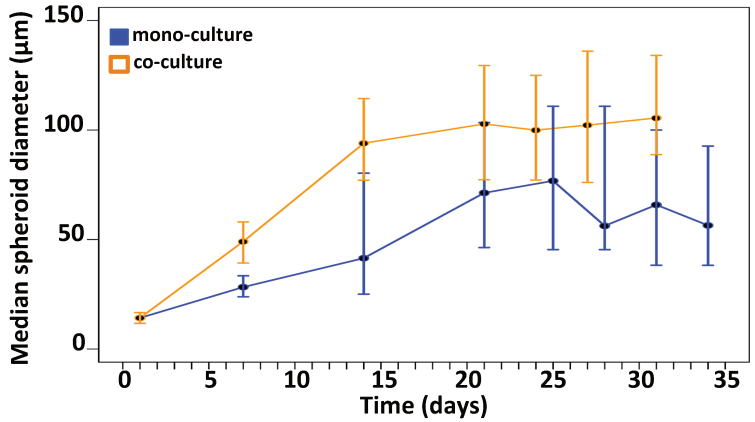
mono-culture
co-culture
Median spheroid diameter (µm)
150
100
50
0
0
5
10
15
20
25
30
35
Time (days)

B

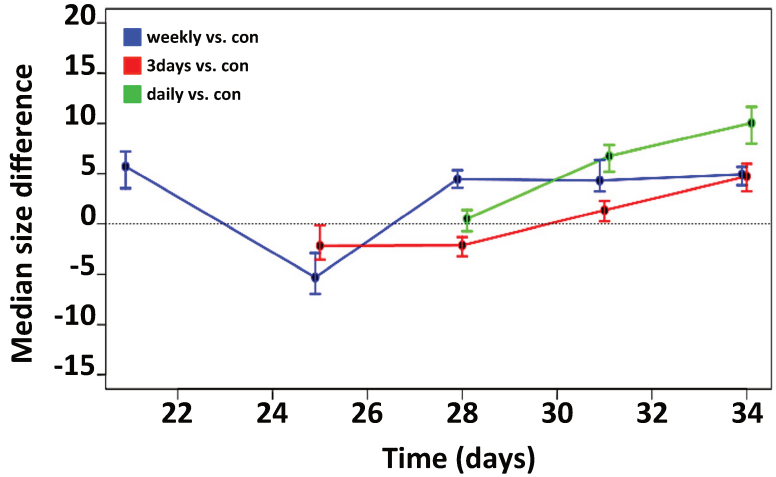
weekly vs. con
3days vs. con
daily vs. con
Median size difference
20
15
10
5
0
-5
-10
-15
22
24
26
28
30
32
34
Time (days)

C

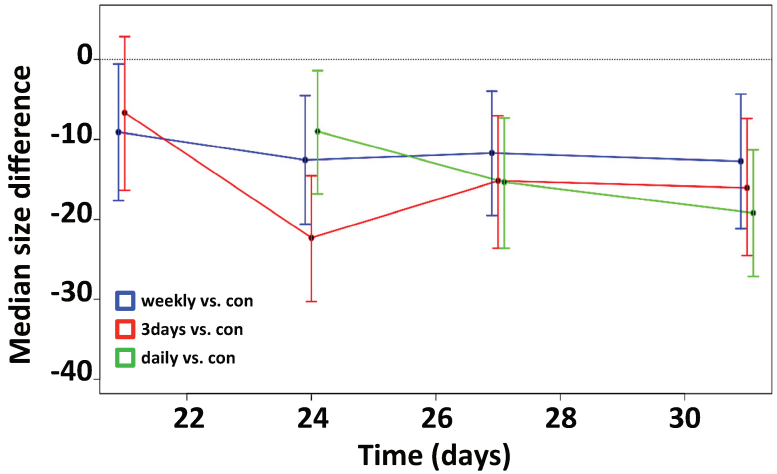
Median size difference
0
-10
-20
-30
-40
weekly vs. con
3days vs. con
daily vs. con
22
24
26
28
30
Time (days)

Figure 3

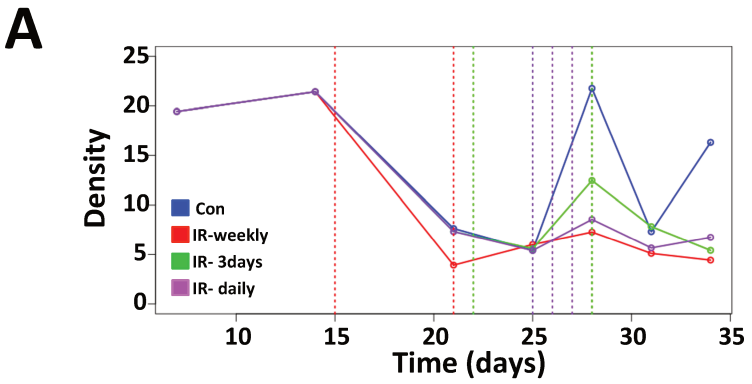

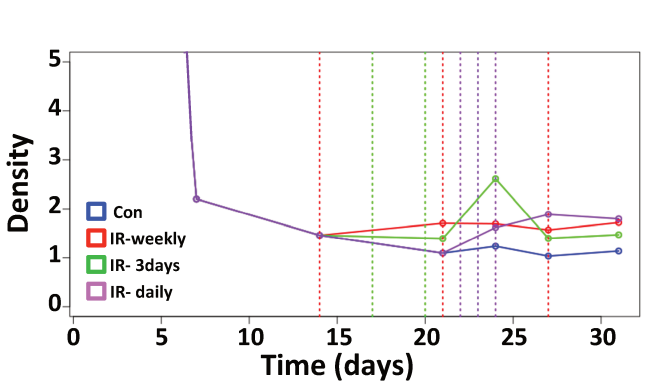

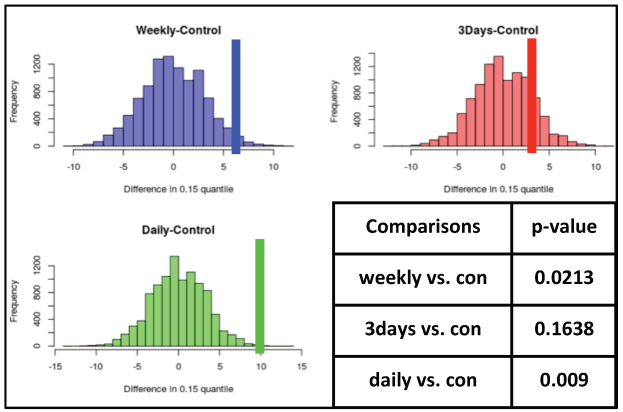

Comparisons	p-value
weekly vs. con	0.0213
3days vs. con	0.1638
daily vs. con	0.009

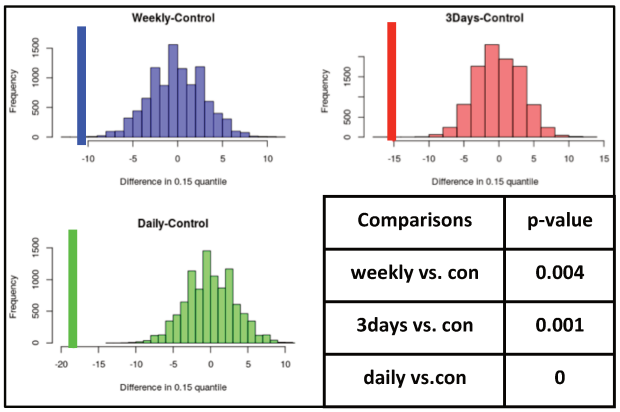

small

Comparisons	p-value
weekly vs. con	0.004
3days vs. con	0.001
daily vs.con	0

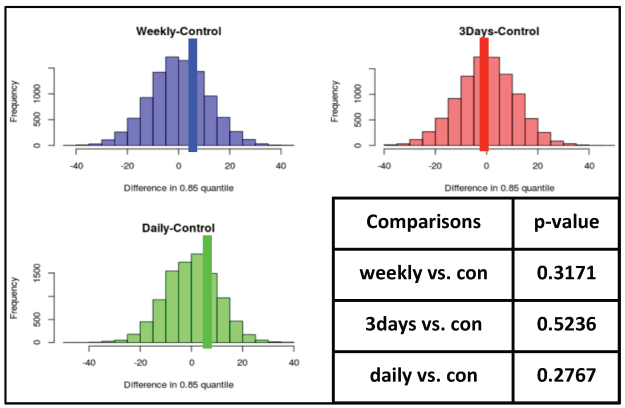

Comparisons	p-value
weekly vs. con	0.3171
3days vs. con	0.5236
daily vs. con	0.2767

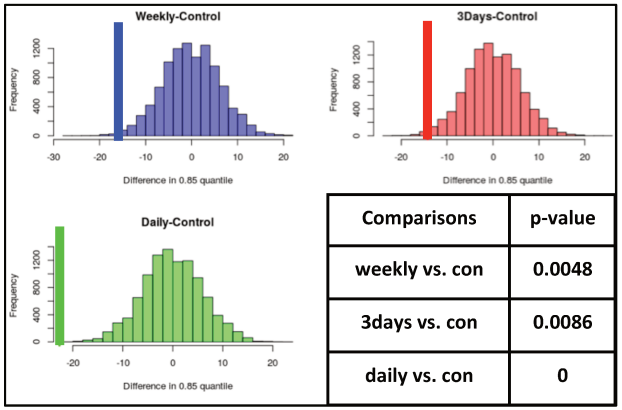

large

Comparisons	p-value
weekly vs. con	0.0048
3days vs. con	0.0086
daily vs. con	0

Figure 4: Density of spheroids in biospheres of mono- and co-cultures

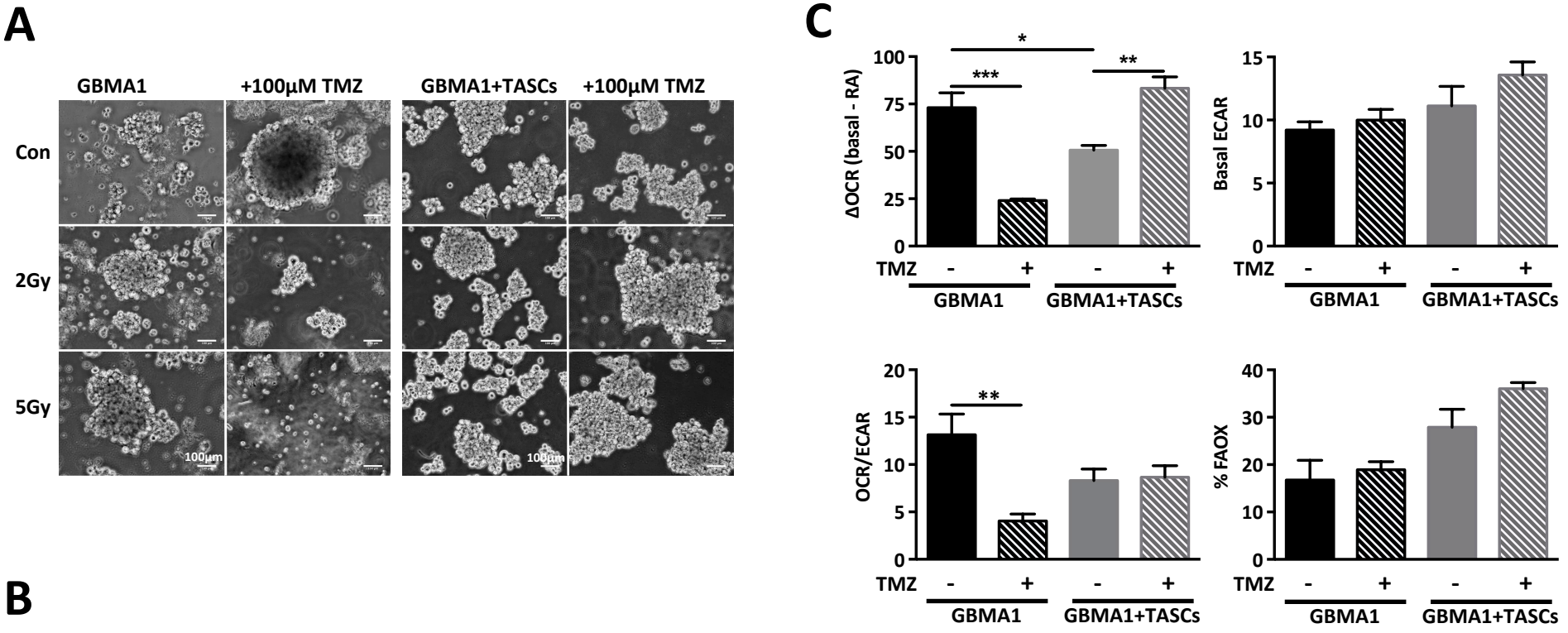
A
GBMA1
+100µM TMZ
GBMA1+TASCs
+100µM TMZ
Con
2Gy
5Gy
100µm
100µm
C
ΔOCR (basal - RA)
Basal ECAR
OCR/ECAR
% FAOX
TMZ
GBMA1
GBMA1+TASCs
B
a
b
MFI (Mitochondria)
TMZ (100µM):
IR:
2Gy
5Gy
Pop.
Events
Median
P1 (APC)
9977
5549,9
9817
941,85
9050
7700,94
9060
8160,17

Figure 5

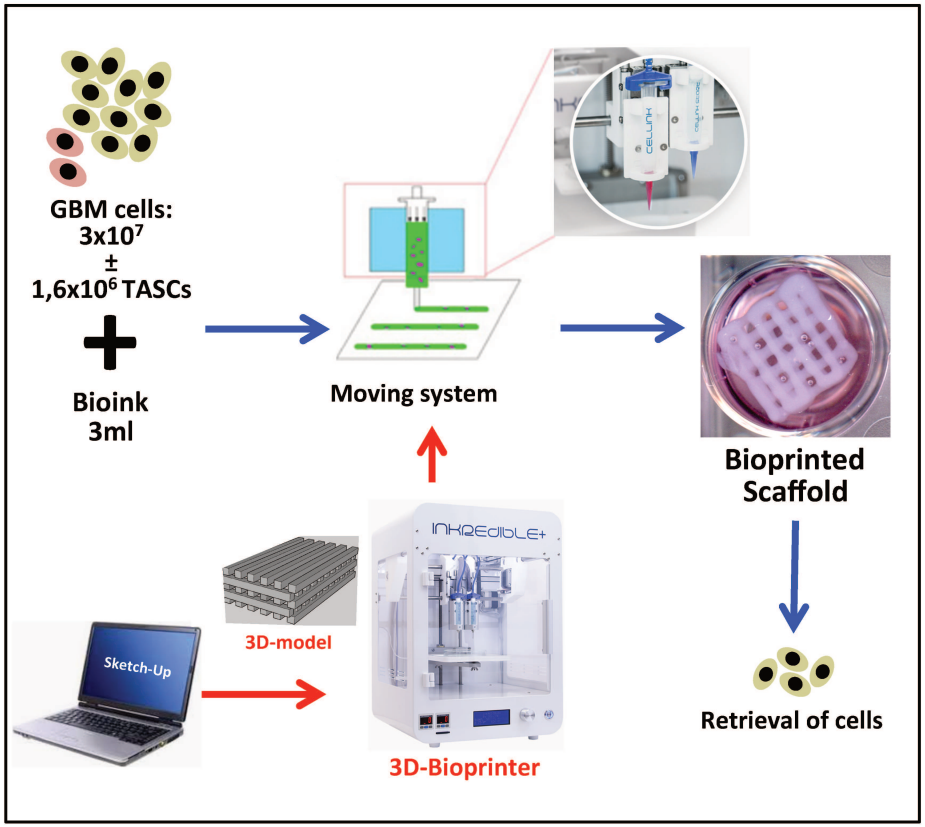
GBM cells:
3x10^7
±
1,6x10^6 TASCs
Bioink
3ml
Moving system
Bioprinted
Scaffold
Retrieval of cells
3D-model
Sketch-Up
3D-Bioprinter

Figure S1

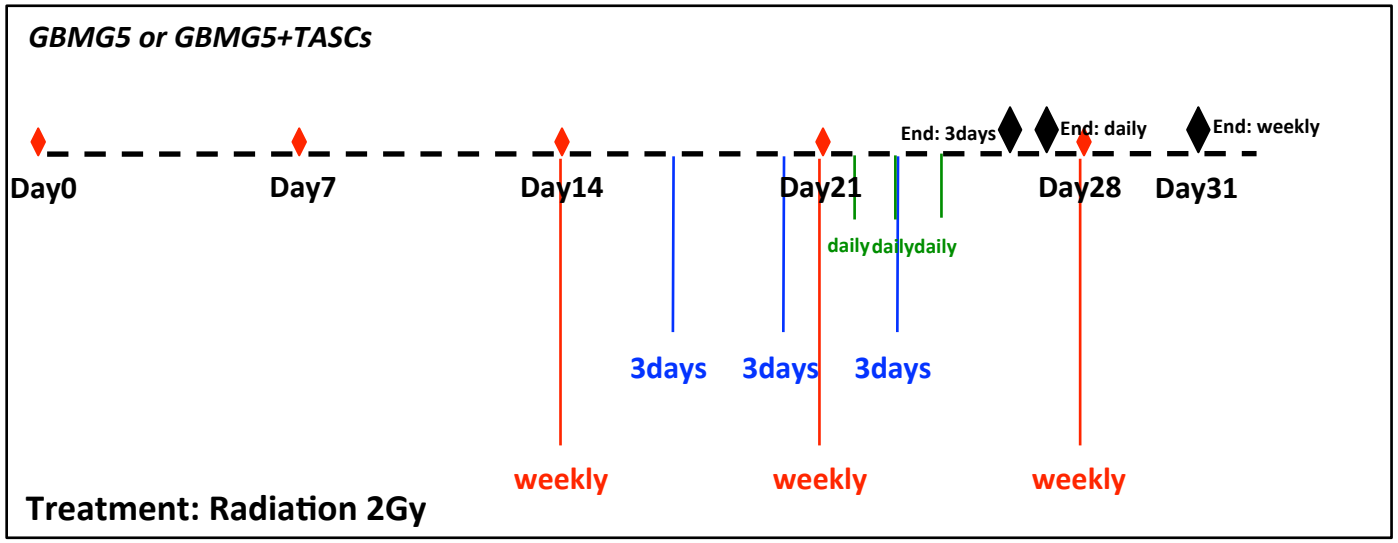
GBMG5 or GBMG5+TASCs
End: 3days
End: daily
End: weekly
Day0
Day7
Day14
Day21
Day28
Day31
daily
daily
daily
3days
3days
3days
weekly
weekly
weekly
Treatment: Radiation 2Gy

Figure S2

GBM	Type	Morphology	Subtype	Treatment	Survival
GBMA1	GBM IV	neurospheres	mesenchymal	Stupp	?
GBM3	GBM IV	adherent	proneural	Stupp	13 m
GBMG5	GBM IV	neurospheres	proliferative	no	?
GBM5	GBM IV	neurospheres	proliferative	Stupp	7 m
GBM8	GBM IV	neuro/adherent	proneural	Stupp	7 m
GBM22	GBM IV	neurospheres	mesenchymal	Stupp	15 m
GBM24	GBM IV	neurospheres	mesenchymal	Stupp	17m
GBM30	GBM IV	neurospheres	mesenchymal	Stupp	18 m
GBM35	GBM IV	adherent	neural	Stupp	10m
GBM37	GBM IV	adherent	neural	Stupp	21m
GBM40	GBM IV recidive	neuro/adherent	nd	Stupp	18 m
GBM71	GBM IV	neurospheres	nd	Stupp	14 m

Table S1

3.2 RESULTATS NON PRESENTES DANS L'ARTICLE

Recrutement des CAF par les cellules cancéreuses de GBM

Nous avons démontré le recrutement des CAF par les cellules cancéreuses de GBM. Que ce soit au sein des tumoroïdes obtenus par scaffolds ou biosphères, les CAF sont toujours attirés et recrutés par les cellules cancéreuses de GBM et jamais l'inverse (Figure 14).

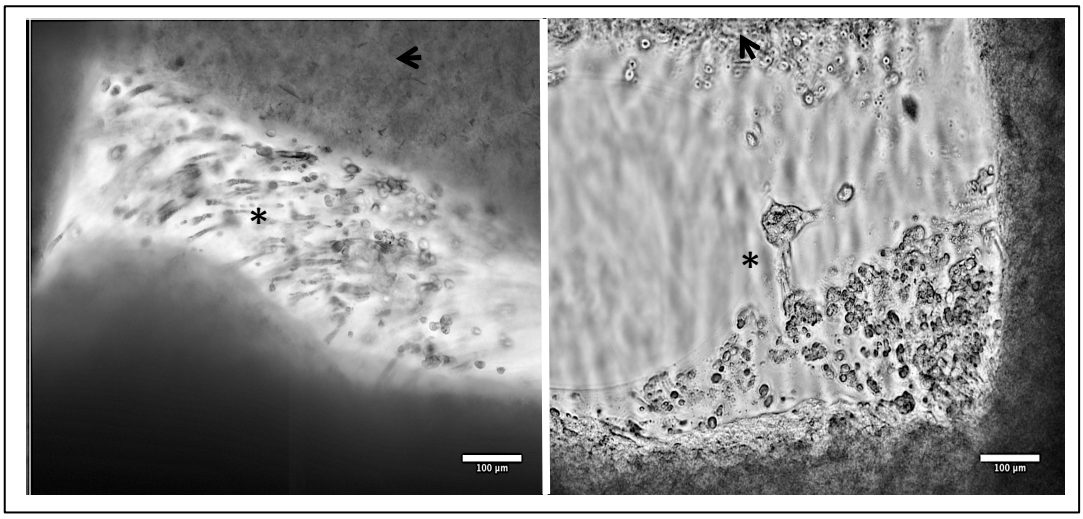

Figure 14. Photographies de scaffolds contenant une co-culture de cellules cancéreuses de GBM et de CAF obtenues par microscopie. Migration des CAF (astériques noires) vers les régions contenant cellules cancéreuses de GBM (têtes de flèches noires) témoignant de leur recrutement.

Chaque GBM comporte des CAF qui lui sont propres

Nous avons démontré que dans chaque primo-culture de GBM, les CAF présentaient des phénotypes différents. Nous avons mis en évidence des marqueurs de surfaces toujours différents entre les CAF provenant de chaque tumeur (Figure 15). Ce constat étoffe une des caractéristiques du GBM, son hétérogénéité interindividuelle.

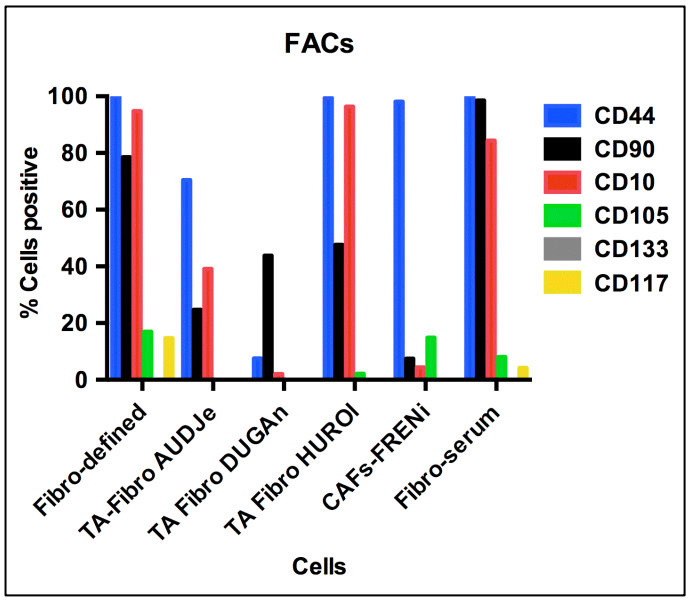

Figure 15. Caractérisation des TASC et d'un CAF. Les phénotypes sont différents entre tous les TASC et le CAF étudiés. Chacun provenant d'une primoculture d'une tumeur d'un patient différent.

3.3 PERSPECTIVES :

Les CAF sont un des éléments déterminants dans l'organisation architecturale de la tumeur. Ils permettent aux cellules cancéreuses de mieux résister au traitement par radiochimiothérapie et de ce fait constituent une cible thérapeutique importante qu'il faut tester. Nous avons démontré qu'il existait des interconnections entre les cellules et que la quantité de mitochondries fonctionnelles présentes dans les cellules cancéreuses en présence des CAF est plus importante. Il est donc nécessaire de comprendre les mécanismes permettant cela.

Dans l'objectif de la plateforme de tumoroïdes que nous souhaitons créer, ces résultats permettent de s'en rapprocher. En effet, notre modèle de tumoroïde est dans la capacité de tester un traitement ciblant directement les CAF de la même manière que la cible thérapeutique peut être les mécanismes d'action de ces CAF. Il est donc important de poursuivre l'étude des CAF en analysant leurs mécanismes d'action.

4 MITOCHONDRIA TRANSFER FROM TUMOR-ACTIVATED STROMAL CELLS (TASCS) TO PRIMARY *GLIOBLASTOMA* CELLS.

Comme nous l'avons démontré dans l'introduction et dans l'article 3, dans les processus de tumorigenèse, le MET joue un rôle important dans le développement, l'infiltration et la résistance tumorale. Les CAF constituent une partie de la population cellulaire du MET. Certains articles rapportent la présence des CAF au sein des GBM cependant leur rôle dans la tumorigenèse et la résistance des GBM n'est pas bien défini.

A partir de notre modèle de tumoroïde de co-culture de cellules de GBM et de CAF, lors des travaux précédents, nous avons constaté que les CAF intervenaient dans la prolifération et dans la résistance aux traitements. Nous avons également constaté des communications directes entre ces deux cellules. Dans notre travail, les CAF ont bien été retrouvés à partir de la tumeur du patient, néanmoins leur durée de vie en culture était limitée. De ce fait, nous avons recréé des CAF à partir de cellules souches mésenchymateuses cultivées avec le milieu conditionné des cellules cancéreuses de GBM. Nous avons nommé ces cellules les TASC (tumor associated stromal cells).

Ce travail avait donc pour objectif d'objectiver ces communications directes intercellulaires et de comprendre comment les CAF permettent en co-culture d'augmenter le taux de mitochondries des cellules cancéreuses.

4.1 PRINCIPAUX RESULTATS :

Les tumoroïdes sont obtenus par co-culture de cellules cancéreuses de primo-cultures de GBM avec des cellules souches mésenchymateuses en présence du milieu conditionné de GBM permettant d'obtenir les TASC.

Les TASC communiquent avec les cellules cancéreuses de GBM par 3 modes : tunneling nano-tubes (TNT), vésicules extra-cellulaires et cannibalisme. Cette interaction cellulaire permet de transférer des mitochondries des TASC aux cellules cancéreuses. Ce transfert augmente la prolifération et la survie des cellules cancéreuses.

ARTICLE 4

Biochemical and Biophysical Research Communications xxx (xxxx) xxx

Contents lists available at ScienceDirect

Biochemical and Biophysical Research Communications

journal homepage: www.elsevier.com/locate/ybbrc

Mitochondria transfer from tumor-activated stromal cells (TASC) to primary *Glioblastoma* cells

Céline Salaud [a, b], Arturo Alvarez-Arenas [c], Fanny Geraldo [a], Juan Belmonte-Beitia [c], Gabriel F. Calvo [c], Catherine Gratas [a, b], Claire Pecqueur [a], Delphine Garnier [a, d], Victor Pérez-Garcià [c], François M. Vallette [a, d, *], Lisa Oliver [a, b, **]

[a] Université de Nantes, INSERM, CRCINA, Nantes, 44007, France
[b] CHU de Nantes, Department of Neurosurgery, Nantes, 44007, France
[c] Department of Mathematics & MOLAB-Mathematical Oncology Laboratory, University of Castilla-La Mancha, 13071, Ciudad Real, Spain
[d] ICO, Laboratoire de Biologie Du Cancer et Théranostics, St Herblain, 44805, France

ARTICLE INFO

Article history:
Received 26 August 2020
Accepted 26 August 2020
Available online xxx

Keywords:
Primary GBM cultures
Mitochondria
Mesenchymal stromal cells
Tunneling nanotubes

ABSTRACT

The tumor microenvironment (TME) controls many aspects of cancer development but little is known about its effect in Glioblastoma (GBM), the main brain tumor in adults. Tumor-activated stromal cell (TASC) population, a component of TME in GBM, was induced *in vitro* by incubation of MSCs with culture media conditioned by primary cultures of GBM under 3D/organoid conditions. We observed mitochondrial transfer by Tunneling Nanotubes (TNT), extracellular vesicles (EV) and cannibalism from the TASC to GBM and analyzed its effect on both proliferation and survival. We created primary cultures of GBM or TASC in which we have eliminated mitochondrial DNA [Rho 0 (ρ^0) cells]. We found that TASC, as described in other cancers, increased GBM proliferation and resistance to standard treatments (radiotherapy and chemotherapy). We analyzed the incorporation of purified mitochondria by ρ^0 and ρ^+ cells and a derived mathematical model taught us that ρ^+ cells incorporate more rapidly pure mitochondria than ρ^0 cells.

1. Introduction

Glioblastoma (GBM) is the most common primary brain tumor in adults, rapidly fatal without treatment. The gold standard for the treatment of GBM is the combination of temozolomide (TMZ) and radiotherapy after maximal surgical removal [1]. The median survival of these patients is around 15 months and <10% of patients survive for more than 5 years [2]. It has long been considered that tumor development and progression depend on the interplay between tumor cells, normal cells and the tumor microenvironment (TME) [3]. Within the TME, cancer-activated fibroblasts, or as designated in this study tumor-activated stromal cells (TASC), are recruited to the tumor by factors released by tumor cells [3]. TASC support multiple aspects of cancer progression (including initiation, invasion, angiogenesis, therapy resistance and metastasis) [4–6]. In GBM, Mesenchymal Stem Cells (MSC) reside in the TME of human gliomas [7] and their presence has been correlated with patient survival and hence GBM aggressiveness [8]. Intercellular communication between tumor cells and other cells present in the TME including TASC or immune cells play an important role in tumor progression. One such interaction is the cellular transfer of mitochondria [9,10] and several studies have shown that transfer through tunneling nanotubes (TNT) confers resistance to chemotherapy and provides a survival advantage [11–14]. In GBM, mitochondrial transplantation through distinct mechanisms (e.g. endocytosis, horizontal transfer …) has been shown to rescue mitochondrial functions and thus tumorigenic potential and cell death pathways *in vitro* [15,16]. In vivo, similar observations have

Abbreviations: 2′,7′-Dichlorodihydrofluorescein diacetate, (DCFDA); Extracellular matrix, (ECM); Extracellular acidification rate, (ECAR); Extracellular vesicles, (EV); Glioblastoma, (GBM); Mesenchymal stem cells, (MSC); MitoTracker, (MitoT); Oxygen consumption rate, (OCR); Reactive oxygen species, (ROS); Rho 0 cells, (ρ^0 cells); Tumor microenvironment, (TME); Tunneling nanotubes, (TNT); Tumor-activated stromal cells, (TASC); Temozolomide, (TMZ).

* Corresponding author. CRCINA, INSERM U1232, Université de Nantes, 8 quai Moncousu, 44007, Nantes, France.
** Corresponding author. CHU de Nantes, Department of Neurosurgery, Nantes, 44007, France.
E-mail addresses: francois.vallette@inserm.fr (F.M. Vallette), lisa.oliver@univ-nantes.fr (L. Oliver).

https://doi.org/10.1016/j.bbrc.2020.08.101
0006-291X/

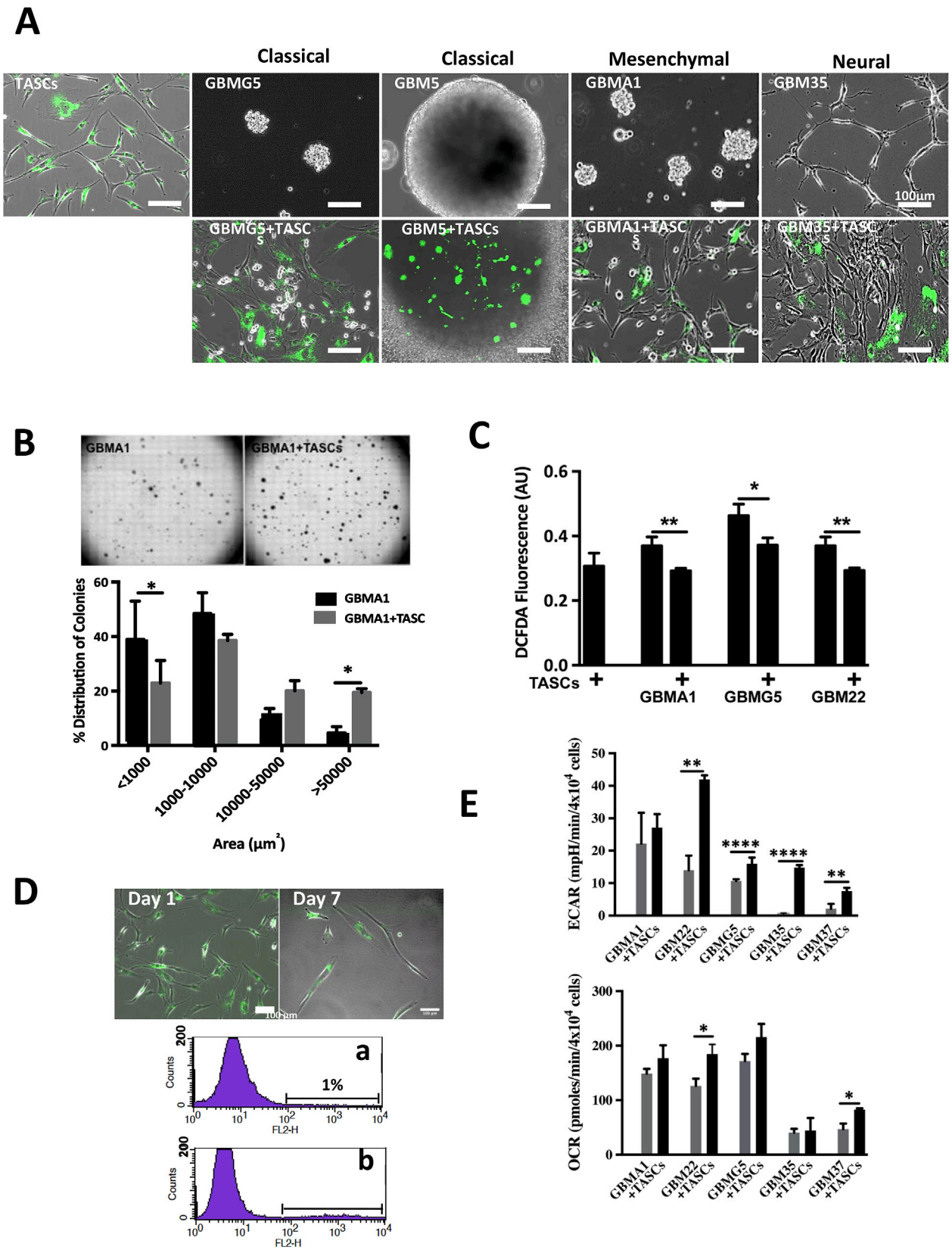

Fig. 1. *Interaction between TASC and GBM cells in co-cultures.* **A.** The morphology of 4 different mono- and co-cultures of GBM cells and actin-GFP labeled-TASC cultured at a ratio of 5:1. The cultures were analyzed microscopically every day over one week. The data presented is that of day 3 and as observed actin-GFP containing particles were visible within GBM cells. Note the formation of neurospheres (organoids) in GBM5 cultures. (Scale bar = 100 µm) **B**. Mono- and co-cultures of GBMA1 and TASC were performed in a soft agar assay and after 21 days the number and size of the colonies were determined. The data are presented as the percentage distribution of the colonies as a function of the number and size. **C.** Total ROS expression was determined in 2×10^3 cells obtained from either mono- or co-cultures of TASC and GBM cells using a DCFDA assay. **D.** *Top:* Actin-GFP labeled-MSCs cultured in defined medium on day 1 and day 7. Note the presence of Actin-GFP labeled cells on day 7. *Bottom:* FACS analyses of co-cultures of GBM cells (**a**: GBMA1 and **b**: GBMG5)

Please cite this article as: C. Salaud et al., Mitochondria transfer from tumor-activated stromal cells (TASC) to primary *Glioblastoma* cells, Biochemical and Biophysical Research Communications, https://doi.org/10.1016/j.bbrc.2020.08.101

been made which suggest that cell-cell interactions and materials exchanges are creating a cellular network that is important for tumor growth and resistance to treatments [17,18].

In this work, we address the question of the existence of similar mechanisms between TASC and cancer cells in GBM.

2. Methods

2.1. Materials

Unless stated otherwise all cell culture material was obtained from Thermo Fisher Scientific (Courtaboeuf, France) and chemicals from Sigma Aldrich (Lyon, France).

2.2. Patient samples and culture

Tumors were obtained from patients diagnosed with high-grade GBM from the "Tumorothèque IRCNA". Characteristics of GBMS used in this study are presented in Table S1. MSC and GBM primary cultures were obtained as described earlier [19,20]. MSC were cultured in a mixture of conditioned medium from GBM primary cultures (48 h) and defined medium at a ratio of 30:70 for at least 7 days as.

2.3. Rho 0 cells

To obtain Rho 0 cells (ρ^0 cells): GBM cells or TASC were cultured in defined medium containing 100-ng/mL EtBr (ethidium bromide), 50-μg/mL uridine and 110-ng/mL pyruvate for at least 4 weeks.

2.4. Co-cultures

Co-cultures were performed by plating 2×10^5 Actin-GFP-labeled-MSC cells (CellLight Actin-GFP BacMam 2.0, Thermo Fisher Scientific) and then 24 h later 10^6 GBM cells were added.

2.5. Quantification of spheroids in agar-agarose

MSC (500 cells/well) were plated in 6-well plates, overlaid with 0.5% agar and then a layer of 0.35% agarose containing 2.5×10^3 GBM cells were added.

2.6. Cell proliferation

Cell counts and viability were performed using the Countess II automated cell counter (Thermo Fisher Scientific) according to manufacturer's instructions.

2.7. Subcellular fractionation

Briefly, after homogenization of MSC (about 2×10^8 cells) the crude mitochondrial fraction was isolated by centrifugation at 10 000 g for 10 min then layered on a 30% Percoll solution and centrifuged at 95 000 g for 30 min. After centrifugation, a dense band of pure mitochondria was observed at the bottom of the tube and a diffused white band of mitochondria-associated membrane at the top of the tube (Table S2).

2.8. Mitochondrial labeling

Pure mitochondria (PM) (1-μg) were incubated with 25-nM MitoTracker (MitoT) deep red at 37 °C for 30 min.

2.9. FACS analysis

MSC were characterized by flow cytometry using the MSC Phenotyping kit (Miltenyi Biotec, Auburn, CA, USA) according to the manufacturer's protocol on a CANTO II (BD Biosciences) flow cytometer equipped with DIVA software, with 10 000 events recorded for each sample.

2.10. ROS analysis

Cells (2×10^3) were loaded into CellTak (BD-Biosciences) coated flat-bottom 96-well plates. CM-H2DCFDA (Thermo Fisher) was added to give a final concentration of 2,5 μM and the cells were incubated for 10 min at 37 °C. The expression of total ROS was determined using a FLUOStar Omega (BMG LabTech) with excitation at 490 nm and emission at 520 nm.

2.11. Electron microscopy

Cells were fixed in 4% glutaraldehyde, then fixed directly for 1 h at 4 °C with 2% OsO_4 in 0.2-M symmetric collidin pH7.2. After washing with 0.2-M symmetric collidin pH7.2, the cells were dehydrated through a graded ethanol series and propylene oxide then embedded in Epox 812 medium. 70–90 nm sections were cut using a Rerchert ultramicrotome and stained with uranyl-acetate and lead-citrate.

2.12. Metabolic analysis

Mitochondrial oxygen consumption rate (OCR) was measured using a XF24 Analyzer (Seahorse, Agilent, Les Ulis, France) and was determined from the mean of 4 values.

2.13. Statistical analyses

Data were analyzed and statistical analyses were performed using GraphPad Prism 7.00 (GraphPad Software, San Diego, CA, USA). Data points are expressed as mean ± SD unless otherwise indicated. *$p < 0.05$, **$p < 0.01$, ***$p < 0.001$.

3. Result

3.1. Interaction between MSC and GBM primary cultures in co-cultures

To determine the interactions in co-cultures between GBM cells and TASC; actin-GFP labeled-TASC were cultured with GBM cells at a ratio of 1:5 and the co-cultures were analyzed every 24 h over 7 days. In parallel, separate monocultures of GBM cells and TASC were also performed. Different GBM subtypes were tested and as shown in Fig. 1A, distinct cellular organizations could be observed: attachment to the Petri dish for neural subtype GBM35, very large spheres for classical subtype GBM5 and smaller spheres for the classical and mesenchymal subtypes GBMG5 and GBMA1. After 48 h we observed the detachment of TASC from the flask and their

and GFP-actin-labeled TASC after 7 days of culture show little or no MSC present in the co-cultures. **E.** Metabolism analysis: glycolysis as measured by ECAR showed a statistical increase in 5 different co-cultures as compared to monocultures. Mitochondrial respiration as measured by OCR showed a statistical difference in 2 out of 5 co-cultures. Seahorse experiments were performed at one week of culture.

Please cite this article as: C. Salaud et al., Mitochondria transfer from tumor-activated stromal cells (TASC) to primary *Glioblastoma* cells, Biochemical and Biophysical Research Communications, https://doi.org/10.1016/j.bbrc.2020.08.101

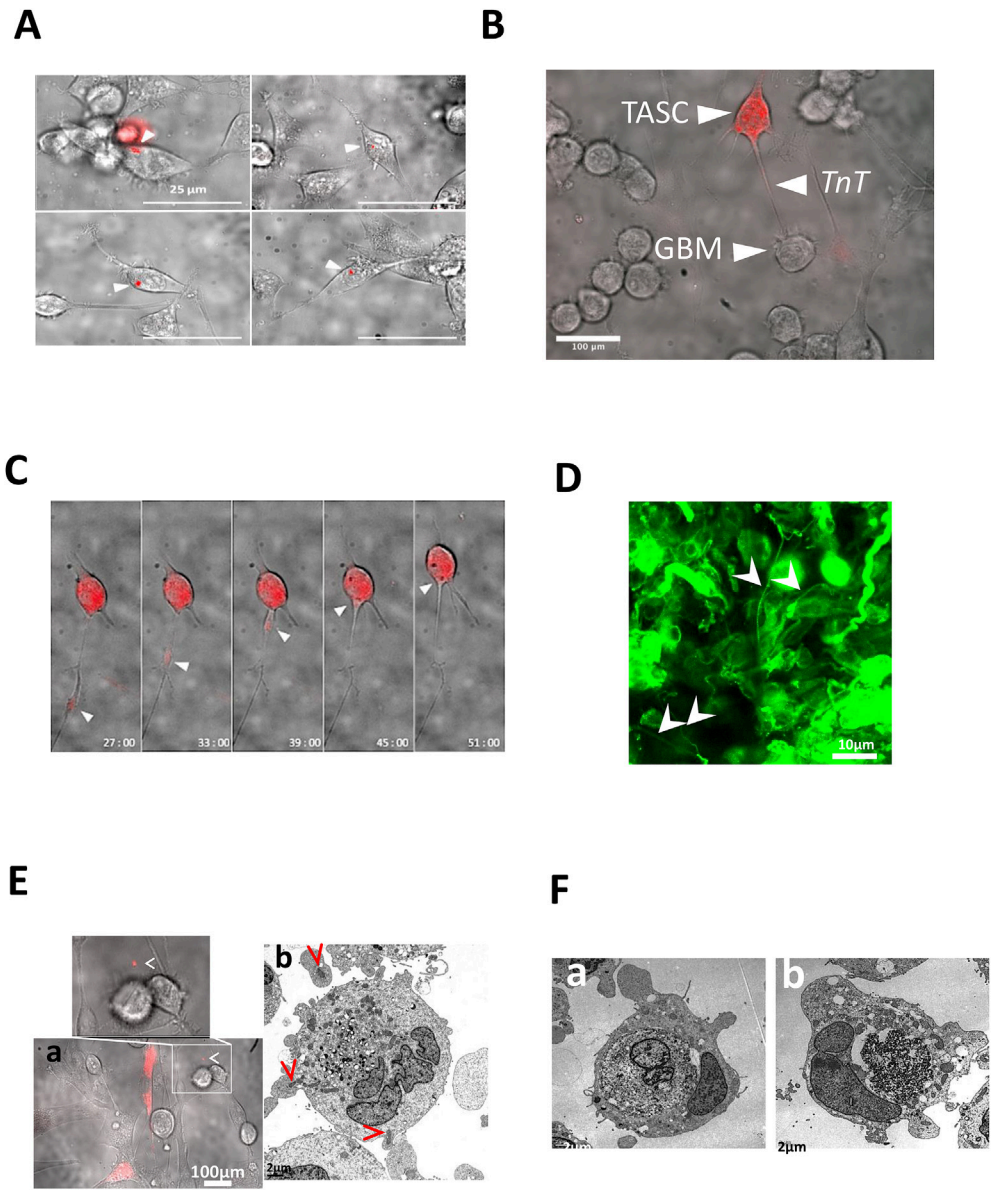

Fig. 2. *Transfer of mitochondria from TASC to GBM cells.* **A**. Co-culture of MitoT-Deep Red labeled-mitochondria containing TASC and GBMA1 cells shows the presence of red-labeled vesicles in GBMA1 cells after 24 h of culture as indicated by the white arrows. **B**. Presence of MitoT-labeled mitochondria in TNT generated by TASC. **C.** Transfer of MitoT-labeled mitochondria from TASC via TNT to GBM cells (**d**). (Scale bar = 100 µm) **C**. Time-Lapse microscopy illustrating the transfer of mitochondria (white head arrows) along TNT and then transfer into GBM cells. (Scale bar = 100 µm) **D**. Confocal microscopic image of organoid of GBM35 showing presence of TNT (Scale bar = 10 µm). **E**. (**a**) Presence of EV containing MitoT-Red labeled mitochondria outside of the cells. (Scale bar = 100 µm) (**b**) Electron microscopy of a neurosphere obtained after co-culture showing the presence of mitochondria in EV-like vesicles outside of the cell as well as mitochondria in protrusions of the cell membrane (red arrows). (Scale bar = 2 µm). **F.** Electron microscopy (as in E) showing incorporation of exogenous cellular materials by GBM cells (a and b: 2 different GBM).

migration into spheroids, followed by incorporation within tumor cells (Fig. 1A).

In a second series of experiments mono- and co-cultures of GBM cells and TASC were performed in soft agar to determine the size and distribution of the colonies. As seen in Fig. 1B, after 3 weeks although the overall number of colonies was higher in mono-cultures, the number of large colonies was higher in the co-cultures as compared to monocultures.

Total ROS expression analyses showed that the presence of TASC caused a significant decrease in the level of ROS in all co-cultures of GBM cells as compared to monocultures (Fig. 1C).

3.2. Effects of co-culture on the metabolism of GBM cells

After 7 days, the co-cultures were recuperated and the presence of actin-GFP labeled TASC was determined by FACS. As shown in Fig. 1D, no actin-GFP-labeled TASC were detected in the co-cultures while they could still be detected in monoculture. This suggests that the TASC in the co-cultures were consumed in the presence of GBM cells. Metabolic analyses using the Seahorse technology were performed on GBM cells after co- and monoculture. Fig. 1E indicates that after 1-week there was a significant increase in glycolysis (measured by ECAR) in 4 out of 5 GBM co-cultures (i.e. when TASC had disappeared). In contrast, analyses of the oxidative phosphorylation (measured by OCR) showed little variations between co-

Please cite this article as: C. Salaud et al., Mitochondria transfer from tumor-activated stromal cells (TASC) to primary *Glioblastoma* cells, Biochemical and Biophysical Research Communications, https://doi.org/10.1016/j.bbrc.2020.08.101

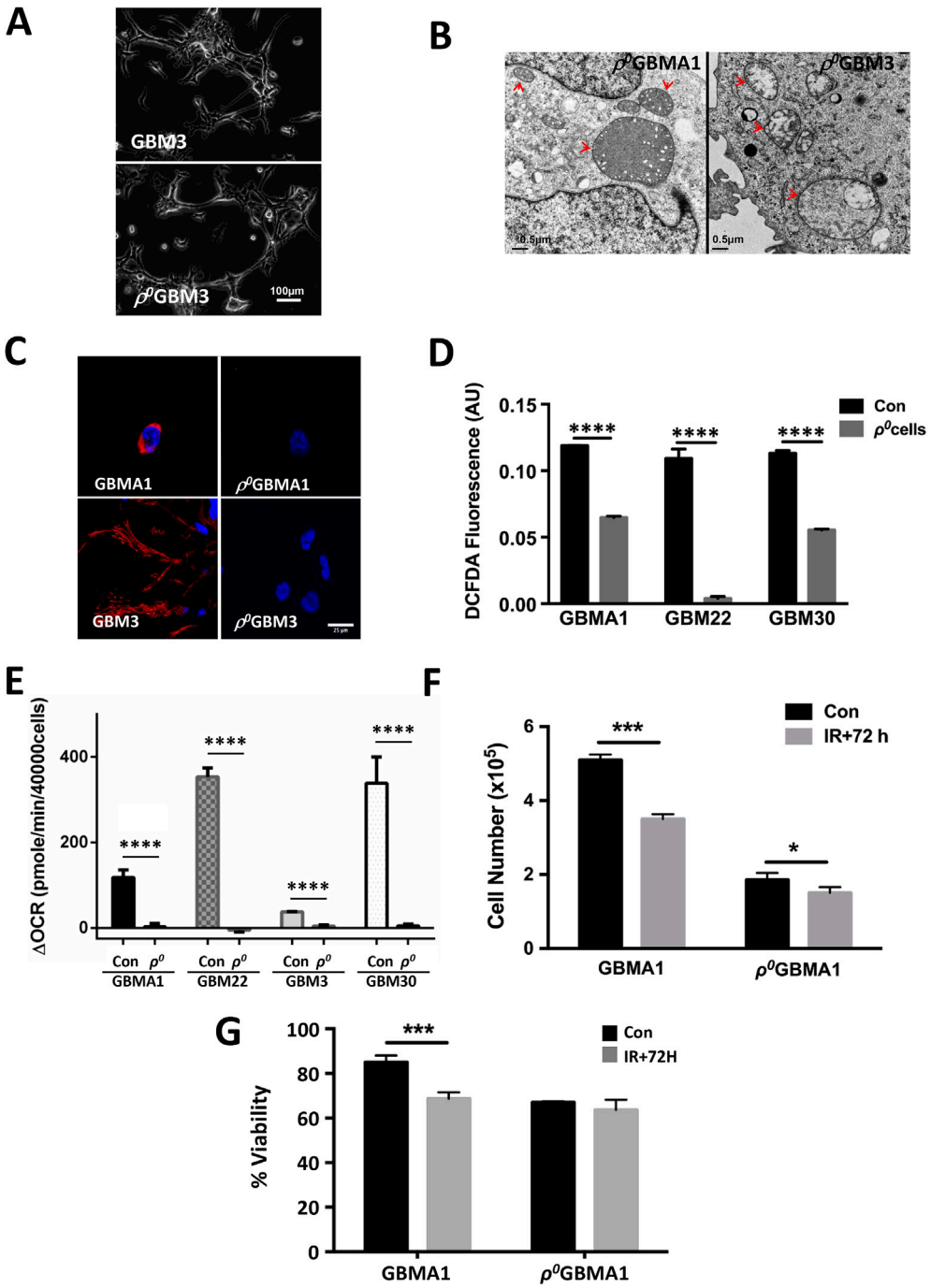

Fig. 3. *Characterization of ρ^0GBM cells.* **A**. Morphology of GBM3 cells and GBM3 cells treated with EtBr for 4 weeks (ρ^0GBM3). (Scale bar = 100 μm) **B**. Electron microscopy of ρ^0GBMA1 and ρ^0GBM3 cells showing the presence of non-functional mitochondria (red arrows). (Scale bar = 0.5 μm) **C**. MitoT-Red-labeled functional mitochondria in GBMA1 and GBM3 cells and the absence of labeled mitochondria in ρ^0GBMA1 and ρ^0GBM3 cells. (Scale bar = 25 μm) **D**. The expression of ROS production in 3 control and the corresponding ρ^0GBM cultures was quantified using a DCFDA assay. Statistical analyses were done using a Grouped two-way ANOVA analysis. **E**. Mitochondrial respiration was assessed using the Seahorse technology in 4 control and ρ^0GBM cultures. The data is expressed as the change in the rate of O_2 consumption. Statistical analyses were done using a Grouped two-way ANOVA analysis. GBMA1 and ρ^0GBMA1 cells were irradiated with 5 Gy and 72 h later the proliferation (**F**) and the viability (**G**) were determined.

and monocultures (Fig. 1E).

3.3. Mitochondria can be transferred to GBM cells via tunneling nanotubes, cannibalism and extracellular vesicles

We investigated the role of mitochondria in the TASC/GBM co-cultures as a significant amount of ROS is formed in mitochondria [20]; and a recent study has shown the incorporation of isolated mitochondria by GBM cells [21]. Mitochondria in TASC were labeled with MitoT deep red and then co-cultured with GBM cells. Microscopic analyses of these co-cultures were done at 24 h and 48 h and 72 h. We observed the presence of labeled mitochondria (hence originating from TASC) in GBM cells 24 h after the initiation of the co-culture (Fig. 2A). Using time-lapse microscopy, we observed the

Please cite this article as: C. Salaud et al., Mitochondria transfer from tumor-activated stromal cells (TASC) to primary *Glioblastoma* cells, Biochemical and Biophysical Research Communications, https://doi.org/10.1016/j.bbrc.2020.08.101

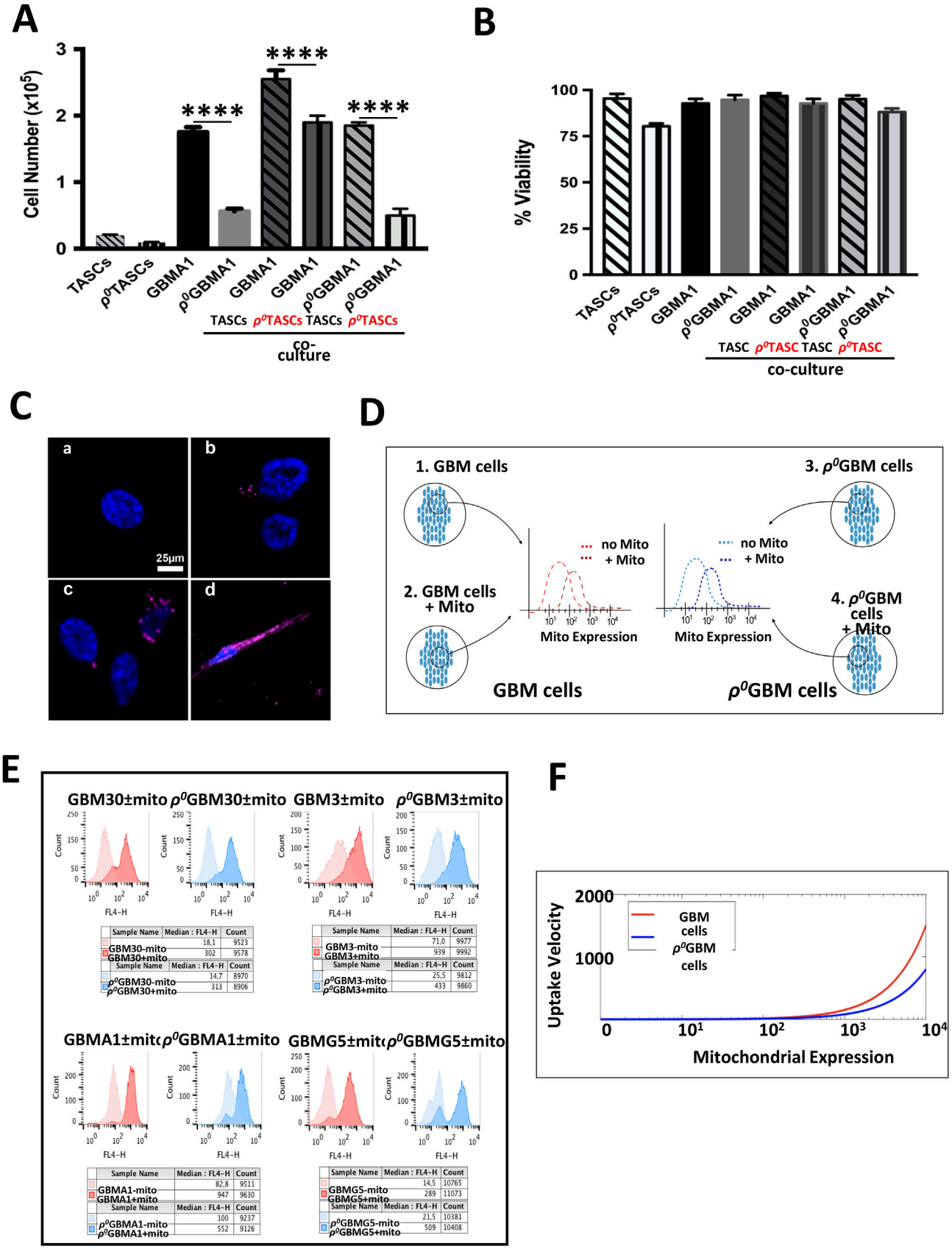

Fig. 4. *Purified mitochondria isolated from MSC transfer to GBM or ρ^0GBM cells.* **A.** Quantification of the proliferation of cells in mono- and co-cultures of GBMA1 cells or ρ^0GBMA1 cells and TASC or ρ^0TASC. GBM cells were plated at 5×10^4 cells/ml in 6-well plates in the presence or absence of 10^4 cell/ml TASC. After 7 days the cells were collected and the number of cells determined. Statistical analyses were done using a Grouped two-way ANOVA analysis. **B.** Effect of TASC or ρ^0TASC on the viability of GBM or ρ^0GBM cells after 72 h of culture. **C.** ρ^0GBM3 cells were incubated with either 25-nM Mito-T (**a**) or 1-µg MitoT-labeled mitochondria for 24 h (**b**), 48 h (**c**) or 72 h (**d**) and then analyzed using a confocal microscope. Note

Please cite this article as: C. Salaud et al., Mitochondria transfer from tumor-activated stromal cells (TASC) to primary *Glioblastoma* cells, Biochemical and Biophysical Research Communications, https://doi.org/10.1016/j.bbrc.2020.08.101

migration of mitochondria along interconnecting tubules, identified as TNT (Fig. 2B and C).

Of note, the presence of nanotubular structures in monocultures of GBM (Fig. 2D) suggests that a transfer of numerous mitochondria between GBM cells via TNT could occur under our conditions.

Aside from the trafficking of mitochondria through TNT, mitochondria can also be transferred inside extracellular vesicles (EV) [22,23]. We identified EV enclosing mitochondria in our co-culture experiments by immunofluorescence as some vesicles containing red-labeled mitochondria from TASC, which was confirmed by electron microscopic analyses (Fig. 2E).

We also observed cannibalism in co-cultures by electron microscopy and light microscopy suggesting that TASC were cannibalized by GBM cells (Fig. 2F). In addition, TASC undergoing fragmentations/cell death were also observed which also could account for mitochondria transfer (Figure S3).

3.4. Characterization of Rho 0 cells

To study the functional importance of mitochondrial transfer from TASC to GBM cells, we generated Rho 0 cells (ρ0 cells). No apparent morphological differences could be discerned between ρ0GBM cells and their control counterparts (Fig. 3A). However, using electron microscopy, morphologically altered mitochondria were present in ρ0GBM cells (Fig. 3B). The fluorescent microscopy on ρ0GBM cells after incubation with the mitochondrial inner potential sensitive MitoT showed no labeling as compared to ρ+GBM cells (Fig. 3C). Next, we quantified the levels of ROS present in these cells and observed a significant reduction in the level of ROS expression in ρ0GBM cells compared to control GBM cells (Fig. 3D) and an absence of oxygen consumption in 4 different ρ0GBM cultures (Fig. 3E). ρ0GBM cells continued to proliferate although much slower than the control cultures (Fig. 3F). Irradiation of ρ0GBM cells indicated that these cells were statistically less sensitive to radiation, showing little changes in cell proliferation or cell death (Fig. 3F and G).

3.5. Proliferation of co-cultures of GBM or ρ^0GBM cells and TASC

We performed co-culture experiments between ρ0GBM cells with TASC or ρ0TASC and vice versa to determine the transfer of mitochondria from TASC to GBM cells. After 7 days of culture the cells were collected and the proliferation of the cells was assessed in co- or monoculture. As shown in Fig. 4A, ρ0 cells proliferated significantly more slowly than control cells both for TASC and GBM cells and as expected, exhibited a reduced metabolism (data not shown). The co-culture with TASC increased the number of ρ+GBM and ρ0GBM. However, addition of ρ0TASC did not affect GBM growth. Nevertheless, no effect on the viability of any of the different cell cultures was observed (Fig. 4B).

3.6. Mitochondria purified from MSC are transferred into GBM cells regardless of their mitochondrial status

Recent study has shown that cancer cells could take up purified mitochondria *in vitro* and restore tumorigenic potential in mitochondrial DNA-deficient cancer cells [16]. We incubated MitoT-labeled mitochondria purified from MSC with GBM cells to compare the uptake of mitochondria by ρ+GBM and ρ0GBM cells (Fig. 4C). The results obtained indicated that ρ0GBM cells were able to incorporate labeled mitochondria as early as 24 h after incubation and that by 72 h a mitochondrial network could be identified (Fig. 4C).

A mathematical model was developed, using the experimental setting described in Fig. 4D, in which a transport equation approach was chosen to reproduce the dynamics of mitochondria uptake (Supplementary Data 2). Such type-equations account for the temporal shifts in the mitochondria expression levels. Experiments where no mitochondria were added to the cultures were used to estimate some of the initial conditions compared to experiments where mitochondria were added in the cultures (Fig. 4E). From this, we were able to estimate the uptake velocity $v_i(x,\ t)$, with x denoting the mitochondria expression level. We found that the velocity that yielded the best fits between the experimental and model data was a linear function $v_i(x,t) = a_i x$ (Figure S1).

According to the experimental results, most of the primary cultures incorporated mitochondria during the first 24 h, since no relevant change in the levels was observed thereafter. Based on the predictions of our model, we concluded that mitochondria uptake is maximal at 24 h and counter intuitively more important for cells with healthy mitochondria than for ρ0GBM cells (Fig. 4F).

4. Discussion

TASC are increasingly studied in many cancers, but there is still very little information about their roles in GBM. However, TASC have been shown to contribute to the increased growth in GBM *in vitro* by the transfer of materials through TNTs and EVs [24–27]. Regulatory factors released from EV have essential roles, including the support of tumor growth, angiogenesis, metastasis and therapy resistance [28-32].

Mitochondria play an active and central role in drug resistance as they constitute a hub for several molecular mechanisms such as apoptosis and metabolic reprogramming. In this study, we have in particular studied the influence of mitochondria exchange between TASC and GBM cells under spheroid conditions (Figs. 1 and 2). We show the transfer of a large number of functional mitochondria from TASC to GBM cells via TNT, EV and possibly through other mechanisms including “cannibalism” (Fig. 3). TNT are transient cytoplasmic extensions connecting non-adjacent cells that can span impressive lengths of several 100 μm, with diameters ranging from 50 to 1500 nm [28]. These TNT are characterized by continuity of both the plasma membrane and the cytoplasm of the two connected cells allowing trafficking of much bigger cargos than gap junctions. TNT can transport a multitude of cellular signals that range from ions, small molecules (miRNA) to entire organelles (mitochondria), or transport of cargos including organelle-derived vesicles and plasma membrane elements [33].

In this study, we demonstrated that functional mitochondria transferred from TASC to GBM cells have a profound impact on GBM cell metabolism and proliferation as well as on survival (Figs. 4–6). Many cancer cells are biased towards the glycolytic metabolism; but they also need oxidative phosphorylation for their pathological requirements. Respiration is important for cancer cell proliferation, tumor progression and metastasis. Cancer cells without mtDNA (ρ^0cells) form tumors after a considerable delay compared to their parental counterparts and tumor progression was associated with the acquisition of mtDNA from the host, resulting in respiration

these experiments were performed on 4 different ρ^0GBM cultures. (Scale bar = 25 μm). **D.** Representations of the 4 different conditions of the experiments performed. GBM cells were incubated with either 1-μg MitoT-labeled pure mitochondria or 25-nM MitoT for different times after which, the cells were analyzed by FACS to determine mitochondria uptake. **E.** The uptake of mitochondrial by GBM or ρ^0GBM cells. GBM30, GBM3, GBMA1 and GBMG5 cells (10^6 cells) and the corresponding ρ^0GBM cells were incubated with 1-μg MitoT-labeled pure mitochondria or without mitochondria for 24 h and then the cells were analyzed by FACS to determine the uptake of MitoT-labeled mitochondria. **F.** Graph displaying the uptake velocities linear profiles: the rate at which GBM and ρ^0GBM cells internalize mitochondria can be different, as shown for GBM3.

Please cite this article as: C. Salaud et al., Mitochondria transfer from tumor-activated stromal cells (TASC) to primary *Glioblastoma* cells, Biochemical and Biophysical Research Communications, https://doi.org/10.1016/j.bbrc.2020.08.101

recovery. The velocity profile of mitochondria uptake, suggested by our mathematical model, implies that its rate is proportional to the mitochondria level present in the cell and thus is not led by the lack of mitochondrial support (Fig. 4). The range of mitochondrial levels observed in the experiments did not show any saturation, particularly in cells displaying higher uptake velocities. However, it cannot be discarded that a certain threshold could exist, so that beyond the linear uptake, dependence breaks down. Since materials exchanged between cancer cells and microenvironment are facilitating proliferation, this exchange would provide a clear selective advantage for cancer cells.

5. Conclusion

Altogether our results highlight the importance of cell-cell cooperation in tumors. This includes the transfer of material (including mitochondria) by different pathways: TNT, microvesicles and cannibalism of cells from the tumor microenvironment. The mechanisms implicated in the transfer of mitochondria to cancer cells might represent an important new therapeutic target in GBM.

Declaration of competing interest

The authors declare no conflict of interest.

Acknowledgments

We thank the platform MicroPicell for their aid with all the microscopic work and the Cytometry Facility Cytocell for expert technical assistance.

Appendix A. Supplementary data

Supplementary data to this article can be found online at https://doi.org/10.1016/j.bbrc.2020.08.101.

Declaration section

Consent for publications

N/A

Availability of data and materials

All data and materials are available upon request to corresponding authors.

Ethics approval and consent to participate

The bio-collection used for this analysis is the Glioblastoma collection belonging to the pediatric research program of the University Hospital of Nantes (Ref. MESR DC-2014-2206, having obtained a favorable opinion from CPP Ouest IV (Dossier 06/15) on 08 / 04/2015).

Funding

This work is supported by grants from “Ligue Grand Ouest Contre le Cance (grant number RN19040NN) and the “Plan Cancer HTE program MoGlimaging” (grant number: HTE C16073NS), “Ministerio de Economía y Competitividad/FEDER, Spain [grant number MTM2015-71200-R]” and James S. McDonnell Foundation (USA)” 21st Century Science Initiative in Mathematical and Complex Systems Approaches for Brain Cancer (Collaborative award 220020450)”. AAA was supported by a fellowship from UCLM [2015/4062].

Authors contributions

CS and LO: performed and analyzed the biological data. AAA, JBB, GFC, VPG performed the mathematical studies. FG, CG, CP, DG: performed experiments for the phenotyping of the cultures. LO and FMV designed and supervised most of the experiments, analyzed the data and wrote the manuscript with the contribution of all the authors.

References

[1] R. Stupp, et al., Radiotherapy plus concomitant and adjuvant temozolomide for glioblastoma, N. Engl. J. Med. 352 (2005) 987–996, https://doi.org/10.1056/NEJMoa043330.
[2] R. Stupp, et al., Effects of radiotherapy with concomitant and adjuvant temozolomide versus radiotherapy alone on survival in Glioblastoma in a randomised phase III study: 5-year analysis of the EORTIC-NCIC trail, Lancet Oncol. 10 (2009) 459–466, https://doi.org/10.1016/S1470-2045(09)70025-7.
[3] C.C. Maley, et al., Classifying the evolutionary and ecological features of neoplasms, Nat. Rev. Canc. 17 (2017) 605–619, https://doi.org/10.1038/nrc.2017.69.
[4] N. Nair, et al., A cancer stem cell model as the point of origin of cancer-associated fibroblasts in tumor microenvironment, Sci. Rep. 7 (2017) 6838, https://doi.org/10.1038/s41598-017-07144-5.
[5] L. Tao, et al., Cancer associated fibroblasts: an essential role in the tumor microenvironment, Oncol. Lett. 14 (2017) 2611–2620, https://doi.org/10.3892/ol.2017.6497.
[6] F. Papaccio, et al., Concise review: cancer cells, cancer stem cells, and mesenchymal stem cells: influence in cancer development, Stem Cells Transl. Med. 6 (12) (2017) 2115–2125, https://doi.org/10.1002/sctm.17-0138.
[7] T.L. Whiteside, Exosome and mesenchymal stem cell cross-talk in the tumor microenvironment, Semin. Immunol. 35 (2018) 69–79, https://doi.org/10.1016/j.smim.2017.12.003.
[8] T. Shahar, et al., Percentage of mesenchymal stem cells in high-grade glioma tumor samples correlates with patient survival, Neuro Oncol. 19 (2017) 660–668, https://doi.org/10.1093/neuonc/now239.
[9] D. Torralba, F. Baixauli, F. Sánchez-Madrid, Mitochondria know No boundaries: mechanisms and functions of intercellular mitochondrial transfer, Front. Cell Dev. Biol. 4 (2016) 107, https://doi.org/10.3389/fcell.2016.00107.
[10] J.L. Spees, et al., Mitochondrial transfer between cells can rescue aerobic respiration, Proc. Natl. Acad. Sci. U.S.A. 103 (2006) 1283–1288, https://doi.org/10.1073/pnas.0510511103.
[11] R. Moschoi, et al., Protective mitochondrial transfer from bone marrow stromal cells to acute myeloid leukemic cells during chemotherapy, Blood 128 (2016) 253–264, https://doi.org/10.1182/blood-2015-07-655860.
[12] A. Caicedo, et al., MitoCeption as a new tool to assess the effects of mesenchymal stem/stromal cell mitochondria on cancer cell metabolism and function, Sci. Rep. 5 (2015) 9073, https://doi.org/10.1038/srep09073.
[13] A. Rustom, et al., Nanotubular highways for intercellular organelle transport, Science 303 (2004) 1007–1010, https://doi.org/10.1126/science.1093133.
[14] Y. Hekmatshoar, et al., The role of metabolism and tunneling nanotube-mediated intercellular mitochondria exchange in cancer drug resistance, Biochem. J. 475 (2018) 2305–2328, https://doi.org/10.1042/BCJ20170712.
[15] C. Sun, et al., Endocytosis-mediated mitochondrial transplantation: transferring normal human astrocytic mitochondria into glioma cells rescues aerobic respiration and enhances radiosensitivity, Theranostics 9 (2019) 3595–3607, https://doi.org/10.7150/thno.33100.
[16] L.-F. Dong, et al., Horizontal transfer of whole mitochondria restores tumorigenic potential in mitochondrial DNA-deficient cancer cells, Elife 6 (2017), e22187, https://doi.org/10.7554/eLife.22187.
[17] M. Osswald, et al., Brain tumour cells interconnect to a functional and resistant network, Nature 528 (2015) 93–98, https://doi.org/10.1038/nature16071.
[18] M. Osswald, et al., A malignant cellular network in gliomas: potential clinical implications, Neuro Oncol. 18 (2016) 479–485, https://doi.org/10.1093/neuonc/now014.
[19] L. Oliver, et al., Differentiation-related response to DNA breaks in human mesenchymal stem cells, Stem Cell. 31 (2013) 800–807, https://doi.org/10.1002/stem.1336.
[20] G.C. Brown, V. Borutaite, There is no evidence that mitochondria are the main source of reactive oxygen species in mammalian cells, Mitochondrion 12 (2012) 1–4, https://doi.org/10.1016/j.mito.2011.02.001.
[21] B. Nzigou Mombo, et al., MitoCeption: transferring isolated human MSC mitochondria to glioblastoma stem cells, JoVE (120) (2017), 55245, https://doi.org/10.3791/55245.
[22] G. van Niel, G. D'Angelo, G. Raposo, Shedding light on the cell biology of extracellular vesicles, Nat. Rev. Mol. Cell Biol. 19 (2018) 213–228, https://doi.org/10.1038/nrm.2017.125.
[23] K.P. Hough, et al., Exosomal transfer of mitochondria from airway myeloid-

derived regulatory cells to T cells, Redox. Biol. 18 (2018) 54–64, https://doi.org/10.1016/j.redox.2018.06.009.
[24] M.L. Vignais, et al., Cell connections by tunneling nanotubes: effects of mitochondrial trafficking on target cell metabolism, homeostasis, and response to therapy, Stem Cell. Int. 2017 (2017) 6917941, https://doi.org/10.1155/2017/6917941.
[25] E. Lou, et al., Imaging tunneling membrane tubes elucidates cell communication in tumors, Trends Cancer 3 (2017) 678–685, https://doi.org/10.1016/j.trecan.2017.08.001.
[26] A.C.C. da Fonseca, B. Badie, Microglia and macrophages in malignant gliomas: recent discoveries and implications for promising therapies, Clin. Dev. Immunol. 2013 (2013), 264124, https://doi.org/10.1155/2013/264124.
[27] N.A. Charles, et al., The brain tumor microenvironment, Glia 60 (2012) 502–514, https://doi.org/10.1002/glia.21264.
[28] A. Clavreul, et al., Isolation of a new cell population in the glioblastoma microenvironment, J. Neuro Oncol. 106 (2012) 493–504, https://doi.org/10.1007/s11060-011-0701-7.
[29] J. Trylcova, et al., Effect of cancer-associated fibroblasts on the migration of glioma cells in vitro, Tumour Biol 36 (2015) 5873–5879, https://doi.org/10.1007/s13277-015-3259-8.
[30] A. Sharma, Role of stem cell derived exosomes in tumor biology, Int. J. Canc. 142 (2018) 1086–1092, https://doi.org/10.1002/ijc.31089.
[31] Y. Komohara, M. Takeya, CAFs and TAMs: maestros of the tumour microenvironment, J. Pathol. 241 (2017) 313–315, https://doi.org/10.1002/path.4824.
[32] M. Wang, et al., Role of tumor microenvironment in tumorigenesis, J. Canc. 8 (2017) 761–773, https://doi.org/10.7150/jca.17648.
[33] P.M. Herst, R.H. Dawson, M.V. Berridge, Intercellular communication in tumor biology: a role for mitochondrial transfer, Front. Oncol. 8 (2018) 344, https://doi.org/10.3389/fonc.2018.00344.

Please cite this article as: C. Salaud et al., Mitochondria transfer from tumor-activated stromal cells (TASC) to primary *Glioblastoma* cells, Biochemical and Biophysical Research Communications, https://doi.org/10.1016/j.bbrc.2020.08.101

GBM	Type	Morphology	Subtype	Treatment	Survival
GBMA1	GBM IV	neurospheres	mesenchymal	Stupp	?
GBM3	GBM IV	adherent	proneural	Stupp	13 m
GBMG5	GBM IV	neurospheres	classical	no	?
GBM5	GBM IV	neurospheres	classical	Stupp	7 m
GBM9	GBM IV	neurosphere/adherent	proneural	Stupp	7 m
GBM15	GBM IV	neurospheres	mesenchymal	no	1.5 m
GBM22	GBM IV	neurospheres	mesenchymal	Stupp	15 m
GBM24	GBM IV	neurospheres	mesenchymal	Stupp	17 m
GBM30	GBM IV	neurospheres	mesenchymal	Stupp	18 m
GBM31	GBM IV	neurospheres	classical	Stupp	21 m
GBM35	GBM IV	adherent	neural	Stupp	10 m
GBM37	GBM IV	adherent	neural	Stupp	21 m

List of primary GBM cultures used in this study. (? = unknown to hospital service) Subtypes were classified according to Verhaak et al. (Cancer Cell. 2010 Jan 19;17(1): 98-110.).

Table S1. Salaud et al.

	Fractions	Volume
H	Homogenate	3.5 ml
MF	Mitochondrial fraction	800 µl
PM	Pure Mitochondria	60 µl
MAM	Mitochondria-Associated Membrane	200 µl
ER	Endoplasmic Reticulum	200 µl
Cyto	Cytosol	3 ml

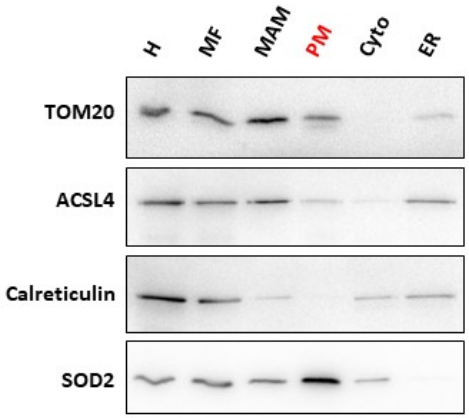

Cellular fractionation of MSC
– 5 µg protein loaded onto gel

Subcellular fractionation by differential centrifugation allows the separation of 6 fractions from MSCs (about $2x10^8$ cells). The list of these fractions with abbreviations, compositions, and total volumes are presented. Protocols can be found in Mignard et al. (J Lipid Res. 2020 61:1025-1037.)

Table S2. Salaud et al.

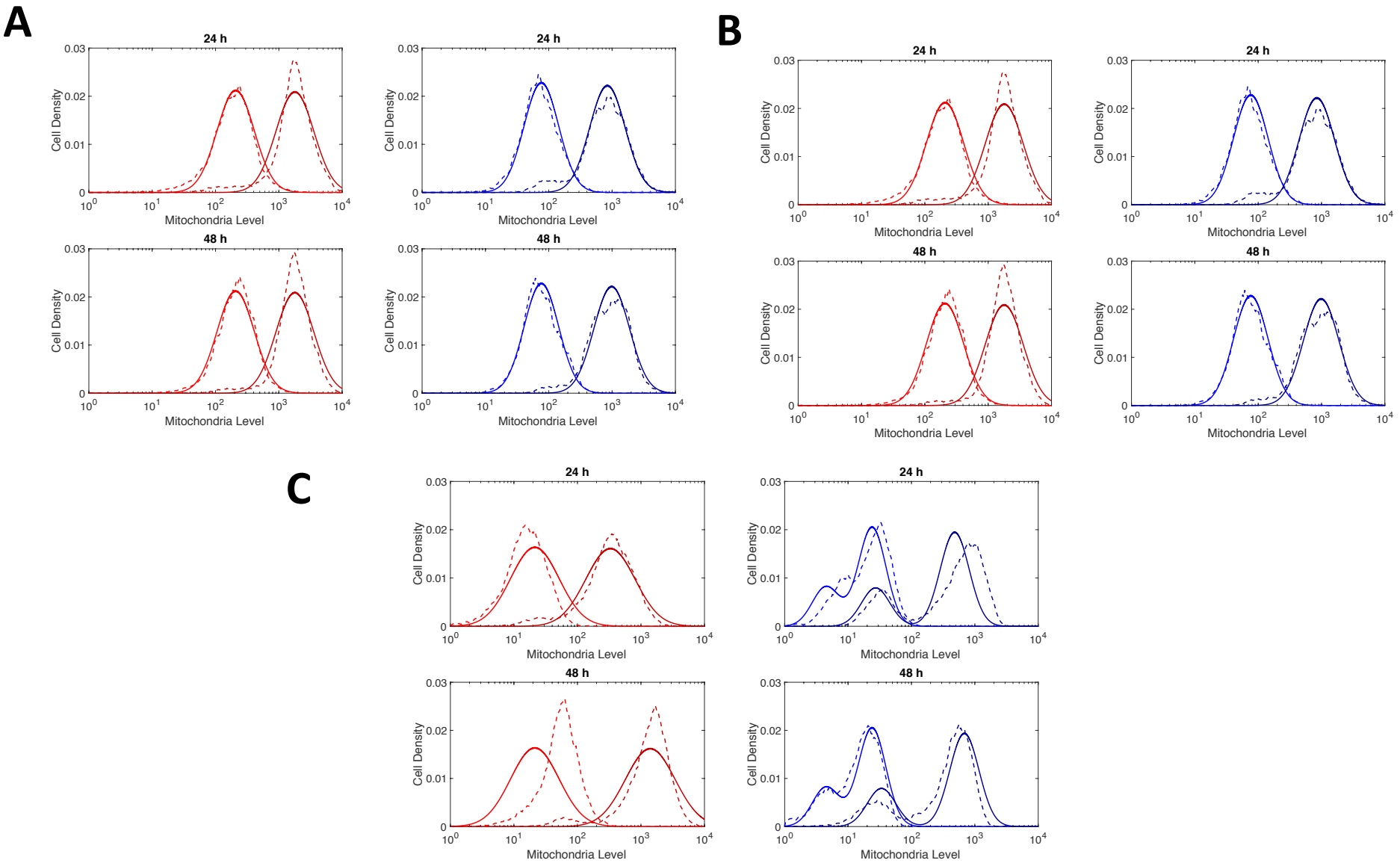

A representative set of fits from the mathematical equation derived from data obtained in figure 4E: Simulation of the uptake of MitoT-labeled pure mitochondria isolated from MSCs by GBMA1 (A), GBM3 (B) and GBMG5 (C). Dashed lines correspond to the experimental data and the solid lines correspond to the numerical simulations. The correspondence of the different lines is as follows: red lines (GBM cells), dark red lines (GBM cells plus MitoT-labeled mitochondria), blue lines (ρ^0GBM cells) and dark blue lines (ρ^0GBM cells plus MitoT-labeled mitochondria).

Figure S1. Salaud et al.

Supplementary informations (Salaud et al.)

Supplementary data 1: additional methods

All procedures involving human participants were in accordance with recommendations of the ethic national research committee. Informed consent was obtained from all individual participants included in this study. The bio-collection used for this analysis is the Glioblastoma collection belonging to the pediatric research program of the University Hospital of Nantes (Ref MESR DC-2014-2206, having obtained a favorable opinion from local Ethics committee (CPP Ouest).

Preparation of GBM primary cultures

GBM primary cultures were obtained as previously described (1). Briefly, Patients diagnosed with high-grade GBM were operated in neurosurgery unit at the "Hôpital Nord Laennec-CHU de Nantes". Immediately after removal of the tumor a fragment of the tumor was placed into 20 ml MACS Tissue Storage Solution (130-100-008, Miltenyi Biotec, Paris, France). Within 4 h the tumor sample was obtained from the "Tumorothèque IRCNA" and treated as follows:

The sample was washed twice with 20 ml PBS and then cut into small fragments of about 2 mm^3. The tumor fragments were then centrifuged for 5 min at 500g after which the supernatant was removed and the pellet suspended in 5 ml PBS - 0.5% BSA - 2mM EDTA and placed into a gentleMACS™ C-tube (130-093-237, Miltenyi Biotec). The cells were then extracted by vortex using a gentleMACS Dissociator (130-093-235, Miltenyi Biotec) then passed through a Falcon® 70 µm cell strainer (352350, Corning, Boulogne-Billancourt, France) The patient derived cells (PDC) recuperated were suspended in defined medium (DMEM/HAM-F12 containing 2 mM L-glutamine, 1x N2 supplement, 1x B27 supplement, 2 µg/ml heparin, 20 ng/ml EGF and 25 ng/ ml bFGF, 100 U/ml penicillin and 100 µg/ml streptomycin) at about $5x10^6$ cells /10 ml. The PDC were cultured in an incubator at 37°C, 5% CO_2 and 95% humidity. As soon as cells started to proliferate in culture aliquots were frozen down to constitute a stock. The culture medium was changed every 2-3 days by replacing 70% of the medium. Primary GBM cell cultures were used for up to 6 months and then discarded and fresh cells were thawed out to prevent derivation of the cultures.

Preparation of MSC

The bone marrow samples used in this study were obtained from healthy donors operated at the Department of Orthopedics at "Centre Hospitalier Universitaire de Nantes France." As previously described (2). The average age of patients was 41 ± 3 years. All human samples were obtained according to the recommendations of the French national ethics committee. The bone marrow cells were isolated by density gradient centrifugation using Ficoll. The cells collected at the interface were cultured in MEM α containing with ribonucleosides and deoxyribonucleosides supplemented with 20% fetal calf serum, 2 mM L-glutamine, 100 U/ml penicillin, and 100 µg/ml streptomycin (complete hMSC medium) and cultured at 37°C in an atmosphere of 5% CO_2 and 95% humidity. Human MSC

cultures were used between passage 2 and 8 passage. Cultures were kept at sub-confluent levels (approximately 75% confluence) and passaged every 5–7 days. Before being used in experiments the phenotype of the MSC was determined by flow cytometry using the MSC Phenotyping kit (130-095-198; Miltenyi Biotec) according to the manufacturer's protocol on a BD FACSCanto II (BD Biosciences, Le Pont de Claix, France) flow cytometer equipped with DIVA software, with 10 000 events recorded for each sample. The data was analyzed using the FlowLogic (Miltenyi Biotec) software. In addition the expression of CD133 (CD133/2-APC; clone 293C3, Miltenyi Biotec), CD44 (CD44-APC, clone BJ18, BioLegend San Diego, CA, USA), CD90 (CD90-PE; 130-095-400, Miltenyi), CD10 (CD10-BV421; clone HI10a, BD Biosciences) and CD105 (CD105-BV421; clone 266, BD Biosciences) were also analyzed.

Co-culture between TASC and GBM

Co-cultures were performed by plating $2x10^5$ MSCs labelled with CellLight Actin-GFP BacMam 2.0 (ThermoFisher Scientific) in 75 mm flasks and 24 h later the cells were washed two times with defined medium and then 10^6 GBM cells in 10 ml defined medium were added to the flasks. The cultures were monitored daily over one week using a Zeiss Axiovert 200-M inverted microscope. At the end of the experiment all the cells were recuperated by incubation for 3 min with Accutase (ThermoFisher Scientific).

To prepare TASC, MSC cells were cultured for a minimum of 5 days in 70% defined medium and 30% of a 48h conditioned medium obtained from the GBM culture that would be used in the co-culture experiment. That is to say that for each co-culture different TASC were prepared.

Labeling of cells with CellLight Actin-GFP BacMam 2.0 (C10582, ThermoFisher Scientific) was performed as follows: briefly $2x10^5$ MSC were allowed to adhere overnight in 75 cm flask and then 15µl was added directly to the cells and the cells were incubated overnight. 16 h later the cells were washed twice and then 10^6 GBM cells in 10 ml defined medium were added to the flasks. The cultures were monitored daily over one week using a Zeiss Axiovert 200-M inverted microscope. On day7, the cells were recuperated by incubation for 3 min with Accutase. The cells were resuspended in PBS-1% BSA and then cell number and viability were determined using the Countess II Automated Cell Counter (ThermoFisher Scientific). Briefly, cells were mixed with Trypan blue (50:50) and loaded into a Countess chamber slide. The image analysis software was used to automatically analyze the acquired images of the samples to give the cell count and viability. 104 cells were immediately analyzed on a BD FACSCanto II (BD Biosciences) flow cytometer equipped with DIVA software, with 10 000 events recorded for each sample. The data was analyzed using the FlowLogic (Miltenyi Biotec) software.

Boyden chamber experiments

24-well cell culture inserts with translucent membranes and 0.4 µm pores were used. Hoechst-33342-stained MSC ($5x10^3$ cells) suspended in complete medium were pipetted into the inner side of the membrane. The cells were allowed to adhere overnight at 37°C in an atmosphere of 95% air/5%

CO_2. The cells were washed 2 times and then replace with 500 μl-defined medium. The insert was placed in a well in 24-well plates prefilled with 1 ml medium (500 µl conditioned medium from different PDCs plus 500 µl defined medium). The cells were incubated for a further 24 h and then the number of MSCs that had traversed the membrane of the insert was counted in 4 different zones using a Zeiss Axiovert 200-M inverted microscope.

Rho 0 cells

To induce mitochondrial damage from cells and to obtain Rho0-like cells (ρ^0 cells); primary GBM cultures or MSC were cultured in defined medium containing 100 ng/mL EtBr (ethidium bromide), 50 µg/mL uridine and 110 ng/mL pyruvate (ρ^0 medium) for at least 4 weeks before testing to determine whether the cells exhibited ρ^0 -like mitochondrial damage. These cells were maintained in ρ^0 medium throughout their period of culture except during experiments when the cells were cultured in defined medium. MSC at passage 3 were used to prepare ρ^0-MSC and used until passage 8 while ρ^0 GBM cells were prepared from freshly thawed cells and frozen down as soon as validated as ρ^0 cells. The ρ^0 GBM were used for 6 months and then discarded to prevent derivation. Prior to use in experiments the cells were stained with MitoTracker deep red every 6-8 weeks to ensure that mitochondria present in the rho0-like cells were still altered".

Agar-agarose culture

Sterile solutions of 2% agar and 1.4% agarose were prepared in Dulbecco's PBS containing $MgCl_2$ and $CaCl_2$. The agar solution was then mixed with defined medium at a ratio of 1:3 and then 1 ml of this solution was added into wells of a 6-well plate and allowed to solidify. During this time 1.4% agarose solution (3 ml) was mixed with 9 ml defined medium and 400 µl PDC (2.5×10^3) were incubated in a 37°C water-bath. When the agar layer had solidified, 1 ml of the cell suspension in agarose was layered on top of the agar layer. The soft agar layer was covered with 1 ml of defined medium. After 3 weeks, the cultures were scanned using a Leica DMI6000B and the Metamorph program.

For co-culture experiments $5x10^4$ Actin-GFP-labeled MSC were plated into 6-well plate 24h before the addition of the agar layer.

Subcellular fractionation

MSC at about 80% confluency were collected from 40 x 75 mm flasks (about $2x10^8$ cells) were homogenized and subcellular fractionation prepared by differential centrifugation.. Briefly, after homogenization the crude mitochondrial fraction was isolated by centrifugation at 10 000g for 10 min. The crude mitochondrial fraction was then layered on a 30% Percoll solution and centrifuged at 95 000g for 30 min. After centrifugation, a dense band of pure mitochondria was observed at the bottom of the tube and a diffused white band of mitochondria-associated membrane at the top of the tube. The fractions were collected with a Pasteur pipette, diluted and then pelleted respectively at 6 300g for 10

min and then 100 000g for 1 h. The different fractions were diluted in different volumes as described in **Table S2**.

Mitochondrial Labeling

Pure mitochondria (PM) (1 µg) were incubated with 25 nM MitoTracker (MitoT) deep red at 37°C for a minimum of 30 min. For the cells: the medium was replaced with pre-warmed medium and then the cells used in experiments. The adherent MitoT-labeled cells were overlaid with unlabeled primary GBM cells and the co-cultures were analyzed by either time-lapse microscopy over 48 h or as end-point experiments after 24 h or 48 h.

Mitochondria (1 µg) were added to 10^6 GBM cells and then incubated for 24, 48 and 72 h. As a control 25 nM MitoT was added to control cells for the same time intervals. For mitochondria: the organelles were centrifuged at 100 000g for 20 min and then used in experiments.

Microscopy

Primary GBM cells were plated on laminin-coated glass coverslips and 24 h later incubated with MitoT deep red for 30 min. The cells were analyzed immediately on a Zeiss Axiovert 200-M inverted microscope.

Time-lapse video-microscopy experiments were performed using a Zeiss Axiovert 200-M inverted microscope and the AxioVision 4.8 program. Dishes were placed inside the Incubator XL-3, on a heating insert M06 (37°C) topped with a CO_2-cover connected to a CO_2 controller that maintained the environmental CO_2 concentration at 5 % for the duration of filming. Digital pictures were acquired and saved every 10 min over 48 h using an AxioCam MR digital camera. The series of photographs were displayed as continuous time-lapse movies for analyses.

Supplementary data 2: mathematical model

The mitochondria expression level in cancer cells was monitored by flow cytometry. The number of cancer cells analyzed at each time frame was about 10000, and histograms were created for the mitochondria intensities in the analyzed populations. The uptake of mitochondria by the cells produces modifications (shifts) in these histograms. To quantify and analyze how the uptake of mitochondria changed over time a mathematical model was proposed.

To capture the histogram dynamics, a density function $u_i(x,t)$ for the population was defined. It denotes the density of cells expressing a level x of mitochondria (i.e. its cellular content) at time t **(5)**. Mitochondria were added to the cell cultures, and their number decreased as they were incorporated into cancer cells. The number of free mitochondria in the culture medium is denoted by $M(t)$. The uptake of mitochondria by cancer cells produces modifications in the histogram; there is

typically a shift to higher values of mitochondria expression. To reproduce such dynamics, an advection equation was chosen since the evolution of different subpopulations fits well to this class of differential equations. The number of cells is not affected by the mitochondria uptake, and this feature is encapsulated in the advection equation due to its inherent mass-conservation structure. The shifts towards higher values of level *x* are considered via a positive velocity $v_i(x,t)$, which gives a measure of the rapidity of uptake of mitochondria for the different cell subpopulations, depending on their level *x* at time *t*. The sub-index *i* represents the possibility that different subpopulations consuming mitochondria at different rates may coexist.

The density function takes values in the following intervals.

$$u_i(x,t)\colon [x_{min}\ x_{max}] \times [0,T] \rightarrow \mathbb{R}^+ \qquad (1)$$

The evolution of the different subpopulations over time is governed by means of the following set of advection equations:

$$\frac{\partial u_i}{\partial t} + \frac{\partial}{\partial x}\big(v_i(x,t)u_i(x,t)\big) = 0 \qquad (2)$$

$$u_i(x,0) = f_i(x) \qquad (3)$$

where $f_i(x)$ is the initial profile of the cell density population *i* having a *x* level of mitochondria. We assume that proliferation (which is low during the studied time frame of 48 h) was not significantly affected by the density functions u_i. Thus, we consider that daughter cells have a similar number of mitochondria as the mother cell. According to our experimental results, there were differences between the initial mitochondria expression (at time 0) with respect to the expression seen at time 24h. However, the differences between 24h and 48h were, in most cases, very small. To reproduce this observation, we included a function accounting for the free mitochondria in the medium. Notice that cells will incorporate mitochondria from the culture medium as long as no complete depletion occurs. Thus, the number of free mitochondria in the medium *M(t)* at time *t* is modeled by means of the differential equation

$$\frac{\partial M(t)}{\partial t} = -\sum_i \int_{x_{min}}^{x_{max}} u_i(x,t)v_i(x,t)dx \qquad (4)$$

If more than one cell subpopulation exists (the summation index *i* can take values higher than one), the differential equations of system Eq. (3) are coupled by means of Eq. (4).

The experiments shown in **Figure 4E** are used to validate our model. We proceeded as follows: 1- the experiments in which no mitochondria were added to the medium were used to estimate the initial conditions $f_i(x)$. (Experiments 1 and 3 in **Figure 4D** were used to estimate the initial conditions for experiments 2 and 4 respectively)
2- in experiments 2 and 4, mitochondria expression at 24h and 48h were used to estimate the uptake velocity $v_i(x,t)$ and the initial condition for free mitochondria in the medium *M(0)*.

A set of fits can be seen in **Figure S4**. From our analysis, the velocity that yielded the best fits was obtained via the following linear dependence

$$v_i(x,t) = a_i x \qquad (5)$$

with different parameters a_i for each primary culture and scenario considered. The velocities v_i have dimensions of mitochondrial expression level over time. **Figure 4F** depicts the uptake velocities for two GBM cell subpopulations (notice that it is represented in a logarithmic scale).

In our analysis two parameters had to be estimated: a_i and *M(0)*. According to the experimental results, most of the primary cultures incorporated the mitochondria during the first 24 h, as no relevant changes in the levels were observed afterwards.

Supplementary references

1. Brocard E, Oizel K, Lalier L, Pecqueur C, Paris F, Vallette FM, Oliver L. Radiation-induced PGE2 sustains human glioma cells growth and survival through EGF signaling. Oncotarget. 2015 Mar 30;6(9):6840-9. doi: 10.18632/oncotarget.3160.
2. Oliver L, Hue E, Séry Q, Lafargue A, Pecqueur C, Paris F, Vallette FM. Differentiation-related response to DNA breaks in human mesenchymal stem cells. Stem Cells. 2013 Apr;31(4):800-7. doi: 10.1002/stem.1336.

Ce travail a été présenté sous forme de poster aux journées scientifiques de l'école doctorale en décembre 2019 et a remporté le prix de la meilleure communication par poster.

Mitochondria transfer from tumor-activated stromal cells (tasc) to primary *glioblastoma* cells.

Céline Salaud[1,2,3], Arturo Alvarez-Arenas Alcami[4], Fanny Geraldo[1,2], Juan Belmonte-Beitia[4], Gabriel F. Calvo[4], Catherine Gratas[1,2], Claire Pecqueur[1,2], Delphine Garnier[1,2,5], François M. Vallette[1,2,5*] and Lisa Oliver[1,2,3*]

[1] CRCINA - INSERM U1232, Nantes 44007 France, [2] Faculté de Médecine, Université de Nantes, Neurochirurgie, Nantes 44007 France, [3] Centre Hospitalier-Universitaire (CHU) de Nantes, Nantes 44007 France, [4] Department of Mathematics & MOLAB-Mathematical Oncology Laboratory, University of Castilla-La Mancha, 13071, Ciudad Real, Spain [5] LabCT- Institut de Cancérologie de l'Ouest - René Gaudducheau, St Herblain

OBJECTIVE: *Glioblastoma Multiforme* (GBM) is the most common primary brain tumor in adults, fatal without treatment. Despite the optimal treatment the overage survival is 15 months.

Within the tumor microenvironment (TME), tumor activated stromal cells (TASC) are recruited to the tumor by factors released by tumor cells. TASC support multiple aspects of cancer progression and cellular interaction such as the cellular transfer of mitochondria via communicating tunneling nanotubules (TNT), which can modulate the phenotype of the tumors. **We address the question of the existence of similar mechanisms between TASC and cancer cells in GBM.**

METHODS:

- *CULTURE CELLS:* Primary GBM cultures were derived from tumors obtained from 20 patients. Normal human mesenchymal stem cells (MSC) were obtained from the "CHU de Nantes". To prepare TASC: MSC were cultured in conditioned medium from primary cultures and defined medium at a ratio of 30:70 for at least 7 day.
- ρ^0 CELLS *OBTENTION*: To elimination mitochondria from cells to obtain ρ^0 cells ; primary GBM cultures or TASC were cultured in defined medium containing 100 ng/mL EtBr, 50 µg/mL uridine and 110 ng/mL pyruvate for at least 4 weeks. Co-cultures were performed by plating 2x10^5 MSC and then 24H later the cells were washed and 10^6 GBM cells in defined medium were added.
- *MITOCHONDRIAL LABELING:* Cells or pure mitochondria were incubated with 25 nM MitoTracker (MitoT). The adherent MitoT-labeled cells were overlaid with unlabeled primary GBM cells and the co-cultures were analyzed by either time-lapse microscopy over 48 H or as end-point experiments after 24 h or 48 H. Mitochondria were added to cells and then incubated for 24, 48 and 72 H.
- *MICROSCOPY:* Primary GBM cells were incubated with MitoT deep red for 30 min. The cells were analyzed on a Zeiss Axiovert 200-M inverted microscope. Digital pictures were acquired and saved every 10 min over 48 h using an AxioCam MR digital camera. The series of photographs were displayed as continuous time-lapse movies for analyses.

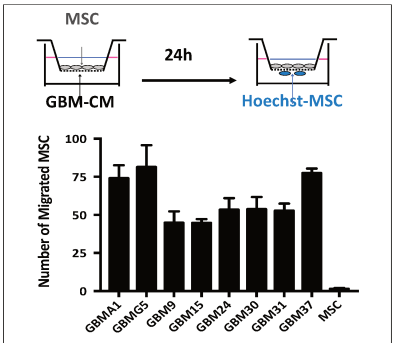

RESULT 1. Induction of TASC phenotype in MSC by GBM cells. MSC have a chemo-attraction after incubation in conditioned media from GBM cultures and hereafter assigned the name TASC to these cells.

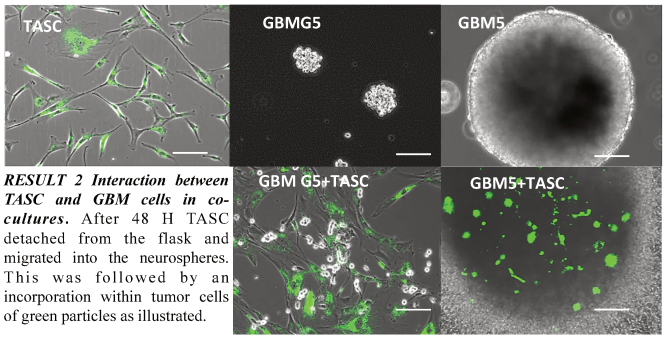

RESULT 2 Interaction between TASC and GBM cells in co-cultures. After 48 H TASC detached from the flask and migrated into the neurospheres. This was followed by an incorporation within tumor cells of green particles as illustrated.

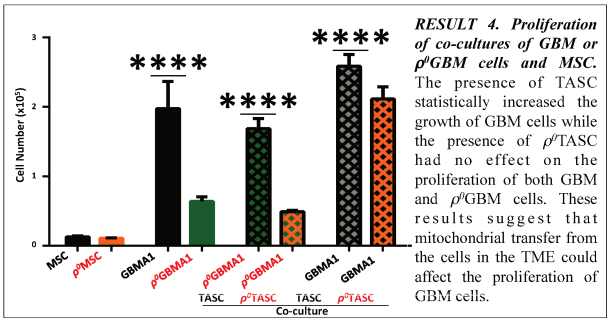

RESULT 4. Proliferation of co-cultures of GBM or ρ^0GBM cells and MSC. The presence of TASC statistically increased the growth of GBM cells while the presence of ρ^0TASC had no effect on the proliferation of both GBM and ρ^0GBM cells. These results suggest that mitochondrial transfer from the cells in the TME could affect the proliferation of GBM cells.

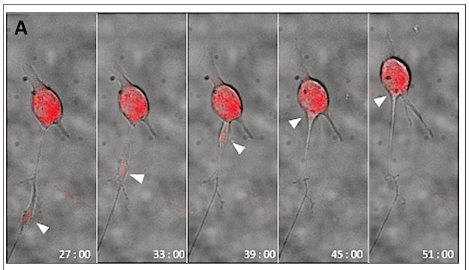

RESULT 3. Mitochondria can be transferred to GBM cells via TNT and exosomes. *A* Presence of labeled mitochondria in GBM cells as early as 24 H after the initiation of the co-culture. Using time-lapse microscopy over 72 H we observed the migration of mitochondria along long interconnecting TNT(white arrow). *B* Mitochondria can also be transferred inside Extracellular Vesicles (red arrows).

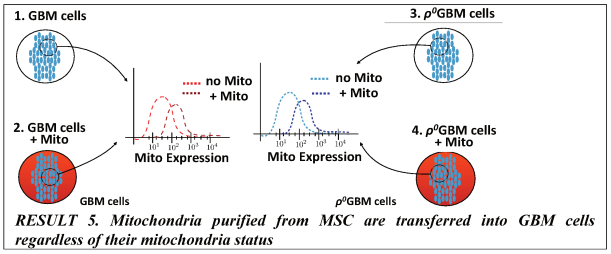

RESULT 5. Mitochondria purified from MSC are transferred into GBM cells regardless of their mitochondria status

CONCLUSION: Mitochondria are exchanged between TASC and GBM cells. Functional mitochondria are transferred from TASC to GBM cells and increase proliferation.

This 3D organoïd culture system contributes to an optimization of an effective *in vitro* model of tumors and shows promise for wide applications in studies of TME/GBM cell interactions and drug discovery fields.

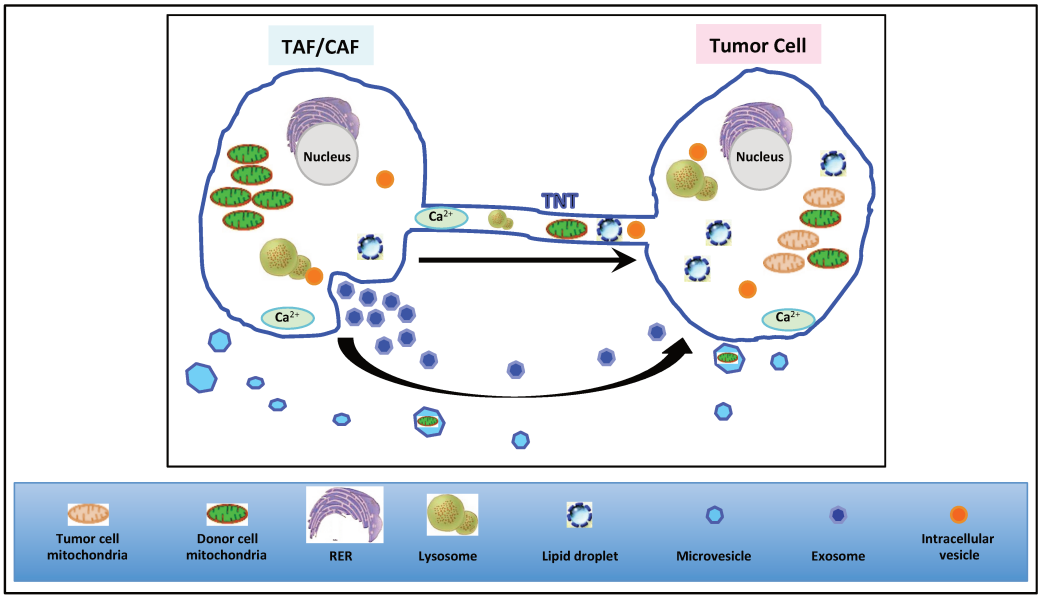

Figure 16. Schématisation des différents moyens de communication entre les cellules tumorales et les CAF. (d'après L. Oliver). Les CAF communiquent avec les cellules cancéreuses par les TNT. Ces TNT permettent les transferts de mitochondries, de lysosomes. Les CAF peuvent également interagir avec les cellules cancéreuses par des exosomes.

4.2 PERSPECTIVE :

Ce travail nous permet de mieux comprendre les mécanismes d'action des CAF dans la résistance au traitement des GBM. Ces mécanismes identifiés et vérifiés sur plusieurs tumoroïdes de GBM permettent de proposer comme cible thérapeutique les mitochondries. Cette thérapeutique pourra être testée pour chaque tumoroïde de chaque patient.

DISCUSSION GÉNÉRALE

IV. DISCUSSION

Les glioblastomes font partie des cancers dont les mécanismes impliqués dans leur formation et leur évolution sont peu compris. Les GBM sont un réel challenge en recherche de par leur complexité intrinsèque, leur hétérogénéité intratumorale et inter-individuelle et leur modification dans le temps. Le traitement de référence est inchangé depuis 2005, basé sur l'étude clinique de Stupp et al. Le traitement actuellement recommandé comporte l'exérèse chirurgicale suivie d'une radiothérapie et chimiothérapie (TMZ) concomitante (16). Malgré ce traitement, la médiane de survie ne dépasse pas 15 mois. Cette évolution fatale à court terme montre les limites de ce traitement et la nécessité absolue de rechercher d'autres thérapeutiques.

Par cette thèse, je me suis intéressée à la résistance des GBM au traitement. En neurochirurgie, nous constatons au quotidien les limites de cette prise en charge pour ces patients. Nous observons, lors des réunions de concertation pluridisciplinaire de neurooncologie, la ré-évolution tumorale très rapide, nécessitant une deuxième ligne de traitement qui, on le sait, ne permet que de gagner du temps.
En travaillant au plus près des scientifiques, je me suis rendue compte de la complexité de la tumorigenèse des cancers, en particulier celle des GBM.

Ce travail a renforcé ma conviction de l'importance d'une collaboration translationnelle, allant de la salle d'opération, à la paillasse, aux essais thérapeutiques. Il paraît incontournable de travailler tous ensemble pour définir la meilleure prise en charge pour chaque patient. Construire une plateforme de criblage des GBM de chaque patient paraît être une solution permettant de tendre vers le traitement personnalisé qui semble être la solution la plus pertinente pour le traitement des cancers et en particulier des GBM.

Dans cet objectif à moyen terme, mon travail de thèse s'est déroulé en quatre phases en se basant sur des questions simples :

-Quels sont, dans les GBM, les mécanismes et les acteurs de la résistance et de la récidive?

-Dans de nombreux cancers, il est décrit le rôle central du MET et de ses composants, comment le recréer de façon fiable et reproductible pour chaque patient?

-Quel est le rôle des CAF dans la résistance et l'évolution des GBM ?

Lors de la première phase, j'ai participé aux travaux de recherche bibliographique afin de faire un état des lieux des différents mécanismes de résistance connus dans les cancers et en particulier dans les GBM. Ce travail a mis en lumière le rôle des cellules dites « quiescentes ». Elles peuvent être un acteur déterminant dans la résistance et donc dans la récidive des GBM. Ces cellules quiescentes peuvent être des cellules souches cancéreuses présentes dans le MET des GBM. L'identification de ces cellules peut permettre de tester un nouveau traitement les ciblant.

La deuxième phase a consisté à développer un modèle pré-clinique simple et reproductible de primocultures de GBM en 3D par technique de bioimpression afin d'étudier dans les meilleurs conditions spatiotemporelles le rôle du MET. L'équipe a donc déterminé la meilleure combinaison de Bioink nécessaire à la technique de bioimpression de ces modèles ainsi que la concentration cellulaire la plus pertinente pour les différentes populations cellulaires étudiées.

Les troisième et quatrième phases avaient pour objectif d'étudier un des composants du MET, les CAF. A partir de notre modèle de culture 3D de GBM, nous avons pu démontrer un des mécanismes de la résistance au traitement actuel des GBM qu'est la communication intercellulaire entre les CAF et les cellules cancéreuses de GBM. Ils permettent à la tumeur de proliférer et de résister aux traitements. Nous avons observé des transferts de mitochondries des CAF aux cellules cancéreuses par différents mécanismes, par l'intermédiaire de connections directes entre ces cellules appelées TNT, par vésicule extracellulaire ou bien par cannibalisme des cellules cancéreuses envers les CAF.

Avantages de notre modèle de tumoroïde et améliorations à venir :

Nous avons détaillé dans l'article 2 la méthodologie de notre modèle de tumoroïde. Celui-ci est reproductible et permet de cultiver plusieurs types cellulaires. Il regroupe les caractéristiques des modèles précliniques pertinents car nous travaillons sur des primocultures de GBM ce qui permet de s'affranchir des inconvénients des lignées cellulaires. C'est un modèle 3D qui permet aux cellules d'interagir dans les 3 plans de l'espace contrairement aux cultures en 2D. Nous avons pour le moment co-cultivé des cellules cancéreuses associées à des CAF, permettant d'analyser leur interaction et de recréer la MEC.

Cependant, ce type de modèles possède encore des limites. Sa taille est très réduite et donc assez éloignée du volume réel de l'organe et de la tumeur qu'il contient. Il y a donc une réelle différence entre l'organoïde/tumoroïde et le cancer in situ. En effet, la diffusion passive des nutriments et de l'oxygène dans ces modèles in vitro est loin des conditions réelles car la tumeur possède une organisation microvasculaire complexe en son sein. Il est donc évident de ce fait que l'absence de vascularisation est une limite de ces modèles in vitro.

Pour permettre à ces modèles d'être vascularisés, il est possible d'injecter par xenogreffes, dans l'organe cible de souris immunodéprimées, le tumoroïde. Néanmoins cela nous renvoie aux limites immuables des modèles murins. Il paraît donc important de générer dans ces modèles 3D in vitro une vascularisation. Vargas-Valderrama et al. ont publié en 2020 une revue de la littérature assez complète sur ce sujet. Ils rapportent plusieurs études ayant tenté d'obtenir une microvascularisation au sein de leur modèles 3D in vitro grâce, par exemple, à la mise en culture d'angioblastes.

Pour le moment, il n'y a pas de modèles recréant réellement cette microvascularisation intrinsèque mais les premiers résultats sont encourageants (67). C'est pourquoi, à court terme, il est prévu de rajouter dans ce modèle des cellules progénitrices endothéliales afin de tenter de recréer cette microvascularisation importante dans les mécanismes de formation et de résistance des GBM.

Afin d'améliorer encore ce modèle, il est également important d'y co-cultiver des cellules immunitaires et plus particulièrement des lymphocytes T. En effet, il est décrit lors d'un processus pathologique intracrânien, tels que les GBM, des phénomènes inflammatoires qui ont pour effet d'engendrer une rupture de la barrière hémato-encéphalique. Cette rupture facilite l'infiltration intratumorale des lymphocytes T en réponse aux phénomènes inflammatoires (81). Il est donc important et tout à fait réalisable de co-cultiver des lymphocytes T afin de recréer l'infiltrat immunitaire présents dans le GBM.

Grace à notre modèle de tumoroïde, nous pouvons sans difficulté rajouter d'autres types cellulaires afin de se rapprocher du MET au complet.

Ce modèle de culture 3D avec ces améliorations décrites ci-dessus devra être comparé à la mise en culture de l'ensemble de la tumeur prélevée dans notre modèle 3D afin de voir la supériorité ou non de cette technique qui paraît très simple à réaliser mais qui possède surement de nombreuses limites.

Cibles thérapeutiques potentielles: CAF / mitochondries?

Ce travail permet de poursuivre la recherche de traitement plus adapté aux GBM. Grâce à nos modèles de tumoroïdes, nous sommes en mesure de tester de nouvelles thérapeutiques à partir d'un échantillon de GBM de différents patients.

Cibler les CAF

Certaines études précliniques ou cliniques de phases I ou II pour différents types de cancers ont testé des traitements qui ciblent des protéines fortement exprimées par les CAF, comme des traitements par anticorps anti-tenascine, un anticorps monoclonal appelé le Sibrotuumab. Les premiers résultats sont encourageants mais restent à confirmer par des essais de phase III et pour le sujet ici traité pour des patients atteints de GBM (52).

Par ailleurs, il été démontré que l'enzyme NAD(P)H oxidase 4 (NOX4) intervenait dans le recrutement des fibroblastes et donc des CAF. Des essais thérapeutiques sur différents cancers par inhibiteur de NOX4 ont été effectués avec pour le moment des résultats peu probants (55).

Cibler les Mitochondries

Nous avons démontré l'importance, dans la résistance au traitement et dans la progression tumorale, du transfert de mitochondries entre les cellules cancéreuses et les CAF. Ces constats ont largement été publiés dans la littérature dans de nombreux autres cancers (82). La mitochondrie peut être ciblée par différentes petites molécules bioactives. Neuzil et al. les ont nommées les « Mitocans » (un mélange de mitochondrie et cancer) (83). Cependant leur action ciblant différents composants de la mitochondrie ne permet pas de distinguer les mitochondries « normales » des mitochondries cancéreuses (38). D'autres traitements ciblant les mitochondries ont été testés, comme certains antibiotiques qui eux, sont capables de cibler les mitochondries des cellules cancéreuses (84).

Perspectives

Ce travail n'est qu'un maillon de la chaine des découvertes et des avancées réalisées au sein de l'équipe. La recherche continue. Les prochaines étapes sont, à court terme, d'améliorer notre modèle de tumoroïdes et de les comparer aux modèles in vivo (représentativité de la réalité, réponse tumorale, résistance en le comparant au patient source).
A plus long terme, l'objectif est de créer une plateforme de tumoroïdes (comportant la biologie, la génétique et les caractéristiques propres à chaque tumeur de patient prélevé) afin de tester pour chaque patient un panel de protocoles thérapeutiques pour lui proposer un traitement personnalisé.

A court terme :

Comme nous l'avons décrit plus haut, nous allons enrichir notre modèle de tumoroïdes en y incluant une microvascularisation et un infiltrat immunitaire.
Par ailleurs, ces tumoroïdes seront injectés par greffes orthotopiques intracérébrales chez les souris afin de comparer ces deux modèles. Cette comparaison se fera en deux temps. Tout d'abord nous analyserons ces deux modèles d'un point de vue morphologique. Puis en administrant le même traitement que le patient au tumoroïde et au modèle animal, nous comparerons l'évolution en taille (par mesure microscopique pour le tumoroïde, par IRM pour le modèle animal et le patient). Cela permettra d'analyser la croissance, l'hétérogénéité et la réponse au traitement de ces deux modèles. Tout cela dans le but de démontrer l'égalité des modèles ou la supériorité d'un des modèles (règle des 3R).

A terme, nous serons capables de reproduire la croissance tumorale du GBM du patient par ces deux modèles, de décortiquer les mécanismes de résistance et de tester des nouvelles thérapies. Cette comparaison permettra également de démontrer la supériorité ou au minimum la non infériorité de notre modèle 3D in vitro dans l'objectif de remplacement des modèles animaux. Dans ce but, une demande de saisine est actuellement soumise au comité d'éthique.

Par ailleurs, il est décrit dans la littérature la présence de cellules sanguines circulantes de GBM dans le sang (85) (86). Cette expression est peut être modifiée dans le temps et laisse envisager un marqueur de modification tumorale qui pourrait témoigner de l'émergence d'une résistance au traitement entre autres par l'intermédiaire des cellules quiescentes comme décrit dans l'article 1. Nous allons donc, en parallèle, effectuer un autre travail. Dans le cadre d'un

Master 2, nous allons analyser la présence ou non dans le sang de cellules tumorales et l'éventuelle modification d'expression dans le temps. Pour faciliter leur mise en évidence, il sera injecté cette fois ci des lignées de cellules tumorales de GBM qui ont l'avantage d'être immunomarquées (U251). L'objectif est de mettre en évidence des cellules sanguines circulantes permettant de rechercher des indices de résistance en cours de traitement.

A plus long terme :

Une fois le modèle validé, l'objectif est de créer une plateforme de tumoroïdes. Dès que le patient sera opéré, un nombre important de tumoroïdes sera créé afin de tester toute une batterie de protocoles thérapeutiques pré-définis (en collaboration avec nos confrères oncologues). Ces tests seront effectués sur une courte durée, pour le plus tôt possible, déterminer le meilleur traitement pour le patient.

La finalité est donc de proposer un traitement personnalisé au patient. Cette approche et ce projet nécessitent de nombreuses étapes en amont mais permet d'espérer à une meilleure survie des patients atteints de GBM.

BIBLIOGRAPHIE

BIBLIOGRAPHIE

1. Lukas RV, Wainwright DA, Ladomersky E, Sachdev S, Sonabend AM, Stupp R. Newly Diagnosed Glioblastoma: A Review on Clinical Management. Oncol Williston Park N. 2019 13;33(3):91–100.
2. Zouaoui S, Rigau V, Mathieu-Daudé H, Darlix A, Bessaoud F, Fabbro-Peray P, et al. Recensement national histologique des tumeurs primitives du système nerveux central : résultats généraux sur 40 000 cas, principales applications actuelles et perspectives. Fr Brain Tumor Database Gen Results 40000 Cases Main Curr Appl Future Prospects Engl. 2012 Feb 1;58(1):4–13.
3. Louis DN, Perry A, Reifenberger G, von Deimling A, Figarella-Branger D, Cavenee WK, et al. The 2016 World Health Organization Classification of Tumors of the Central Nervous System: a summary. Acta Neuropathol (Berl). 2016;131(6):803–20.
4. Louis DN, Ohgaki H, Wiestler OD, Cavenee WK, Burger PC, Jouvet A, et al. The 2007 WHO Classification of Tumours of the Central Nervous System. Acta Neuropathol (Berl). 2007;114(2):97.
5. Daumas-Duport C, Beuvon F, Varlet P, Fallet-Bianco C. [Gliomas: WHO and Sainte-Anne Hospital classifications]. Ann Pathol. 2000 Oct;20(5):413–28.
6. Brouland JP, Hottinger AF. [Revised WHO classification 2016 of gliomas : what's new ?]. Rev Med Suisse. 2017 Oct 18;13(579):1805–9.
7. Baldi I, Huchet A, Bauchet L, Loiseau H. [Epidemiology of glioblastoma]. Neurochirurgie. 2010 Dec;56(6):433–40.
8. Sanson M. Gliomes avec mutation IDH : profil génomique et perspectives cliniques. Morphologie. 2016 Sep 1;100(330):172–3.
9. Salvati M, Tariciotti L, Brunetto GMF, Gallo G, Santoro F, Frati A, et al. Glioblastoma: Molecular profile and immunophenotypic analysis as prognostic tools for tailored therapy and decision making in a recent surgical series. Interdiscip Neurosurg [Internet]. 2020 Jun 1 [cited 2020 Sep 27];20:100697. Available from: http://www.sciencedirect.com/science/article/pii/S221475191930369X
10. Hai Yan, Parsons W, Jin G, Mclendon R, Rasheed A, Weishi Yuan, et al. IDH1 and IDH2 mutations in gliomas. N Engl J Med. 2009;(8):765.
11. Brennan CW, Verhaak RGW, McKenna A, Campos B, Noushmehr H, Salama SR, et al. The somatic genomic landscape of glioblastoma. Cell. 2013 Oct 10;155(2):462–77.

12. Van Meir EG, Hadjipanayis CG, Norden AD, Shu H-K, Wen PY, Olson JJ. Exciting new advances in neuro-oncology: the avenue to a cure for malignant glioma. Ca. 2010;(3):166.

13. Verhaak RGW, Hoadley KA, Purdom E, Wang V, Qi Y, Wilkerson MD, et al. Integrated genomic analysis identifies clinically relevant subtypes of glioblastoma characterized by abnormalities in PDGFRA, IDH1, EGFR, and NF1. Cancer Cell. 2010 Jan 19;17(1):98–110.

14. Wang Q, Hu B, Hu X, Kim H, Squatrito M, Scarpace L, et al. Tumor Evolution of Glioma-Intrinsic Gene Expression Subtypes Associates with Immunological Changes in the Microenvironment. Cancer Cell. 2017 10;32(1):42-56.e6.

15. Schernberg A, Marabelle A, Massard C, Armand J-P, Dumont S, Deutsch E, et al. Mise au point sur les glioblastomes : des thérapies ciblant les cellules tumorales aux thérapies ciblant les cellules immunitaires. Whats Glioblastoma Treat Tumor-Target Immune-Target Ther Engl. 2016 May 1;103(5):484–98.

16. Stupp R, Mason WP, van den Bent MJ, Weller M, Fisher B, Taphoorn MJB, et al. Radiotherapy plus concomitant and adjuvant temozolomide for glioblastoma. N Engl J Med. 2005 Mar 10;352(10):987–96.

17. Alieva M, Leidgens V, Riemenschneider MJ, Klein CA, Hau P, van Rheenen J. Intravital imaging of glioma border morphology reveals distinctive cellular dynamics and contribution to tumor cell invasion. Sci Rep. 2019 Feb 14;9(1):2054.

18. Feuvret L, Antoni D, Biau J, Truc G, Noël G, Mazeron J-J. [Guidelines for the radiotherapy of gliomas]. Cancer Radiother J Soc Francaise Radiother Oncol. 2016 Sep;20 Suppl:S69-79.

19. Glaser SM, Dohopolski MJ, Balasubramani GK, Flickinger JC, Beriwal S. Glioblastoma multiforme (GBM) in the elderly: initial treatment strategy and overall survival. J Neurooncol. 2017;134(1):107.

20. Qazi MA, Vora P, Venugopal C, Sidhu SS, Moffat J, Swanton C, et al. Intratumoral heterogeneity: pathways to treatment resistance and relapse in human glioblastoma. Ann Oncol Off J Eur Soc Med Oncol. 2017 Jul 1;28(7):1448–56.

21. Hegi ME, Diserens A-C, Gorlia T, Hamou M-F, de Tribolet N, Weller M, et al. MGMT gene silencing and benefit from temozolomide in glioblastoma. N Engl J Med. 2005 Mar 10;352(10):997–1003.

22. Zanders ED, Svensson F, Bailey DS. Therapy for glioblastoma: is it working? Drug Discov Today. 2019 May;24(5):1193–201.

23. Behnan J, Finocchiaro G, Hanna G. The landscape of the mesenchymal signature in brain tumours. Brain J Neurol. 2019 Apr 1;142(4):847–66.
24. Bastien JIL, McNeill KA, Fine HA. Molecular characterizations of glioblastoma, targeted therapy, and clinical results to date. Cancer. 2015 Feb 15;121(4):502–16.
25. Behnan J, Isakson P, Joel M, Cilio C, Langmoen IA, Vik-Mo EO, et al. Recruited brain tumor-derived mesenchymal stem cells contribute to brain tumor progression. Stem Cells Dayt Ohio. 2014 May;32(5):1110–23.
26. Alexander BM, Pinnell N, Wen PY, D'Andrea A. Targeting DNA repair and the cell cycle in glioblastoma. J Neurooncol. 2012 May;107(3):463–77.
27. Ke C, Tran K, Chen Y, Di Donato AT, Yu L, Hu Y, et al. Linking differential radiation responses to glioma heterogeneity. Oncotarget. 2014 Mar 30;5(6):1657–65.
28. Ramírez-Expósito MJ, Martínez-Martos JM. The Delicate Equilibrium between Oxidants and Antioxidants in Brain Glioma. Curr Neuropharmacol. 2019;17(4):342–51.
29. Rabé M, Dumont S, Álvarez-Arenas A, Janati H, Belmonte-Beitia J, Calvo GF, et al. Identification of a transient state during the acquisition of temozolomide resistance in glioblastoma. Cell Death Dis. 2020 06;11(1):19.
30. Hermida MA, Kumar JD, Schwarz D, Laverty KG, Di Bartolo A, Ardron M, et al. Three dimensional in vitro models of cancer: Bioprinting multilineage glioblastoma models. Adv Biol Regul. 2020 Jan 1;75.
31. Clavreul A, Guette C, Faguer R, Tétaud C, Boissard A, Lemaire L, et al. Glioblastoma-associated stromal cells (GASCs) from histologically normal surgical margins have a myofibroblast phenotype and angiogenic properties. J Pathol. 2014 May;233(1):74–88.
32. D'Alessio A, Proietti G, Sica G, Scicchitano BM. Pathological and Molecular Features of Glioblastoma and Its Peritumoral Tissue. Cancers. 2019 Apr 3;11(4).
33. Quail DF, Joyce JA. The Microenvironmental Landscape of Brain Tumors. Cancer Cell. 2017 13;31(3):326–41.
34. Martínez-Ramos C, Lebourg M. Three-dimensional constructs using hyaluronan cell carrier as a tool for the study of cancer stem cells. J Biomed Mater Res B Appl Biomater. 2015 Aug;103(6):1249–57.
35. Virga J, Szemcsák CD, Reményi-Puskár J, Tóth J, Hortobágyi T, Csősz É, et al. Differences in Extracellular Matrix Composition and its Role in Invasion in Primary and Secondary Intracerebral Malignancies. Anticancer Res. 2017;37(8):4119–26.
36. Virga J, Szivos L, Hortobágyi T, Chalsaraei MK, Zahuczky G, Steiner L, et al. Extracellular matrix differences in glioblastoma patients with different prognoses. Oncol Lett.

2019 Jan;17(1):797–806.
37. Ford K, Hanley CJ, Mellone M, Szyndralewiez C, Heitz F, Wiesel P, et al. NOX4 Inhibition Potentiates Immunotherapy by Overcoming Cancer-Associated Fibroblast-Mediated CD8 T-cell Exclusion from Tumors. Cancer Res. 2020 May 1;80(9):1846–60.
38. D'Souza GGM, Wagle MA, Saxena V, Shah A. Approaches for targeting mitochondria in cancer therapy. BBA - Bioenerg. 2011 Jan 1;1807(6):689–96.
39. Shi Y, Du L, Lin L, Wang Y. Tumour-associated mesenchymal stem/stromal cells: emerging therapeutic targets. Nat Rev Drug Discov. 2017 Jan;16(1):35–52.
40. Lathia JD, Mack SC, Mulkearns-Hubert EE, Valentim CLL, Rich JN. Cancer stem cells in glioblastoma. Genes Dev. 2015 Jun 15;29(12):1203–17.
41. Schonberg DL, Lubelski D, Miller TE, Rich JN. Brain tumor stem cells: Molecular characteristics and their impact on therapy. Mol Aspects Med. 2014 Oct;39:82–101.
42. Shu HK, Kim MM, Chen P, Furman F, Julin CM, Israel MA. The intrinsic radioresistance of glioblastoma-derived cell lines is associated with a failure of p53 to induce p21(BAX) expression. Proc Natl Acad Sci U S A. 1998 Nov 24;95(24):14453–8.
43. Wang J, Wakeman TP, Lathia JD, Hjelmeland AB, Wang X-F, White RR, et al. Notch promotes radioresistance of glioma stem cells. Stem Cells Dayt Ohio. 2010 Jan;28(1):17–28.
44. Bao S, Wu Q, McLendon RE, Hao Y, Shi Q, Hjelmeland AB, et al. Glioma stem cells promote radioresistance by preferential activation of the DNA damage response. Nature. 2006 Dec 7;444(7120):756–60.
45. Whiteside TL. Exosome and mesenchymal stem cell cross-talk in the tumor microenvironment. Semin Immunol. 2018;35:69–79.
46. Chen J, Li Y, Yu T-S, McKay RM, Burns DK, Kernie SG, et al. A restricted cell population propagates glioblastoma growth after chemotherapy. Nat Int Wkly J Sci. 2012;488(7412):522.
47. Appaix F, Nissou M-F, van der Sanden B, Dreyfus M, Berger F, Issartel J-P, et al. Brain mesenchymal stem cells: The other stem cells of the brain? World J Stem Cells. 2014 Apr 26;6(2):134–43.
48. Hossain A, Gumin J, Gao F, Figueroa J, Shinojima N, Takezaki T, et al. Mesenchymal Stem Cells Isolated From Human Gliomas Increase Proliferation and Maintain Stemness of Glioma Stem Cells Through the IL-6/gp130/STAT3 Pathway. Stem Cells. 2015;(8):2400.
49. Shahar T, Rozovski U, Hess KR, Hossain A, Gumin J, Gao F, et al. Percentage of mesenchymal stem cells in high-grade glioma tumor samples correlates with patient survival. Neuro-Oncol. 2017 01;19(5):660–8.

50. Clavreul A, Etcheverry A, Chassevent A, Quillien V, Avril T, Jourdan M-L, et al. Isolation of a new cell population in the glioblastoma microenvironment. J Neurooncol. 2012 Feb;106(3):493–504.

51. Miyai Y, Esaki N, Takahashi M, Enomoto A. Cancer-associated fibroblasts that restrain cancer progression: Hypotheses and perspectives. Cancer Sci. 2020 Apr;111(4):1047–57.

52. Xing F, Saidou J, Watabe K. Cancer associated fibroblasts (CAFs) in tumor microenvironment. Front Biosci Landmark Ed. 2010 Jan 1;15:166–79.

53. Liu T, Zhou L, Li D, Andl T, Zhang Y. Cancer-Associated Fibroblasts Build and Secure the Tumor Microenvironment. Front Cell Dev Biol. 2019;7:60.

54. Sahai E, Astsaturov I, Cukierman E, DeNardo DG, Egeblad M, Evans RM, et al. A framework for advancing our understanding of cancer-associated fibroblasts. Nat Rev Cancer. 2020 Mar;20(3):174–86.

55. Barnett RM, Vilar E. Targeted Therapy for Cancer-Associated Fibroblasts: Are We There Yet? J Natl Cancer Inst. 2018 Jan 1;110(1).

56. Mishra PJ, Mishra PJ, Humeniuk R, Medina DJ, Alexe G, Mesirov JP, et al. Carcinoma-associated fibroblast-like differentiation of human mesenchymal stem cells. Cancer Res. 2008 Jun 1;68(11):4331–9.

57. Mezawa Y, Orimo A. The roles of tumor- and metastasis-promoting carcinoma-associated fibroblasts in human carcinomas. Cell Tissue Res. 2016;365(3):675–89.

58. Trylcova J, Busek P, Smetana K, Balaziova E, Dvorankova B, Mifkova A, et al. Effect of cancer-associated fibroblasts on the migration of glioma cells in vitro. Tumour Biol J Int Soc Oncodevelopmental Biol Med. 2015 Aug;36(8):5873–9.

59. Wang Z, Tan Y, Yu W, Zheng S, Zhang S, Sun L, et al. Small role with big impact: miRNAs as communicators in the cross-talk between cancer-associated fibroblasts and cancer cells. Int J Biol Sci. 2017;13(3):339–48.

60. Luo X, Weiss WA. Utility of Human-Derived Models for Glioblastoma. Cancer Discov. 2020 Jul;10(7):907–9.

61. Lopes-Coelho F, Gouveia-Fernandes S, Serpa J. Metabolic cooperation between cancer and non-cancerous stromal cells is pivotal in cancer progression. Tumour Biol J Int Soc Oncodevelopmental Biol Med. 2018 Feb;40(2):1010428318756203.

62. Lee C, Abelseth E, de la Vega L, Willerth S m. Bioprinting a novel glioblastoma tumor model using a fibrin-based bioink for drug screening. Mater Today Chem. 2019 Jun 1;12:78–84.

63. Lagerweij T, Dusoswa SA, Negrean A, Hendrikx EML, de Vries HE, Kole J, et al. Optical clearing and fluorescence deep-tissue imaging for 3D quantitative analysis of the brain tumor microenvironment. Angiogenesis. 2017;1.
64. Lopez M. Les modèles murins de cancers : synthèse bibliographique et contribution à la mise en place d'un modèle orthotopique de cancer du colon pour des études précliniques d'évaluation thérapeutique. :86.
65. Baker BM, Chen CS. Deconstructing the third dimension: how 3D culture microenvironments alter cellular cues. J Cell Sci. 2012 Jul 1;125(Pt 13):3015–24.
66. Lancaster MA, Knoblich JA. Organogenesis in a dish: modeling development and disease using organoid technologies. Science. 2014 Jul 18;345(6194):1247125.
67. Vargas-Valderrama A, Messina A, Mitjavila-Garcia MT, Guenou H. The endothelium, a key actor in organ development and hPSC-derived organoid vascularization. J Biomed Sci. 2020;27(1).
68. Kaushik G, Ponnusamy MP, Batra SK. Concise Review: Current Status of Three-Dimensional Organoids as Preclinical Models. Stem Cells Dayt Ohio. 2018 Sep;36(9):1329–40.
69. Clevers H. Modeling Development and Disease with Organoids. Cell. 2016 Jun 16;165(7):1586–97.
70. Aberle MR, Burkhart RA, Tiriac H, Olde Damink SWM, Dejong CHC, Tuveson DA, et al. Patient-derived organoid models help define personalized management of gastrointestinal cancer. Br J Surg. 2018;105(2):e48–60.
71. Heinrich MA, Liu W, Jimenez A, Yang J, Akpek A, Liu X, et al. 3D Bioprinting: from Benches to Translational Applications. Small Weinh Bergstr Ger. 2019 Jun;15(23):e1805510.
72. Hubert CG, Rivera M, Spangler LC, Wu Q, Mack SC, Prager BC, et al. A Three-Dimensional Organoid Culture System Derived from Human Glioblastomas Recapitulates the Hypoxic Gradients and Cancer Stem Cell Heterogeneity of Tumors Found In Vivo. Cancer Res. 2016 15;76(8):2465–77.
73. Gomez-Roman N, Stevenson K, Gilmour L, Hamilton G, Chalmers AJ. A novel 3D human glioblastoma cell culture system for modeling drug and radiation responses. Neuro-Oncol. 2017 01;19(2):229–41.
74. Gomez-Roman N, Stevenson K, Gilmour L, Hamilton G, Chalmers AJ. A novel 3D human glioblastoma cell culture system for modeling drug and radiation responses. Neuro-Oncol. 2017 01;19(2):229–41.
75. Dai X, Ma C, Lan Q, Xu T. 3D bioprinted glioma stem cells for brain tumor model

and applications of drug susceptibility. Biofabrication. 2016 11;8(4):045005.

76. Hubert CG, Rivera M, Spangler LC, Wu Q, Mack SC, Prager BC, et al. A Three-Dimensional Organoid Culture System Derived from Human Glioblastomas Recapitulates the Hypoxic Gradients and Cancer Stem Cell Heterogeneity of Tumors Found In Vivo. Cancer Res. 2016 15;76(8):2465–77.

77. Heinrich MA, Bansal R, Lammers T, Zhang YS, Michel Schiffelers R, Prakash J. 3D-Bioprinted Mini-Brain: A Glioblastoma Model to Study Cellular Interactions and Therapeutics. Adv Mater Deerfield Beach Fla. 2019 Apr;31(14):e1806590.

78. Yi H-G, Jeong YH, Kim Y, Choi Y-J, Moon HE, Park SH, et al. A bioprinted human-glioblastoma-on-a-chip for the identification of patient-specific responses to chemoradiotherapy. Nat Biomed Eng. 2019 Jul;3(7):509–19.

79. Lancaster MA, Knoblich JA. Generation of cerebral organoids from human pluripotent stem cells. Nat Protoc. 2014 Oct;9(10):2329–40.

80. Linkous A, Balamatsias D, Snuderl M, Edwards L, Miyaguchi K, Milner T, et al. Modeling Patient-Derived Glioblastoma with Cerebral Organoids. Cell Rep. 2019 Mar 19;26(12):3203-3211.e5.

81. Binder DC, Davis AA, Wainwright DA. Immunotherapy for cancer in the central nervous system: Current and future directions. Oncoimmunology. 2015 Sep 11;5(2):e1082027.

82. Hekmatshoar Y, Nakhle J, Galloni M, Vignais M-L. The role of metabolism and tunneling nanotube-mediated intercellular mitochondria exchange in cancer drug resistance. Biochem J. 2018 Jul 31;475(14):2305–28.

83. Neuzil J, Dong L-F, Rohlena J, Truksa J, Ralph SJ. Classification of mitocans, anti-cancer drugs acting on mitochondria. Mitochondrion. 2013 May 1;13(3):199–208.

84. Lamb R, Ozsvari B, Lisanti CL, Tanowitz HB, Howell A, Martinez-Outschoorn UE, et al. Antibiotics that target mitochondria effectively eradicate cancer stem cells, across multiple tumor types: treating cancer like an infectious disease. Oncotarget. 2015 Mar 10;6(7):4569–84.

85. Chistiakov DA, Chekhonin VP. Circulating tumor cells and their advances to promote cancer metastasis and relapse, with focus on glioblastoma multiforme. Exp Mol Pathol. 2018;105(2):166–74.

86. Krol I, Castro-Giner F, Maurer M, Gkountela S, Szczerba BM, Scherrer R, et al. Detection of circulating tumour cell clusters in human glioblastoma. Br J Cancer. 2018;119(4):487–91.

DOCTORAT BIOLOGIE BRETAGNE SANTE LOIRE

UNIVERSITÉ DE NANTES

Titre : Reconstruction in vitro d'un glioblastome par techniques de bioimpression

Mots clés : Glioblastome, culture 3 Dimensions, microenvironnement tumoral, TASC, mécanismes de résistance

Résumé : Les glioblastomes (GBM) sont des tumeurs cérébrales de mauvais pronostic dont le traitement repose sur l'exérèse suivi d'une radiochimiothérapie, leur médiane de survie est de 15 mois.
Il est démontré que le microenvironnement tumoral (MET) des GBM, comporte de nombreuses cellules comme les fibroblastes associés au cancer (CAF) et joue un rôle important dans la survie, la croissance et la résistance. Il est donc nécessaire de trouver un modèle pré-thérapeutique le plus proche des conditions humaines afin de comprendre les mécanismes de tumorigenèse du GBM.
Dans un premier temps, nous avons étudié la littérature pour identifier tous les mécanismes de résistance. Il semblerait que les cellules quiescentes, présentes dans le MET, soient déterminantes.
Dans un second temps, nous avons mis au point un modèle de tumoroïde 3D en utilisant des cultures dérivées de patients. Nous avons défini la composition de la matrice ainsi que les concentrations optimales des cellules en culture. Un modèle mathématique a été développé pour déterminer la prolifération et la forme des tumoroïdes.
Nous avons ensuite étudié le rôle des CAF. Ils transfèrent leurs mitochondries par des tunneling nanotubes (TNT), des vésicules extracellulaires ou par cannibalisme aux cellules cancéreuses. Ce transfert contribue à la prolifération et à la résistance au traitement.
Ces modèles de cultures primaires de GBM en 3D sont la première étape indispensable pour espérer créer des traitements personnalisés basés sur les prélèvements tumoraux des patients.

Title : In vitro reconstruction of Glioblastoma by 3D bioprinting

Keywords : Glioblastoma, 3 Dimensional culture, tumor microenvironment, CAF, resistance mechanism

Abstract : Glioblastomas (GBMs) are brain tumors with a poor prognosis, treatment is based on surgical removal followed by radiochemotherapy and the median survival is 15 months.
The reason of therapeutic resistance is complex. GBMs are extremely heterogeneous in their composition. Tumor microenvironment (TME) is composed of numerous different populations including cancer-associated fibroblast (CAF) and plays an important role in survival, growth and resistance of the tumor.
It is therefore necessary to find a pre-therapeutic model closest to the in vivo conditions to improve our knowledge of tumoregenesis.
Fist, we present a review of literature of resistance mechanisms. The quiescent cells, present in the TME, may have an important role.
Second, we developed a 3D tumoroid model using patient-derived cultures. We determined optimal matrix composition and cell concentration. A mathematical model was developed to determine proliferation and form of tumoroids.
Third, using our tumoroid models, we showed CAF protection to GBM cells to therapy.
Fourth, we studied interaction between CAF and GBM cultures in co-culture. CAF transfer mitochondria by tunnelling nanotubes (TNT), extracellular vesicles or cannibalism. Mitochondrial transfer contributes to proliferation and resistance to treatment.
These 3D tumor models are the first step to create personalized treatments based on tumor samples from patients.